DISS. ETH NO. 27172

Natural Knee Kinematics

-

The Role of Limb Alignment and Activity on Knee Joint Motion

A thesis submitted to attain the degree of

DOCTOR OF SCIENCES of ETH ZÜRICH

(Dr. sc. ETH Zürich)

presented by

Barbara Elisabeth Postolka

MSc in Human Movement Sciences, ETH Zürich

born on 17.05.1989

citizen of Zürich, ZH

accepted on the recommendation of

Prof. Dr. William R. Taylor, examiner

Dr. Renate List, co-examiner

Dr. Pascal Schütz, co-examiner

Prof. Dr. Věra Pinskerová, co-examiner

2020

Statement of originality

I hereby confirm that I am the sole author of the written work here enclosed and that I have compiled it in my own words. Parts excepted are corrections of form and content by the supervisors and/or co-authors of the published articles (Chapters 2-6).

Barbara Elisabeth Postolka

Acknowledgements

During my PhD, I have received guidance, advice and help from many people to whom I am extremely grateful. Without their great support this thesis would not have been possible.

First and foremost, I would like to thank my supervisor Prof. Dr. William R. Taylor for his continuous support and dedication towards my project. Your inputs and visions have helped me to critically think about my project and sometimes also outside the box. I have greatly benefited from your passion for writing and have learned lot about scientific writing. Thank you for your trust and support to travel the world and present my work at scientific meetings.
I also sincerely like to thank my co-examiners Dr. Renate List and Dr. Pascal Schütz. Since my first internship within the group you have been of great support. You have taught me how to run experiments in the lab and your patience while working with subjects was always an example for me. Thank you for always having an open door for all my questions, problems and ideas. Our discussions and your valuable input and constructive feedback were of great benefit and imporved the outcome of this project. I deeply like to thank you for everything.
Many thanks are also owed to Prof. Dr. Věra Pinskerová for accepting to be a co-examiner of this thesis. Your continuous interest in my work, our discussions and your effort in reading and evaluating the thesis was of great value.

During my time as a PhD student, I received valuable support in measuring, post-processing and analysing of my data from many students. I especially like to thank Katrin Dätwyler, Edwina Huber and Bernhard Birner who wrote their thesis within this project and contributed to its successful completion.

I like to express my sincere gratitude to all the participants of my study. Without your interest, time and patience during the measurement sessions this thesis would not have been possible.

I would also like to thank PD Dr. med. Sandro F. Fucentese for the clinical guidance and inputs to the study and Nathalie Kühne for organising all clinical assessment sessions.
The financial support from Medacta International and the Commission for Technology and Innovation (CTI) was greatly appreciated.

I would not have been able to perform the measurements in the lab without a lot of helping hands. Thank you to Michael Angst, Dr. Fabio D'Isidoro, Lynn Ellenberger, Marina Hitz, Michael Plüss, Longfeng Rao, Samara Monn, Lorena Suter, Dr. Thomas Zumbrunn and all students for their support during all the hours in the lab.
Furthermore, I like to sincerely thank Peter Schwilch and Marco Hitz for their technical help and support with the FluMo and in the lab.

A big thank you to Reto Togni for assuring the FluMo and I are pictured in the right light. Your effort in taking and editing these pictures was greatly appreciated.

I also like to thank all the current and past members of the Laboratory for Movement Biomechanics. Thanks for making such a great working environment. The coffee breaks, grill lunches on the terrace, Monday sports sessions, the time spend in Brisbane, Dublin and Calgary and all other events we have spent together have created a memorable working atmosphere. I especially like to thank Dr. Niklas Ignasiak, Deepak Ravi Kumar, PD Dr. Dr. Silvio Lorenzetti, Dr. Hamed Hosseini Nasab, Prof. Dr. Mark Sayers, Dr. Florian Schellenberg, Dr. Navrag Singh, Dr. Colin Smith, Stefan Plüss, Rosa Visscher, Dr. Florian Vogl and Dr. Roland Zemp.

A special thank to Fabian Ammann for proofreading the introduction of this thesis and providing valuable feedback.

Thank you to my family and friends. Thanks for sharing joyful and stressful times, being curious of my work and accompanying me on this journey.
From the bottom of my heart I like to thank Mami, Papi and Claudia. Thank you for your lifelong loving and emotional support for everything I do.
I am deeply thankful to my partner Marco. You have challenged me with your questions, motivated me when needed and always had an open ear. Thank you for traveling the world with me and being the best home office companion I could ever wish for. Thank you for your countless support.

Abstract

Joint motion of the natural knee is guided by an interconnected system of bones, soft tissue structures and muscles providing guidance for a complex set of tibio-femoral rotations and condylar translations along all six degrees of freedom. Accurate knowledge of knee kinematics is essential for a clear understanding of knee joint function, but also provides the foundation for assessing joint pathologies and the efficacy of musculoskeletal interventions. In general, subject-specific differences have been reported, with inter-subject variability dominating the magnitudes and patterns of condylar translation. However, while general agreement has been achieved for tibio-femoral kinematics during repetitive flexion tasks, controversial results and contradictory findings have been presented for dynamic activities such as walking, especially for the tibial rotation, condylar translation, and the resultant centre of rotation. Here, comparisons between studies are complicated by the variety of measurement systems and analysis approaches used, but also due to challenges in interpreting three dimensional multi-segment and dynamic kinematic data. Until now, research into knee kinematics has generally been limited to spatially restricted activities in patients possessing metallic implants due the accessibility of only static videofluoroscopy and image registration techniques that require sharp image contrast. However, recent developments in mobile videofluoroscopy and image analysis approaches that enable skeletal registration now allow more advanced assessments of the natural knee during fully functional activities, including investigation into the role of specific musculoskeletal and anatomical variations on natural knee kinematics. Specifically, anatomical differences in constitutional varus or valgus limb alignment pose considerable challenges during total knee arthroplasty, requiring an improved understanding of the impact of its role on tibio-femoral kinematics before individualised biomechanical models are able to support clinical decision-making. Such knowledge could help guide surgical approaches through subject-specific implant selection and optimised surgical alignment of total knee arthroplasty components based on an understanding of the individual's joint kinematics.

This thesis therefore aims to gain an in-depth understanding of the role of limb alignment and activity on tibio-femoral kinematics of the natural knee during functional activities of daily living.

Using the moving fluoroscope developed at the Institute for Biomechanics at ETH Zürich, tibio-femoral kinematics were assessed in 27 subjects (with limb alignment ranging from 8° valgus to 9° varus) during complete gait cycles of free level walking, downhill walking and stair descent. Real-time tracking of the subject's knee motion resulted in the ability to capture radiographic images of the knee at 25 - 30 Hz. To allow analysis of the three dimensional positions of both the femur and tibia, a novel intensity-based 2D/3D registration algorithm was initially developed and validated, resulting in reconstructions with an in-plane error of < 1 mm, out-of-plane error of < 7.1 mm, and rotational error of $< 1°$. While for some images the registration was performed extremely well, image properties, as well as the contralateral knee crossing the image twice per gait cycle, complicated a successful registration of other images, necessitating occasional manual intervention.

To better understand physiologically healthy knee kinematics, tibio-femoral rotation and condylar translation was evaluated in the subgroup of subjects with neutral limb alignment (3° valgus to 3° varus). Despite a significant increase in the range of joint flexion from level walking to downhill walking to stair descent, the ranges of condylar antero-posterior translation remained comparable. However, distinct differences in the rotational as well as translational ranges of motion between the loaded and unloaded phases of gait emphasise the need to analyse complete gait cycles. In support of previous studies in the literature, a general central to medial tibio-femoral centre of rotation in the transverse plane was found.

From this initial investigation into knee joint kinematics, it became evident that the analysis approach used was critical for understanding and interpreting the resulting tibio-femoral motion. As a consequence, condylar antero-posterior translation during multiple trials of knee bending and level walking was evaluated and compared using six different kinematic analysis approaches. Clear differences between the methods were evident for certain flexion angles and phases of the gait cycle. In particular, both contact based approaches (nearest point and tibio-femoral separation) revealed significantly different translations compared to the functional flexion axis, the cylinder axis, and the transepicondylar axis. In addition, significant differences occurred between the functional flexion axis and the transepicondylar axis. The results clearly demonstrate that interpretation of joint kinematics is dependent on the analysis approached used. In order to

minimise crosstalk, joint translations should be reported using functional flexion axes. To provide comparison and reach consensus on the interpretation of tibio-femoral kinematics, reporting joint translations using at least two different approaches is recommended.

To investigate the role of limb alignment on tibio-femoral kinematics, all 27 subjects were analysed during complete cycles of level walking and stair descent according to their hip-knee-ankle angle grouping. Surprisingly, no differences in the ranges of tibio-femoral rotation or condylar translation were found for either activity. However, significant differences between the varus and valgus group were found for the translational motion characteristics of the lateral condyle during certain phases of a complete gait cycle of stair descent. Although subject-specific limb alignment only revealed a minor influence on tibio-femoral kinematics, differences between individual subjects were evident, suggesting that other factors (e.g. soft tissue sufficiency) are responsible for the observed inter-subject variability.

In conclusion, this thesis has, for the first time, successfully analysed *in vivo* knee joint kinematics throughout complete gait cycles of level walking, downhill walking and stair descent in a unique subject cohort with neutral, varus, and valgus limb alignments. While limb alignment was found to play only a minor role in governing tibio-femoral kinematics, differences between the loaded and unloaded phases of the gait cycle emphasise the need to assess complete gait cycles. In addition, dissimilarities between kinematic analysis approaches highlight the importance of selecting a suitable analysis approach and, for better comparison between different studies, possible also report kinematic data using different methodologies. Comparison against previously measured tibio-femoral kinematics in total knee arthroplasty patients using the same measurement set-up, suggests that individual pre-operative joint movement patterns could be targeted by selecting specific implants and therefore provide solutions for both varus and valgus subjects. These data can provide a basis for clinical decision-making regarding implant selection and surgical alignment, as well as help to further improve surgical procedures aiming to restore natural knee joint motion.

Zusammenfassung

Die Bewegung des natürlichen Kniegelenks wird durch ein komplexes Zusammenspiel verschiedener Gelenksstrukturen wie Knochen, Bändern, Sehnen und Muskeln ermöglicht und geführt. Genaue Kenntnisse über die individuellen Bewegungen ermöglichen ein detailliertes Verständnis der Kniegelenksfunktion. Dieses Wissen bildet die Grundlage um pathologische Veränderungen am Knie sowie die Wirksamkeit von operativen Eingriffen besser zu verstehen. Die vorhandene Literatur zeigt eine generelle Übereinstimmung für die Bewegung des Knies in isolierten Flexionsbewegungen. Jedoch sind die wissenschaftlichen Resultate zur Bewegung des Knies während dynamischen Aktivitäten, wie z.B. ebenes Gehen, eher widersprüchlich. Ein Vergleich der verschiedenen Studien wird durch die Vielzahl verwendeter Mess- und Auswertungsmethoden zusätzlich erschwert.

Aufgrund des limitierten Aufnahmevolumen und der benötigten Bildkontraste bei der Verwendung von bildgebenden Verfahren wie Röntgen, war bis jetzt die Forschung am Knie mehrheitlich auf räumlich begrenzte Aktivitäten mit Probanden mit einer totalen Knieprothese beschränkt. Die Entwicklung neuer Mess- und Auswertungsmethoden ermöglicht nun die radiologische Erfassung und Analyse der Bewegung des gesunden Knies während kompletten funktionalen Aktivitäten, einschliesslich der Untersuchung des Einflusses unterschiedlicher muskuloskelettalen oder anatomischen Variationen des gesunden Knies. Unterschiedliche Beinlängsachsenstellungen stellen eine Schwierigkeit beim Einsetzen von totalen Knieprothesen dar und erfordern ein verbessertes Verständnis der Auswirkungen auf die Bewegung des Knies. Detaillierten Kenntnisse der individuellen Bewegung können dazu beitragen chirurgische Eingriffe durch eine entsprechende Auswahl und Ausrichtung der Implantat-Komponenten weiter zu verbessern und die Patientenzufriedenheit zu erhöhen.

Diese Doktorarbeit hatte daher zum Ziel, Erkenntnisse über den Einfluss der individuellen Beinlängsachsenstellung, sowie der ausgeführten Aktivität auf die individuelle Bewegung des natürlichen Knies zu liefern.

Mit Hilfe des «Moving Fluoroscope» wurden 27 Probanden, mit einer Beinlängsachsenstellung von 8° valgus (X-Bein) bis 9° varus (O-Bein), während kompletten Gangzyklen ebenen Gehens, Bergabgehen sowie Treppenabsteigen untersucht. Durch Echtzeitverfolgung der Kniebewegung folgt das Fluoroskop dem Probanden und ermöglicht so die Aufnahme von Röntgenbildern des Knies über einen kompletten Gangzyklus. Um die Analyse der dreidimensionalen Position und Ausrichtung des Ober- und Unterschenkelknochens im Raum zu ermöglichen, wurde zuerst ein neuartiger Auswertungsalgorithmus entwickelt und validiert. Basierend auf einer intensitätsbasierten Registrierung der dreidimensionalen Knochenstruktur auf dem zweidimensionalen Röntgenbild, kann die Position des Knochens mit einem Fehler von < 1 mm in der Bildebene, < 7.1 mm normal zur Bildebene sowie einem Rotationsfehler von $< 1°$ bestimmt werden. Während die Registrierung für einige Bilder extrem gut funktioniert, erschweren unter anderem geringe Bildkontraste, Helligkeit und die Position der Knochen eine erfolgreiche Registrierung der Bilder und erfordern daher ein manuelles Positionieren der Knochen.

Um die physiologisch gesunde Kniebewegung besser zu verstehen wurden die Gelenks-Rotationen und Translationen der Probanden mit einer neutralen Beinlängsachsenstellung (3° valgus bis 3° varus) untersucht. Trotz eines signifikanten Anstiegs der Knieflexion vom ebenen Gehen zum Bergabgehen und Treppenabsteigen, zeigten sich keine Unterschiede im Umfang der Tibiarotation, der Abduktion/Adduktion sowie der antero-posterioren Translation. Jedoch verdeutlichen Unterschiede zwischen der belasteten Standphase und der unbelasteten Schwungphase die Notwendigkeit komplette Gangzyklen zu untersuchen. Wie in einigen früheren Studien schon erwähnt, resultierten die Bewegungen um ein zentrales bis mediales Rotationszentrum innerhalb der Transversalebene.

Basierend auf dieser initialen Untersuchung der Kinematik des Kniegelenks, wurde ersichtlich, dass die gewählte Auswertungsmethode das Verständnis sowie die Interpretation der resultierenden Bewegung entscheidend beeinflusst. Um ein besseres Verständnis des Einflusses der einzelnen Auswertungsmethoden auf die Resultate zu erhalten, wurde die antero-posteriore Translation der medialen und lateralen Femurkondyle während mehreren Versuchen einer isolierten Kniebeuge sowie ebenem Gehen analysiert. Zwischen den sechs analysierten Auswertungsmethoden zeigten

sich klare Unterschiede in der kondylären Translation für bestimmte Gelenkswinkel und Zeitpunkte des Gangzyklus. Insbesondere die beiden Methoden zur Bestimmung der Kontaktpunkte zwischen Femur und Tibia (nächster Punkt des Femurs zur Tibia Ebene sowie tibio-femoraler Abstand) zeigten signifikant unterschiedliche Translationen im Vergleich zu einer funktionellen Flexionsachse, der Zylinderachse sowie der transepikondylären Achse. Darüber hinaus waren signifikante Unterschiede zwischen der funktionellen Flexionsachse und der transepikondylären Achse ersichtlich. Diese Ergebnisse zeigen deutlich, dass die verschiedenen kinematischen Auswertungsmethoden unterschiedliche Aspekte der dreidimensionalen Bewegung beschreiben. Für einen besseren Vergleich zwischen den unterschiedlichen Studien und um eine gemeinsame Übereinstimmung zu erreichen, empfehlen wir, insbesondere kondyläre Translationen basierend auf mindestens zwei Methoden darzustellen.

Um den Einfluss der Beinlängsachsenstellung auf die tibio-femorale Kinematik besser zu verstehen, wurden alle 27 Probanden während ebenem Gehen sowie Treppenabsteigen untersucht und anhand ihrer individuellen Beinlängsachsenstellung in Gruppen eingeteilt. Für beide Bewegungen wurden keine Unterschiede im Umfang der tibio-femoralen Rotation oder kondylären Translation gefunden. Jedoch zeigte die laterale Kondyle während Treppenabsteigen signifikant unterschiedliche Translationsmuster zwischen der varus und valgus Gruppe. Obwohl die individuelle Ausrichtung der Beinlängsachse nur einen geringen Einfluss auf die tibio-femorale Kinematik hatte, waren deutliche Unterschiede zwischen den Probanden ersichtlich und deuten darauf hin, dass andere Faktoren wie z.B. die Eigenschaften der Seitenbänder für die individuellen Unterschiede verantwortlich sind.

Diese Doktorarbeit hat zum ersten Mal die *in vivo* Bewegung des gesunden Kniegelenks während kompletten Gangzyklen des ebenen Gehens, des Bergabgehens sowie des Treppenabsteigens in einer einzigartigen Probandengruppe mit neutraler, varus oder valgus Beinlängsachsenstellung analysiert. Während die Beinlängsachsenstellung nur einen geringen Einfluss auf die tibio-femorale Kinematik hatte, unterstreichen die Unterschiede zwischen den belasteten und unbelasteten Phasen des Gangzyklus die Notwendigkeit, komplette Gangzyklen zu analysieren. Des weiteren verdeutlichen die Unterschiede zwischen den verwendeten kinematischen Auswertungsmethoden die Bedeutung der Wahl einer geeigneten Auswertungsmethode. Um einen besseren Vergleich zwischen verschiedenen Studien zu gewährleisten, sollten kinematische Daten mittels unterschiedlichen Auswertungsmethoden dargestellt werden. Ein Vergleich der tibio-femoralen Kinematik mit zuvor gemessenen Patienten mit einer totalen Knieprothese zeigte zudem, dass

individuelle, präoperative Bewegungsmuster durch die Auswahl spezifischer Implantat ermöglicht werden können und daher als geeignete Lösung für varus und valgus Patienten dienen können. Die erhaltenen Resultate können als Grundlage dienen, um Entscheidungen betreffend idealem Implantat oder der Beinängsachsenstellung zu treffen und damit einen Beitrag zur Wiederherstellung einer natürlichen Kniebewegung leisten.

Contents

List of Figures

List of Tables

Abbreviations

2D	two dimensional
3D	three dimensional
A-P	antero-posterior
Abd/add	abduction/adduction
ANOVA	mixed-model analysis of variances
CA	cylinder axis
CAD	computer-aided design
CCD	charge-coupled device
CoR	centre of rotation
CT	computed tomography
DAP	dose area product
DRR	digitally reconstructed radiograph
EFC	extension facet centre
FFA	functional flexion axis
FFA_P	functional flexion axis point
FFA_P_{lat}	lateral functional flexion axis point
FFA_P_{med}	medial functional flexion axis point
FFC	flexion facet centre
Flex/ex	flexion/extension
GCA	geometric centre axis
HKA	hip-knee-ankle
IMU	inertial measurement unit
Int/ext	tibial internal/external rotation
Max	maximum
Min	minimum
M-L	medio-lateral
MRI	magnetic resonance imaging
N_P	nearest point
N_P_{lat}	lateral nearest point
N_P_{med}	medial nearest point
NP	nearest point approach
P-D	proximal-distal
RMS	root mean square
RoM	range of motion
RSA	roentgen stereo photogrammetric analysis

SARA	symmetrical axis of rotation approach
SD	standard deviation
SEP	tibio-femoral separation approach
SPM	statistical parametric mapping
STA	soft tissue artefact
TEA	transepicondylar axis
TKA	total knee arthroplasty
X_{Femur}	antero-posterior axis of the femoral anatomical coordinate system
X_{Tibia}	antero-posterior axis of the tibial anatomical coordinate system
Y_{Femur}	longitudinal axis of the femoral anatomical coordinate system
Y_{Tibia}	longitudinal axis of the tibial anatomical coordinate system
Z_{Femur}	medio-lateral axis of the femoral anatomical coordinate system
Z_{Tibia}	medio-lateral axis of the tibial anatomical coordinate system

Chapter 1

Introduction and motivation

The human knee joint consists not only of the distal femur, the proximal tibia and the patella, but also of multiple soft tissue structures such as the cruciate and collateral ligaments, the menisci as well as numerous muscles acting at and around the knee. While the cruciate and collateral ligaments serve as primary passive stabilisers, the medial and lateral menisci provide a more conforming articular surface to the joint. The kinematics of the knee are guided by this interconnected system of bones, soft tissue structures and muscles, resulting in a complex set of translations and rotations in all six degrees of freedom [1].

With an aging and more active society, the prevalence for musculoskeletal interventions, such as ligament reconstruction, meniscus or cartilage restoration surgery or ultimately, substituting joint surfaces using total knee arthroplasty (TKA) to restore pain free functionality of the knee joint are increasing [2]. These surgical interventions intend to restore physiological kinematics, including sufficient range of motion (RoM) as well as avoiding overloading of the surrounding soft tissue structures. Accurate knowledge of natural, healthy tibio-femoral kinematics can not only provide critical information for assessing knee joint functionality, but also lay the foundation for understanding these joint pathologies as well as further assess and develop musculoskeletal interventions.

Although, TKA surgery has become a standard surgical procedure with a general high success rate, almost 20% of all patients undergoing TKA surgery remain uncertain or unsatisfied with the received outcome [3]. More precisely, up to 13% of all patients were dissatisfied with the implant function during activities of daily living, especially when high flexion angles are required [4]. To further increase patient satisfaction and minimise revision surgeries, an improved understanding of anatomical factors, such as varus and valgus limb alignment, and their role on

tibio-femoral kinematics are needed. Based on an improved understanding of individual tibio-femoral kinematics, idividualised approaches could help guide clinical decision-making through subject-specific implant selection and optimised surgical alignment.

1.1 Assessing tibio-femoral kinematics

Increased scientific interest to better understand knee joint motion has led to the development of different measurement techniques to accurately assess tibio-femoral kinematics. In order to understand tibio-femoral kinematics in a comprehensive three dimensional (3D) aspect and to describe the time-dependent relative motion between the femur and tibia in a two dimensional (2D) representation, different methodological conventions and approaches have been used.

1.1.1 Measurement technologies

In a clinical setting, conventional goniometers can be used to assess flexion while standing. Although easy to use, flexion/extension measurements can be affected by errors of up to 10°, while assessment of longitudinal rotation as well as abduction/adduction is not possible using goniometers [5].

To evaluate dynamic knee kinematics, optical motion capture systems together with active or passive skin markers are a well established tool. Covering a large measurement volume, full body motion of a variety of dynamic activities can be captured. However, soft tissue artefacts (STA), caused by movement of the skin relative to the underlying bone, critically affect these measurements and limits their accuracy [1, 6–8]. Although procedures to minimise STA as well as correction measures have been presented in the literature [9–12], their usage to assess smallest changes in e.g. antero-posterior (A-P) translation are limited. To directly assess *in vivo* bony kinematics, pins screwed directly into the subject's bone can be used in combination with optical motion capture systems [13–16]. But such procedures are highly invasive and therefore limited to studies within small cohorts.

Comparable to skin marker analysis, approaches using inertial measurement units (IMUs) attached to the subject's skin have been proposed. Most of these sensors, incorporate accelerometers, gyroscopes and magnetometers. By using two or more IMU sensors, data from multiple

segments can be acquired synchronously, enabling estimation of joint kinematics [17]. While not being tied to a laboratory environment, IMUs allow measuring long term kinematics in different surroundings [17]. However, post processing of the acquired data requires a prolonged procedure. After defining the 3D orientation of the sensor, an anatomical calibration is needed to determine the orientation of the sensor with respect to the underlying bone [17].

To directly assess knee kinematics in a less invasive manner, different imaging techniques have been successfully established. Roentgen stereo photogrammetric analysis (RSA) [18] and magnetic resonance imaging (MRI) analysis [19–23] have been used to investigate tibio-femoral kinematics, but are limited to static or quasi-static movements due to their imaging modality. Videofluoroscopy using single-plane [24–28] and dual-plane [29–32] set-ups has been intensively used to study the knee during functional activities *in vivo*. Although being able to capture dynamic movements, most of these systems are limited by the size and static configuration of the imaging intensifier, leading to a restricted measurement volume and resulting in the analysis of motion tasks with a limited range of movement such as lunging [32–38], squatting [19, 28, 39–43], kneeling [28, 39, 44, 45], or other flexion activities [21, 46–50], as well as only portions of a gait cycle [24, 28, 31, 39, 42, 44, 47, 51, 52]. To overcome the limitations of a static imaging set-up and therefore enable measurements of complete gait cycles, procedures to re-orientate the fluoroscope during different trials to enhance the field of view have been investigated [32, 53]. Although the walking speed was kept constant, this technique can be influenced by kinematic and temporal changes between different gait cycles [53]. As a further improvement, mobile systems that allow tracking of the knee during dynamic movements [54] as well as consecutive cycles of gait activities [30] have been developed. While the MoBiX system, a dual-plane fluoroscopic imaging system presented by Guan et al. [30] is able to measure a complete gait cycle of level walking, the moving fluoroscope, established at the Institute for Biomechanics (ETH Zürich, Switzerland), is not only capable of tracking the knee throughout multiple complete cycles of level walking (Figure 1.1), but also while downhill walking and stair descent. All these videofluoroscopic systems expose the subject to radiation and data collection should therefore be kept to a minimum for each subject. Using subject-specific models, based on computed tomography (CT) or MRI scans, 2D/3D registration of the fluoroscopic images provides accurate knowledge of the 3D position and orientation of each bone in space. Approaches for single-plane fluoroscopy presented in the literature [46, 51, 55–61], generally share high in-plane translational accuracy, but substantial differences for out-of-plane translational and rotational accuracy.

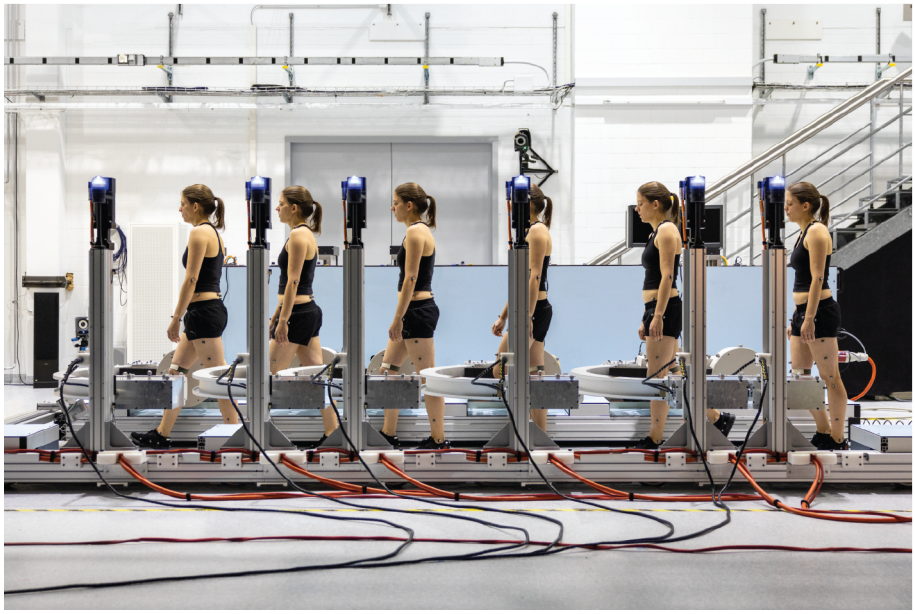

Figure 1.1: Moving fluoroscope enabling tracking of the knee throughout complete cycles of free level walking (pictured), downhill walking and stair descent

1.1.2 Anatomical coordinate systems and methodological conventions

Relative movement of two rigid bodies, each having a local Cartesian coordinate system, can be described using a rotation matrix and the translation vector or the combined 4 x 4 transformation matrix. To understand the orientation of the proximal segment with respect to the distal segment (e.g. the femur with respect to the tibia), the relative position form one to the other can be quantified using a parametrisation of the transformation matrix such as Euler/Cardan angles, the Helical axis, Helical angles or the Joint Coordinate System proposed by Grood & Suntay [62].
To obtain clinically meaningful rotations and joint angles, a clinical reference system needs to be defined and joint angles are then described with respect to the reference system. Mostly, rotations in the sagittal plane are defined as flexion/extension, rotational movements towards or away of the sagittal plane as abduction/adduction and rotations around the longitudinal axis as internal/external rotation.

To determine the femoral anatomical coordinate system, most studies use the flexion/extension axis, along the medio-lateral direction, as the primary axis. Predominantly, functional approaches as well as anatomical definitions, based on clinical characterizations and subject-specific anatomical features, are used.

Using the relative movement of the femur and tibia, functional approaches determine the optimised axis of rotation. Different mathematical conventions to define a functional flexion axis (FFA) have been presented in the literature including fitting approaches based on least square estimations [50, 63–65], a mean helical axis approach [66] or the symmetrical axis of rotation approach (SARA) (Figure 1.2 A) [67]. The transepicondylar axis (TEA) is a widely used anatomical axis, defined as the connection line of the most prominent point on the medial and lateral epicondyles (Figure 1.2 B) [68–70]. The geometric centre axis (GCA) and the cylinder axis (CA) are based on the fitting of circular, cylindrical or spherical shapes to the posterior portion of the femoral condyles (Figure 1.2 C) [49, 71, 72]. Additionally, based on the tibio-femoral contact surface during flexion, an anterior and posterior circular surface can be defined and used to fit a circle resulting in an extension and flexion facet centre (EFC & FFC) (Figure 1.2 D) [20].
The femoral anatomical coordinate system is then completed with a longitudinal and an antero-posterior axis, that are generally based on anatomical landmarks and defined in order to build an orthogonal right-handed coordinate system.

The tibial anatomical coordinate system is mainly defined using anatomical features and bony landmarks. Most studies incorporate the longitudinal axis of the tibial shaft as the primary axis [32, 39, 53, 73–75]. The medio-lateral axis can then be defined parallel to the posterior edge of the tibia [32, 39, 42, 73] or based on the line connecting circles fitted to the medial and lateral tibial plateau [47, 75]. The antero-posterior axis is set perpendicular to the longitudinal and medio-lateral axes to complete the right-handed tibial anatomical coordinate system.

Most studies use these local anatomical coordinate systems applied to the Joint Coordinate System proposed by Grood & Suntay [62] to report tibio-femoral rotations. Based on the femoral medio-lateral axis, the tibial longitudinal axis and a floating axis, a non-orthogonal coordinate system is defined and used to describe tibio-femoral rotations (Figure 1.3) [62].

Beside tibio-femoral rotations, relative translations between the two bones, measured as the translation between the origins of the anatomical coordinate systems, but also the relative translations of the medial and lateral condyles individually, have been investigated. Among all studies, A-P translations of the femoral condyles are generally reported with respect to the posterior tibial cortex [21, 23] or the tibial midline [46, 47, 76].

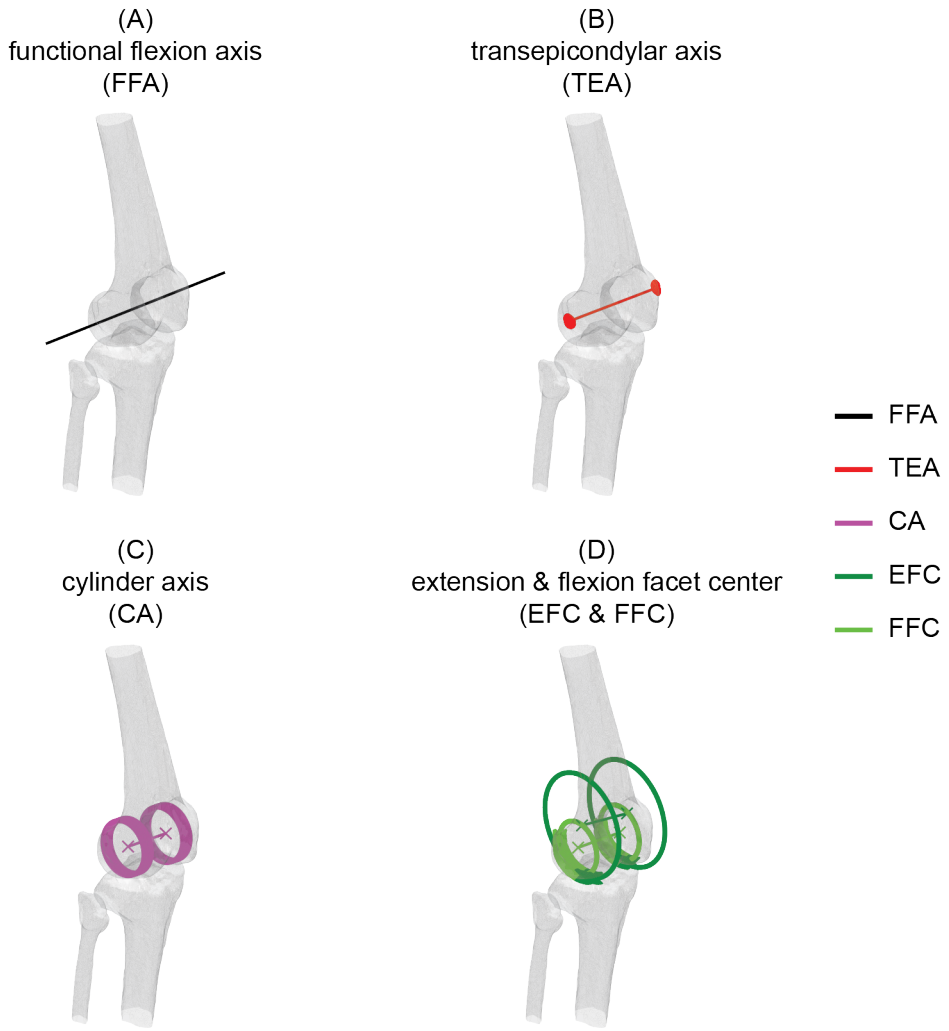

Figure 1.2: Exemplary illustration of the (A) functional flexion axis (FFA), (B) transepicondylar axis (TEA), (C) cylinder axis (CA) and the (D) extension and flexion facet centres (EFC & FFC), depicted in a right knee.

Using the aforementioned functionally or anatomically defined medio-lateral femoral axes (Figure 1.2), a medial and lateral point can be described (e.g. the centre of the fitted circle) and individual translations with respect to the tibial coordinate system can then be evaluated. In addition, condylar translation has also been analysed using tibio-femoral contact points. With knowledge of the tibio-femoral cartilage, the centroid of the area formed by the overlap of the femoral and tibial cartilage can be defined as the contact point [33]. However, as most studies are lacking information about the tibio-femoral cartilage, the nearest point of the medial and lateral femoral condyle in relation to the tibia [46], a plane parallel to the tibial joint surface [49] or the lowest point of each femoral condyle [47] were used in various studies [33, 46, 47, 49, 74]. To account for missing information about the tibio-femoral cartilage, the geometric centre of the region having less than 6 mm tibio-femoral separation has also been used [28].

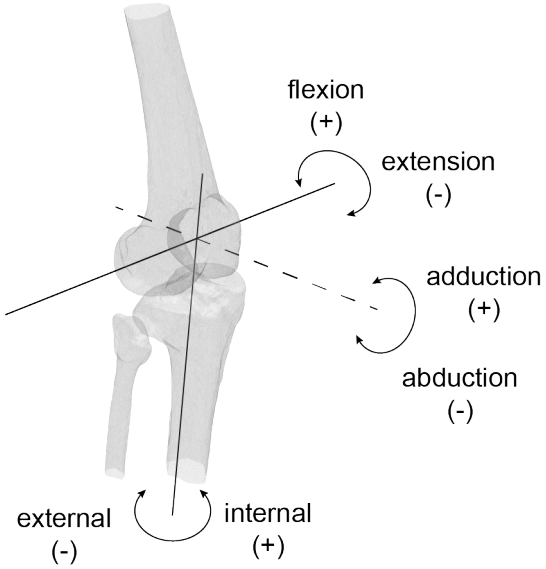

Figure 1.3: Tibio-femoral rotations according to the Joint Coordinate System based on Grood & Suntay [62]. Flexion/extension occurs around the femoral medio-lateral axis, tibial internal/external rotation around the tibial longitudinal axis and abduction/adduction around the floating axis (depicted as a dashed line).

1.2 Tibio-femoral kinematics of the natural knee

For most studies, tibio-femoral rotations are reported as flexion/extension, abduction/adduction and tibial (or femoral) internal/external rotation. While the RoM for abduction/adduction and tibial internal/external rotation is limited by the soft tissue structures, the predominant rotation occurs for flexion/extension, with an active RoM of about 120 - 130° and a passive RoM up to 160° [21, 77].

In general, studies analysing tibio-femoral kinematics can be divided into three groups, firstly studies performing *in vitro* experiments using cadaver material, secondly *in vivo* studies on static or quasi-static flexion activities in an unloaded or loaded situation and thirdly *in vivo* studies evaluating dynamic activities such as walking.

1.2.1 *In vitro* experiments

Studies applying passive knee flexion to cadaver specimens found a continuous tibial internal rotation over the course of flexion [22, 72, 78]. Within the frontal plane, an initial tibial adduction (varus movement) was followed by an abduction (valgus movement) with on overall RoM of less than 5° [72].

Using femur fixed axes (FFC, GCA, TEA), a continuous posterior movement of the lateral condyle was found but with substantial differences in the amount of A-P translation between the methods [20, 22, 43, 72, 78]. For the medial condyle, minimal posterior translation was found using the FFC approach [20, 22, 43]. A sphere and circle fit, resulted in an initial anterior translation until mid-flexion followed by posterior translation [72, 78], whereas the TEA revealed continuous posterior translation over the full flexion range [78]. Only one study analysed tibio-femoral contact paths and found equal posterior translation for both condyles [43].

1.2.2 Flexion activities

Lunges [32–38] and squats [19, 28, 39–43] but also kneeling [28, 39, 44, 45] and various other flexion activities [21, 46–50] have been used to study tibio-femoral kinematics during weight-bearing flexion from slight extension (-10°) up to 150° of flexion. Comparable to the cadaver studies, a continuous internal rotation of the tibia was found [21, 28, 32, 34, 35, 38, 39, 42, 44–47, 50, 72, 76], with the majority of rotation occurring within the first 30° of flexion [21, 38, 46, 47]. Less has been reported about the abduction/adduction behaviour over continuous flexion. Minimal RoM has been described, with a slight trend towards more tibial abduction (valgus movement) with increasing flexion [34, 35, 38, 39, 44, 45].

Unloaded flexion activities, acquired in a laying or seated position, revealed limited movement of the medial condyle and posterior translation of the lateral condyle when using the FFC approach [19, 43, 77] as well as a circle/spherical fit [79, 80]. For the medial and lateral tibio-femoral contact points however, a equal continuous posterior translation, was found [23, 43, 79].

For loaded knee flexion activities, an anterior translation until mid-flexion followed by posterior translation was found for the medial condyle using geometric and anatomical approaches (FFC, GCA, TEA) while the corresponding lateral condyle experienced a posterior translation [19, 21, 35, 39–41, 43, 48, 49, 72]. Overall, the lateral condyle tended to have a larger range of A-P translation compared to the medial condyle, indicating a medial centre of rotation (CoR) [21, 39, 40, 50]. At high flexion angles, more equal ranges of translation were found, resulting in a more bicondylar posterior translation [21, 39, 40]. All studies assessing A-P translations using contact approaches, reported posterior translation of the medial and lateral condyle. While studies using the nearest or lowest point of the femur in respect to the tibia showed a trend of larger translations for the lateral compared to the medial condyle [33, 35, 46, 47, 49, 76], more equal

translations were found for the contact points calculated based on the tibio-femoral articular cartilage overlap [33, 36–38, 43, 48].

1.2.3 Dynamic gait activities

For dynamic gait activities, most studies have evaluated portions of the complete gait cycle [52, 81, 82], mainly the stance phase [13, 16, 24, 31, 32, 51, 83–86], and only limited studies have successfully examined tibio-femoral kinematics over a complete gait cycle of walking [1, 15, 74, 87, 88]. Among all studies, consistent findings were presented for tibio-femoral flexion/extension. After a first peak, observed at contralateral toe-off (end of loading response) the knee extended before returning to flexion, with a maximum knee flexion during swing phase, shortly after toe-off [1, 13, 15, 16, 31, 32, 74, 85, 87, 88]. For tibial internal/external rotations varying results have been reported. Most studies observed an externally rotated tibia at heel-strike, followed by an internal rotation during early stance phase, reaching a first peak shortly after contralateral toe-off [1, 15, 16, 31, 32, 52, 74, 82, 85, 87, 88]. For mid stance, the tibia was shown to experience no to minimal external rotation, followed by an additional internal rotation in preparation for toe-off [15, 16, 31, 32, 74, 85, 88]. Peak tibial internal rotation was reported to occur around toe-off [1, 15, 31, 74, 87, 88]. During the unloaded swing phase, tibial external followed by internal rotation in preparation for the following heel-strike was found [1, 15, 74, 87, 88]. Contrary to this common understanding of tibial rotation, initial tibial external rotation after heel-strike followed by internal rotation during mid-stance and external rotation until toe-off, was described by two studies [13, 51]. Rotations in the frontal plane (abduction/adduction) were reported to have the smallest RoM of all three tibio-femoral rotations [1, 13, 74, 83, 88]. Minimal abduction/adduction during the loaded stance phase [1, 13, 15, 31, 52, 74, 87, 88], but tibial adduction until maximum flexion followed by abduction have been reported for the unloaded swing phase [1, 74, 87, 88]. Despite the small RoM, the individual rotational patterns for abduction/adduction showed clear subject-specific differences [15].

Compared to studies analysing level walking, less has been published about tibio-femoral kinematics of downhill walking and stair descent, especially for abduction/adduction and tibial internal/external rotation. While the initial flexion at heel-strike remained constant, the range of flexion/extension was significantly higher for downhill walking compared to level walking [89–91]. Due to the step height when ascending or descending a set of stairs, the range of tibio-femoral flexion was also increased in stair activities. Overall, less is known about the alterations of abduction/adduction and tibial rotation during downhill walking as well as stair activities.

As for the loaded flexion activities, different approaches were used to assess the A-P translation of the medial and lateral femoral condyle with respect to the tibia. Analysing the complete gait cycle, the GCA showed significant more translation for the lateral compared to the medial condyle resulting in an overall medial CoR [74]. Using tibio-femoral contact approaches, a similar behaviour was reported for the loaded stance phase [24, 51, 81] as well as the full gait cycle [74]. In contrast to these findings, a contradictory translational behaviour was described, with larger A-P translations for the medial GCA, TEA and cartilage contact compared to their lateral counterpart [31, 86]. Earlier as well as recent publications, supported this data with reporting a lateral CoR for the stance phase of walking [52, 84].
For downhill walking, individual condylar A-P translations were only analysed for the early stance phase (weight acceptance), with reported equal translations for the medial and lateral contact point [82, 92]. More studies have analysed stair like activities such as step down and step up [18, 24, 28, 51, 75, 93]. Using tibio-femoral contact measures as well as the TEA resulted in equal anterior translation with knee extension during a step up activity [28, 75]. For the FFC and GCA, the medial condyle translated posterior with extension whereas the lateral condyle translated anterior, but with no significant differences between the condyles [18, 75, 93]. During stair descent, the translational patterns of the tibio-femoral contact points were comparable to a flexion activity, with slight anterior translation of the medial and posterior translation for the lateral contact point, but with differences on the amount between the studies [24, 51]. For both activities, downhill walking and stair descent, analysis of condylar A-P translation during the unloaded swing phase remains missing.

1.3 Limb alignment

The axial alignment of the lower limb in the frontal plane is traditionally defined by the hip-knee-ankle (HKA) or mechanical tibio-femoral alignment measured by the angle between the mechanical axes of the femur and tibia. In general, a HKA angle of $0 \pm 3°$ is quantified as neutral alignment, while HKA angles of $> 3°$ and $< -3°$ are defined as varus and valgus alignment, respectively (Figure 1.4).
Recently, kinematic alignment of TKA implant components based on the patients preoperative limb alignment has gained interest among the orthopeadic community. To better understand surgical outcomes and support clinical decision-making, knowledge about the role of subject-specific variances on tibio-femoral kinematics is needed.

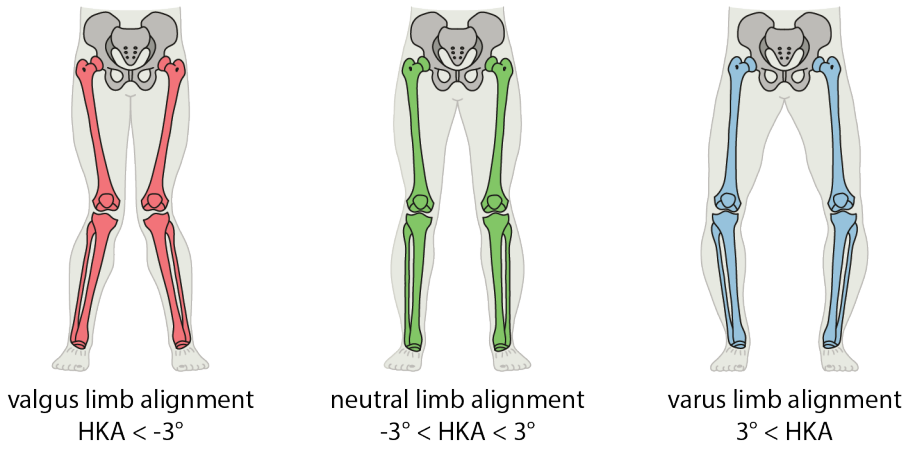

Figure 1.4: Description of neutral, varus and valgus limb alignment based on the hip-knee-ankle (HKA) angle.

1.3.1 Measurement techniques

The current gold standard for assessing limb alignment is a standing, weight-bearing A-P full limb radiograph ranging from the pelvis to the ankle [94–99]. Despite excellent inter- as well as intra-observer correlations [94], full limb radiographs are a 2D representative of the limb alignment, which has been shown to be highly affected by the position of the subject at the time of image acquisition [97]. Malpositioning of the limbs, loading condition as well as hip, knee and ankle rotational position have all been found to critically influence the resultant limb alignment [97, 100–102].

Alternatively, the scout view of a CT scan can be used to define mechanical alignment of the femur and tibia. Although providing a 3D assessment of the lower limb, it is also affected by rotational misplacement or malpositioning of the lower extremities while scanning and is acquired in a supine, non-weight-bearing position [97].

To simplify the analysis, a number of low cost, instant and quick limb alignment assessment methods have been proposed in the literature, including visual observation [103] and methods using callipers or goniometers [104–106]. Although these methods do not expose the subject to radiation and generate a fast and easily accessible limb alignment classification, contradictory results have been found when comparing the results with the weight-bearing A-P full limb radiograph (gold standard) [107, 108].

Likewise, marker-based lower limb alignment measures have been proposed as a non-invasive, 3D alternative in a weight-bearing posture [109–112]. Based on skin markers attached to anatomical landmarks, these approaches were able to reproducible calculate the HKA angle and showed good correlations to the gold standard measures [109, 110, 112]. Limited studies have also used skin marker based analysis to assess dynamic HKA angulation during level walking but only limited correlations were found between static and dynamic HKA [113, 114]. However, the accuracy of these approaches are critically affected by the skin marker placing and the influence of STA on correctly identifying the joint centres. Due to the time consuming procedure and limited availability in clinics, marker-based lower limb alignment assessments are only rarely performed, but provide a great potential, especially in combination with 3D gait analysis [112].

Over the last decade, the EOS imaging system (EOS^{TM} Imaging, Paris, France) has been established as an alternative system to accurately assess lower limb alignment using low dose bi-planar X-ray [115]. Consisting of two perpendicular X-ray units, mounted on a C-arm, the EOS is capable of simultaneously acquiring full length, weight-bearing images in the frontal and sagittal plane [116, 117]. Post-processing of the bi-planar radiographs can be performed using the incorporated software allowing 3D reconstruction of the bone surfaces and automatic computation of clinical lower limb parameters, such as HKA angle or femoral and tibial mechanical angle [97, 118]. This process has been shown to enable reconstructions with high inter- as well as intra-observer reproducibility [117, 119]. Due to its 3D modality, the EOS system not only measures limb alignment under an upright weight-bearing condition, but also accounts for extension deficits or modifications of the rotational alignment of the limb [97]. Although also exposing the subject to radiation, the absorbed radiation dose per scan is reduced compared to conventional A-P full length radiographs or CT scans [117, 120, 121]. Overall, limb alignment parameters calculated using the EOS system are clinically comparable to traditional A-P full length radiographs or supine CT scans, although some significant differences have been reported [97, 117, 119]. Therefore, the EOS provides a promising analysis tool to not only assess limb alignment but to thoroughly quantify anatomical lower limb parameters in a standing, weight-bearing position.

1.3.2 Constitutional varus

In general, neutral limb alignment is considered the normal condition among healthy subjects. In a large cohort study using full limb radiographs, a mean limb alignment of $1.33 \pm 2.34°$ was found, with 24.6% and 2.4% of all subjects exhibiting a varus or valgus alignment, respectively [122].

This trend was later confirmed in a retrospective study analysing supine, non-weight-bearing CT images [123]. Using both image modalities, women were found to experience significantly more valgus alignment compared to men [122, 123].

1.3.3 Role of limb alignment on tibio-femoral kinematics and kinetics

Frontal plane alignment of the lower limb has been shown to critically affect tibio-femoral joint loading [124–126] as well as influence the risk and progression of osteoarthritis in the knee [127–129]. While effects on joint loading have been analysed in various studies, less is known about the altered tibio-femoral kinematics in subjects with extreme limb alignment, especially *in vivo* during activities of daily living.

In subjects with a neutrally aligned leg, the ground reaction force (GRF) vector was shown to pass medially of the knee joint centre while standing. As a result, an external adduction moment was found at the knee with increasing knee joint forces in the medial compared to the lateral compartment [125]. With varus or valgus alignment, the line of action of the GRF vector as well as the distribution of the compartment loading changes [108, 111, 128, 130]. Based on musculoskeletal modelling, it has been shown that varus and valgus alignment increase the total knee joint contact forces during gait activities [124, 126]. Additionally, a shift of the contact force towards the medial or lateral compartment was found with varus and valgus alignment, respectively [126].

Limited literature is available on the influence of varus and valgus alignment on tibio-femoral rotations or translations. Maderbacher, Baier and co-workers have shown that the HKA angle critically influences the tibio-femoral internal/external rotational and adduction/abduction patterns during continuous knee flexion [131, 132]. While varus knees showed a continuous external rotation of the femur with increasing flexion, valgus subjects exhibited an internal rotation over the same flexion range [131]. However, these experiments were performed *in vitro*, using cadaver specimens, or intra-operatively in a non-weight-bearing situation. Only one study was found comparing osteoarthritic subjects with varus and valgus alignment with a control group while performing a barefoot walking task [133]. As for the aforementioned studies, differences in the adduction/abduction angle were found, together with a reduced flexion/extension RoM for the varus and valgus subjects.

1.4 Motivation and aims of thesis

The overall motivation for this thesis was to gain an in-depth understanding of the role of limb alignment and activity on tibio-femoral kinematics of the natural knee joint during functional activities of daily living, including complete gait cycles.

Numerous studies have analysed tibio-femoral kinematics of the knee *in vitro*, during isolated flexion activities as well as during dynamic activities, such as walking. For isolated flexion activities, general agreement on tibio-femoral rotations and condylar translation was achieved. While both femoral condyles translated posteriorly with increasing flexion, larger posterior translation of the lateral compared to the medial condyle induced a medial pivot pattern with an overall medial CoR. However, for dynamic activities, contradictory results for longitudinal tibio-femoral rotation, condylar translation and the resultant CoR have been presented. Subject-specific differences have been observed and inter-subject variability for the magnitudes and pattern of condylar translation were reported. Comparison between the different studies is not only complicated by the variety of measurement systems, set-ups and analysis approaches used, but also by the challenge of interpreting 3D, time-dependent, multi-segment kinematic data. As a result, no general consensus has yet been reached on the tibio-femoral kinematics of the healthy, natural knee, especially during dynamic gait activities.

In addition, the studies have reported subject-specific differences with inter-subject variability, especially for condylar translations. Therefore, an in-depth understanding of the role of specific musculoskeletal and anatomical variations on individual knee joint motion remains missing.

With the Institute for Biomechanics' moving fluoroscope, a unique technology is available to quantitatively assess *in vivo* tibio-femoral kinematics of the knee not only during static flexion activities but also throughout complete gait cycles of level walking, downhill walking and stair descent. Using this technology, the leading aim of this thesis was to gain an improved understanding of the role of limb alignment and activity on natural, healthy tibio-femoral kinematics and thereby advancing the knowledge of factors influencing healthy knee kinematics.

In particular, this doctoral thesis was based on the following aims:

Aim 1: Evaluation of a measurement set-up to analyse tibio-femoral kinematics of the natural knee joint using dynamic videofluoroscopy

To successfully analyse tibio-femoral kinematics throughout complete gait cycles of level walking, downhill walking and stair descent, the knee joint is required to be visible within the field of view of the moving fluoroscope and the 3D position and orientation of the bones need to be accurately registered. Therefore, the tracking ability of the moving fluoroscope was assessed among ten subjects with a total knee arthroplasty and the accuracy and reliability of the 2D/3D registration procedure was evaluated using fluoroscopic images of radiopaque and natural bones.

Aim 2: Understanding tibio-femoral kinematics of the healthy knee during gait activities

Despite several studies assessing the healthy knee during portions of or complete gait cycles, tibio-femoral kinematics are still controversially discussed and no clear consensus has yet been reached on the movement of the healthy knee throughout complete gait cycles of dynamic activities. It remains unclear whether the observed discrepancies have occurred on the basis of the performed activity, the cohort studied or the analysis method. Therefore, *in vivo* tibio-femoral kinematics were analysed in ten healthy subjects throughout multiple complete gait cycles of level walking, downhill walking and stair descent.

Aim 3: Comparison of methodological concepts for assessing natural tibio-femoral kinematics

While Aim 2 resulted in clear subject-specific differences in condylar translation of the functional flexion axis as well as a medial and lateral contact point, comparison to the existing literature was challenging. For a detailed comparison of different kinematic analysis approaches and their effect on the reported kinematics, condylar A-P translations were calculated based on identical videofluoroscopy data of ten healthy subjects but using six different kinematic analysis approaches.

Aim 4: Understanding the role of limb alignment on tibio-femoral kinematics

Kinematic alignment of TKA implants by restoring the native anatomical alignment of a patient has recently gained interest in the orthopaedic community. However, less is known about the altered tibio-femoral kinematics in subjects with varus or valgus alignment compared to individuals with a neutral alignment. Therefore, three subject cohorts with varus, neutral and valgus limb alignment were analysed during level walking and stair descent and the impact of subject-specific limb alignment on tibio-femoral rotations and condylar translations was investigated.

1.5 Outline of thesis

This thesis is structured in seven chapters. In addition to the current chapter, providing background information as well as outlining the motivation and specific aims of this doctoral thesis, **Chapters 2 to 6** are based on scientific articles that have been peer-reviewed and published or are in the review process for publication in international scientific journals. These chapters form the core of this doctoral thesis and intend to address the previously specified aims.

Chapter 2 provides a detailed description of the Institute for Biomechanics' moving fluoroscope, including an assessment of its tracking capability to maintain the knee within the field of view of the image intensifier.

Chapter 3 describes the ability of a novel intensity-based 2D/3D registration algorithm to successfully and accurately register fluoroscopic images of the natural knee by investigating its accuracy, reliability and repeatability for registering radiopaque bone models as well as natural femora and tibiae.

Chapter 4 focuses on the tibio-femoral kinematics throughout complete gait cycles of level walking, downhill walking and stair descent. Using ten healthy subjects with a neutral limb alignment, tibio-femoral rotations and condylar translation were analysed by moving videofluoroscopy.

Chapter 5 compares the magnitude of transverse plane knee joint motion from identical dynamic videofluoroscopy data but using six different kinematic analysis approaches. This study emphasizes the importance of reporting kinematics based on multiple approaches to gain an in-depth knowledge about the underlying movement.

Chapter 6 presents tibio-femoral kinematics of 27 subjects with varus, neutral or valgus limb alignment and investigates the role of limb alignment on tibio-femoral rotations as well as condylar translations during level walking and stair descent.

In **Chapter 7**, the major findings, presented in the previous chapters, are summarised and jointly discussed. In addition, the limitations of the presented work are discussed and an outlook for future research in the field of tibio-femoral kinematics is provided.

Chapter 2

A moving fluoroscope to capture tibio-femoral kinematics during complete cycles of free level and downhill walking as well as stair descent

adapted from:

Renate List, Barbara Postolka, Pascal Schütz, Marco Hitz, Peter Schwilch, Hans Gerber, Stephen J. Ferguson*, William R. Taylor*

*These authors contributed equally to this work

Institute for Biomechanics, ETH Zürich, Zürich, Switzerland

Plos One, 12(10):e0185952, 2017

DOI: 10.1371/journal.pone.0185952

open access

2.1 Abstract

Videofluoroscopy has been shown to provide essential information in the evaluation of the functionality of total knee arthroplasties. However, due to the limitation in the field of view, most systems can only assess knee kinematics during highly restricted movements. To avoid the limitations of a static image intensifier, a moving fluoroscope has been presented as a standalone system that allows tracking of the knee during multiple complete cycles of level and downhill walking, as well as stair descent, in combination with the synchronous assessment of ground reaction forces and whole body skin marker measurements. Here, we assess the ability of the system to keep the knee in the field of view of the image intensifier. By measuring ten total knee arthroplasty subjects, we demonstrate that it is possible to maintain the knee to within 1.8 ± 1.4 cm vertically and 4.0 ± 2.6 cm horizontally of the centre of the intensifier throughout full cycles of activities of daily living. Since control of the system is based on real-time feedback of a wire sensor, the system is not dependent on repeatable gait patterns, but is rather able to capture pathological motion patterns with low inter-trial repeatability.

2.2 Introduction

It is well accepted that the accurate quantification of *in vivo* knee joint kinematics and kinetics is essential for a thorough understanding of knee functionality [6], particularly after total knee arthroplasty (TKA). Such knowledge allows the verification and improvement of new surgical procedures and rehabilitation techniques, the development of new concepts for knee implants and the advancement or validation of numerical models. In human movement analysis, skin marker based measurement is currently still the most employed tool. However, this method is critically affected by soft tissue artefact (STA), which reduces the ability to assess skeletal kinematics [1, 7].

In the past two decades, single-plane videofluoroscopic analysis [55, 56, 134–137] as well as dual-orthogonal fluoroscopy [76] have provided valuable information in the study of the three dimensional (3D) motion of TKAs and normal knees. These technologies work by applying low-dosage radiographic imaging at sufficient frame rates to allow a dynamic assessment of the skeletal kinematics, and have the advantage that they are not affected by STA. Here, 3D registration of the two dimensional (2D) images is generally performed using computer-aided design (CAD) models of the implant components, or the segmented geometry from computed tomography (CT)

or magnetic resonance imaging (MRI) scans of the bones, together with a 2D/3D registration algorithm [55–58, 138, 139]. One drawback of this methodology, however, is the limited field of view of the generally stationary image intensifier, resulting in assessments of only highly restricted movements, as the knee must remain within the field of view of the image intensifier. Thus, past research has mainly focused on examining the kinematics of the knee during rising up from a chair (or sitting down), step-up/step-down and deep knee bend activities, often capturing only a portion of the whole motion [140, 141]. However, the negotiation of stairs is considered to be one of the primary daily activities that cause difficulties for subjects afflicted with knee disorders. Due to the larger joint moments [142], as well as higher variability and left-right asymmetries [143] compared to level walking, many TKA subjects develop compensatory movements to safely complete the task in a pain free manner. Given that downhill walking shows an increase in knee flexion, in the magnitude of the first peak of the vertical ground reaction force, in the braking force of the anterio-posterior component, as well as in knee joint moments [90, 91], it is no great surprise that walking down an inclined surface is also known to be challenging for TKA subjects. Recent approaches suggest merging the information gained from subsequent videofluoroscopic and skin marker measurements [144–146]. Although this concept exploits the large measurement field provided by conventional skin marker gait analysis and the accuracy of videofluoroscopy, the limitations of STA and the restricted field of view of the static image intensifier still remain. The utilization of treadmills has also been proposed in order to confine the movement of the knee to the field of view of a videofluoroscope [147–149]. However, temporal [150–155], joint kinematic [150, 151, 153, 155, 156], as well as kinetic gait parameters [151, 155] are known to differ significantly between level and treadmill walking. Furthermore, individuals first need to be familiarized with treadmill walking [157], which can cause difficulties especially for elderly subjects or patients with a pathological gait pattern [155, 156].

A couple of research groups have been working on the development of mobile X-ray systems [54, 135, 158–160], and recently Guan et el. [30] presented a mobile bi-plane X-ray system used for tracking of the knee joint during level walking. The system was capable of moving the X-ray units 3.6 m horizontally and 0.5 m vertically at peak velocities of 5 m/s and 1.2 m/s respectively with peak accelerations of 20 m/s^2 and 12 m/s^2. Knee position was captured using a marker-camera sensor system, but the tracking of the system combined this data with a learned velocity profile. The resulting ability of the system to maintain the knee within the field of view was therefore dependent upon the repeatability of the motion task.

To overcome the limitations of a static image intensifier and allow tracking of the knee throughout complete cycles of level walking, Zihlmann et al. [137] presented a mobile fluoroscope that was

capable of real-time tracking, thereby allowing natural variations in the gait cycle to be captured. One major advantage of the system is that it allowed the synchronous assessment of ground reaction forces. However, the system has not yet been assessed in its ability to accurately follow the knee throughout activities of daily living, and was only able to move horizontally. With the vision to allow the examination of more strenuous activities such as downhill walking and stair descent, the aim of this study was to further develop the system to additionally allow vertical tracking as well as to examine the accuracy with which the knee can be maintained within the field of view during different activities of daily living.

2.3 Materials and methods

2.3.1 The moving fluoroscope

The moving fluoroscope has been developed to track the human knee joint over complete cycles of activities of daily living, and is composed of a modified BV Pulsera C-arm (Philips Medical Systems, Switzerland) mounted onto a moving trolley (Figure 2.1). The horizontal displacement of the trolley is achieved with six synchronous servo-motors (Mavilor BLS 113A, Infranor, Switzerland), which are controlled by six servo drives (XtrapulsCD1-a-400/45, Infranor, Switzerland), resulting in an ability to move the C-arm at up to 5 m/s with maximum accelerations of up to 9 m/s^2. The vertical displacement of the C-arm is performed by two electrically geared and motorised (Movinor LH97, Infranor, Switzerland) linear actuators, one on the same side as the image intensifier (TKK30-325AL, Rexroth Bosch Group, Germany), and one on the side of the radiation source (LM4.2.0800BR020.1.04.0S, Line Tech AG, Glattbrugg, Switzerland). In this manner, the C-arm can achieve a maximum vertical velocity of 1.33 m/s and an acceleration of up to 4 m/s^2. The relative location of the knee with respect to the trolley is measured using a wire sensor (WS17KT, ASM Sensor, Germany) in combination with a digital goniometer (05.2420.0020, Kuebler, Germany) that are attached to the leading bar of the trolley (Figure 2.2). The end of the wire is attached to an elastic velcro-strap that is secured around the thigh above the subject's knee to be measured (Figure 2.2).

Based on the real-time excursion and inclination of the sensor wire, the motors were driven according to a feedback controller to keep the knee joint in the field of view of the video fluoroscope both horizontally and vertically. Here, a PC running LabVIEW Real Time (LV 2014, National Instruments, Austin TX, USA) hosted a motion controller (PCI-7354, National Instruments,

Austin TX, USA) and a DAQ-card (NI PCIe-6323, National Instruments, Austin TX, USA), which in combination with the software, transformed the knee sensor signal into vertical and horizontal coordinates for the motion controller. These calculations ran at a loop iteration frequency of 5 kHz. The vertical axis ran as a closed loop proportional integration controller in the displacement mode following the pre-determined set point. For the horizontal axis, the difference between the knee position and the pre-determined set point was used as a direct input signal for the motor drives, which were configured in velocity mode (a control range from 0 to 25 cm corresponded to 0 to 5 m/s).

Since the moving fluoroscope is mounted on a standalone trolley, horizontal walking distance is only limited by cable length and the existing lab configuration, thus allowing a range of about 10 m. In the vertical direction, the moving fluoroscope allows tracking of the joint between 0.4 m and 1.05 m above ground.

Finally, the fluoroscopy system was modified with the incorporation of a standalone charge-coupled device (CCD) camera (camera: IMPERX IPX-1M48-L, Imperx Inc., Boca Raton, USA; framegrabber: Matrox Solios eCL/XCL-B, Matrox Electronic Systems Ltd., Quebec, Canada) to allow a shutter time of 1 ms and an image resolution of 1000 x 1000 pixels with a grayscale resolution of 12 bit. Imaging parameters of the X-ray system were: pulse frequency 25 Hz, pulse width 8 ms, voltage around 60 - 70 kV and current around 10 - 12 mA.

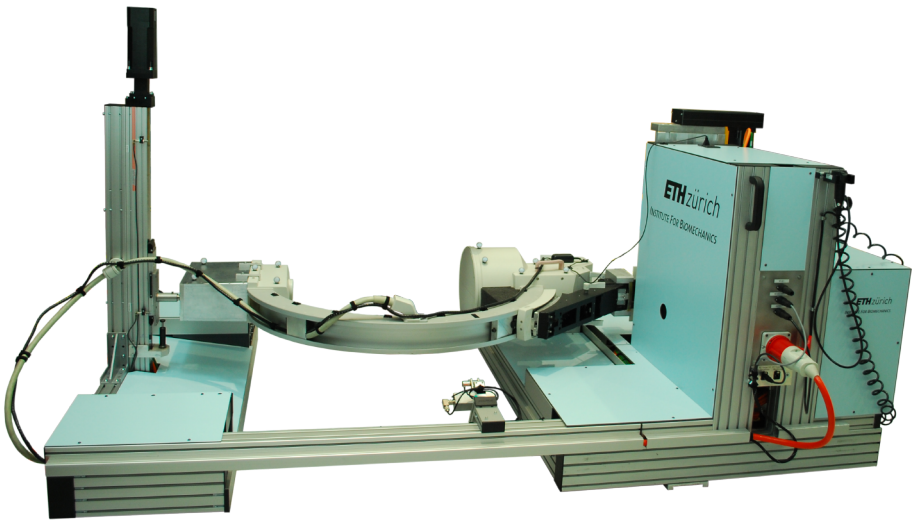

Figure 2.1: Moving fluoroscope developed at the Institute for Biomechanics. Consisting of a C-arm mounted on a moving trolley, allows real time tracking of the knee throughout complete cycles of level walking, stair descent and ramp descent activities. The figure shows the set-up for measurements of the left knee. For measurements of the right knee, the C-arm is rotated by 180° around its out-of-plane axis and the front bar, including wire sensor is reconfigured to the other side of the trolley, such that the C-arm always leads away from the subject due to safety considerations

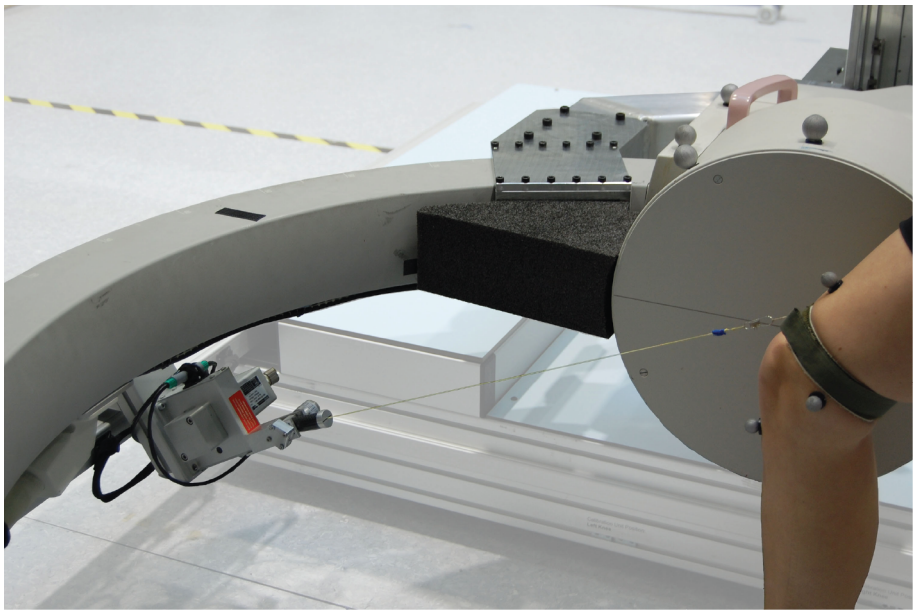

Figure 2.2: Wire sensor. Tracking of the trolley is achieved by positional feedback of the subject's knee using a wire sensor and digital goniometer, thus allowing tracking of the knee joint both horizontally and vertically

2.3.2 Coupled force, fluoroscope and reflective marker measurements

The videofluoroscopic image assessment was coupled with a motion capture system (VICON MX system, Oxford Metrics Group, UK) and force plates (Kistler, Switwerland). In order to time synchronize all three systems, a trigger signal was sent from the X-ray generator to an analog input of the motion capture system for each radiographic image.

The orientation and position of the fluoroscopy coordinate system was registered in the global laboratory coordinate system by using a grid of metal beads (also later used for image distortion correction), which was additionally equipped with six reflective markers affixed at predefined positions. The grid was rotated and displaced into multiple positions on the image intensifier, such that the grid's beads were assessed by the fluoroscopic system while the locations of the reflective markers were simultaneously captured by the motion capture system. Since the positions of the reflective markers were identified in both the fluoroscopy and the laboratory coordinate systems, the transformation between the two coordinate systems was determined using a least-squares fit of point clouds [161]. Furthermore, to track the position of the moving fluoroscope during measurements, the C-arm was equipped with five reflective markers on the X-ray source and six on the image intensifier (Figure 2.1).

The set-up of the force plates used for level walking consisted of five force plates fixed in a straight line, each with a dimension of 40 x 60 cm (2x Type 9281B, 2x Type 9285, 1x Type

9281C; Kistler, Winterthur, Switzerland). The force plates were decoupled from vibrations of the surrounding floor by installation on a separate concrete pillar constructed on the building foundation [137].

For stair descent, a three-step staircase equipped with two mobile force plates (Type 9286AA, Kistler, Winterthur, Switzerland), was fastened alongside the force plates fixed in the floor, thus also decoupled from any vibration in the surrounding floor. Each step of the staircase measured 280 x 180 x 800 mm in depth, height and width respectively (Figure 2.3).

For downhill walking, a ramp was constructed that included two mobile force plates (Type 9286AA, Kistler, Winterthur, Switzerland) that were also mounted onto the decoupled force plates in the ground (Figure 2.3).

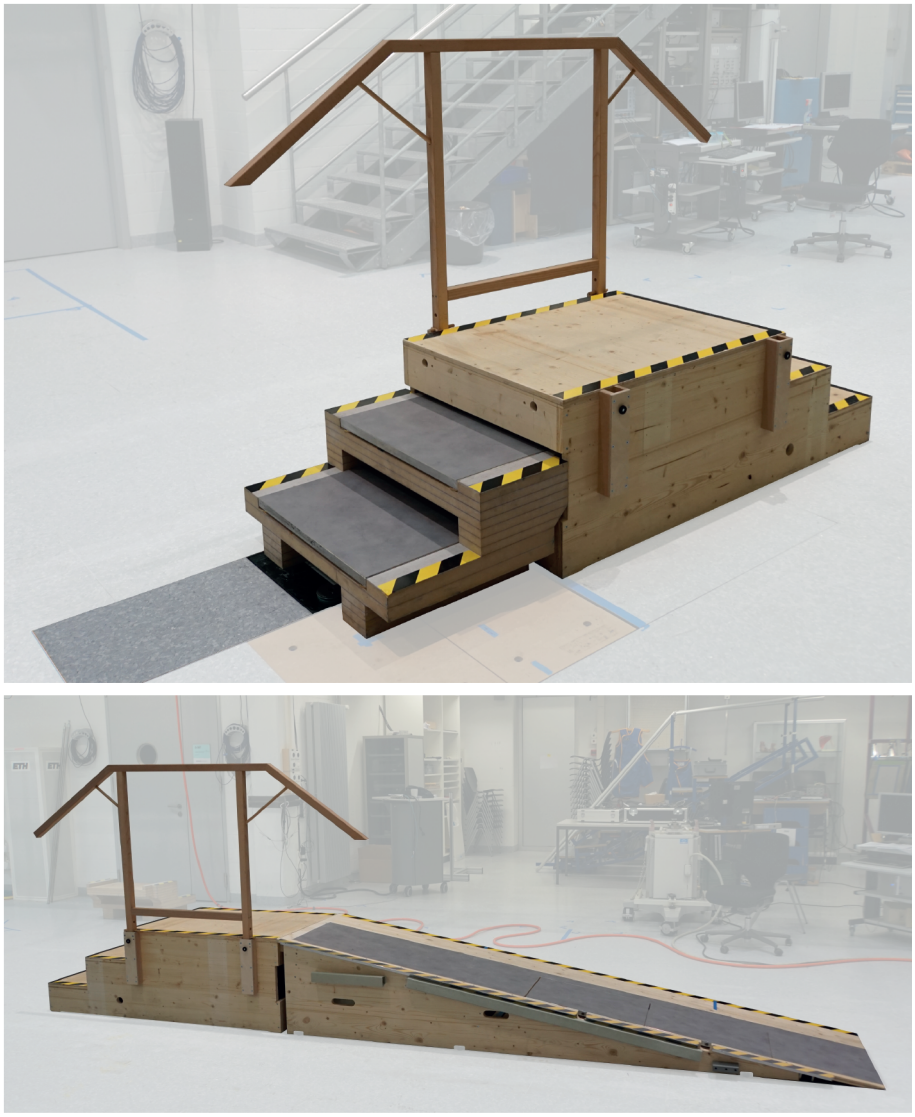

Figure 2.3: Staircase and ramp (10° inclination) including two mobile force plates

2.3.3 Feasibility study on ten TKA subjects

The ability of the moving fluoroscope to track the knee within the image area was assessed in ten TKA subjects (three female and seven male, six GMK PS fixed-bearing TKA and four GMK Sphere TKA (Medacta International, Switzerland), at least one year postop, good outcome, no/very low pain with a Visual Analogue Scale score < 2, average age of 69.6 $\pm$ 7.9 years and average BMI of 26.4 $\pm$ 2.9 kg/m^2), who participated in an on-going study on TKA kinematics [162]. All subjects provided written, informed consent to participate in this study, which was approved by the cantonal ethical committee of Zürich (KEK-ZH-Nr. 2015-0140).
Prior to each experiment, each subject was given sufficient time to get accustomed to the moving fluoroscope without being exposed to radiation (two to four walking trials). For each motion task (level walking, stair descent, downhill walking) a minimum of five gait cycles were assessed. TKA kinematics by means of fluoroscopy, whole body kinematics based on skin markers, as well as ground reaction forces, were measured simultaneously. Data processing of the fluoroscopic images included image distortion correction by a local algorithm operating on a reference grid, assessment of the projection parameters of the videofluoroscopic system (focal distance, location of the principle point in the image plane) determined by a least-squares optimization using five images of a calibration tube, as well as 2D/3D registration based on the CAD models of the implant components [135, 138, 163]. In addition, the following parameters were computed to evaluate tracking capability of the moving fluoroscope:

Gait parameters

Gait velocity was calculated based on the midpoint between the two skin markers located on the posterior spina iliaca processes. Knee velocity and acceleration were tracked based on the knee markers on the lateral epicondyle.

Parameters reflecting motion of the moving fluoroscope

Maximal velocity and acceleration of the moving fluoroscope while tracking of the knee was evaluated in both the horizontal and vertical directions.

Tracking

The tracking was evaluated by the location of the knee joint centre, defined as the origin of the femoral implant coordinate system (mid point between medial and lateral epicondyles on femoral flexion axis), relative to the image intensifier.

2.4 Results

The average gait velocity of the ten subjects was 0.94 m/s for level walking (Table 2.1). In the horizontal direction for level and downhill walking, the maximal accelerations that were recorded by the moving fluoroscope were below the maximal knee accelerations, whereas the maximal velocities of the moving fluoroscope were larger than maximal knee velocities (Table 2.1). For stair descent, horizontal velocities and accelerations of the moving fluoroscope were comparable to the knee parameters. In the vertical direction, the maximal accelerations and velocities of the moving fluoroscope tended to be larger than those of the knee (Table 2.1).

The horizontal motion of the moving fluoroscope was stable in its trajectory, reflected by the absence of medio-lateral motion ($<$ 13 mm deviation in medio-lateral direction from linear motion).

The knee joint centre for all ten subjects remained within the field of view of the image intensifier for all walking tasks and all trials, with an average distance between the knee joint centre and the centre of the image intensifier: vertical 1.8 $\pm$ 1.4 cm, horizontal 4.0 $\pm$ 2.6 cm (Figure 2.4, S1 Video).

2.5 Discussion

The ability to reconstruct the skeletal kinematics of the human tibio-femoral as well as patello-femoral joints in 3D, without the influence of soft tissue artefact and throughout complete cycles of activities of daily living, provides critical new perspectives for understanding knee pathology and improving implant design. In this study, a moving fluoroscope has been developed and its ability to maintain the knee within the field of view of the image intensifier during level gait, stair descent and downhill walking has been demonstrated in ten TKA subjects.

The construction of the moving fluoroscope as a C-arm mounted on a standalone trolley allows the usage within a variety of settings, since no construction or fixed installation on the floor is needed. In addition, the construction offers the ability to combine kinematic and ground reaction force measurements, and is only limited in walkway distance by cable length. The major disadvantage of this more mobile set-up is the possibility of wheel slippage over the floor at higher gait accelerations, which can be overcome with optimal combinations of wheel and floor materials.

The presented moving fluoroscope is based on only a single C-arm, and therefore has both advantages and disadvantages compared to static systems or dual-plane systems. Due to its dynamic

Table 2.1: Gait parameters and parameters of the motion of the moving fluoroscope. Mean and standard deviations over all ten subjects

		gait velocity [m/s]		**maximum velocity** [m/s]		**maximum acceleration** [m/s^2]	
		horizontal	vertical	horizontal	vertical	horizontal	vertical
subject	level walking	0.94 ± 0.11					
	stair descent	0.51 ± 0.09	0.26 ± 0.03				
	downhill walking	0.78 ± 0.13	0.14 ± 0.03				
knee	level walking			1.87 ± 0.16		7.87 ± 0.72	
	stair descent			1.20 ± 0.19	0.35 ± 0.30	4.61 ± 0.83	3.74 ± 0.97
	downhill walking			1.59 ± 0.20	0.25 ± 0.19	6.93 ± 1.16	3.10 ± 0.60
FluMo	level walking			2.06 ± 0.19		6.72 ± 0.41	
	stair descent			1.18 ± 0.20	0.39 ± 0.24	4.62 ± 0.86	4.32 ± 1.14
	downhill walking			1.73 ± 0.26	0.34 ± 0.10	6.54 ± 0.56	4.02 ± 0.80

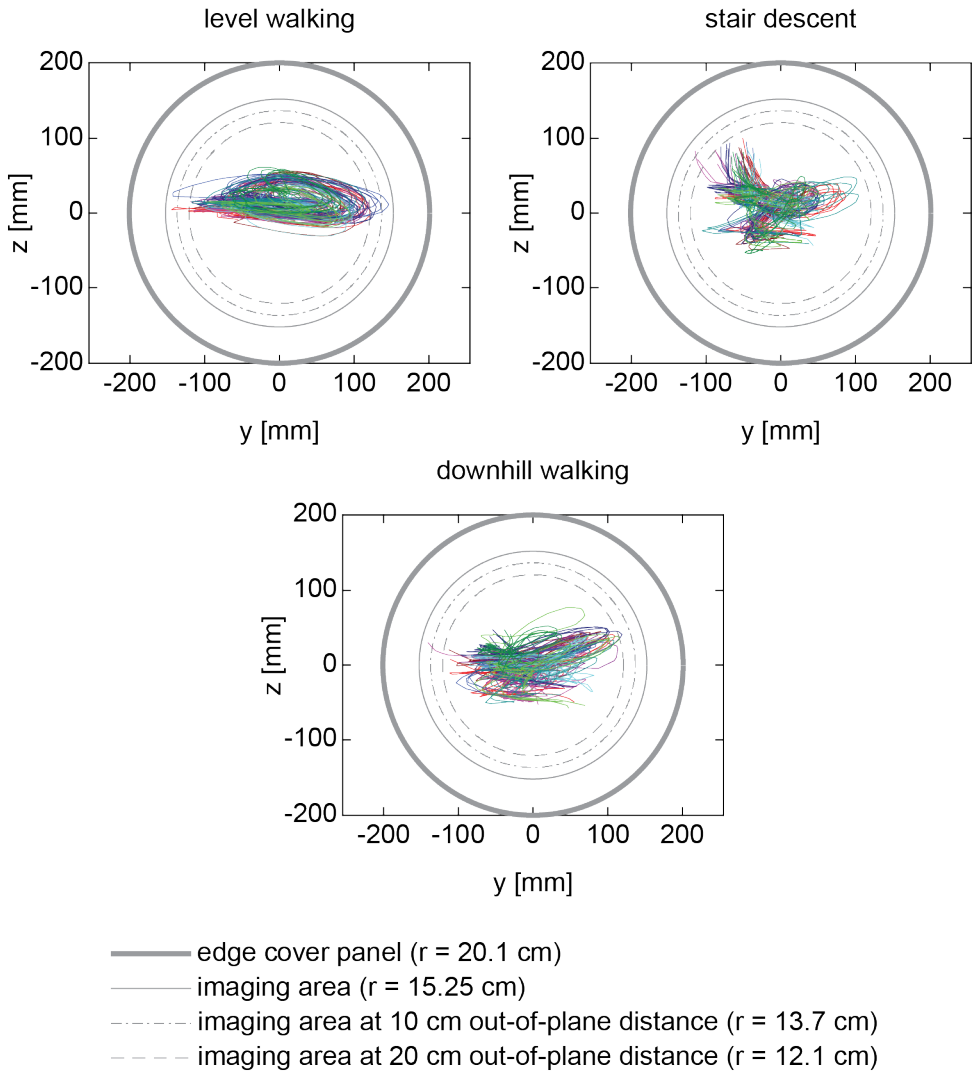

Figure 2.4: Movement of the knee joint centre relative to the image intensifier during level walking, stair descent and downhill walking. All trials for all ten subjects are shown (one colour for each subject)

nature, subjects are clearly aware of being accompanied by such a system during walking, both from a physical presence, as well as a noise perspective. As a result, gait velocities of the TKA subjects were lower than have been observed in healthy subjects [164, 165], but have been shown to become comparable to TKA subjects [166]. A previous study on subjects that were actively tracked by a robotic imaging system found only small and clinically non-relevant adjustments in gait patterns [54]. However, although gait velocity as well as ground reaction force patterns of the present study were comparable to TKA subjects of earlier skin marker studies, a future study should investigate if there is any influence of the presented moving fluoroscope, especially of the sound of the fluoroscope on the gait pattern of subjects walking with the moving fluoroscope. Another aspect of a single-plane fluoroscope compared to a dual-plane counterpart is the lower level of 2D/3D registration accuracy achievable, especially in the out-of-plane direction [167]. While this presents a considerable disadvantage, especially in the registration of natural bones, the approach also has clear advantages. A mobile single-plane system provides a larger effective field of view than a static dual-plane system. Dual-plane systems physically constrain the measurement volume in two directions, thus confining the natural motion of the subject. Radiation exposure is also a critical, yet often neglected consideration; dual-plane systems expose the subject to substantially higher levels of radiation. In this study, we have demonstrated the ability of the system to maintain the knee within the field of view (both horizontally and vertically) during a variety of activities of daily living – and this has been made possible by the wire sensor that provides a direct contact with the body of the subject. While the influence of the wire on gait is expected to be very small (it only applies an external force of about 4 N), a clear advantage is that the time delay is small enough to allow real-time control. In other systems [30] tracking includes a learned velocity profile and since, especially for pathological gait, gait repeatability can be reduced, this can lead to deficiencies in being able to keep the knee in the field of view. Due to the weight of the system, the presented real-time tracking is certainly not perfect. For a few frames, in which the knee joint centre reaches a location close to the edge of the image intensifier, part of the implant was out of the field of view. Although the information was sufficient to perform a 2D/3D registration, it is clear that if less information is available, reduced accuracy must be expected. Furthermore, any motion of the TKA relative to the image intensifier leads to the possibility of motion blur and therefore reduced accuracy in the 2D/3D registration. In the presented set-up, however, the rapid shutter time of 1 ms decreases motion blur, but a small amount of motion blur is still visible (see S1 Video), resulting in a lower Image Quality Measure [168] for some images during gait trials in comparison to static standing trials. As an example, the Image Quality Measure based on De and Masilamani [168] showed a range of 0.0006 - 0.0015

for the images of the gait trial presented in S1 Video in comparison to the Image Quality Measure of 0.0011 - 0.0012 in the images of a standing trial of the same subject.

The accuracy of the resulting tibio-femoral kinematics after 2D/3D registration is clearly influenced by the image quality and the registration algorithm itself, but is also strongly dependent on the object geometry, thus type and size of the implant and joint investigated. Previous validation of the aforementioned 2D/3D registration algorithm resulted in rotational and translational RMS errors of 0.2°/0.4 mm for in-plane and 1.3°/2.1 mm for out-of-plane for the Mobility^{TM} total ankle arthroplasty [163], and 0.15°/0.3 mm for in-plane and 0.25°/1 mm for out-of-plane for the balanSys® TKA [135]. Other studies using single-plane systems have reported slightly higher errors of between 0.3° to 1.4° and about 0.5 mm for in-plane rotations and translations and between 1.5° and 2.3° and between 4.0 and 6.6 mm for out-of-plane rotations and translations [55, 56, 167]. A similar accuracy can be expected for the two implant designs and various implant sizes included in the present study. For natural tibio-femoral kinematics, the errors are expected to be larger due to lower contrast and less prominent geometric features in comparison to TKAs.

2.6 Conclusions

A moving fluoroscope has been presented that is a standalone system, and which allows the kinematic assessment of the tibio-femoral and patella-femoral joints by means of single-plane videofluoroscopy during level gait, stair descent and downhill walking in combination with synchronous reflective marker and ground reaction force measurements. Its ability to keep the knee within the field of view of the image intensifier has been demonstrated in ten TKA subjects. Since the fluoroscope is moved based on real-time control, its usage is not dependent on gait repeatability and will allow the evaluation of healthy as well as pathological gait patterns without the requirement for the joint to follow pre-determined paths.

2.7 Acknowledgements

Many people have played an important role in the development of the moving fluoroscope, especially Dr. Mauro Foresti, who has done a tremendous amount of work in making the moving fluoroscope a reality.

2.8 Supplementary materials

Supplementary material associated with this chapter can be found in the online version of the published paper (https://doi.org/10.1371/journal.pone.0185952.s001).

S1 video: Videofluoroscopic video of the knee, as well as time synchronised whole body skin marker and ground reaction force data during level walking. Furthermore, the trigger signal, that was sent from the X-ray generator to an analog input of the motion capture system for each radiographic image, is displayed.

Chapter 3

Evaluation of an intensity-based algorithm for 2D/3D registration of natural knee videofluoroscopy data

adapted from:

Barbara Postolka*[1], Renate List*[1], Benedikt Thelen[2], Pascal Schütz[1], William R. Taylor[1], Guoyan Zheng[2]

*These authors contributed equally to this work

[1]Institute for Biomechanics, ETH Zürich, Zürich, Switzerland

[2]Institute for Surgical Technology & Biomechanics, University of Berne, Bern, Switzerland

Med Eng Phys, 77:107-113, 2020

DOI: 10.1016/j.medengphy.2020.01.002

open access

Keywords

in vivo kinematics, knee, videofluoroscopy, 2D/3D registration

3.1 Abstract

The accurate quantification of *in vivo* tibio-femoral kinematics is essential for understanding joint functionality, but determination of the 3D pose of bones from 2D single-plane fluoroscopic images remains challenging. We aimed to evaluate the accuracy, reliability and repeatability of an intensity-based 2D/3D registration algorithm. The accuracy was evaluated using fluoroscopic images of two radiopaque bones in 18 different poses, compared against a gold-standard fiducial calibration device. In addition, three natural femora and three natural tibiae were used to examine registration reliability and repeatability. Both manual fitting and intensity-based registration exhibited a mean absolute error of < 1 mm in-plane. Overall, intensity-based registration of the femoral bone model revealed significantly higher translational and rotational errors than manual fitting, while no statistical differences (except for y-axis translation) were found for the tibial bone model. The repeatability of 108 intensity-based registrations showed mean in-plane standard deviations of 0.23 – 0.56 mm, but out-of-plane position repeatability was lower (mean SD: femur 7.98 mm, tibia 6.96 mm). Standard deviations for rotations averaged 0.77 – 2.52°. While the algorithm registered some images extremely well, other images clearly required manual intervention. When the algorithm registered the bones repeatably, it was also accurate, suggesting an approach that includes manual intervention could become practical for efficient and accurate registration.

3.2 Introduction

The accurate quantification of *in vivo* tibio-femoral kinematics and kinetics is essential for a detailed understanding of knee joint functionality [6] as well as pathological movement patterns, but also for refining surgical procedures, rehabilitation techniques, and implant design. Although skin marker based analysis is currently still the most employed tool in human movement analysis, its accuracy is known to be limited by soft tissue artefact [1, 6–8]. As a result, more accurate single- [163, 169, 170] as well as dual-plane [30, 76] videofluoroscopy techniques have gained in-

creasing employment in the study of three dimensional (3D) joint motion. Here, image based 3D geometries of the natural bones, or computer-aided design (CAD) models of the implant components are registered to the two dimensional (2D) fluoroscopic images using a 2D/3D registration approach [55–58, 138]. Using such techniques, registration of natural bones remains challenging due to the generally lower contrast and less prominent geometric features of the bones compared to the higher-contrast shadows of metallic components. 2D/3D image registration is further challenged due to low out-of-plane accuracy [59, 60, 167, 171]. To overcome this issue, a variety of 2D/3D registration algorithms have been proposed [51, 56, 60, 139, 167, 172].

Two main categories of 2D/3D registration algorithms exist: feature- [51, 59, 173–175] and intensity-based [60, 61, 176–182] methods. Feature-based methods require a surface model of the bone, generally created from the segmentation of computed tomography (CT) scan data. Importantly, these techniques are only able to utilise surface information, and are unable to consider information originating from the internal structure of the bone. In contrast, intensity-based methods directly compare the 2D radiographic images with digitally reconstructed radiographs (DRRs), which are obtained by simulating X-ray projections through the CT volume. With the aim to determine the correct position and orientation of the bone in 3D space, the complete CT data stack is repeatedly transformed in an iterative optimization process until maximum similarity is achieved between the DRR and the 2D fluoroscopic image.

While most 2D/3D approaches used for analysing 2D fluoroscopic images of the natural knee are feature-based [46, 51, 55–59] and only use the surface characteristics of each subjects' bone to guide registration, two validated intensity-based approaches have also been presented in the literature [60, 61]. All of these methodologies show a standard deviation (SD) of the in-plane translational error of less than 1 mm, whereas the SD for the out-of-plane translation as well as the rotational error vary considerably between the different approaches (Table 3.1). Recently, an intensity-based registration algorithm has been proposed by Zheng and co-workers [183–185]. Different from previous work [60, 61], the proposed algorithm incorporated a robust similarity measure that was derived from information and Markov random field theories [185]. Additionally, in order to speed up the registration process, it used the cubic splines data model to compute the multi-resolution data pyramids for both the CT data and the X-ray images, the DRRs, as well as the gradient and the Hessian of the robust similarity measure. Registration is then performed from the coarsest resolution until the finest one by maximizing the similarity measure using a Levenberg-Marquardt non-linear least-squares optimizer. However, before this approach can be used towards understanding the functional kinematics of the natural knee, a validation of the algorithm is clearly required. As a result, the goal of this study was to determine the accuracy

of the intensity-based 2D/3D registration algorithm, as well as to evaluate its reliability and repeatability for fitting femoral and tibial bones in 3D space.

3.3 Materials and methods

In the developed software ("KneeFit") several previously introduced techniques [183–185] were integrated into a graphical user interface for efficient utilisation of 3D kinematic information from 2D fluoroscopic images. The accuracy and reliability of the 3D pose registration algorithm were then evaluated using fluoroscopic images of radiopaque and natural bones in different poses, compared against a gold-standard fiducial marker calibration device, as described below:

3.3.1 Image acquisition for assessing algorithm accuracy

A calibration object consisting of 16 spherical, radiopaque calibration fiducials (seven with a diameter of 5.0 mm and nine with a diameter of 2.5 mm) at known positions (accuracy: $\pm$ 0.1 mm) was rigidly mounted onto an artificial femur and tibia with radiopaque properties (Femur 1130-177, Tibia 1117-42, Sawbones, Vashon Island, USA) (Figure 3.1 A) [186]. To obtain volumetric models, full-length CT scans (resolution 0.5 x 0.5 mm, slice thickness 1 mm; Brilliance 64, Philips Healthcare, Netherlands) of the artificial bones were acquired. Bone volume models were created by segmenting the CT data-stack using the open-source software MITK-GEM [187].
Videofluoroscopic images were acquired using the Institute for Biomechanics' moving fluoroscope at ETH Zürich [135, 137, 188], which consists of a modified videofluoroscope (BV Pulsera, Philips Healthcare, Netherlands) operating at a pulse frequency of 25 Hz and a field of view of 30.5 cm. The system was modified by incorporating a stand-alone charge-coupled device (CCD) camera to allow a shutter time of 1ms and an image resolution of 1000 x 1000 pixels with a greyscale resolution of 12 bits [163]. The videofluoroscopic image coordinate system was defined with the x- and y-axes lying in the image plane and the z-axis perpendicular to the image plane. The origin of the videofluoroscopic image coordinate system was set to the X-ray source [163]. Image distortion was eliminated using a local correction algorithm [135] based on a reference grid with 1761 beads. The projection parameters of the videofluoroscopic system (focal distance, location of the principle point in the image plane) were determined by a least-squares optimization based on five images of a calibration tube (300 mm long with two Plexiglas® plates), consisting of 25 metal fiducials at known positions (accuracy: $\pm$ 0.03 mm) within the base plates [135].

Table 3.1: Precision of 2D/3D registration methods based on 3D CT models and 2D single-plane fluoroscopic images of natural knees (registration precision = average standard deviation of the error).

		SD translation [mm]		**SD rotation [°]**	**registration**	
		in-plane	out-of-plane	all axes	feature	intensity
Fregly et al. 2005 [59]	femur/tibia$^{\diamond}$	0.42	5.6	1.30	x	
Komistek et al. 2003 [51]	femur/tibia	0.34	-	0.35	x	
Scarvell et al. 2010 [60]	femur	0.36	0.74	0.4		x
	tibia	0.38	0.55	0.47		
Tsai et al. 2010 [61]	femur	0.72	3.23	0.83		x
	tibia	0.86	4.61	1.21		

feature = feature-based approach; intensity = intensity-based approach; $^{\diamond}$synthetic fluoroscopic images

Each bone model was fluoroscopically imaged in 18 different static positions (different poses throughout the imaging volume that encompassed all different perspectives and planes) (Figures A.1 & A.2), as well as dynamically (40 images) during a movement that was similar to the within-image motion observed during tracked walking (Figure 3.1 B).

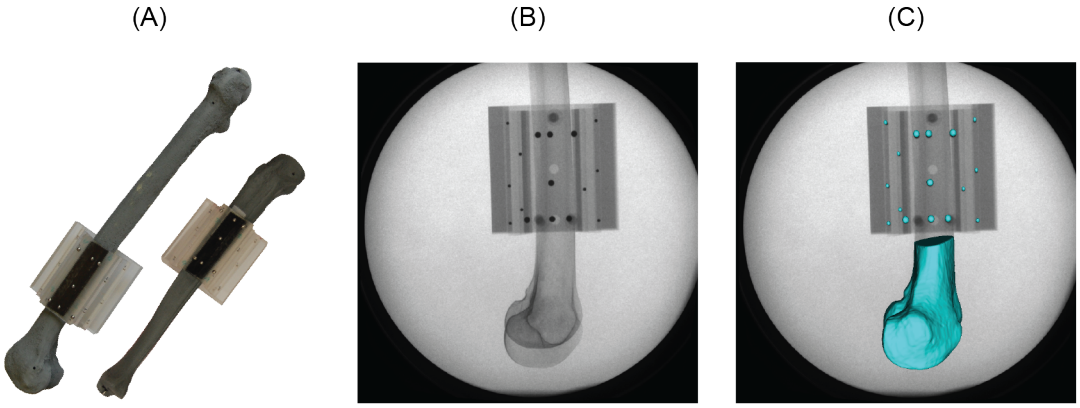

Figure 3.1: (A) Femur (left) and tibia (right) bone models with radiopaque image properties, each equipped with a rigidly attached fiducial marker device [186], (B) Videofluoroscopic image of the femur bone model with the fiducial marker device, (C) registered image of the femur bone model and the fiducial marker device.

3.3.2 2D/3D registration algorithm

An accurate similarity measure, based on a least-squares approach that can be effectively minimized by derivative-based optimization methods, was used as the objective function [185]. A continuous image model-based cubic spline was used to accurately interpolate the 3D volume data as well as the 2D fluoroscopic image [184]. This cubic-spline data model allows a well-defined gradient of the objective function, enabling the use of a multi-resolution Levenberg-Marquardt optimizer for fast convergence.

3.3.3 2D/3D manual fitting and computational registration

The CT volume data was firstly manually manipulated ("fitted") such that the projection of the bone surface models optically best matched each fluoroscopic image. These manually fitted poses were stored as 3D geometric transformations, and afterwards used as initial poses for registration using the intensity-based registration algorithm.

3.3.4 Evaluation of algorithm accuracy

To evaluate the accuracy of the 2D/3D bone registration in three planes and around all three axes, the manually fitted and intensity-based registered 3D poses of the femur and tibia were compared to the positions obtained using the fiducial calibration device (Figure 3.1 C). Here, in order to obtain the pose of the fiducial device for each frame, the centre of each fiducial sphere was firstly acquired in the CT image coordinate system [189], including the corresponding projection centre of each fiducial in each fluoroscopic image [190]. A closed-form solution [191] was then used to compute the ground truth transformation for the fiducial device between the CT and the fluoroscopic image coordinate systems.
In order to allow interpretation of the fitting and registration accuracy, as well as ensure consistency with later assessment of joint motion in natural knees, the translational differences were calculated at a point close to the intercondylar notch (femur) and at a point close to the intercondylar eminence (tibia). For rotational differences, all three axes of the rotation matrix were decomposed in the image coordinate system. To evaluate errors in the manual fitting and computational registration processes, the mean absolute differences and SD as well as the range (min, max) of the error between the fiducial reference and the two registration methods were calculated. Furthermore, the root-mean-square (RMS) error for the two in-plane translations and all three rotations were analysed. Additionally, registration precision was determined as the average standard deviation of the error. The limits of agreement according to Bland and Altman [192] were used to evaluate out-of-plane bias.

3.3.5 *in vivo* repeatability test

In contrast to the Sawbone-based accuracy tests described above, repeatability was evaluated using the fluoroscopic images of three healthy subjects (2 male/1 female, 23 $\pm$ 1 years, BMI 22.2 $\pm$ 0.3 kg/m^2) captured during functional activities. All subjects provided written, informed consent to participate in this study, which was approved by the Zürich cantonal ethics committee (BASEC-Nr. 2016-00410) and carried out in accordance to the declaration of Helsinki. CT scans of all subjects were performed in the same manner described previously, spanning approximately 20 cm inferior and up to 20 cm superior of the knee joint line. Fluoroscopic images were then captured using the Institute for Biomechanics' moving fluoroscope [135, 137, 188] during standing, as well as throughout complete cycles of level walking and deep knee bending, due to their usage within our standard measurement protocol [188, 193, 194]. For each of the three subjects, one

pose at about 90° of knee flexion, one during mid-stance and one during standing were selected for evaluating the repeatability of the 2D/3D registration process (Figure A.3). To the best of their ability, each of the 4 observers manually fitted all 9 images (3 subjects, each 3 images) on multiple occasions (3 different days). Similar to the evaluation of the algorithm accuracy (above), each of these manually fitted images was then used as the initial position for the intensity-based registrations.

For each image, the repeatability of the 3D pose (tibia and femur) was determined based on the standard deviation of the 12 times (3 days, 4 observers) the image was manually fitted or computationally registered. The *in vivo* accuracy of the 2D/3D registration of the natural knees was not assessed in this setting, as no gold standard was present.

3.3.6 Post-processing

Post-processing of the registration data was performed using Matlab (Matlab 2017a, Mathworks, USA). A Wilcoxon signed-rank test was used to evaluate whether the accuracy differed between the manual fitting and the intensity-based registration. All statistical analyses were performed using SPSS (SPSS V24, IBM, USA) with a significance level set to $p < 0.05$.

3.4 Results

3.4.1 Accuracy assessment

Firstly, the poses of the manually fitted femur and tibia, as well as their intensity-based 2D/3D registrations were compared to the position obtained using the gold-standard calibration device. Combined evaluation of the static and dynamic trials (58 images) for each of the femoral and tibial bone models was performed for both manual fitting and intensity-based registration. In general, the largest absolute fitting and registration errors were observed in the out-of-plane (Err_T_z) direction, while for the in-plane directions (Err_T_x/Err_T_y), the mean absolute errors were < 1 mm (Table 3.2).

For the femur, all mean absolute translational errors using the intensity-based registration were significantly larger than for manual fitting. For the tibia, however, no significant differences were found, except for Err_T_y, where significantly smaller errors were observed using the intensity-based registration. Similarly, all mean absolute rotational errors for the intensity-based registered

femur were significantly larger than for manual fitting, while no significant differences were found for the tibia.

In the imaging plane, all images for the femur and 50 of 58 images for the tibia exhibited in-plane translational root-mean-square errors of < 1 mm using manual fitting. Using the intensity-based registration algorithm, only 34 of 58 images for the femur, but 57 of 58 images for the tibia showed errors < 1 mm.

The Bland-Altman plots for the out-of-plane translational error (Err_T_z) showed no obvious progressive trends, for either approach or bone (Figure 3.2), indicating no confounding factors. However, both approaches and bone models exhibited a negative bias (mean error).

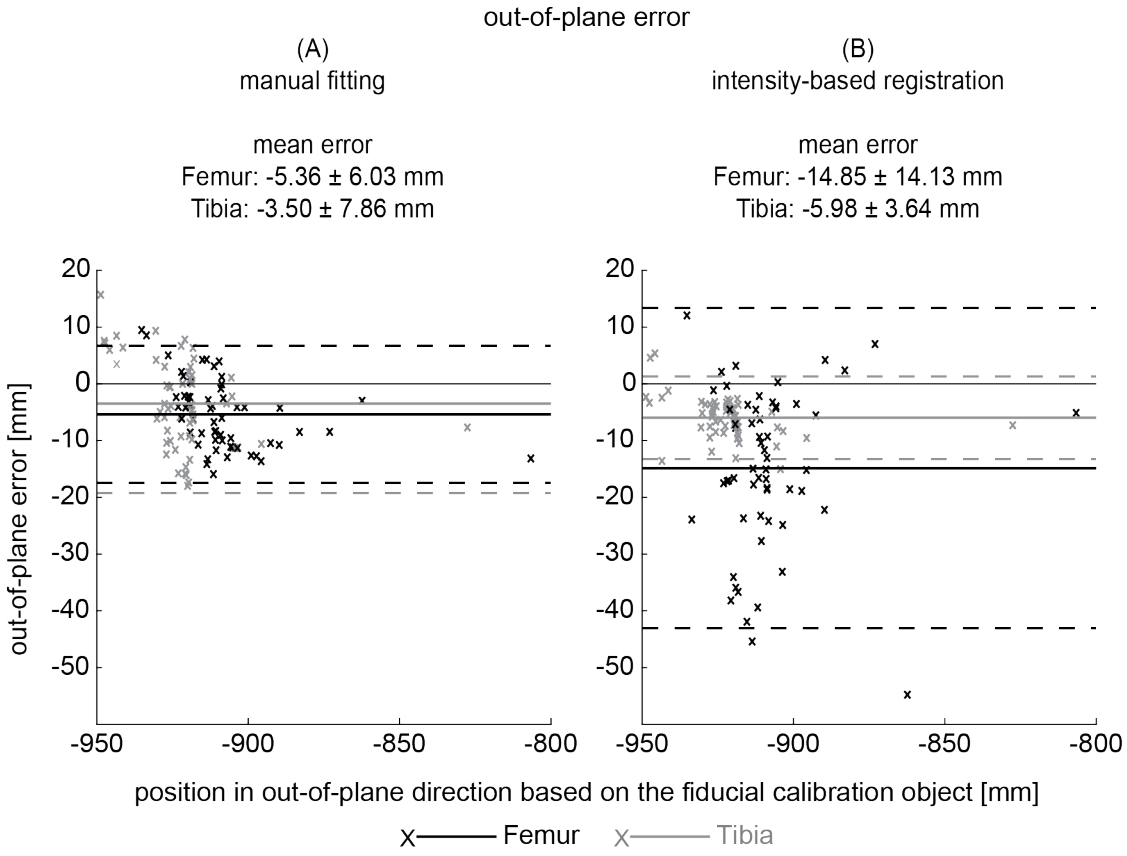

Figure 3.2: Bland-Altmann plots showing the translational out-of-plane agreement between the manually fitted (A) or the intensity-based registration (B) and the gold-standard fiducial position for each image. The mean difference between the two methods is plotted as the centre line (solid). The upper and lower dotted lines show the limits of agreement, between which 95% of the errors are expected to fall.

Table 3.2: Mean ± standard deviation as well as range (min, max) of the absolute translational [mm] and rotational [°] errors for the manual fitting and intensity-based registration

		translation error [mm]			**rotation error [°]**		
		Err_T$_x$	Err_T$_y$	Err_T$_z$	Err_R$_x$	Err_R$_y$	Err_R$_z$
manual	**femur**						
	mean ± STD	0.24 ± 0.19	0.45 ± 0.30	6.87 ± 4.20	0.45 ± 0.30	0.43 ± 0.33	0.28 ± 0.22
	(range)	(0.00, 0.80)	(0.01, 1.25)	(0.09, 15.92)	(0.00, 1.27)	(0.00, 1.68)	(0.00, 0.92)
	tibia						
	mean ± STD	0.52 ± 0.42	0.60 ± 0.41	7.12 ± 4.77	0.93 ± 0.79	0.86 ± 0.90	1.00 ± 0.82
	(range)	(0.01, 1.74)	(0.01, 1.49)	(0.00, 17.98)	(0.06, 4.27)	(0.01, 6.04)	(0.06, 4.35)
intensity	**femur**						
	mean ± STD	0.88 ± 0.60*	0.86 ± 0.88*	15.93 ± 12.88*	1.32 ± 1.35*	1.35 ± 0.96*	1.82 ± 1.38*
	(range)	(0.01, 2.73)	(0.00, 2.97)	(0.29, 54.79)	(0.00, 8.56)	(0.06, 3.72)	(0.03, 5.50)
	tibia						
	mean ± STD	0.46 ± 0.25	0.29 ± 0.28*	6.33 ± 2.99	0.85 ± 0.54	0.96 ± 0.72	0.93 ± 0.52
	(range)	(0.03, 1.15)	(0.02, 1.45)	(1.20, 15.03)	(0.02, 2.34)	(0.05, 2.79)	(0.01, 2.38)

*significant difference between manual fitting and intensity-based registration

3.4.2 *in vivo* repeatability test

The repeatability of the 108 manual fittings (4 observers, 3 days, 9 images) showed mean SD for the in-plane positions (SD_T$_x$/SD_T$_y$) of 0.43 - 0.83 mm, with the largest SD within a single image observed at the tibia (1.29 mm) (Table 3.3). Out-of-plane position repeatability (SD_T$_z$) was much lower (mean SDs femur: 8.31 mm, tibia 8.43 mm), with greatest SDs for single images of up to 14.46 mm for the femur and 13.65 mm for the tibia. SDs for rotations averaged 1.15 - 2.53°, but peaked at 3.11° and 4.63° for single images of the femur and tibia respectively.
For the computational intensity-based registration, the same repeatability tests showed mean SDs for the in-plane positions (SD_T$_x$/SD_T$_y$) of 0.23 - 0.56 mm, with the largest SD observed at the tibia (1.54 mm). Out-of-plane position repeatability (SD_T$_z$) was much lower (mean SDs 7.98 mm for femur, 6.96 mm for tibia), with greatest SDs for single images of up to 19.26 mm for the femur and 16.85 mm for the tibia. SDs for rotations averaged 0.75 - 2.52°, but were as high as 3.34° for the femur and 6.70° for the tibia.

3.5 Discussion

The 3D registration of skeletal position and orientation from 2D fluoroscopic images is an emerging technology that allows an understanding of internal joint kinematics. However, manual 2D/3D registration approaches are generally limited by the considerable time and expertise needed by the researcher to register the segmented data to the images. To overcome this limitation, as well as reduce subjective fitting errors, we aimed to investigate the accuracy and repeatability of a novel intensity-based 2D/3D registration algorithm for the analysis of natural knee kinematics during functional activities using a femoral and tibial radiopaque bone model as well as natural knee data. Generally, our 2D/3D intensity-based algorithm was able to successfully and accurately register fluoroscopic images of the natural knee, but seemed unable to find an optimal solution for some images. As a result, manual process control and occasional manual fitting still seem to be required in order to ensure an acceptable outcome.
Manual fitting as well as intensity-based registration were shown to be affected by a mean absolute translational registration error of less than 1 mm in-plane for the femur and tibia bone models (Table 3.2). Unsurprisingly, the out-of-plane translational errors were substantially higher than the in-plane errors for all cases [59, 135]. The precision of in-plane registration (indicated by the

Table 3.3: Repeatability (standard deviations) over 12 manual fittings (left) and 12 intensity-based registrations (right) for each image. The smallest and largest SDs for each degree of freedom for both bones are highlighted in bold italics

		manual fitting						**intensity-based registration**					
		SD translations [mm]			SD rotations [°]			SD translations [mm]			SD rotations [°]		
		SD_T$_x$	SD_T$_y$	SD_T$_z$	SD_R$_x$	SD_R$_y$	SD_R$_z$	SD_T$_x$	SD_T$_y$	SD_T$_z$	SD_R$_x$	SD_R$_y$	SD_R$_z$
	1	0.55	0.49	7.82	0.95	***0.99***	0.99	***0.03***	***0.01***	***0.65***	***0.03***	***0.01***	***0.05***
	2	0.57	0.42	7.03	1.10	1.09	0.77	***1.23***	0.56	***19.26***	1.35	***1.79***	1.22
	3	0.79	0.34	6.82	1.19	2.78	2.59	0.21	0.13	6.59	0.92	0.59	0.40
femur	4	0.55	0.29	7.22	***0.68***	1.06	***0.73***	0.30	0.17	4.71	0.64	0.11	0.52
image	5	***0.34***	0.56	***6.26***	0.75	1.11	0.81	0.22	0.20	7.68	0.71	0.92	0.73
number	6	***0.94***	0.45	7.68	1.52	***3.11***	2.04	0.16	0.13	7.28	0.72	0.65	0.12
	7	0.85	***0.68***	***14.46***	***1.96***	2.46	***2.79***	1.06	***0.58***	7.74	***2.53***	***1.79***	***3.34***
	8	0.44	0.43	10.15	0.91	***0.99***	0.97	0.41	0.11	8.97	0.14	0.35	0.39
	9	0.42	***0.24***	7.33	1.31	1.32	1.19	0.08	0.20	8.97	0.86	0.49	0.18
mean SD		**0.60**	**0.43**	**8.31**	**1.15**	**1.66**	**1.43**	**0.41**	**0.23**	**7.98**	**0.88**	**0.75**	**0.77**
	1	0.58	0.60	8.41	0.95	2.45	2.16	0.32	0.39	7.80	0.89	2.85	1.64
	2	0.93	0.58	7.75	***0.90***	2.53	2.17	0.60	0.69	6.06	1.71	3.42	1.41
	3	0.76	***0.38***	7.18	***2.39***	2.13	2.217	0.17	0.10	2.30	***0.22***	0.16	0.13
tibia	4	0.85	0.60	7.90	1.89	3.10	2.59	***1.23***	1.21	***16.85***	2.97	***6.70***	***2.77***
image	5	***0.49***	***0.67***	***6.16***	1.60	***1.48***	1.79	0.13	0.06	***1.47***	0.89	2.59	1.60
number	6	0.71	0.45	7.72	1.18	***4.63***	***3.92***	0.32	0.33	7.81	0.42	0.46	0.17
	7	***1.29***	0.50	***13.65***	2.10	3.23	2.92	1.03	***1.54***	10.89	***4.75***	5.36	2.66
	8	1.17	0.60	10.49	1.63	1.72	1.56	0.46	0.60	6.57	0.87	0.98	0.55
	9	0.69	0.54	6.84	1.14	1.53	***1.49***	***0.06***	***0.08***	2.92	***0.22***	***0.14***	0.24
mean SD		**0.83**	**0.55**	**8.43**	**1.53**	**2.53**	**2.31**	**0.48**	**0.56**	**6.96**	**1.44**	**2.52**	**1.24**

SD of the error) was comparable to most other studies [51, 59–61, 172, 195] (Table 3.1). However, our algorithm was somewhat less precise for registering out-of-plane position, and considerably worse than Scarvell and co-workers [60], who had specifically targeted a reduction of this error. Compared to literature reports, the precision of bone rotation found in our study was similar for the tibia but slightly worse for the femur. Unfortunately, a direct comparison of the femoral and tibial registration accuracy was not possible, as the mean of the absolute error was not generally reported.

Interestingly, intensity-based registration of the femur bone model revealed significantly higher translational and rotational errors than using manual fitting, whereas no statistical differences (except for translation along the y-axis) were found for the tibia bone model. This unusual difference plausibly originates from the manner in which intensity-based registration and manual fitting approaches address the problem. It is clear that the human eye is able to utilise all forms of visual information, including not only changes in intensity of the images, but also the apparent contours of the structures. In comparison, our intensity-based approach exclusively used information regarding the pixel greyscale values, and did not consider surface features. Under these conditions, it seems likely that the tibia has considerable intensity information that registration approaches are able to successfully utilise, whereas the femur possesses large and clear structural information that is easily accessible to the human eye (and possibly also model based fitting approaches), but that may present insufficient intensity changes to allow an equal quality of registration. As a result, a combination of feature- and intensity-based registration could plausibly produce further improvement to the registration quality achieved.

For all registration methods found in the literature, as well as the approaches used in this study, the out-of-plane translational values showed the highest errors, as well as the lowest precision. Similar to our study, Fregly and co-workers [59] reported a significant negative bias for out-of-plane translation, leading to the bones being reconstructed closer to the image intensifier than in reality, possibly the result of beam-hardening. Since movement of the femur relative to the tibia during functional activities of daily living mainly occurs in the sagittal plane, it seems that a correction to align the bones, or at least limit the relative movement between them in the out-of-plane direction, would be entirely possible. Consequently, relative out-of-plane movement (in our case the medio-lateral direction) between the bones should be interpreted with extreme caution.

Knowledge about the repeatability and reproducibility of the proposed registration algorithm is crucial, as usage is planned for different study cohorts as well as by different researchers, where a repeatable approach is critical. Manual fitting showed lower consistency, indicated by higher

SDs within single images than intensity-based registration. In addition, the best intensity-based registrations achieved an accuracy of under 0.1 mm in-plane and 0.3 mm out-of-plane, and $< 0.1°$ in all three planes – hence demonstrating that excellent levels of accuracy can be reached using these methods. Therefore, a semi-automatic procedure whereby the repeatability of an automatic procedure can be combined with manual intervention to exclude clearly incorrect intensity-based solutions, is a clear step towards improving overall mean accuracy. When considering the time and resources required to manually fit images (up to 3 min per image), such a process could potentially provide up to 70% saving for each successfully registered image.

In-plane translational repeatability for both bones and rotational repeatability for the femur was comparable to another study [195]. However, in our results, the tibia showed less rotational repeatability, and out-of-plane translational repeatability for both bones was worse. SDs for manual fitting were relatively low, likely supported by simply excluding clearly incorrect results, which the computational registration may not pick up due to the focus on different intensity concentrations. Consequently, low SDs for multiple registrations are achievable despite different manual initialisations. This indicates that the registration process is more dependent on the quality of the image (e.g. exposure, contrast, and bone pose) than the initial manual position.

Despite the registration errors reported here and in other studies, it is important to note that our approach will predominantly be used to assess tibio-femoral kinematics, mainly antero-posterior (A-P) translations and relative rotations [170, 193, 194] of the femur and tibia. Compared to known tibio-femoral kinematics of the natural knee (A-P translations 7.62 - 15.38 mm for the medial and lateral femoral condyles during walking [15, 74] with SDs of up to 3.7 mm during the swing phase [15]), our registration accuracy exhibits sufficient ability to assess differences between the A-P translation of the medial and lateral condyles, as well as rotations around all three axes. Other approaches to assess knee motion use dual-plane fluoroscopy [30, 32, 167, 196] in which out-of-plane error is reduced to a minimum. As expected, the SD for all three translations found in our study were higher than those found for a dual-plane set-up [30, 32]. Interestingly, however, rotational precision was not substantially better using dual-plane fluoroscopy, and importantly the ability to track the motion of subjects' knees throughout complete cycles of functional activities is still in its infancy [74].

Our validation study is affected by certain limitations. The achieved registration precision is not only affected by the applied registration modality but also by the accuracy of the distortion correction algorithm applied to all fluoroscopic images before the 2D/3D registration. If the pin-cushion distortion is not perfectly eliminated, a systematic error will be introduced. In addition, the artificial bones with radiopaque image properties used in this study were unlikely to fully

reproduce the properties of a natural femur and tibia, where sharper images may well be offset by an increased internal structural homogeneity. Although the used gold standard is also subject to fitting errors, the sharp imaging shadows of the metallic fiducials, together with extremely accurate manufacturing, greatly limits the introduction of possible errors [186]. Moreover, the absence of soft tissue will also play a role on the acquired images. Increased knee size on the fluoroscopic images, achieved by moving the measured joint towards the radiation source, would increase the number of pixels per bone, hence simplifying the intensity-based registration. In our study, however, we aimed to mimic an *in vivo* measurement set-up by placing the knee as close to the image intensifier as possible in order to maximize capture volume during the movement. Finally, no ground truth was available to provide an accurate assessment of repeatability in our study, which clearly needs to be addressed in future studies.

3.6 Declaration of competing interest

There are no conflicts of interest.

3.7 Acknowledgements

The authors like to thank Alper Akcoeltekin for processing of the fiducial calibration device data as well as Dr. Colin Smith and Longfeng Rao for the manual fitting of the repeatability data. The work was financially supported by the Commission for Technology and Innovation (Bern, Switzerland, Project Number: 17078.1 PFLS-LS) and Medacta International SA (Castel San Pietro, Switzerland).

3.8 Ethical approval

All subjects provided written, informed consent to participate in this study, which was approved by the Zürich cantonal ethics committee (BASEC-Nr. 2016-00410) and carried out in accordance to the declaration of Helsinki.

3.9 Supplementary materials

Supplementary material associated with this chapter can be found in Appendix A.

Chapter 4

Tibio-femoral kinematics of the healthy knee joint throughout complete cycles of gait activities

adapted from:

Barbara Postolka[*1], Pascal Schütz[*1], Sandro F. Fucentese[2], Michael A.R. Freemann[3†], Vera Pinskerova[4], Renate List[1,5], William R. Taylor[1]

[*]These authors contributed equally to this work

[†]Died 14^{th} September 2017

[1]Institute for Biomechanics, ETH Zürich, Zürich, Switzerland

[2]Balgrist University Hospital, Zürich, Switzerland

[3]Royal London Hospital, London, United Kingdom

[4]Medical Faculty, Charles University, Prague, Czech Republic

[5]Human Performance Lab, Schulthess Clinic, Zürich, Switzerland

J Biomech, 110:109915, 2020

DOI: 10.1016/j.jbiomech.2020.109915

open access

Keywords

in vivo knee kinematics, tibio-femoral kinematics, fluoroscopy, gait, stair descent, ramp descent

4.1 Abstract

Accurate assessment of 3D tibio-femoral kinematics is essential for understanding knee joint functionality, but also provides a basis for assessing joint pathologies and the efficacy of musculoskeletal interventions. Until now, however, the assessment of functional kinematics in healthy knees has been mostly restricted to the loaded stance phase of gait, and level walking only, but the most critical conditions for the surrounding soft tissues are known to occur during high-flexion activities. This study aimed to determine the ranges of tibio-femoral rotation and condylar translation as well as provide evidence on the location of the centre of rotation during multiple complete cycles of different gait activities.

Based on radiographic images captured using moving fluoroscopy in ten healthy subjects during multiple cycles of level walking, downhill walking and stair descent, 3D femoral and tibial poses were reconstructed to provide a comprehensive description of tibio-femoral kinematics.

Despite a significant increase in joint flexion, the condylar antero-posterior range of motion remained comparable across all activities, with mean translations of 6.3 - 8.3 mm and 7.3 - 9.3 mm for the medial and lateral condyles respectively. Only the swing phase of level walking and stair descent exhibited a significantly greater range of motion for the lateral over the medial compartment. Although intra-subject variability was low, considerable differences in joint kinematics were observed between subjects. The observed subject-specific movement patterns indicate that accurate assessment of individual pre-operative kinematics together with individual implant selection and/or surgical implantation decisions might be necessary before further improvement to joint replacement outcome can be achieved.

4.2 Introduction

Kinematics of the human knee are guided by an interconnected system of bones, soft tissue structures and muscles acting around the joint. The resulting joint function in healthy knees is known to exhibit motion in all six degrees of freedom, presenting a complex set of translations

and rotations [1]. Accurate knowledge of tibio-femoral movement can hence provide critical information for assessing knee joint functionality [6], but also lay the foundations for understanding joint pathologies and musculoskeletal interventions. Total knee arthroplasty (TKA) or ligament reconstruction surgeries generally aim to restore pain-free functionality to the joint, based on physiological kinematics. However, the motion patterns of the native tibio-femoral joint itself are still discussed controversially [24, 31, 51, 74, 84]. Nevertheless, novel implant designs have been introduced that aim to mimic healthy joint kinematics, even though a comprehensive understanding of tibio-femoral kinematics during different gait activities remains missing.

While early studies used cadaveric material to examine tibio-femoral motion, optical motion capture using skin-mounted markers has become commonplace for assessing dynamic joint function. However, these measurements are known to be critically affected by soft tissue artefact (STA) [1, 7, 8]. Errors associated with STA can be avoided using pins screwed directly into the subjects' bones [15, 16], but such procedures are highly invasive and therefore limited to small cohort studies. To directly assess tibio-femoral kinematics in a less invasive manner, single-plane [24, 26–28, 44, 188] and dual-plane [29–32] fluoroscopic analyses have provided valuable and accurate data. The predominant drawback of most systems, however, relates to the small size and static nature of the intensifier, hence restricting measurements to a limited field-of-view. Consequently, most studies have analysed quasi-static activities such as knee bending, squatting and sit-to-stand or assessed only a portion of the gait cycle [24, 28, 31, 39, 42, 44, 47, 51]. To overcome the limitations of static imaging set-ups, procedures to enhance the fluoroscopic field-of-view have been investigated [32]. Moreover, mobile fluoroscopic systems have emerged that allow tracking of the knee during dynamic movements [54] and consecutive cycles of gait activities [30, 188].

Due to their strong radiographic image contrast and associated ease of 2D/3D registration to fluoroscopic images, the kinematics of total knee replacements have been studied in detail [24, 47, 55, 193, 194, 197]. The movement patterns of the natural knee have, however, proven far more difficult to access. While most available studies have evaluated the loaded stance phase of walking [13, 16, 24, 31, 51, 84], only few studies have successfully examined tibio-femoral kinematics over a complete cycle of walking [1, 15, 32, 74]. While consistent findings were presented for joint flexion, with a first peak observed at contralateral toe-off and a maximum knee flexion shortly after toe-off [1, 13, 15, 16, 31, 32, 74, 82, 85], contradictory patterns were reported for the other two rotations. Most studies observed an internally rotated tibia at heel-strike, followed by further internal rotation during early stance phase, reaching a first peak shortly after contralateral toe-off [1, 15, 16, 31, 32, 74, 82]. The tibia is then thought to rotate externally through

mid-stance, before rotating internally once again prior to toe-off [15, 16, 31, 32, 74]. Contrary to this common understanding of knee motion, tibial external rotation during early stance phase was described in two studies [13, 51], where tibial internal rotation during mid-stance was followed by external rotation from 66% of the stance phase until toe-off. In the few studies that were able to assess the unloaded swing phase, peak tibial internal rotation was found shortly after toe-off, followed by external rotation until just before heel-strike, with tibial internal rotation occurring in preparation for the following heel-strike [1, 15, 74]. Throughout the complete gait cycle, minimal changes in abduction/adduction were observed, but with clear subject-specific differences [1, 15, 31].

Only few studies have examined the antero-posterior (A-P) translation of the two femoral condyles relative to the tibia individually. Here, a larger translation has generally been observed for the lateral compared to the medial condyle during the loaded stance phase [24, 51], as well as over complete gait cycles [74], indicating an overall medial centre of rotation (CoR). In contrast, Koo & Andriacchi [84] observed more translation of the medial compared to the lateral condyle during the loaded stance phase of gait, which was later supported by Kozanek and co-workers [31].

Beyond these reports, quantifying knee motion during more challenging activities of daily living such as downhill walking and stair descent are critical for understanding knee function. In the limited literature, no consistent trend of A-P translation of the medial versus the lateral condyle was reported for either of the two activities, and analysis of the unloaded swing phase remains missing [24, 51, 92].

As a result, tibio-femoral movement patterns during functional gait activities are still discussed controversially. Importantly, comparison of condylar A-P translation is complicated by the method used for analysing the movement: the tibio-femoral contact path [24, 51, 74], geometric condylar centres [31, 74], or points on the transepicondylar axis [31] have all been used to describe condylar translation, plausibly also contributing to the inconsistent observations. However, it also remains unclear whether the observed variations resulted from differences in performing the activities, the cohorts studied, or simply because of variability in soft tissue structure or anatomy. Therefore, the aim of this study was to determine the ranges of tibio-femoral rotation and condylar translation during complete cycles of free level walking, downhill walking, and stair descent, as well as provide evidence on the location and possible movement of the centre of joint rotation in the transverse plane in healthy knees.

4.3 Methods

4.3.1 Subjects

Ten subjects (5 female/5 male, aged 23.7 ± 3.2 years, BMI 21.7 ± 2.2 kg/m^2) provided written, informed consent to participate in this study, which was approved by the local ethics committee (KEK-ZH-Nr. 2016-00410). All subjects underwent a clinical knee examination (including testing of ligament condition) by an experienced knee surgeon, and subject-specific limb alignment (mean varus angle of 0.6 ± 1.4°) was evaluated using a biplanar X-ray system (EOS imaging, France) in a standing position [116]. Subjects with significant problems at the lower extremities or exhibiting a limb alignment > 3° varus/valgus were excluded from this study.

4.3.2 Measurement set-up

Tibio-femoral kinematics were assessed using the ETH moving fluoroscope [188], synchronised with a 22 camera optical motion capture system (Vicon MX System, Oxfords Metrics Group, UK) as well as five floor-mounted force plates (Kistler AG, Switzerland), while an additional two mobile force plates instrumented the ramp and stairs respectively (Figure 4.1). The subjects performed all motion tasks in a pair of self-selected sports shoes.

4.3.3 Motion tasks

After a standing trial and activity-specific familiarisation trials, all subjects were measured throughout at least five valid cycles each of straight level walking, downhill walking (10° declined slope), and stair descent (three steps, each 18 cm in height) – in this study collectively considered to be gait activities. Trials were considered valid when the knee remained within the field-of- view of the image intensifier throughout the stance as well as the swing phase, and all force plates were hit correctly. The ground reaction forces were used to determine heel-strike and toe-off with a threshold of 25 N. For downhill walking, the second heel-strike, marking the end of swing phase, was defined based on the trajectory of a heel marker. Overall, for each participant the mean dose area product (DAP) was 7.9 ± 1.2 Gycm^2 (diameter image intensifier 30.5 cm) leading to a total average effective dose of 0.11 ± 0.02 mSv for the fluoroscopic measurement.

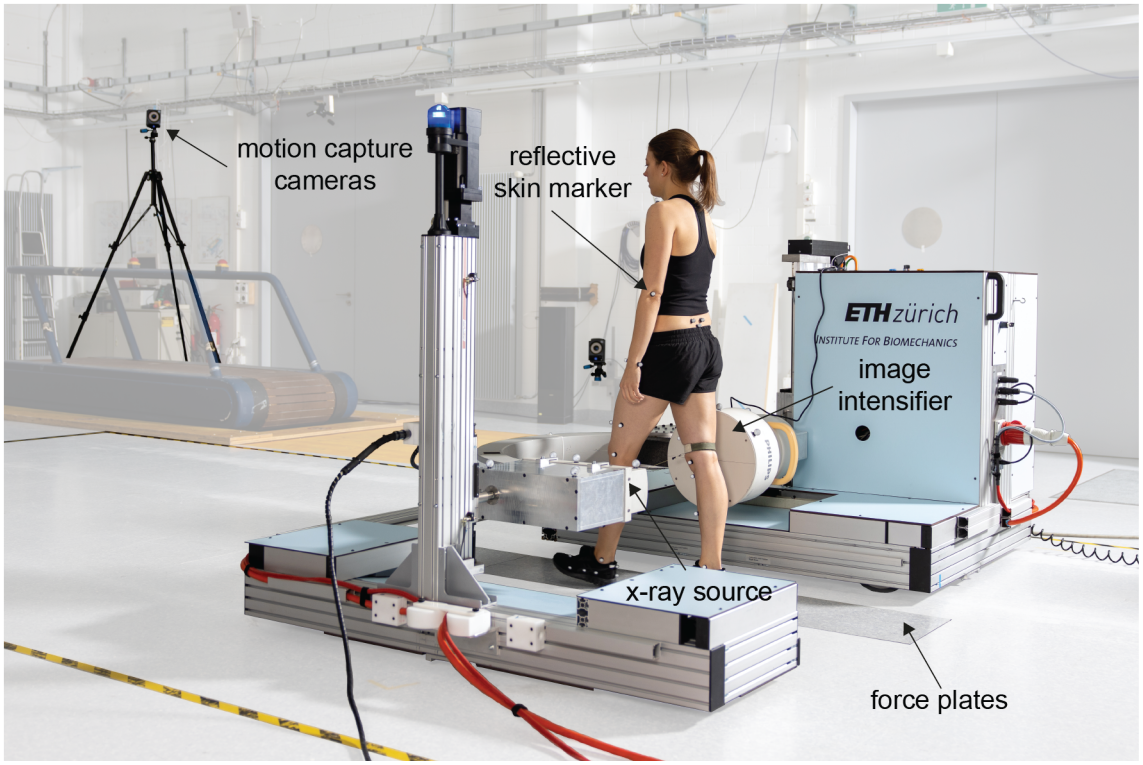

Figure 4.1: Measurement set-up during level walking. Radiographic images of the knee were captured using a moving fluoroscope, imaging at 25 Hz (1 ms shutter time) with an image resolution of 1000 x 1000 pixels [135, 188]. The moving fluoroscope was equipped with five optical markers on the x-ray source and six on the image intensifier to track its position [188]. Fifty-five skin markers, placed at specific anatomical locations [198], were tracked at 100 Hz using a 22 camera system (Vicon MX system, Oxford Metrics Group, UK). Five force plates embedded in the floor (decoupled from the surrounding ground) and two mobile force plates mounted on the ramp and stairs (Kistler Instrumentation, Switzerland) were used to measure undisturbed ground reaction forces at a sampling frequency of 2000 Hz.

4.3.4 3D tibio-femoral kinematics

Subject-specific volumetric models were obtained based on a CT scan of each subject's knee (approximal 20 cm proximal/distal of the joint line, resolution 0.5 x 0.5 mm, slice thickness 1 mm), followed by manual segmentation of the data using the open-source software MITK-GEM [187]. All fluoroscopic images were distortion corrected and the optical projection parameters (focal distance, principal point) were determined [135]. The 3D position and orientation of the femur and tibia were evaluated using a semi-automatic 2D/3D registration software [199], with reported mean absolute errors of $< 1^\circ$ for rotations around all three axes, < 0.6 mm for in-plane, and < 7.1 mm for out-of-plane translations using artificial bones with radiopaque image properties.

Local femoral and tibial anatomical coordinate systems were established to calculate relative

tibio-femoral rotations (Figure 4.2 A&B) [62]. The functional flexion axis (FFA) was defined based on kinematics derived from the fluoroscopic imaging data of a maximal deep knee bending trial using the symmetrical axis of rotation approach [67]. Condylar A-P location was calculated based on a medial (FFA_P$_{med}$) and lateral (FFA_P$_{lat}$) point on the functional flexion axis of the femur (Figure 4.2 C). Translation of each femoral condyle was then described as the movement of these points with respect to the mid-coronal plane of the tibia. All A-P translations were scaled using a subject-specific coefficient, scaled to a ratio of the mean condylar width divided by the subject's condylar width [74]. To allow comparison and interpretation throughout complete gait cycles, tibio-femoral kinematic data was linearly interpolated to 101 data points. To allow comparison of joint kinematics against other studies, tibio-femoral translation is additionally presented using the nearest point (N_P) approach (same normalisation and interpolation) on the surface of each femoral condyle (N_P$_{med}$ and N_P$_{lat}$) relative to a plane parallel to the tibial articular surface, as described by Asano and co-workers [49].
Finally, the CoR in the transverse plane was calculated using the symmetrical centre of rotation estimation based on the locations of FFA_P$_{med}$ and FFA_P$_{lat}$ [200].

4.3.5 Statistics

A total of four mixed-model analysis of variances (ANOVAs) with subject as random effect were performed. Three mixed-model ANOVAs were performed to investigate the influence of the task and gait phase on the ranges of tibio-femoral rotation using the ranges of rotation (flexion/extension, ab/adduction, tibial internal/external) as the dependent variables, with task (three levels: level walking, downhill walking, stair descent) and gait phase (two levels: stance phase, swing phase) as independent variables. One ANOVA was applied to test the effect of task, side, and gait-phase on the range of A-P translation (FFA_P approach). Here, the range of A-P translation was set as the dependent variable, while task (three levels: level walking, downhill walking, stair descent), gait phase (two levels: stance phase, swing phase) and side (two levels: medial A-P, lateral A-P) were set as the independent variables. The least significant differences approach was used for post-hoc comparisons and the levels of significance were corrected for multiple comparisons, starting at $\alpha = 0.05$, using Bonferroni correction. No statistical tests were performed for the A-P translation of the N_P approach. Statistics were conducted in SPSS (SPSS 24, IBM, USA).

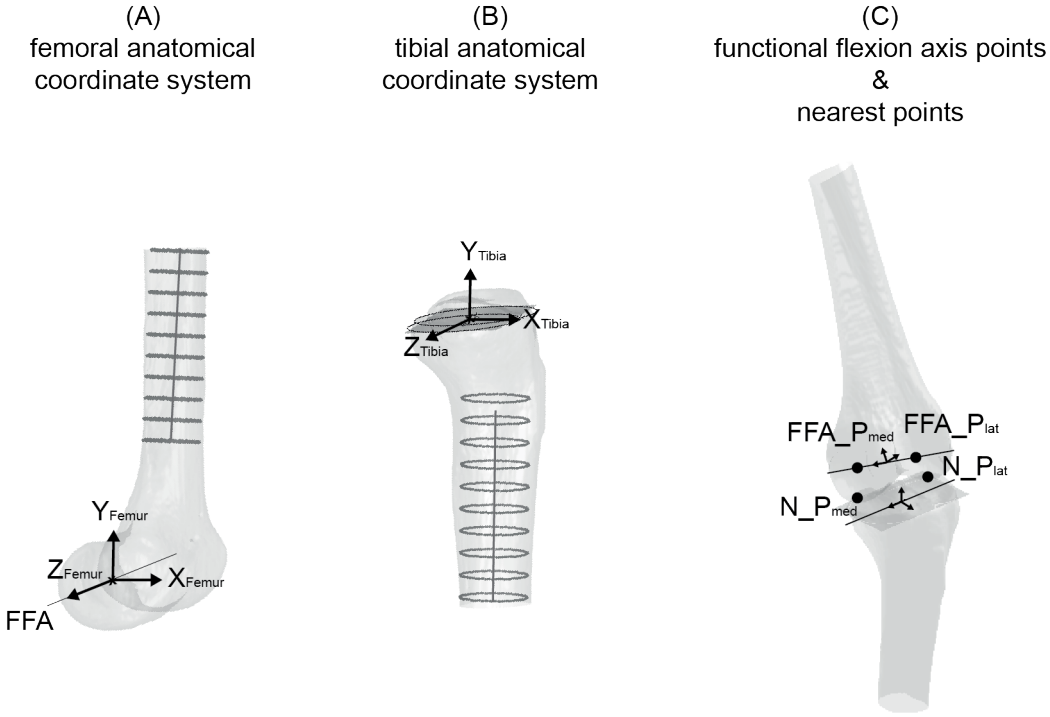

Figure 4.2: (A) Femoral anatomical coordinate system pictured in a left femur. Based on the fluoroscopic imaging data of a maximal deep knee bending trial, the functional flexion axis (FFA) was defined using the functional symmetrical axis of rotation approach [67]. The origin was defined as the midpoint between the most medial and lateral point of the femur on the FFA. The medio-lateral axis (Z_{Femur}), was oriented along the FFA, pointing medially. A cylinder (depicted as multiple circles) was then fitted to the most proximal 10 cm of the femoral shaft, defining the shaft axis. The antero-posterior axis (X_{Femur}) was orthogonal to Z_{Femur} and the shaft axis. In right knees, X_{Femur} pointed posterior, while in left knees it was directed anteriorly. The longitudinal axis (Y_{Femur}) was orthogonal to both X_{Femur} and Z_{Femur} to complete the right-handed coordinate system. (B) Tibial anatomical coordinate system pictured in a left tibia. A plane parallel to the posterior tibial slope was constructed, resecting the condylar cartilage. Two circles were manually fitted in the plane, such that the maximum possible circle perimeter fitted to the tibial cortex. The midpoint between the two circles' origins was set as the origin of the tibial anatomical coordinate system. Similar to the femur, a cylinder was fitted to the most distal 10 cm of the tibial shaft (depicted as multiple circles). However, for the tibia, the longitudinal axis (Y_{Tibia}) was consistent with the orientation of the shaft axis, but passed through the origin. The antero-posterior axis (X_{Tibia}) was orthogonal to Y_{Tibia} and the line connecting the circle centres. Similar to the femur, the X_{Tibia} pointed posteriorly in right knees, but anteriorly in left knees. The medio-lateral axis (Z_{Tibia}) was orthogonal to the X_{Tibia} and Y_{Tibia} to complete the right-handed coordinate system. (C) The nearest points (N_P_{med} & N_P_{lat}) between the femoral condyles and the tibial plane were calculated as the weighted means of the ten nearest points (mean point separation 0.4 mm) for the medial and the lateral condyles. Two points on the functional flexion axis (FFA_P_{med} & FFA_P_{lat}) were then defined based on the projection of N_P_{med} & N_P_{lat} during standing onto the FFA. These points were used to describe condylar A-P translation relative to the tibia.

4.4 Results

Mean average velocities over the complete gait cycle were 0.87 ± 0.06 m/s during level walking, 0.81 ± 0.07 m/s during downhill walking, and 0.5 ± 0.05 m/s for stair descent.

4.4.1 Tibio-femoral rotations

During standing, a mean knee flexion of -2.6 ± 5.6° and tibial external rotation of 2.8 ± 9.9° (range 13.1° internal to 16.4° external) were recorded.

As expected, a significant increase in range of joint flexion was observed from level walking to downhill walking and stair descent (Table 4.1). For all three activities, the knee joint was slightly flexed at heel-strike, followed by an activity-specific flexion/extension behaviour, with peak knee flexion occurring shortly after toe-off (level walking: 62.8 ± 5.5°; downhill walking: 70.1 ± 4.7°; stair descent 95.0 ± 5.7°) (Figure 4.3).

After heel-strike, the tibia generally rotated internally during the stance phase, reaching a maximum internal rotation shortly before toe-off (level walking: -9.9 ± 6.9°, downhill walking: 10.6 ± 7.7°, stair descent: -12.3 ± 7.6°) followed by an external rotation in preparation for the subsequent heel-strike (Figure 4.3). Initial tibial internal/external rotation at heel-strike was highly subject specific, with individual values ranging from 14.5° internal to 11.1° external rotation between the three activities. However, each subject exhibited consistent internal/external rotation characteristics, with a mean standard deviation (SD) of 1.5 - 3.4° across all subjects.

Repeatable ab/adduction was found for the individual subjects (mean subject SDs: 0.9 - 1.8°), but these were highly individual, and no clear ab/adduction patterns could be established over a complete gait cycle for any of the activities (Figure B.1).

4.4.2 Condylar translation

During standing, the mean FFA_P$_{med}$ (-10.6 ± 7.0 mm) and FFA_P$_{lat}$ (-8.7 ± 5.7 mm) over all subjects were located posterior to the tibial mid-coronal plane.

Following a short posterior translation after heel-strike, FFA_P$_{med}$ moved anteriorly, peaking shortly before toe-off for both level and downhill walking. This motion was followed by a short posterior and again anterior translation, reaching a second peak before returning to its initial position at heel-strike (Figure 4.4). For all three activities, a significant difference was found for the amount of A-P translation of the FFA_P$_{med}$ between the stance and the swing phases

Table 4.1: Range of motion (RoM) for all three tibio-femoral rotations. Mean and standard deviations across all ten subjects are presented for the loaded stance and unloaded swing phases of level walking, downhill walking and stair descent.
Flex/ex: flexion/extension, int/ext: tibial internal/external rotation, ab/add: abduction/adduction

RoM[°]	**loaded stance phase**			**unloaded swing phase**		
	flex/ex	int/ext	ab/add	flex/ex	int/ext	ab/add
level walking	39.1 ± 4.8 ^{*a,b}	12.9 ± 2.1	5.4 ± 1.5 ^{*d}	65.6 ± 4.0 ^{*f,g}	12.2 ± 3.9	6.3 ± 1.7
downhill walking	55.3 ± 3.2 ^{*a,c}	13.5 ± 3.1	5.2 ± 1.1 ^{*e}	72.0 ± 3.4 ^{*f,h}	11.6 ± 3.3 ^{*i}	6.2 ± 1.8
stair descent	79.9 ± 5.2 ^{*b,c}	13.0 ± 2.6	6.5 ± 1.2 ^{*d,e}	93.1 ± 4.6 ^{*g,h}	13.3 ± 2.4 ^{*i}	5.6 ± 1.3

*significant differences are presented between lettered pairs (a - i) based on the adjusted level of significance of $\alpha = 0.017$

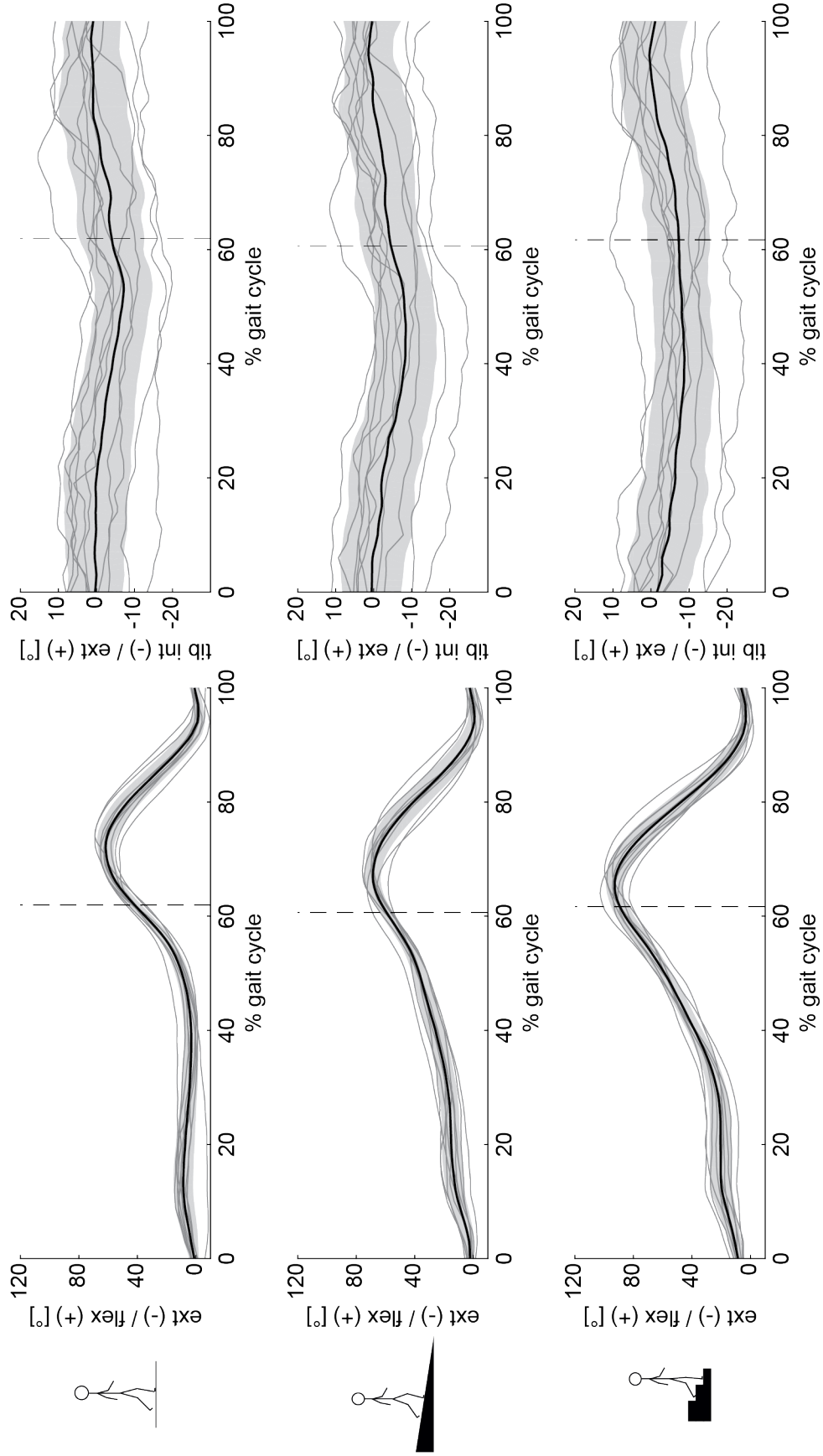

Figure 4.3: Tibio-femoral flexion/extension (flex/ex) and tibial internal/external rotations (tib int/ext) throughout complete cycles of level walking (top), downhill walking (middle) and stair descent (bottom). The mean across all subjects (black line), standard deviations across all subjects (grey shading), as well as means for every subject (dark grey lines) are presented. The average instance of toe-off across all subjects is indicated as a vertical dashed line.

(Table 4.2). The FFA_P_{lat} moved posteriorly after heel-strike, reaching a minimum around toe-off. Extension of the knee during the unloaded swing phase was then associated with an anterior translation of the FFA_P_{lat} for all three activities and all subjects (Figure 4.4). Overall, FFA_P_{med} and FFA_P_{lat} showed comparable ranges of A-P translation, with only the swing phase of level walking and stair descent showing significant differences (Table 4.2). Intra-subject repeatability was high for both FFA_P_{med} and FFA_P_{lat} A-P translation, with overall mean SDs of only 0.8 - 2.0 mm across all repetitions of each different task (Figure B.2, B.3 and B.4). For comparison, the N_Ps were located anteriorly to the mid-coronal plane while standing (N_P_{med}: 4.7 ± 5.4 mm; N_P_{lat}: 11.3 ± 9.7 mm). As opposed to the FFA_P, a considerable difference between the A-P translations of N_P_{med} compared to N_P_{lat} was found for both phases of all three activities (Table 4.2). While N_P_{med} showed a consistent pattern of A-P translation for all subjects over all activities, high inter-subject variability was observed for N_P_{lat}, especially during mid-stance of level walking and shortly before heel-strike in all activities (Figure 4.4). However, the mean intra-subject variability (1.2 - 3.0 mm) was comparable to both FFA points throughout the entire gait cycles (Figure B.2, B.3 & B.4).

4.4.3 CoR in the transverse plane

Over all subjects, a slightly medial mean CoR was observed for the entire gait cycle of all activities with the swing phase (level walking: 13.7 ± 14.4 mm; downhill walking: 11.7 ± 9.0 mm; stair descent: 14.6 ± 9.8 mm, all medial) nearly always presenting a more medial CoR than the stance phase (level walking: 7.2 ± 7.4 mm; downhill walking: 6.7 ± 8.8 mm; stair descent: 9.4 ± 14.3 mm, all medial) (Figure 4.5, Table B.1 - B.9). Intra-subject variability of the location of the FFA_P_{med} and FFA_P_{lat} within a task was high (Figures B.5 - B.34), and resulted in SD's ranging from 0.9 - 23.3 mm for the mean location of the subject-specific CoR over a gait phase (Table B.1 - B.9).

4.5 Discussion

A comprehensive understanding of human knee joint kinematics is critical for guiding the design of total knee replacement components that aim to mimic healthy joint motion. Until now, movement of the tibio-femoral joint has been discussed controversially, but only rarely analysed over multiple cycles of different activities. For the first time in healthy knees, moving fluoroscopy has

Table 4.2: Range of antero-posterior (A-P) translation for the medial and lateral condyle point using the functional flexion axis (FFA_P$_{med}$ & FFA_P$_{lat}$) and the nearest point (N_P$_{med}$ & N_P$_{lat}$). Mean and standard deviations across all ten subjects are presented for the loaded stance and unloaded swing phases of level walking, downhill walking and stair descent.

RoM [mm]		**loaded stance phase**		**unloaded swing phase**	
		medial condyle	lateral condyle	medial condyle	lateral condyle
FFA_P	level walking	8.3 ± 1.8 ^{*k}	8.2 ± 1.4	6.6 ± 1.6 ^{*k,o}	8.1 ± 1.8 ^{*o}
	downhill walking	8.0 ± 2.5 ^{*l}	8.5 ± 1.5 ^{*m}	6.3 ± 1.7 ^{*l}	7.3 ± 1.9 ^{*m,q}
	stair descent	8.2 ± 2.6 ^{*n}	9.3 ± 2.1	6.7 ± 1.7 ^{*n,p}	9.1 ± 2.2 ^{*p,q}
N_P	level walking	10.3 ± 3.2	15.5 ± 6.1	13.3 ± 4.3	21.7 ± 8.5
	downhill walking	9.5 ± 2.5	17.4 ± 8.8	13.0 ± 4.2	21.8 ± 8.7
	stair descent	9.7 ± 2.1	15.4 ± 6.4	10.7 ± 3.3	20.9 ± 6.3

*significant differences are presented between lettered pairs (k - q) based on the adjusted level of significance of $\alpha = 0.0083$
no statistical tests were conducted for the N_P approach

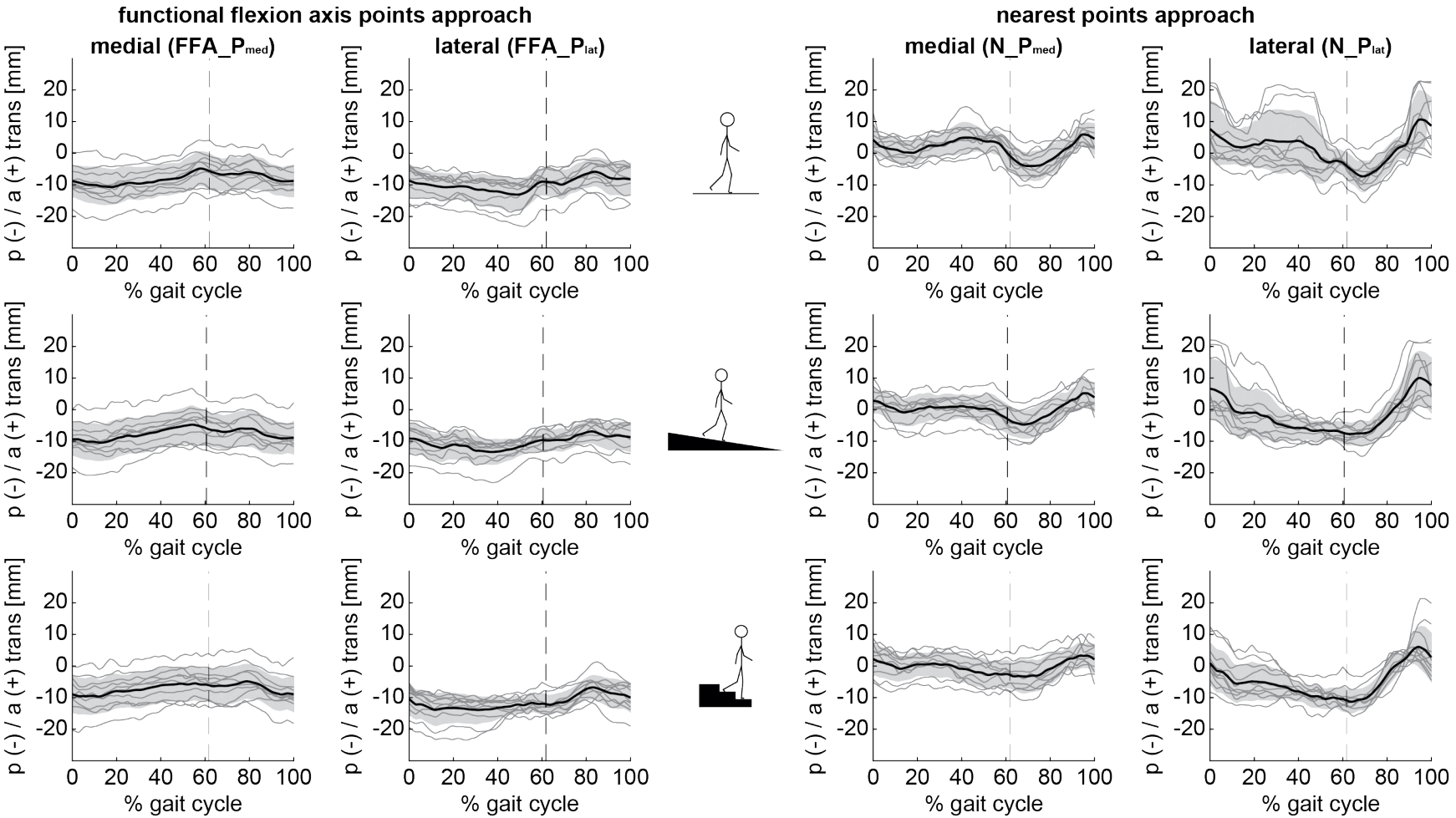

Figure 4.4: Antero (a) – posterior (p) translation of the medial and lateral functional flexion axis points (left) as well as the nearest points (right) throughout complete cycles of level walking (top), downhill walking (middle) and stair descent (bottom). The mean across all subjects (black line), standard deviations across all subjects (grey shading), as well as means for every subject (dark grey lines) are presented. The average instance of toe-off across all subjects is indicated as a vertical dashed line.

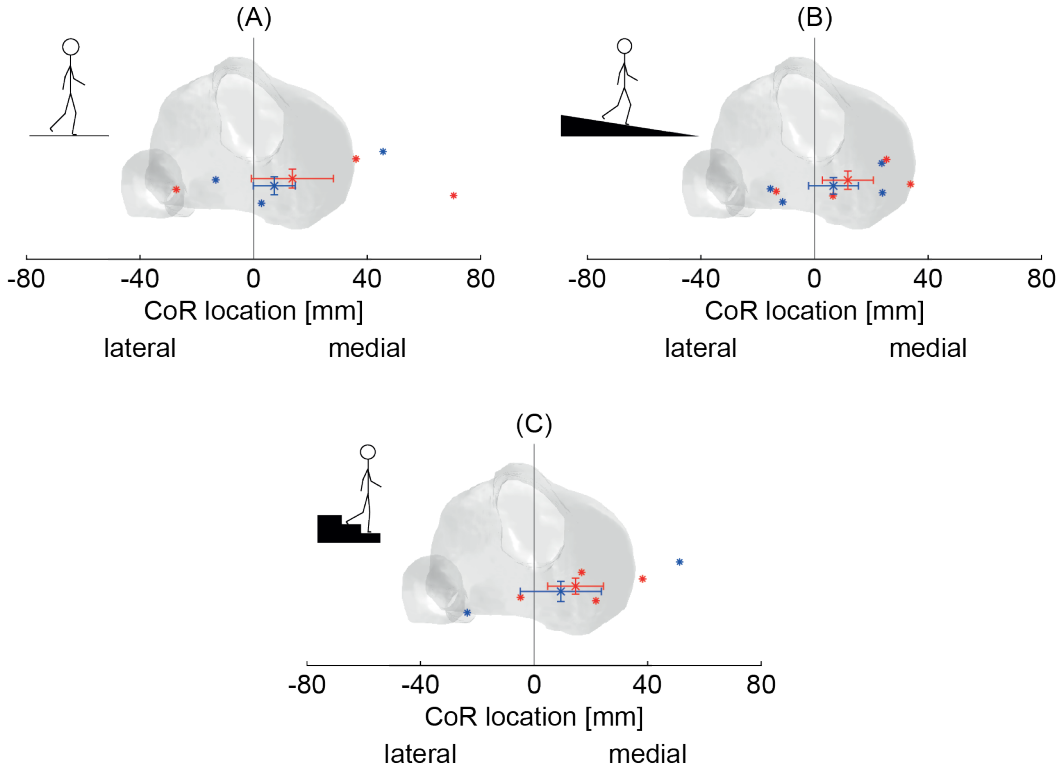

Figure 4.5: Location of the centre of rotation (CoR) shown on the plateau of a left tibia during the loaded stance (blue) and the unloaded swing (red) phases of level walking (A), downhill walking (B) and stair descent (C). The mean across all subjects as well as the standard deviations in the antero-posterior and medio-lateral directions are indicated with whiskers. The most extreme points in each direction across all subjects and trials are presented as *.

been used in this study to determine the *in vivo* tibio-femoral rotations and translations that occur throughout complete cycles of downhill walking and stair descent, in addition to free level walking, using the same subject cohort as well as the same measurement set-up. Only a limited task-dependency was observed for ranges of A-P translation, despite clear differences in knee flexion angles (Table 4.1, 4.2). Overall, the data have revealed a predominantly central to medial CoR in the transverse plane, even though it is located laterally in some individuals and during some phases of different activity cycles.

The flexion/extension patterns during level walking found in this study were consistent with those reported in the literature [15, 74]. Furthermore, our tibio-femoral internal-external rotation patterns were comparable to the limited evidence available on complete gait cycles during level walking [74], even though the absolute values differed. This variation likely originates from differences in the definition of the femoral and tibial anatomical coordinate systems [15, 74]. In our study, similar ranges of A-P translation were observed for both compartments (using FFA_P$_{med}$ and FFA_P$_{lat}$), but with larger A-P translations on the lateral side of the joint for the unloaded swing phase of level walking and stair descent. Such data is consistent with

previous studies that suggested a medial pivot during unloaded flexion [20, 43]. The magnitude of the overall translations of the medial compartment (FFA_P$_{med}$) were comparable to values presented in the literature, whereas for the lateral compartment (FFA_P$_{lat}$), contradictory results were found [31, 74]. As the subject-specific FFA was optimised over the full range of motion during deep knee bending, the true instantaneous flexion axis at a specific instant of time might vary from the mean FFA, possibly introducing an A-P translation error around the flexion axis. Further investigation is clearly required in order to understand the influence of such secondary errors, including their role relative to different activities and flexion axis approaches.

To allow cross-study comparison, we have also presented condylar kinematics using the nearest point approach. While the range of A-P translation for some subjects was in line with the literature [74], others exhibited a substantially larger range of A-P translation. An assessment of the femoral geometries revealed a relatively flat region on the lateral condyle (similar to previous observations in cadaveric studies [20]) for some subjects, plausibly resulting in a "jump" of the N_P$_{lat}$ during phases of knee extension (Figure 4.4, right). As a result, it seems that this method is sensitive to local contact conditions, but does not necessarily describe the relative movement between the tibia and the femur. Additional research into the influence of subject-specific anatomy on the translation of the contact points is thus needed before a thorough understanding of the large variability in A-P translation between subjects can be gained.

The mean CoR was located on the medial tibial plateau for all three activities. Nevertheless, the location of trial specific mean CoRs varied among subjects and tasks (Table B.1 - B.9). These results are generally in line with previous findings [24, 74], although a mean lateral CoR has also been presented [31, 84]. Calculation of the mean CoR over the complete gait cycle seems to be more robust than for either the stance or swing phase individually, resulting in SDs of less than 5 mm for most of the subjects, in line with previous research [24]. Furthermore, individual movement patterns were clearly observed, thus emphasising the need to analyse multiple trials for individual subjects.

Overall, the majority of studies fail to capture the unloaded stance phase, which, based on the results of our study, differs from the loaded stance phase. Analysis of this phase of gait provides clear insights into the largest joint rotations that are critical for understanding soft tissue loading as well as possible overloading [201, 202]. Accurate assessment of complete cycles of daily activities could therefore be key for planning subject-specific component implantation to achieve pain-free post-operative outcome.

Walking with the moving fluoroscope potentially influenced the natural gait patterns of our subjects in the present study, especially as walking speeds are known to be reduced compared to free

level walking [143]. However, the changes in gait parameters have been shown to be small, and gait patterns remain comparable to those exhibited during slow walking [203]. While kinematics captured in this study may not be completely natural, they still represent the state-of-the-art in understanding joint motion over complete cycles and for different daily activities. The predominant drawback, however, is the subject's exposure to radiation, necessitating that data collection using such technologies is kept to a minimum.

Overall, comparison with the existing literature is challenging, mainly due to the variety of approaches used. While the geometric centre axis as well as the transepicondylar axis are widely used, their definition is highly dependent on the protocol and experience of the examiner. Within this study, we aimed to minimise the observers input to receive an independent axis that is only based on the subject's deep knee bending movement (using the fluoroscopic based reconstruction of the bone segments). Only the tibial coordinate system in our study was defined based on subject-specific anatomy, but it is indeed entirely plausible that individual differences could have added variation to the presented results.

Although the current single-plane set-up in combination with the semi-automatic 2D/3D registration possesses high accuracy in the in-plane direction [199], a combination of errors for different segments could plausibly lead to larger total relative errors. The greatest source of error is likely to arise from the contralateral knee crossing through the image twice during each gait cycle, hence cumulatively limiting the accuracy of the 2D/3D registration at these instances. In addition, out-of-plane registration errors could play a role in the determination of the CoR in the transverse plane. To overcome this limitation as well as to improve out-of-plane accuracy, a dual-plane set-up could provide considerable advantages, however this would increase the overall radiation dosage applied to the subject.

This study provides the first analysis of knee kinematics during multiple complete cycles of free level walking, downhill walking and stair descent. The results suggest that the CoR is primarily located medially, but varies between subjects and gait phases. It therefore seems that the recent movement towards medial congruent implant designs [194] is warranted, but further investigation is clearly needed to elucidate the role of limb alignment and anatomical inter-subject variability on knee joint kinematics, particularly with regard to the loading and possible overloading of the surrounding soft tissues [201]. Importantly, however, the subject-specific movement patterns observed in this study indicate that individual implant selection and/or surgical implantation decisions might be necessary before further improvement to joint replacement outcome can be achieved, possibly supported by the accurate assessment of each individual's pre-operative knee joint kinematics to guide clinical decision-making.

4.6 Acknowledgement

The study was partially financed by the Commission for Technology and Innovation (Bern, Switzerland, Project Number 17078.1 PFLS-LS) and Medacta International SA (Castel San Pietro, Switzerland). The sponsor was not involved in the data collection, nor in the analysis or the interpretation of the data. Furthermore, the authors would like to thank all the subjects who participated in the study, as well as Nathalie Kühne (Balgrist University Hospital) for the organisation of the clinical examinations and all the students for their help in the data collection.

4.7 Conflict of interest statement

RL has received speaker's fees from Medacta. SFF and VP receive advisory fees from Medacta as part of their consultancy work. MARF has received consultancies from Medacta.

4.8 Supplementary materials

Supplementary material associated with this chapter can be found in Appendix B.

Chapter 5

Interpretation of natural tibio-femoral kinematics critically depends upon the kinematic analysis approach: A survey and comparison of methodologies

adapted from:

Barbara Postolka[1], William R. Taylor[1], Katrin Dätwyler[1], Markus O. Heller[2], Renate List[1,3], Pascal Schütz[1]

[1]Institute for Biomechanics, ETH Zürich, Zürich, Switzerland

[2]School of Engineering, University of Southampton, Southampton, United Kingdom

[3]Human Performance Lab, Schulthess Clinic, Zürich, Switzerland

in preparation

Keywords

in vivo knee kinematics, tibio-femoral kinematics, kinematic analysis, transversal plane kinematics, antero-posterior translation

5.1 Abstract

A variety of kinematic conventions based on different coordinate systems and rotational axes have been proposed and applied in an attempt to describe tibio-femoral motion. However, no consensus has yet been reached on the physiological ranges of A-P translation of the condyles nor the location of the centre of rotation. Therefore, the goal of this study was to compare the magnitudes of transverse-plane knee joint kinematics as well as the centre of rotation derived from identical dynamic videofluoroscopic data of ten subjects during continuous flexion as well as complete gait cycles using six different kinematic analysis approaches.

The condylar A-P translations showed observable differences between the approaches. In particular, the contact point approaches (nearest point and tibio-femoral separation) revealed significantly different A-P translation compared to the femur fixed axes for certain flexion angles and phases of the gait cycle. For all approaches and both activities, the resulting position of the centre of rotation in the transverse plane was located slightly medially. However, medio-lateral variability between subjects was high, resulting in a lateral centre of rotation for certain subjects. Our analysis achieved similar A-P translations to previous studies, but the interpretations of joint kinematics were considerably different depending on the analysis approach applied, despite our analysis of identical tibio-femoral joint movement. Axis approaches that are based on anatomical landmarks seem to be subject to high levels of cross-talk. Our recommendation is therefore that joint translations based on functional flexion axes should be reported in preference to anatomically based axes. Moreover, we recommend that joint kinematics are reported using at least two different approaches in order to provide standardised comparisons and reach consensus on the interpretation of tibio-femoral joint kinematics during functional activities *in vivo*.

5.2 Introduction

The accurate assessment of tibio-femoral kinematics in both healthy and pathological joints is essential for the quantification and understanding of not only knee joint functionality [5, 50] but also for developing joint prostheses [55, 194]. The motion of the knee joint is thought to be characterised by a complex combination of mainly flexion/extension together with internal/external rotation and antero-posterior (A-P) translation of the femur relative to the tibia [1]. Despite the employment of novel measurement techniques based on magnetic resonance imaging (MRI) [19, 21, 43] or videofluoroscopy [24, 26–32, 44, 188] to accurately assess knee joint kinematics, scientific and clinical agreement on the movement patterns of natural knees remains lacking. Critically, no consensus has yet been reached on the physiological range of A-P translation of the medial versus the lateral epicondyles (pivoting movement of the femoral epicondyles on the tibial plateau), or the path of the centre of rotation (CoR) during dynamic and functional activities. As a result, our understanding of the parameters that govern joint movement, and consequently the effect of loading, limb alignment, pathology, and prosthesis design remain limited.
From a mechanical perspective, it is possible for many trajectories to be followed by a joint with six degrees of freedom such as the knee. Specifically, the difficulties in describing three dimensional (3D), time-dependent, multi-segment kinematics within a static, two dimensional (2D) representation are evident. Consequently, a variety of kinematic conventions based on different segment proximity measures, coordinate systems, and/or rotational axes, have been proposed and applied to describe tibio-femoral motion. The proposed approaches can generally be categorised into three groups:

1. Contact points:

   Here, a point on each of the medial and lateral condyles is defined to describe the location of contact between the tibial and femoral surfaces. These are typically the nearest points [46, 49] or the lowest point of each femoral condyle in a tibial coordinate system [47]. With knowledge of the tibio-femoral cartilage thickness, the centroid of the area formed by the overlap of the femoral and tibial cartilage surfaces can also be defined as the contact point or region [33]. To account for missing information about the tibio-femoral cartilage and its deformation, the geometrical centre of the region having less than 6 mm separation has been considered as acceptable threshold for contact region definition [28].

2. Functional axes:

   Functional axes of rotation are derived from the relative movement between two segments. Different mathematical conventions have been introduced, including axis fitting approaches based on e.g. least square estimates [50, 63–65], mean helical axes [66], or the symmetrical axis of rotation approach (SARA) [67]. In applications assessing knee joint motion, functional axes can either be fixed to the femur or tibia.

3. Anatomical axes:

   Anatomical axes of rotation are usually determined based on clinical definitions and subject-specific anatomical features. While the transepicondylar axis (TEA) is defined according to bone landmarks [68–70], the geometrical centre axis (GCA) or the cylinder axis (CA) are based on the fitting of circular, cylindrical or spherical shapes to the femoral condyles [49, 71, 72]. Similarly, based on the geometry of the femoral surface in contact with the tibia, anterior and posterior circular surfaces can be used to define an extension facet centre (EFC) and a flexion facet centre (FFC) [20]. The respective points are then joined to create a femur fixed axis.

Importantly, these approaches are sensitive to different aspects of intersegmental kinematics and have therefore resulted in conflicting information about the most prevalent location of the transverse plane CoR during loaded flexion tasks (Table 5.1 & 5.2), as well as the stance and swing phases of level walking (Table 5.3). As a result, different conclusions have been drawn regarding the kinematics of the knee:

For loaded knee flexion activities, the lateral condyle showed an overall larger A-P translation compared to the medial condyle for analyses using anatomical axes [19, 21, 40, 41, 43, 49, 50] as well as contact points [24, 28, 33, 34, 36, 42, 46, 49, 51], but some studies have reported almost equal translation for both condylar contact points [37, 38, 43, 47] (Table 5.1 & 5.2). Functional movements such as level walking are discussed more controversially in the literature, however. A medial CoR, indicating more A-P translation of the lateral compared to the medial compartment, was found using contact points [24] but also the GCA [74], as well as the functional flexion axis [204]. Conversely, larger medial than lateral A-P translations were found using GCA, TEA as well as cartilage contact measures [31, 86]. Evidence has also been presented reporting a lateral CoR during the loaded stance phase of level walking [52, 84] (Table 5.3).

Given the current state of research, particularly the inconsistent findings, fundamental questions remain about knee kinematics – not only as to how the natural tibio-femoral joint actually moves under loaded and unloaded conditions – but also what role anatomy and pathology play in

governing changes to tibio-femoral joint motion. This lack of consensus regarding knee kinematics poses obvious barriers, for example to the design of novel implants or the development of specific rehabilitation programs that aim to mimic or restore natural knee function. More than basic differences between study conditions (e.g. patient characteristics, task, measurement technique etc.), it is entirely conceivable that the different kinematic analysis approach and convention used for reporting the study outcomes may have led to misunderstandings and contradictory conclusions of what are, in fact, similar motion patterns. Based on an in-depth survey of the literature (Table 5.1, 5.2 & 5.3), it is hypothesised that different approaches to analyse joint kinematics lead to differences in the interpretation of transverse plane knee joint motion, hence explaining some of the contradictory results reported in the literature. Therefore, the goal of this study, was to compare the magnitudes of transverse plane knee joint motion for a data set of dynamic videofluoroscopy data, analysed using six different kinematic analysis approaches.

5.3 Materials & methods

5.3.1 Tibio-femoral data capture

Kinematic data was acquired for ten healthy subjects (5 female/5 male, aged 23.7 ± 3.2 years, BMI 21.7 ± 2.2 kg/m^2) during standing (2 trials), deep knee bending (continuous knee flexion from full extension to maximum flexion, 3 - 4 trials) as well as complete cycles of level walking (5 - 6 trials) using a dynamic videofluoroscope [188]. A detailed description of the motion tasks and the measurement procedure has been published previously [204], however a brief description is provided here: Single-plane videofluoroscopic images were captured at 25 Hz (1 ms shutter time, 1000 x 1000 pixels image resolution) in combination with ground reaction force data (2000 Hz) using five force plates (2x 9281B, 2x 9285B, 1x 9281C; Kistler AG, Switzerland). The vertical ground reaction force was used to define heel-strike and toe-off during level walking (threshold 25 N). In order to perform 2D/3D registration of the fluoroscopic images, a CT scan of each subject's knee (∼20 cm proximal/distal of the joint space, resolution 0.5 x 0.5 mm, slice thickness 1 mm) was manually segmented to generate subject-specific femur and tibia models [187]. Semi-automatic 2D/3D registration was then performed using the KneeFit software, resulting in registration errors of < 0.6 mm for in-plane translations, < 7.1 mm for out-of-plane translations and $< 1^\circ$ for all rotations [199]. Each frame was examined visually to ensure reasonable medio-lateral alignment between the femur and tibia and corrected where necessary. All subjects

Table 5.1: Part 1: Summary of antero-posterior translations and the centre of rotation during loaded knee flexion using different kinematic analysis approaches

author	**# knees (age)**	**imaging modality**	**RoM evaluated**	**method**	**A-P translation**		**CoR**
					medial	**lateral**	
Asano et al. [49]	6 (25-43 y)	biplane x-ray	0-120°	GCA	3.8mm a	17.8mm p	medial pivot
				NP	0-30°: 6.9mm p 30-120°: -	0-120°: 27.4mm p	medial pivot
Asano et al. [50]	9 (25-43 y)	biplane x-ray	0-90°	FFA	n.a.	n.a.	medial pivot
DeFrate et al. [33]	5 (21-41 y)	dual-plane fluoroscopy	0-90°	NP	4.5±3.3mm p	13.3±5.7mm p	n.a.
Dennis et al. [24]	5	single-plane fluoroscopy	0-90°	CP	n.a.	n.a.	medial pivot
Dennis et al. [46]	10 (22-44 y)	single-plane fluoroscopy	0-120°	NP	1.9±1.9mm p	21.1±9.3mm p	n.a.
Grieco et al. [47]	10 (57.4±7.1 y)	single-plane fluoroscopy	0-120°	NP	0-30°: 4.7±2.2mm p 30-60°: 0.2±1.1mm p 60-90°: 0.4±2.2mm a 90-120°: 0.6±1.6mm a	0-30°: 11.8±4.4mm p 30-60°: 3.2±2.8mm p 60-90°: 1.4±2.7mm p 90-120°: 3.4±5.1mm p	n.a.
Hamai et al. [34]	5 (28-30 y)	single-plane fluoroscopy	85-150°	CP	2mm p	8mm p	medial
Hill et al. [19]	7 (22-35 y)	MRI	-5-90°	EFC/FFC	10-90°: 4mm a	posterior	n.a.

A-P: antero-posterior, CoR: centre of rotation, RoM: range of motion, y: year, a: anterior, p: posterior, GCA: geometric centre axis, EFC: extension facet centre, FFC: flexion facet centre, FFA: functional flexion axis, TEA: transepicondylar axis, NP: nearest point, CP: contact point

Table 5.2: Part 2: Summary of antero-posterior translations and the centre of rotation during loaded knee flexion using different kinematic analysis approaches

author	**# knees (age)**	**imaging modality**	**RoM evaluated**	**method**	**A-P translation**		**CoR**
					medial	**lateral**	
Johal et al. [21]	10 (20-30 y)	MRI	-5-140°	EFC/FFC	-5-90°: 2.2±1.5mm a 90-120°: 3.6±2.0mm p 120-140°: 9.4±2.1mm p	-5-120°: 21.1±4.7mm p 120-140°: 9.8±2.1mm p	n.a.
Komistek et al. [51]	4 (29-44 y)	single-plane fluoroscopy	0-90°	CP	1.5mm p (3.0mm a - 4.6mm p)	14.1mm p (5.8-24.7mm p)	medial pivot
Li et al. [36]	5 (25±5 y)	dual-plane fluoroscopy	0-90°	CP	∼1.5mm p	∼9mm p	n.a.
Li et al. [37]	9 (19-38 y)	dual-plane fluoroscopy	0-90°	CP	11.1±2.4mm p	11.8±4.3mm post	n.a.
Moro-oka et al. [28]	6 (28-31 y)	single-plane fluoroscopy	0-150°	NP	posterior	posterior	>80°: medial pivot
Pinskerova et al. [43]	5	MRI	-5-120°	EFC/FFC CP	- 19mm p	20mm p 22mm p	medial n.a.
Qi et al. [38]	8 (23-49 y)	dual-plane fluoroscopy	-5-150°	CP	11.1±3.3mm p	14.6±3.7mm p	n.a.
Tanifuji et al. [40]	20 (24-61 y)	single-plane fluoroscopy	0-140°	GCA	0-100°: 5.5±3.7mm a 100-140°: 3.9±2.9mm p	0-140°: 15.6±5.0mm p	0-120°: medial pivot
Tanifuji et al. [41]	20 (24-61 y)	single-plane fluoroscopy	0-140°	TEA	0-30°: 3.6±3.0mm a 30-140°: 18.1±3.7mm p	0-140°: 31.7±7.3mm p	n.a.
Yamaguchi et al. [42]	8 (41±7 y)	single-plane fluoroscopy	-10-110°	CP	n.a.	n.a.	medial

A-P: antero-posterior, CoR: centre of rotation, RoM: range of motion, y: year, a: anterior, p: posterior, GCA: geometric centre axis, EFC: extension facet centre, FFC: flexion facet centre, FFA: functional flexion axis, TEA: transepicondylar axis, NP: nearest point, CP: contact point

Table 5.3: Summary of antero-posterior translations and the centre of rotation during level walking using different kinematic analysis approaches

author	**# knees (age)**	**imaging modality**	**gait phase**	**method**	**A-P translation**		**CoR**
					medial	**lateral**	
Dennis et al. [24]	5	single-plane fluoroscopy	stance	CP	0.8mm	7.3mm	medial pivot
Gray et al. [74]	15 (30.5±6.2 y)	dual-plane fluoroscopy	stance & swing	GCA	7.6mm	11.6mm	medial
				NP	9.7mm	15.4mm	n.a.
Komistek et al. [51]	4 (29-44 y)	single-plane fluoroscopy	stance	CP	0.9mm a	4.3mm p	n.a.
Koo & Andriacchi [84]	23 (37±12 y)	skin marker	stance	n.a.	n.a.	n.a.	lateral
Koo & Koo [52]	7 (23±2 y)	dual-plane fluoroscopy	mid swing - mid stance	CP	n.a.	n.a.	lateral
Kozanek et al. [31]	8 (32-49 y)	dual-plane fluoroscopy	stance	TEA	9.7±0.7mm	4.0±1.7mm	n.a.
				GCA	17.4±2.0mm	7.4±6.1mm	n.a.
Liu et al. [86]	8 (32-49 y)	dual-plane fluoroscopy	stance	CP	3.6±0.3mm	1.6±0.4mm	lateral pivot
Postolka et al. [204]	10 (23.7±3.2 y)	single-plane fluoroscopy	stance & swing	FFA	st: 8.3±1.8mm sw: 6.6±1.6mm	st: 8.2±1.4mm sw: 8.1±1.8mm	medial
				NP	st: 10.3±3.2mm sw: 13.3±4.3mm	st: 15.5±6.1mm sw: 21.7±8.5mm	n.a.

A-P: antero-posterior, y: year, CoR: centre of rotation, a: anterior, p: posterior, st: stance; sw: swing; GCA: geometric centre axis, EFC: extension facet centre, FFC: flexion facet centre, FFA: functional flexion axis, TEA: transepicondylar axis, NP: nearest point, CP: contact point

provided written, informed consent to participate in this study, which was approved by the local ethics committee (KEK-ZH-Nr. 2016-00410).

5.3.2 Anatomical coordinate systems

In order to obtain physiological segment rotations and translations, local femoral and tibial anatomical coordinate systems were defined according to Postolka et al. [199]. The medio-lateral axis for the femur was defined using the symmetrical axis of rotation approach [67] derived from the kinematics of a deep knee bending trial. The antero-posterior axis was defined orthogonal to the medio-lateral axis and a temporary femoral shaft axis. The right-handed coordinate system was then completed by creating an orthogonal longitudinal axis, with its origin located at the midpoint between the most medial and lateral point on the medio-lateral axis. The origin of the tibial coordinate system was defined as the midpoint between two circles intersecting the bone's surface, fitted to a proximal plane, parallel to the tibial articular surface [47]. The longitudinal axis was defined along the length of the shaft, while the antero-posterior axis was defined orthogonal to the longitudinal axis and the line connecting the circle centres. The medio-lateral axis was then defined to complete the right-handed, orthogonal coordinate system.

5.3.3 Kinematic analysis

Based on the 3D position and orientation of the femur relative to the tibia during all motion tasks, condylar A-P translations were analysed using six different kinematic analysis approaches (Table 5.4): The location of the nearest points (NP), the centres of the contact regions defined by < 6 mm tibio-femoral separation (SEP), and the extension facet and flexion facet centres (EFC/FFC) of each condyle were calculated accordingly. To ensure consistency for the functional flexion axis (FFA), the transepicondylar axis (TEA), and the cylinder axis (CA), the distance between the medial and lateral points was defined according to the distance between the nearest points during standing. A-P translation of each femoral condyle was then described as the translation of these points with respect to the tibial anatomical coordinate system. To normalise joint kinematics to the individual subject sizes, all A-P translations were scaled using a subject-specific coefficient based on the mean condylar width divided by the subject's condylar width [74, 204]. A-P translations during continuous knee flexion were analysed as a function of tibio-femoral flexion angle, while A-P translations during level walking were normalised to a complete gait cycle. For each approach, the location of the CoR in the transverse plane was calculated using the

Symmetrical Centre of Rotation Estimation [200] based on the location of the respective medial and lateral points.

5.3.4 Statistics

Two mixed-model analyses of variances (ANOVA), one for continuous knee bending and one for level walking, were performed to investigate differences in the ranges of A-P translation between the medial and lateral condyles, as well as the effect of the analysis approach. The range of A-P translation was set as the dependent variable. Approach (six levels: FFA, TEA, CA, EFC/FFC, NP, SEP) and condyle (two levels: medial, lateral) were set as fixed effects, with subject as random effect. Post-hoc comparisons were conducted using a least significant difference approach, and significance levels were adjusted for multiple comparisons using Bonferroni correction. The ANOVA analysis was conducted using the SPSS software suite (SPSS v24, IBM, USA).
In order to analyse the effects of the different kinematic analysis approaches on A-P translation over the whole time series, one-dimensional statistical parametric mapping (SPM) was performed [206] using the open-source toolbox SPM-1D (T.C. Pataky 2017, v. M.0.4.5). For each activity, two one-way ANOVAs were performed, one for each condyle. A-P translation was set as the dependent variable and the analysis approach (six levels: FFA, TEA, CA, EFC/FFC, NP, SEP) as the independent variable. Post-hoc comparisons were conducted using a two-sample t-test and significance levels were adjusted for multiple comparisons using Bonferroni correction.

5.4 Results

A significant interaction was found between the kinematic analysis approach and the condyle (medial/lateral), hence limiting the statistical model. Therefore, statistical analysis was based on the post-hoc pairwise comparisons.

5.4.1 Standing

The FFA was located most posteriorly, followed by the CA and the TEA (Figure 5.1). Both contact point approaches (NP, SEP) indicated tibio-femoral contact at a more anterior location. Across all approaches, the lateral point was on average located anteriorly compared to the medial point.

Table 5.4: Description of all six kinematic analysis approaches used

Approach	Definition
Nearest point (NP)	Weighted mean of the ten nearest points of the medial and lateral femoral condyle relative to a plane parallel to the tibial articular surface.
Tibio-femoral separation point (SEP)	Based on the nearest point of each femoral condyle relative to a plane parallel to the tibial articular surface, a separation threshold was set by adding 6 mm to the nearest point (to account for missing articular cartilage [28]). The tibio-femoral separation point was then calculated as the geometric centre of the femoral region with less separation than the threshold.
Functional flexion axis (FFA)	Medio-lateral axis of the femoral anatomical coordinate system, defined based on bone kinematics of a deep knee bending trial and calculated using the symmetrical axis of rotation approach [67].
Transepicondylar axis (TEA)	The most prominent medial and lateral epicondylar regions were manually selected from the segmented femoral surfaces (r = 5 mm) using the Rhinoceros software (Rhinoceros v5, Robert McNeel & Associates). The medial and lateral epicondylar points (mean of all selected surface points) were connected to form the TEA.
Cylinder axis (CA)	Cylinders on each of the medial and lateral condylar surfaces were defined that intersected the most distal (lowest) point of each femoral condyle (in the sagittal plane). The cylinder axis was defined as the common axis of the two cylinders.
Extension facet centre (EFC) & flexion facet centre (FFC)	Based on the location of the nearest points during standing, deep knee bending and level walking, the corresponding surface points on the medial and lateral condyles were extracted at maximum extension, 20° flexion and 120° flexion. The surface points between the point at maximal extension and 20° flexion were used to fit an extension circle, while the surface points at 20° and 120° flexion were used to fit a flexion circle. The circles were fitted using the approach suggested by Taubin [205], with the anatomical medio-lateral axis set as the normal axis of the fitted circles. The centres of the circles were used as the extension facet centres and flexion facet centres. Due to the absence of knee extension in one subject in our study, no extension facet centres could be detected and therefore EFC/FFC was not analysed for this subject.

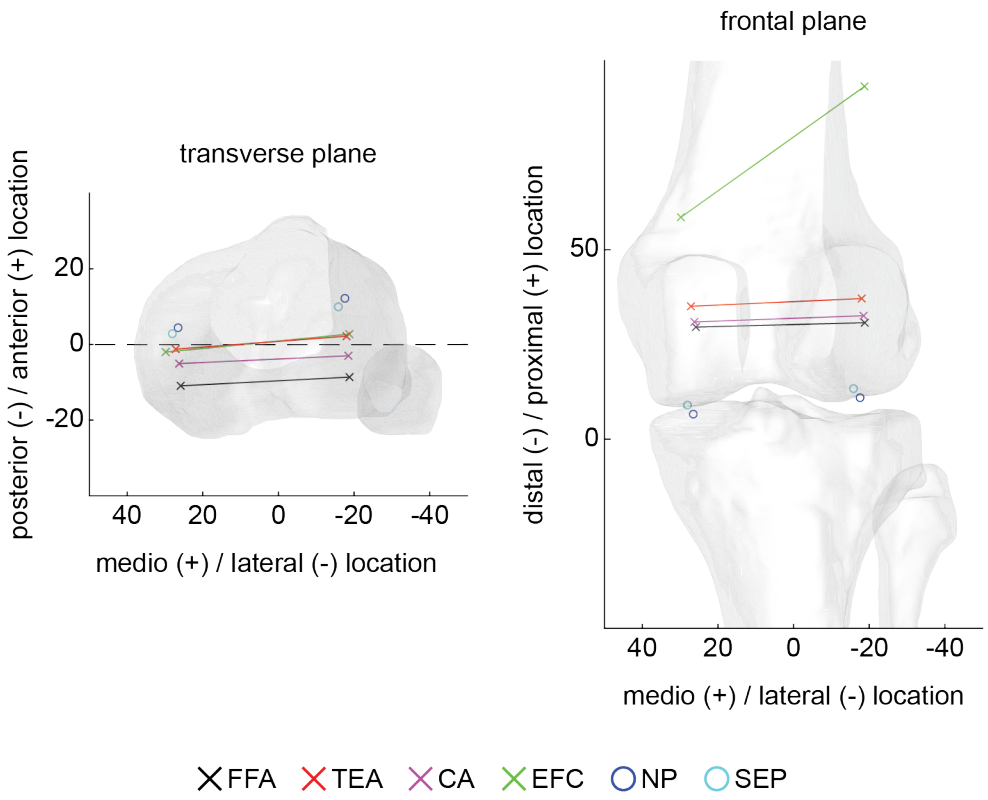

Figure 5.1: 3D location of the medial and lateral condylar points during standing. Mean location across all 10 subjects within the tibial anatomical coordinate system using the functional flexion axis (FFA), transepicondylar axis (TEA), cylinder axis (CA), extension facet centres (EFC), nearest point (NP) and tibio-femoral separation (SEP) are presented in the transverse plane (left) and frontal plane (right).

5.4.2 Continuous knee flexion

Across all subjects and all trials of deep knee bending, flexion ranged from -11.0° to 162.7°. A range of 25° to 119° was covered by all subjects and therefore used for statistical comparison. Apart from the FFA, a significantly larger range of A-P translation was observed for the lateral compared to the medial condyle (Figure 6.2, Table 5.5). The CoR in the transverse plane was therefore located slightly medially for all kinematic analysis approaches (Figure 5.4, Table C.1). However, variability between subjects and kinematic analysis approaches was high, resulting in a mean lateral CoR for a few subjects (Table C.1).
The range of A-P translation for the medial as well as the lateral condyle exhibited significant differences between the approaches (Table 5.6), predominantly at low and high flexion angles (med: 25° - 38° / 72° - 119°; lat: 25° - 42° / 46° - 52° / 70° - 119°) (Figure C.1). At low flexion, differences occurred between the FFA and both contact approaches. At higher flexion angles the contact approaches exhibited significantly different translational patterns than the TEA and CA but differences between the FFA and TEA were also evident (Figure 5.2, Table C.2).

5.4.3 Functional gait activity

Over the complete gait cycle of level walking, the lateral condyle point experienced significantly more A-P translation than the medial condyle point for all six kinematic analysis approaches (Table 5.5), resulting in an overall medial position of the CoR in the transverse plane (Figure 5.4, Table C.1).
In a comparison between analysis approaches, significant differences were found during the early and late stance phases, as well as the swing phase (med: 0 - 32% / 49 - 100%; lat: 0 - 32% / 52 - 100%) (Figure C.1), but also for both the medial and lateral ranges of A-P translation (Table 5.6). Overall, the largest differences occurred between the FFA, TEA and CA compared to the contact approaches, but dissimilarities between the FFA and TEA were also apparent (Figure 5.3, Table C.2).

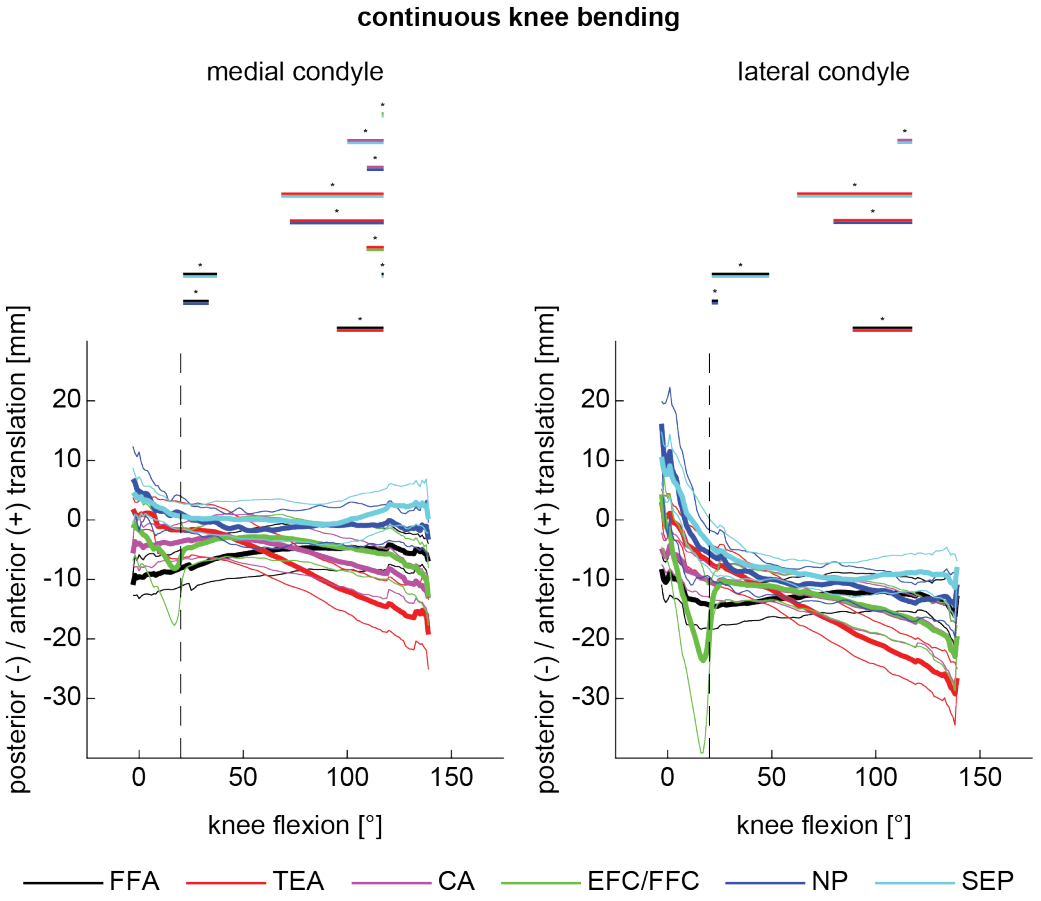

Figure 5.2: Antero-posterior translation of the medial (left) and lateral (right) condyle using the functional flexion axis (FFA), transepicondylar axis (TEA), cylinder axis (CA), extension facet centres and flexion facet centres (EFC/FFC), nearest point (NP) and tibio-femoral separation (SEP) during continuous knee bending are shown as a function of the flexion angle. Mean across all subjects (thick line) and standard deviations across all subjects (thin lines) are presented. Significant differences between approaches are indicated with bars in the colours of the respective approaches with an adjusted level of significance of $\alpha = 0.0033$. The dashed black line is indicating 20° of flexion.

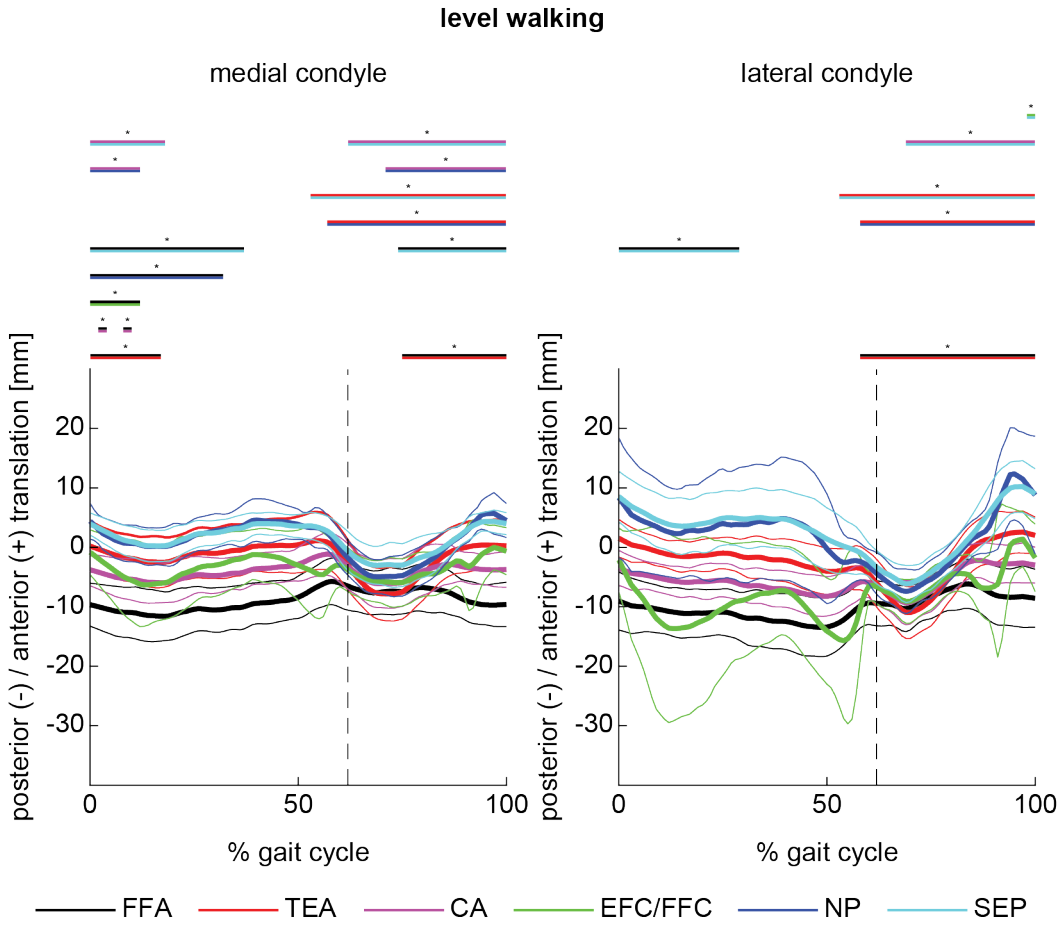

Figure 5.3: Antero-posterior translation of the medial (left) and lateral (right) condyle using the functional flexion axis (FFA), transepicondylar axis (TEA), cylinder axis (CA), extension facet centres and flexion facet centres (EFC/FFC), nearest point (NP) and tibio-femoral separation (SEP) over a complete gait cycle of level walking. Mean across all subjects (thick line) and standard deviations across all subjects (thin lines) are presented. Significant differences between approaches are indicated with bars in the colours of the respective approaches with an adjusted level of significance of $\alpha = 0.0033$. The dashed black line is indicating the average toe-off across all subjects.

Table 5.5: Range of antero-posterior translation (mean ± standard deviation) of the medial and lateral condyle during continuous knee bending and level walking using the functional flexion axis (FFA), transepicondylar axis (TEA), cylinder axis (CA), extension facet centres and flexion facet centres (EFC/FFC), nearest point (NP) and tibio-femoral separation (SEP). In addition, the resultant p-value of the performed ANOVA to investigate differences in the range of A-P translation between the medial and lateral condyle for each approach are indicated.

RoM [mm]	**FFA**	**TEA**	**CA**	**EFC/FFC**	**NP**	**SEP**
continuous knee bending						
medial	7.2 ± 1.8	17.9 ± 7.5	10.4 ± 1.9	11.7 ± 5.8	8.9 ± 4.7	6.9 ± 2.9
lateral	8.5 ± 1.9	25.5 ± 5.2	15.0 ± 4.1	25.7 ± 17.1	20.9 ± 10.1	16.7 ± 6.9
p-value	*0.275*	*0.000**	*0.001**	*0.000**	*0.000**	*0.000**
level walking (complete cycle)						
medial	8.8 ± 2.0	12.1 ± 2.5	8.7 ± 1.3	12.6 ± 5.5	14.7 ± 3.4	11.1 ± 3.0
lateral	11.5 ± 1.9	17.0 ± 3.6	12.1 ± 2.6	27.8 ± 13.0	25.5 ± 5.6	19.2 ± 4.2
p-value	*0.002**	*0.000**	*0.000**	*0.000**	*0.000**	*0.000**

*significant difference on an adjusted level of significance of $\alpha = 0.0083$

Table 5.6: Resultant p-values of the performed ANOVAs to investigate differences in the range of A-P translation of the medial and lateral condyle between the functional flexion axis (FFA), transepicondylar axis (TEA), cylinder axis (CA), extension facet centres and flexion facet centres (EFC/FFC), nearest point (NP) and tibio-femoral separation (SEP).

			SEP	**NP**	**EFC/FFC**	**CA**	**TEA**
continuous knee bending	medial condyle	FFA	0.887	0.108	0.000*	0.022	0.000*
		TEA	0.000*	0.000*	0.000*	0.000*	
		CA	0.032	0.491	0.152		
		EFC/FFC	0.000*	0.036			
		NP	0.143				
	lateral condyle	FFA	0.000*	0.000*	0.000*	0.000*	0.000*
		TEA	0.000*	0.009	0.372	0.000*	
		CA	0.145	0.000*	0.000*		
		EFC/FFC	0.000*	0.001*			
		NP	0.001*				
level walking (complete cycle)	medial condyle	FFA	0.009	0.000*	0.000*	0.787	0.000*
		TEA	0.294	0.002*	0.617	0.000*	
		CA	0.004	0.000*	0.000*		
		EFC/FFC	0.128	0.011			
		NP	0.000*				
	lateral condyle	FFA	0.000*	0.000*	0.000*	0.582	0.000*
		TEA	0.012	0.000*	0.000*	0.000*	
		CA	0.000*	0.000*	0.000*		
		EFC/FFC	0.000*	0.008			
		NP	0.000*				

*significant difference on an adjusted level of significance of $\alpha = 0.0033$

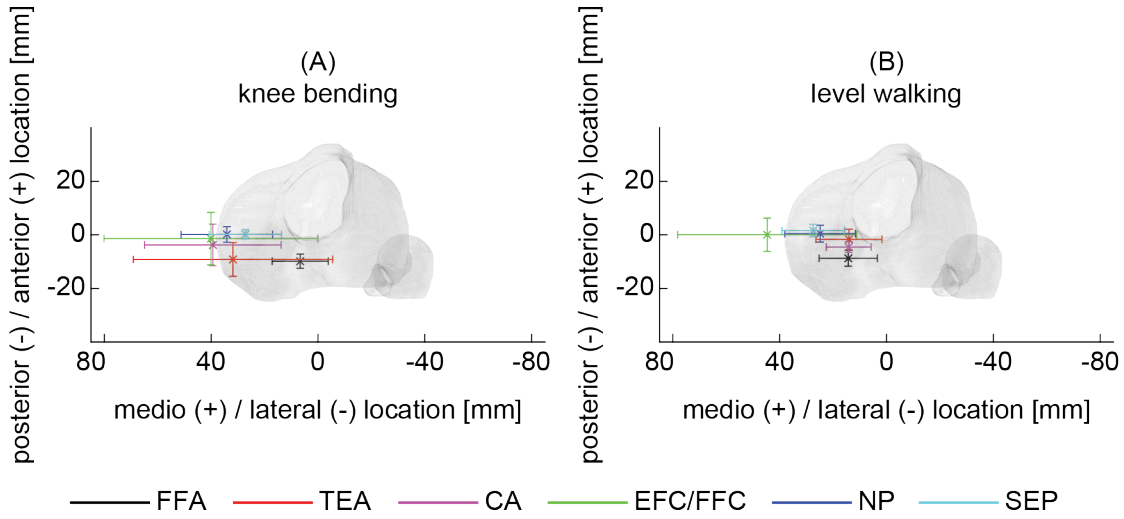

Figure 5.4: Location of the centre of rotation (CoR) shown on the tibial plateau during (A) continuous knee bending and (B) complete cycle of level walking using the functional flexion axis (FFA), transepicondylar axis (TEA), cylinder axis (CA), extension facet centres and flexion facet centres (EFC/FFC), nearest point (NP) and tibio-femoral separation (SEP). The mean across all subjects as well as the standard deviations in antero-posterior and medio-lateral directions are indicated with whiskers.

5.5 Discussion

A clear understanding of tibio-femoral kinematics is a prerequisite for a detailed understanding of joint functionality and treatment outcomes. However, differences in the interpretation of movement data inhibit a general consensus on kinematics of the healthy knee. This study compared six kinematic analysis approaches in order to understand their differences and initiate discussions to reach agreement on how tibio-femoral kinematics should best be reported. Our results, based on videofluoroscopy data of ten healthy subjects during multiple trials of continuous knee bending as well as complete cycles of free level walking, clearly demonstrate the impact of the kinematic analysis approach used and its effect on the interpretation of identical 3D tibio-femoral motion.

During complex movements such as walking, the tibio-femoral axis of rotation is constantly changing. An instantaneous axis of rotation can provide a qualitative description of where and in what plane these relative joint movements occur. However, since such instantaneous axes constantly move relative to the bone segments, they are unable to provide quantitative data on relative poses. The use of segment fixed axes faces other challenges, however, since deviations from the instantaneous axis of rotation (e.g. as anatomical points rotate about the true axis) will be associated with an erroneous translation. As a result, any segment fixed axis might be able to reconstruct relative segment motion at certain instances, but will introduce translational errors

over other periods of the movement cycle. It is therefore clear that such cross-talk errors result in a deviation and misunderstanding of the true joint kinematics. The resulting challenge is to identify approaches that best describe joint kinematics in a robust and reliable manner [207], but that is also appropriate to the intended application.

Within the current study, the FFA most closely approximated to the instantaneous axis of rotation and was therefore assumed to be least affected by kinematic cross-talk. However, as the FFA is generally based on a single movement trial, variations in reference axes for other trials of the same subject are inherently plausible. Contrary to this knowledge of relative segment motion, contact point approaches can provide knowledge of localised contact conditions at the condylar surface. However, individual anatomical differences in femoral and tibial geometry can affect condylar translations and result in large inter-subject variability.

While the FFA, TEA, and CA showed similar (parallel) translational behaviour at low flexion angles, dissimilarities, most likely due to kinematic cross-talk errors, were evident during deep flexion. These errors clearly resulted in much larger ranges of A-P translation, which could plausibly explain some of the differences in joint kinematics described in the literature:

Continuous knee bendig: While an initial anterior translation of the medial TEA and GCA has been reported in the literature, the present study found continuous posterior translation at low flexion angles. However, comparable ranges of lateral translation were found for both the TEA – our study: 25.5 mm vs. 31.7 mm [41] – as well as the GCA – 15.0 mm vs. 15.6 - 17.8 mm [40, 49]. Comparison of the reported values using the EFC/FFC approach was challenging in the current study due to the variability between subjects' anatomies, but our data do support previously studies indicating more A-P translation for the lateral compared to the medial condyle [19, 21, 43]. Over a comparable range of flexion, translations using the medial and lateral contact point approaches (NP & SEP) presented similar trends to previous studies, indicating more translation on the lateral (16.7 - 20.9 mm vs. 19.8 - 27.4 mm) than the medial side (6.9 - 8.9 mm vs. 1.9 - 6.9 mm) [46, 47, 49]. Two studies have also presented equal translation of both condyles, which could not be replicated within the present study [38, 43].

Level walking: Over the complete gait cycle, our results using the CA (medial: 8.7 mm; lateral: 12.1 mm) are in line with translations reported using a GCA (medial: 7.6 mm; lateral: 11.6 mm) [74]. However, contrary results have been reported for the loaded stance phase: While we observed posterior translation of both condyles during early stance, more translation was evident for the lateral condyle. In comparison Kozanek and co-workers [31] reported an initial anterior peak and anterior translation of the medial condyle prior to toe-off (GCA: 17.4 mm; TEA: 9.7 mm) together with limited A-P translation of the lateral condyle until late stance,

followed by anterior translation in pre-swing (GCA: 7.4 mm; TEA: 4.0 mm). Our results also indicate more A-P translation for both condyles than presented in the literature when using contact approaches [24, 51, 74, 86]. In particular, our observation of large inter-subject differences for the lateral condyle during the stance phase has not been previously reported.

Importantly, these observations confirm that different interpretations of joint kinematics exist across studies depending on the analysis approach used. Accordingly, our analyses result in remarkably similar tibio-femoral A-P translations to each individual study when using their analysis approach during the more standardised assessment of continuous knee bending. We therefore provide plausible evidence that similar kinematic patterns have indeed been captured across many different previous studies, but their interpretation according to the analysis approach used has resulted in seemingly different movement patterns. Conversely, the data for walking was less convincing. While knee bending is a guided and restricted movement that can be captured using standardised measurement techniques, the assessment of functional activities such as walking are subject to much greater variation in measurement technologies [24, 30, 31, 188]. Moreover, large inter-subject variability is known to exist during gait activities, further complicated by treadmill vs. free level walking.

While the present study could clearly demonstrate the effect of various kinematic analysis approaches, despite the assessment of identical tibio-femoral kinematics, there were obvious limitations to our study. Although walking with the moving fluoroscope requires a reduced gait speed (present study: 0.87 ± 0.06 m/s), the resultant tibio-femoral kinematics were shown to remain comparable to those presented for slow walking [203]. As a result of the single-plane set-up, out-of-plane registration errors were large. In this study, these errors were mitigated by observational checks of outliers and ensuring reasonable medio-lateral alignment between the femur and tibia, also including the path of movement throughout the time-series [199]. Finally, all axes and anatomical landmarks identified manually were subject to observer induced variability, hence contributing to reduced analysis reliability, but such inaccuracies are a fundamental aspect of the analysis approaches themselves, which should be considered in their application.

The results of this study clearly demonstrate that interpretation of joint kinematics is dependent on the analysis approach used. It is therefore critical that the biomechanics community reaches consensus on when each specific analysis approach should be used in order to provide a fundamental basis for comparing joint kinematic patterns. While functionally determined femur fixed axes seem to report the relative positions of the tibia and femur, and can therefore be used to assess the 3D movement of the joint, axes approaches that are based on anatomical landmarks seem to be subject to higher levels of kinematic cross-talk. Our recommendation is therefore that

joint translations based on functional flexion axes should be reported in preference to anatomical based axes. On the other hand, contact point approaches seem to provide information regarding the localised contact conditions at the condylar surfaces, and should therefore be reported to inform on loading, overloading, and/or wear of the joint. Finally, since no clear solution to this problem has yet been found, we would recommend that kinematics are reported using at least two different approaches, a functionally determined axis as well as a contact point approach, such that a more standard comparison and interpretation of tibio-femoral joint kinematics during functional activities *in vivo* can be achieved.

5.6 Acknowledgement

This project has been partially funded by Medacta International SA (Castel San Pietro, Switzerland) and the Commission for Technology and Innovation (Bern, Switzerland, Project Number 17078.1 PFLS-LS). Furthermore, the authors would like to thank Maryam Hajizadeh for her initial work in comparing different kinematic analysis approaches.

5.7 Supplementary materials

Supplementary material associated with this chapter can be found in Appendix C.

Chapter 6

Limb alignment plays only a minor role on tibio-femoral kinematics: A dynamic videofluoroscopy study

adapted from:

Barbara Postolka[1], William R. Taylor[1], Sandro F. Fucentese[2], Renate List[1,3], Pascal Schütz[1]

[1]Institute for Biomechanics, ETH Zürich, Zürich, Switzerland

[2]Balgrist University Hospital, Zürich, Switzerland

[3]Human Performance Lab, Schulthess Clinic, Zürich, Switzerland

in preparation

Keywords

in vivo knee kinematics, tibio-femoral kinematics, varus alignment, valgus alignment, videofluoroscopy, gait

6.1 Abstract

In-depth knowledge of individual tibio-femoral kinematics is essential for a detailed understanding of knee joint functionality. With the recent tendency towards kinematic alignment of total knee arthroplasties in subjects with a constitutional varus or valgus limb alignment, detailed understanding of the relationship between limb alignment and subject-specific tibio-femoral kinematics is of key importance to support clinical decision-making. While altered tibio-femoral joint loadings and the risk and progression of osteoarthritis have been reported for subjects with varus or valgus limb alignment, less is known about the changes in tibio-femoral kinematics during activities of daily living. Therefore, the objective of this study was to investigate the role of limb alignment on knee joint kinematics in subjects with neutral, varus and valgus limb alignment during gait activities.

Tibio-femoral rotations, condylar antero-posterior translations and the location of the centre of rotation were analysed in twelve neutral, ten varus and five valgus subjects throughout complete gait cycles of level walking and stair descent using dynamic videofluoroscopy. No significant differences in the ranges of tibio-femoral rotation nor the ranges of condylar antero-posterior translation were found between the three alignment groups. However, significant differences between the varus and valgus subjects were found for the translational patterns of the lateral femoral condyle (FFA_P_{lat}) during mid-stance and early swing (44 - 55% & 70 - 75% gait cycle) of stair descent. For all three alignments and both activities, an overall medial centre of rotation was found.

Based on the presented data, limb alignment seems to play only a minor role in modulating tibio-femoral kinematics throughout dynamic gait activities. However, subject-specific differences were evident, suggesting other factors to be responsible for the individual differences (e.g. soft tissue sufficiency). In combination with musculoskeletal modelling, this data can provide a basis for clinical decision-making regarding anatomical alignment and further improve surgical procedures aiming to restore natural knee joint motion.

6.2 Introduction

Tibio-femoral kinematics of the healthy knee are guided by a complex system of bones and soft tissue structures, including muscles, enabling a complex set of rotations and translations along all six degrees of freedom [1]. In-depth knowledge of the joint motion is not only essential for understanding knee joint functionality as well as pathologies and injuries of the knee, but also to improve patient outcomes while aiming to restore natural knee function. However, tibio-femoral motion patterns of the healthy knee are still controversially discussed in the literature [24, 31, 51, 52, 74, 84, 86, 204] with only limited studies analysing tibio-femoral kinematics over complete cycles of walking without the influence of soft tissue artefacts [74, 85, 88, 204]. These variable findings, result in contrary conclusions about the predominant location of the centre of rotation (CoR) in the transverse plane [24, 52, 74, 84, 86, 204]. In addition, comparison of reported rotations and translations has been shown to be difficult, as different measurement techniques as well as various definitions of the anatomical coordinate systems have been used. *In vivo* analysis is generally limited to small cohort studies, resulting in large standard deviations between subjects. However, the influence of anatomical variations, such as limb alignment or ligament condition, on inter-subject variability remain unclear [131, 204].

Limb alignment is a common anatomical variation, with a substantial fraction of the healthy adult population exhibiting limb alignment of more than 3° of varus or valgus respectively [95, 122, 123]. It has been shown to critically affect tibio-femoral joint loading [1, 124–126] as well as influence the risk and progression of osteoarthritis in the knee [127–129]. However, less is known about the altered tibio-femoral kinematics in subjects with extreme limb alignment, especially *in vivo* during activities of daily living. The hip-knee-ankle (HKA) angle was found to affect tibio-femoral internal/external rotations and abduction/adduction during continuous knee flexion using cadaver specimens and intra-operative measures [131, 132]. But only one study compared osteoarthritic subjects with varus and valgus alignment with a control group while performing a barefoot walking task [133]. Like the aforementioned studies, differences in the abduction/adduction angle were found. In addition, the varus and valgus subjects showed a reduced range of flexion/extension over the stance phase. However, no study has yet investigated the relationship of lower limb alignment and the resultant tibio-femoral kinematics during multiple, *in vivo*, weight-bearing gait activities in healthy subjects.

With the recent tendency towards kinematic alignment during total knee arthroplasty (TKA) surgeries in subjects with a constitutional varus or valgus limb alignment, an in-depth understanding of the relationship between limb alignment and subject-specific tibio-femoral kinematics

is crucial for supporting clinical decision-making. Therefore, the goal of the present study was to analyse tibio-femoral kinematics in non-osteoarthritic subjects with different limb alignment. The primary aim of the study was to identify differences in the tibio-femoral kinematics based on limb alignment.

6.3 Methods

6.3.1 Subjects

12 left and 15 right knees of healthy subjects with no signs of knee disorders were included in this study (Table 6.1 & Table 6.2). Subject-specific limb alignment was evaluated using the EOS biplane X-ray system (EOS imagine, France) in a standing position [116]. Subjects with a limb alignment between $\pm$ 3° varus and valgus were classified as neutral, subjects with $<$ -3° as valgus and subjects with $>$ 3° as varus, all subjects were then grouped according to their limb alignment (Table 6.2).

The study was approved by the local ethics committee (KEK-ZH-Nr. 2016-00410) and carried out in accordance with the declaration of Helsinki. All subjects provided written informed consent prior to the first measurement session.

Table 6.1: Inclusion and exclusion criteria for subjects to participate in this study

inclusion criteria	**exclusion criteria**
– female or male – age: 18+ years – BMI: $\leq$ 33 – good health condition, adequate for test procedure	– significant problem on lower extremities – any arthroplasty at the lower extremities – subject incapable to understand and sign informed consent – pregnancy at time of testing – incapable of performing the motion tasks – any disease process that would preclude accurate evaluation (e.g. neuromuscular, psychiatric or metabolic disorder)

Table 6.2: Group characteristics in terms of sex (female (F)/male (M)), side (right (R)/left (L)), age, body mass index (BMI) and hip-knee-ankle (HKA) angle. Mean (min, max) are presented for each group

group characteristics	**neutral (n = 12)**	**varus (n = 10)**	**valgus (n = 5)**
sex (F/M)	6F / 6M	4F / 6M	4F / 1M
side (R/L)	6R / 6L	7R / 3L	2R / 3L
age [years]	24.0 (20, 31)	25.8 (20, 46)	37.2 (22, 67)
BMI [kg/m^2]	21.3 (18.7, 25.4)	20.6 (17.0, 23.6)	23.0 (20.1, 26.2)
HKA [°]	0.5 (-2, 3)	5.7 (4, 9)	-5.6 (-8, -4)

HKA: varus = positive angle, valgus = negative angle

6.3.2 Experimental procedure

First, all subjects underwent a clinical knee examination to ensure no knee disorders (Table 6.1), followed by an EOS and CT scan (∼20 cm proximal/distal of the joint line, resolution 0.5 x 0.5 mm, slice thickness 1 mm).

To assess tibio-femoral kinematics during standing (2 trials), complete cycles of free level walking (5 - 6 trials), and complete cycles of stair descent (5 trials, three 18 cm steps), the Institute for Biomechanics' moving fluoroscope was used (Figure 6.1 A) [188]. Fluoroscopic images were acquired at 25 - 30 Hz (1 ms shutter time) with an image resolution of 1000 x 1000 pixels (Figure 6.1 B) [188]. Synchronised ground reaction forces were obtained using five force plates embedded in the floor and two additional mobile force plates mounted on the stairs (Kistler, Instrumentation, Switzerland), operating at a sampling frequency of 2000 Hz. Full description of the measurement set-up has been previously published [204].

Upright standing and level walking were measured for all 27 subjects. Due to technical problems during the experiment, the data for stair descent could not be analysed for one subject.

6.3.3 Data analysis

Using the incorporated software of the EOS system, subject-specific limb alignment was identified [97]. The open-source software MTIK-GEM [187], was used to generate individual subject-specific volumetric models of the femur and tibia, based on each subjects knee CT scan.

Distortion correction was applied to all fluoroscopic images and the optical projection parameters were calculated [135]. 2D/3D registration of the fluoroscopic images was performed using a semi-automatic 2D/3D registration software (Figure 6.1 C) with reported mean absolute registration errors of $< 1°$ for all three rotations, < 0.6 mm for in-plane and < 7.1 mm for out-of-plane

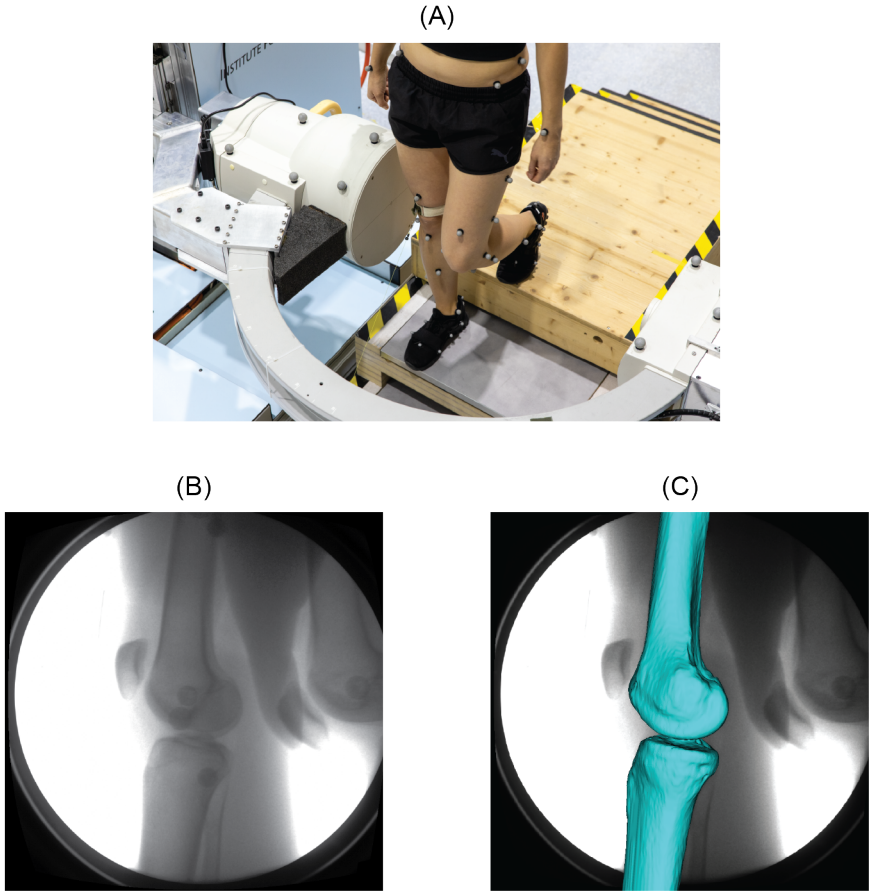

Figure 6.1: (A) Subject tracked by the moving fluoroscope during a trial of stair descent. (B) Fluoroscopic image during stair descent. (C) Registered subject-specific femur and tibia model during stair descent.

translations of a single bone specimen [199].

Relative rotations were calculated based on the functional flexion axis (medio-lateral axis) of the femur and the longitudinal axis of the tibia, using the Joint Coordinate System approach [62]. Antero-posterior (A-P) translations of the medial and lateral condyle were assessed using a medial and lateral point on the functional flexion axis (FFA_P$_{med}$ & FFA_P$_{lat}$) as well as the nearest point of each femoral condyle relative to a plane parallel to the tibial articular surface (N_P$_{med}$ & N_P$_{lat}$) [204]. A-P translations were calculated with respect to the mid coronal plane of the tibia and scaled to the average condylar width of the neutral subjects [204]. Based on the location of the FFA_P$_{med}$ and FFA_P$_{lat}$, a mean CoR in the transverse plane was calculated over the complete gait cycle, using the symmetrical centre of rotation estimation [200].

Heel-strike and toe-off were determined based on the ground reaction forces, using a threshold of 25 N. All rotations and translations during level walking and stair descent were normalised to 101 data points per complete gait cycle.

6.3.4 Statistics

Three mixed-model analysis of variance (ANOVA) were performed to test the effect of limb alignment on the ranges of tibio-femoral rotation. The rotational range of motion (RoM) was set as the dependent variable while group (three levels: neutral, varus, valgus) and activity (two levels: level walking, stair descent) were set as fixed effects and subjects as random effect. Another ANOVA was performed to compare the ranges of A-P translation between the medial and lateral condyle as well as the three limb alignment groups. The range of A-P translation was set as the dependent variable. The group (three levels: neutral, varus, valgus), activity (two levels: level walking, stair descent) and condylar side (two levels: medial, lateral) were used as fixed effects and the individual subjects as random effect. Post-hoc comparisons were conducted using a least significant difference approach, with significance levels adjusted for multiple comparisons using Bonfferoni correction. All ANOVA's were conducted using the SPSS software suite (SPSS v24, IBM, USA).
In order to analyse the effect of the different limb alignment groups on rotations and A-P translations of the FFA_P$_{med}$ and FFA_P$_{lat}$ at specific time points over the time series of a gait cycle, one-dimensional statistical parametric mapping (SPM) was performed [206]. A total of ten one-way ANOVAs was performed. The rotation or translation respectively, was set as the dependent variable, while the group (three levels: neutral, varus, valgus) was used as the independent variable. If the ANOVA revealed significant differences between the groups, a post-hoc two sample t-test was performed with significance levels adjusted for multiple comparisons using Bonferroni correction.

6.4 Results

During level walking and stair descent, the subjects walked with an absolute average velocity of 0.82 ± 0.08 m/s and 0.56 ± 0.05 m/s, respectively.

6.4.1 Frontal plane

Between all subjects, individual limb alignment measured using the EOS ranged from 8° valgus to 9° varus whereas the adduction angle during upright standing measured using the moving fluoroscope ranged from -7° to 9.3° (Figure 6.2 A).

For dynamic level walking and stair descent no significant differences in abduction/adduction between the limb alignment groups were found for the range nor the pattern over the complete time series of a gait cycle (Table 6.3, Figure 6.3, Figure D.1, Figure D.3).

6.4.2 Sagittal plane

The ranges and rotational pattern of flexion/extension were comparable between the three limb alignment groups for both activities (Table 6.3, Figure 6.3, Figure D.1, Figure D.3).

6.4.3 Transverse plane

In the upright standing position, the neutral and valgus subjects showed an almost equal mean location of the medial and lateral point using both approaches. For the varus subject, the positions for both approaches, slightly differed from the other two groups (Figure 6.2 B).
No significant differences between the alignment groups were found for the ranges and rotational pattern of tibial internal/external rotation during level walking and stair descent (Table 6.3, Figure 6.3, Figure D.1, Figure D.3).
The neutral and varus subgroup exhibited significant more condylar translation for the FFA_P_{lat} compared to the FFA_P_{med} for both activities (Table 6.4). While the valgus group exhibited a similar difference for stair descent, equal ranges of A-P translation of the FFA_P_{lat} and FFA_P_{med} were found for level walking (Table 6.4). Although comparable ranges of translation were found for both activities and both condyle points, limb alignment significantly influenced the translational patterns of the FFA_P_{lat} during stair descent (Table 6.4, Figure 6.4, Figure D.1, Figure D.4). A significant difference between the varus and valgus group was found for mid stance and early swing (44 - 55% & 70 - 75% gait cycle) (Figure 6.4, Figure D.2).
Overall, a medial CoR resulted for each limb alignment group during both activities (Figure 6.6). However, variability between subjects was high for all three groups, even resulting in a more central to lateral CoR for certain subjects (Figure D.6).
For comparison, translations of the nearest point approach were also presented (Figure 6.5). Comparable A-P translations between the limb alignment groups were found for the N_P_{med}, but large standard deviations, especially during phases of low flexion, were evident for the N_P_{lat}. Overall these larger variations indicate more inter-subject variability in the resultant motion patterns.

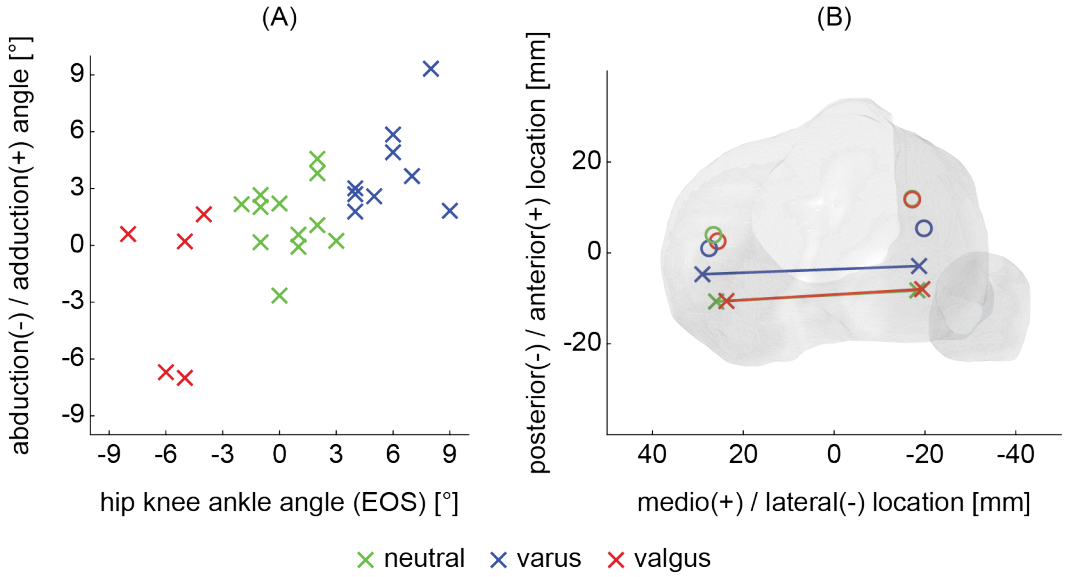

Figure 6.2: (A) Hip-knee-ankle angle measured in EOS versus abduction (-)/adduction (+) angle during upright standing measured using videofluoroscopy. (B) Mean location of the medial and lateral functional flexion axis points (x) and nearest points (o) within the tibial anatomical coordinate system for each subgroup, presented in the transverse plane.

Table 6.3: Range of motion for all three tibio-femoral rotations. Mean and standard deviations across all subjects for the neutral, varus and valgus group are presented for the complete gait cycle of level walking and stair descent. Flex/ex: flexion/extension, tibial int/ext: tibial internal/external rotation, abd/add: abduction/adduction

RoM [°]		**neutral**	**varus**	**valgus**
level walking	flex/ex	66.1 ± 3.9	63.3 ± 4.0	63.5 ± 6.4
	int/ext	15.5 ± 2.6	13.8 ± 1.6	13.3 ± 0.8
	abd/add	7.0 ± 1.9	5.7 ± 1.6	7.6 ± 2.3
stair descent	flex/ex	93.1 ± 4.9	90.7 ± 3.9	92.1 ± 6.9
	int/ext	16.2 ± 2.2	14.7 ± 2.6	15.5 ± 2.5
	abd/add	7.1 ± 1.4	6.4 ± 1.6	8.8 ± 2.2

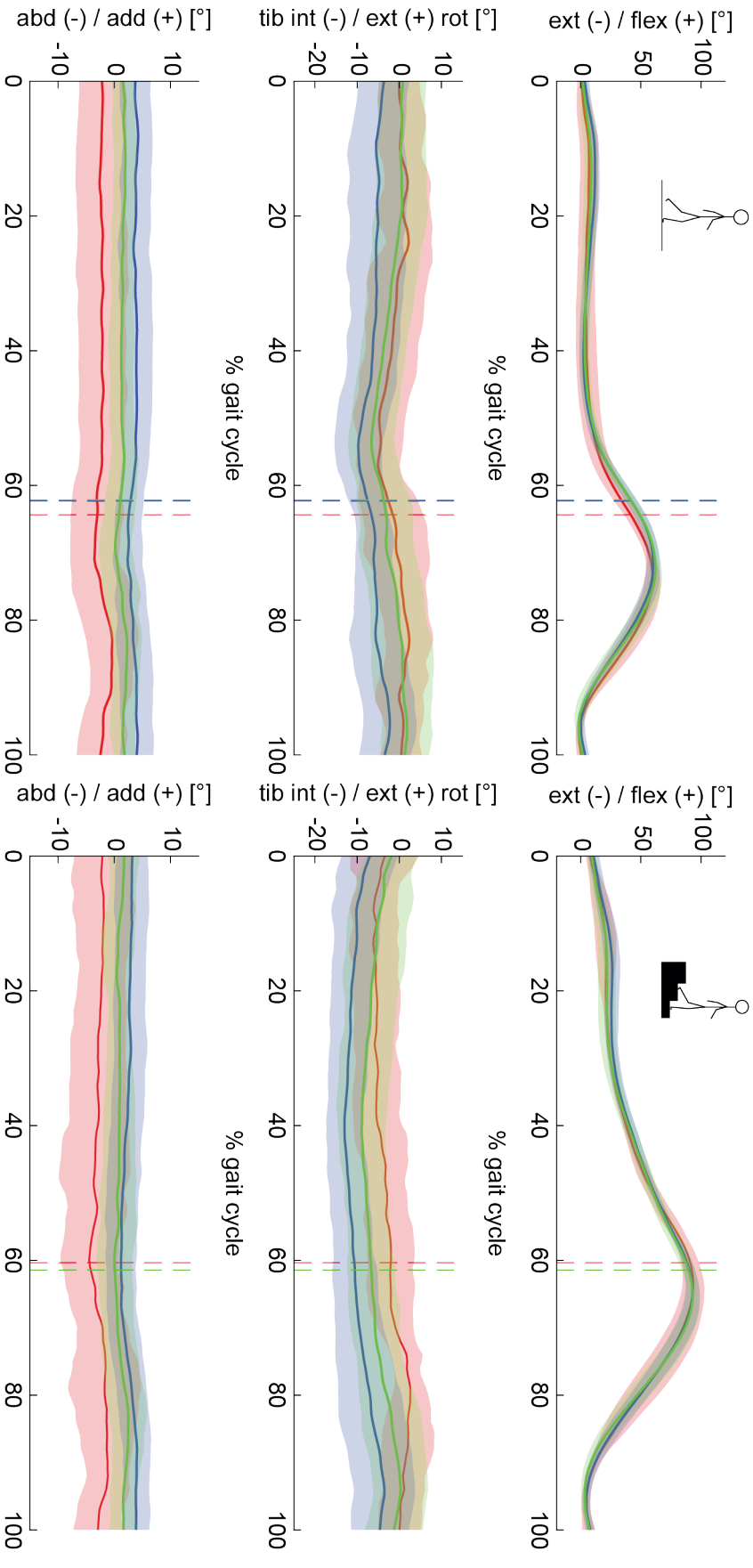

Figure 6.3: Tibio-femoral flexion/extension (flex/ext), tibial internal/external rotation (tib int/ext rot) and abduction/adduction (abd/add) throughout complete cycles of level walking (left column) and stair descent (right column). The mean (thick line) and standard deviations (shaded area) across each group are presented. The average instance of toe-off across all subjects of each group is indicated as a vertical dashed line.

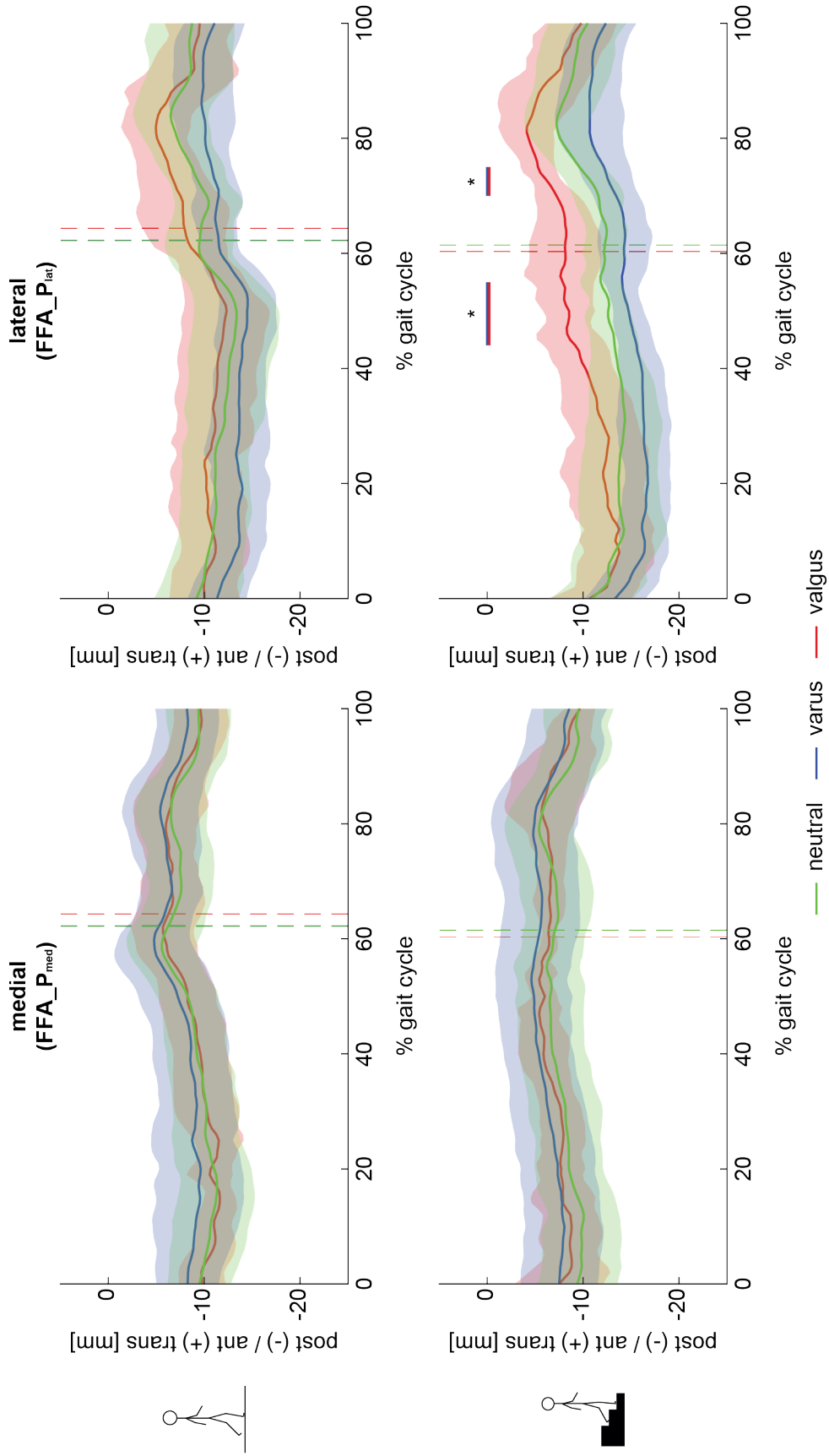

Figure 6.4: Antero (ant) – posterior (post) translation of the medial and lateral functional flexion axis points (FFA_P$_{med}$, FFA_P$_{lat}$) throughout complete cycles of level walking (top) and stair decent (bottom). The mean (thick line) and standard deviations (shaded area) across each group are presented. The average instance of toe-off across all subjects of each group is indicated as a vertical dashed line. Significant differences between approaches are indicated with bars in the colours of the respective approaches with an adjusted level of significance of $\alpha = 0.017$.

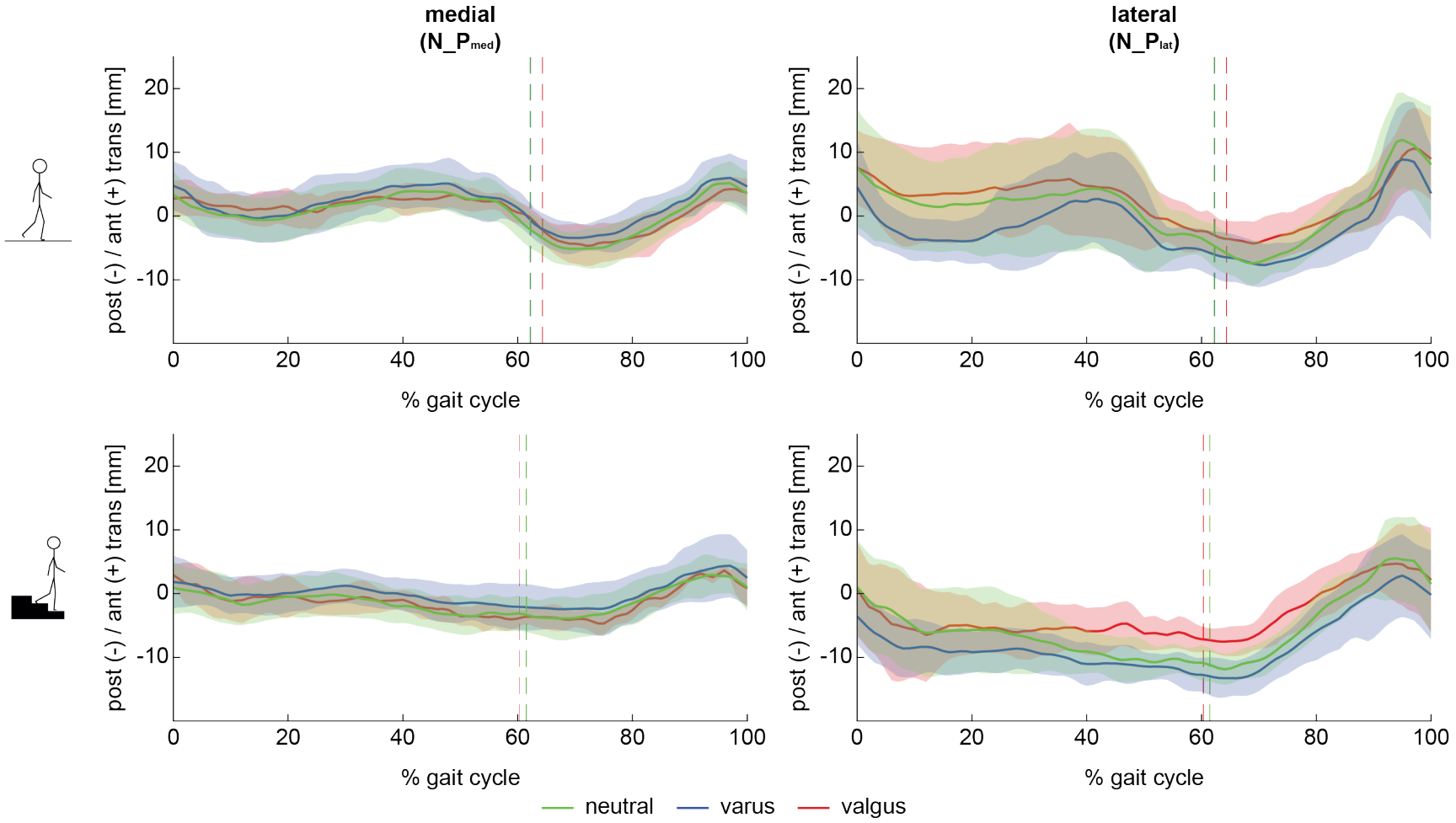

Figure 6.5: Antero (ant) – posterior (post) translation of the medial and lateral nearest points (N_P$_{med}$, N_P$_{lat}$) throughout complete cycles of level walking (top) and stair decent (bottom). The mean (thick line) and standard deviations (shaded area) across each group are presented. The average instance of toe-off across all subjects of each group is indicated as a vertical dashed line.

Table 6.4: Range of antero-posterior (A-P) translation of the medial and lateral condyle using the functional flexion axis (FFA_P$_{med}$ & FFA_P$_{lat}$) and the nearest point approach (N_P$_{med}$ & N_P$_{lat}$). Mean and standard deviations for the neutral, varus and valgus subgroup are presented over the complete gait cycle of level walking and stair descent.

RoM [mm]		**neutral**	**varus**	**valgus**
level walking	FFA_P$_{med}$	8.8 ± 1.8	8.6 ± 1.0	9.8 ± 0.8
	FFA_P$_{lat}$	10.9 ± 2.2	9.9 ± 2.1	10.3 ± 3.0
	p-value FFA_P	*0.000**	*0.000**	*0.422*
	N_P$_{med}$	14.3 ± 3.3	13.7 ± 2.2	14.3 ± 3.4
	N_P$_{lat}$	24.6 ± 6.3	21.9 ± 6.3	19.6 ± 4.1
stair descent	FFA_P$_{med}$	8.7 ± 1.9	7.4 ± 1.5	8.7 ± 1.0
	FFA_P$_{lat}$	11.8 ± 2.5	10.5 ± 1.4	12.9 ± 2.2
	p-value FFA_P	*0.000**	*0.000**	*0.000**
	N_P$_{med}$	12.4 ± 2.7	11.5 ± 2.5	12.2 ± 2.5
	N_P$_{lat}$	22.3 ± 6.7	19.9 ± 6.2	18.6 ± 1.8

*significant difference based on an adjusted level of significance of $\alpha = 0.0083$

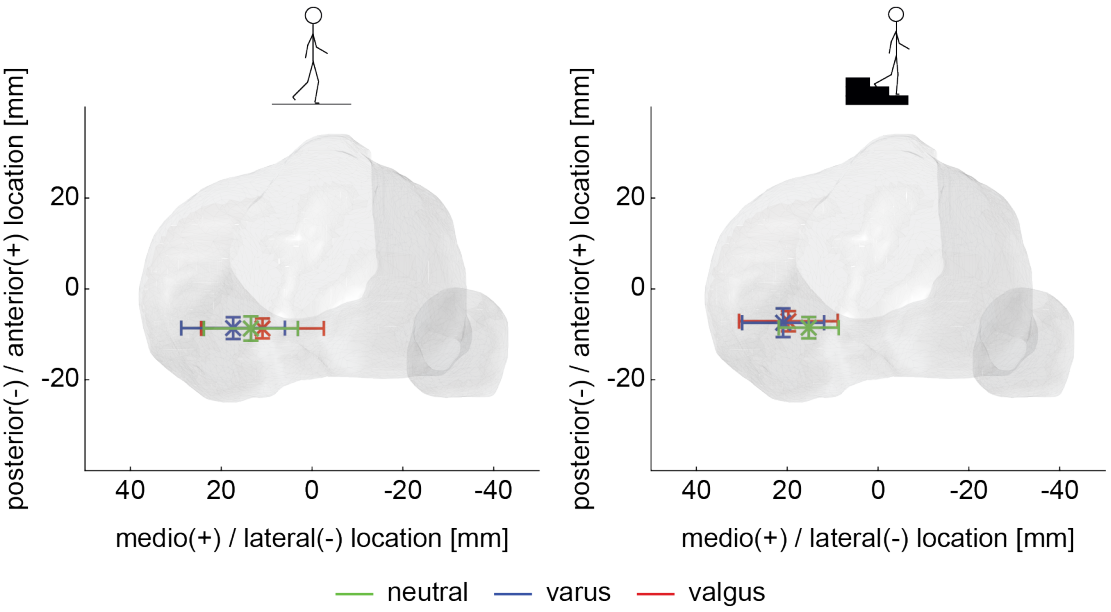

Figure 6.6: Location of the centre of rotation (CoR) shown on the tibial plateau during complete cycles of level walking (left) and stair descent (right). The mean across each group as well as the standard deviations in the antero-posterior and medio-lateral directions are indicated with whiskers.

6.5 Discussion

A comprehensive knowledge of subject-specific knee motion is crucial for a clear understanding of knee joint functionality and clinical decision-making. Within the recent tendency towards kinematic alignment in TKA in subjects with constitutional varus or valgus limb alignment, detailed knowledge of the relationship between limb alignment and subject-specific tibio-femoral kinematics is crucial for restoring natural knee kinematics and the aim to further improve patient outcome. However, motion of the natural knee remains controversially discussed and a comprehensive understanding of the role of limb alignment on tibio-femoral kinematics is missing. To our knowledge, this is the first *in vivo* study analysing tibio-femoral kinematics in healthy subjects with neutral, varus or valgus alignment throughout complete dynamic gait activities using dynamic videofluoroscopy. The present data revealed only a minor role of limb alignment on condylar translation and no influence on tibio-femoral rotations.

A comparison to the limited literature available on altered kinematics in knees with varus or valgus limb alignment showed only low agreement [131–133]. While a significant decrease in range of flexion and altered mean adduction angles over the loaded stance phase were found in osteoarthritic varus and valgus subjects [133], the results of this study have indicated no differences in the rotational RoM between the groups. Nevertheless, for both activities, the varus subjects generally showed the larges adduction angles over the course of the gait cycle, whereas the valgus subjects showed less adduction (Figure 6.3). The low agreement to the literature is inherently plausible based on the different subject characteristics. While our study has analysed healthy, pain free subjects without symptoms of osteoarthritis, the literature is based on subjects with osteoarthritis or subjects undergoing a TKA surgery.

Generally, limb alignment is classified based on the HKA. In the present study, the HKA angle extracted from the EOS measurement was compared against the videofluoroscopic abduction/adduction angle calculated during upright standing (Figure 6.2 A). While the position of the subject is comparable in both situations, the angle is calculated differently. The EOS is based on anatomical axes whereas the adduction angle is calculated based on the FFA and the longitudinal tibial shaft axis. As the FFA is based on a functional calibration movement (deep knee bending), differences to anatomical measures are likely to be observed. For a direct comparison of the two imaging modalities, comparable axes should be used for both calculations.

Furthermore, identical HKA angles can be caused by different combinations of the femoral and tibial mechanical angles resulting in altered orientations of the joint line [208]. Therefore, deviations of the tibio-femoral kinematics could be more affected by these measures instead of the

general HKA. In addition, femoral and tibial torsion influence the relative position of the femur and tibia to each other but also with respect to the hip and ankle joint. Influence on tibio-femoral rotation and condylar translations are inherently conceivable and additional research on the individual anatomical factors is required.

The presented study is clearly limited by the low number of subjects with a valgus limb alignment. Recruitment of the respective subjects was challenging, especially as constitutional valgus is only present in a low number of men and women [122]. However, to enhance the statistical power of this study, more valgus subjects would be needed.

A shift of the ground reaction force vector in subjects with mal-alignment has been previously reported [126]. Within this study no difference in the location of the CoR was found between the three alignments groups for either activity. As shown in a study using the CAMS knee dataset [170], the loading distribution within the joint does not necessarily correlate with the pivoting location [209]. It is therefore conceivable, that despite longitudinal rotations occurring around a medial CoR, changes to the loading within the joint exist among the three limb alignment groups. As a result, analysis of the tibio-femoral loading condition within the presented cohort should be done in further studies.

Within the currently used single-plane videofluoroscopic setup, 2D/3D registration of the fluoroscopic images is limited by the out-of-plane error [199]. While the registration errors could affect the determination of the CoR in the transverse plane, relative rotations and in plane translations are less influenced. In addition, relative errors between the femur and tibia are unknown. As previously reported, walking with the moving fluoroscope significantly reduces the walking speed but the reported walking patterns remain comparable to slow walking [203].

Small influence of individual limb alignment on tibio-femoral kinematics but large differences between subjects, suggest that other factors (e.g. soft tissue sufficiency) are responsible for individual differences. While the collateral ligaments are known to differ substantially in subjects with varus or valgus limb alignment [131], musculoskeletal modelling can provide additional insights in the elongation pattern of the collateral and cruciate ligaments throughout complete cycles of activities of daily living therefore enhance the understanding of soft tissue constraints and laxity on tibio-femoral kinematics.

Based on the presented data, and in combination with musculoskeletal modelling, further insights in the influence of anatomical parameters on tibio-femoral kinematics can be gained and thus enhance clinical decision-making towards further improvement of surgical outcomes aiming to restore natural knee joint motion.

6.6 Acknowledgement

This study was partially financed by the Commission for Technology and Innovation (Bern, Switzerland, Project Number 17078.1 PFLS-LS) and Medacta International SA (Castel San Pietro, Switzerland). Medacta was not involved in the data collection, nor in the analysis or the interpretation of the data.
The authors would like to thank all the subjects who participated in the study, as well as Nathalie Kühne (Balgrist University Hospital) for the organisation of the clinical examinations and all the students for their help in collection and processing of the data. Furthermore, we like to thank Edwina Huber and Bernhard Birner for their work analysing parts of the data during their thesis.

6.7 Conflict of interest statement

RL has received speaker's fees from Medacta. SFF receives advisory fees from Medacta as part of his consultancy work.

6.8 Supplementary materials

Supplementary material associated with this chapter can be found in Appendix D.

Chapter 7

Synthesis

A comprehensive understanding of natural knee joint motion along all its six degrees of freedom is not only needed to gain a detailed understanding of healthy knee joint function but also to understand pathologies and injury mechanisms of the knee. In addition, this knowledge can help to improve patient outcome by restoring a pain free functionality of the joint with sufficient range of motion (RoM) and avoid overloading of the soft tissue structures. While a general agreement on tibio-femoral kinematics of isolated flexion activities has been achieved, controversial findings have been presented for dynamic movements, such as walking. As a result, detailed knowledge of the underlying factors such as differences in the performed activity or anatomical variances between the studied subjects remains missing.

The overall objective of this doctoral thesis was to investigate the role of limb alignment and activity on natural knee joint motion throughout dynamic gait activities to gain an improved understanding of the mechanisms governing tibio-femoral kinematics. Within this thesis a unique subject cohort with neutral, varus, and valgus limb alignment was measured using the Institute for Biomechanics' moving fluoroscope. As the first study analysing tibio-femoral kinematics throughout complete gait cycles of level walking, downhill walking and stair descent in subjects with different limb alignment, this thesis has found no influence of the limb alignment on tibio-femoral rotations and only a minor effect on condylar translations. While the performed activity was found to significantly alter the range of tibio-femoral flexion, but to a lesser extent the ranges of tibial rotation, abduction/adduction and condylar translation. However, clear differences in the range of motion between the loaded stance and unloaded swing phase illustrate the need to analyse complete gait cycles to fully understand tibio-femoral kinematics.

7.1 Assessment of natural tibio-femoral kinematics

Accurate tracking, of the subject walking with the moving fluoroscope, is a prerequisite for the knee to stay within the field of view of the image intensifier and therefore successfully capturing tibio-femoral kinematics. Using real-time tracking of the knee motion, the moving fluoroscope is able to follow the knee despite natural variations and is therefore able to react to changes in the subject's walking pattern. Overall, the moving fluoroscope is able to travel with up to 5 m/s (maximal acceleration 9 m/s^2) and 1.33 m/s (maximal acceleration 4 m/s^2) in the horizontal and vertical direction, respectively.
The tracking ability of the moving fluoroscope was investigated in ten good outcome total knee arthroplasty (TKA) subjects during level walking, downhill walking and stair descent (Chapter 2). Across all three activities and all subjects, the average distance between the knee joint centre and the centre of the image intensifier was 4.0 ± 2.6 cm and 1.8 ± 1.4 cm for the horizontal and vertical direction, respectively (Figure 2.4). With its ability to maintain the knee centred within the field of view, the moving fluoroscope shows adequate tracking of the knee for all three gait activities. By reacting on subject-specific movement patterns rather than follow predefined paths, the moving fluoroscope was shown to be a promising tool to not only measure subjects with a TKA but also healthy subjects.

To obtain the three dimensional (3D) positions of the femur and tibia in space, accurate registration of the 3D bone geometries onto the two dimensional (2D) fluoroscopic images is needed. Until now, the imaging set-up was primarily used to assess tibio-femoral kinematics of TKA subjects [137, 193, 194]. Therefore, a novel, intensity-based 2D/3D registration algorithm was implemented, which not only utilises bone surface information but also incorporates the internal bone structure. By simulating x-ray projections through the computed tomography (CT) volume, a digitally reconstructed radiograph (DRR) is generated and directly compared with the original 2D videofluoroscopic image.
Using a radiopaque femur and tibia bone model, the accuracy of this novel intensity-based 2D/3D registration algorithm was evaluated by comparing manual fitting with intensity-based registration (Chapter 3). Absolute fitting and registration errors for the out-of-plane direction were substantially higher than for the two in-plane directions. Overall, manual fitting revealed smaller mean absolute errors compared to intensity-based registration for all three translations and rotations of the femur. For the tibia, the mean absolute errors along the vertical axis of the image intensifier were significantly smaller using the intensity-based registration, whereas

no differences were found for the other two translations and all three rotations (Table 3.2). In addition, data of three natural knees was used to examine the reliability and repeatability of a repetitive registration performed by different examiners. Comparable to the mean absolute error, the repeatability analysis showed small standard deviations (SD) for in-plane translations but larger SDs for the out-of-plane translation. SDs were comparable for all three rotations (Table 3.3). Although the obtained registration was extremely precise for certain images, manual registration was more accurate for a substantial amount of images. As a result, a semi-automatic 2D/3D registration procedure, with manual fitting of challenging images, was used to process the natural knee data presented in this thesis.

The structure of the knee enables rotations and translations along all six degrees of freedom and individual knee joint motion has been presented using a variety of kinematic analysis approaches. The Joint Coordinate System originally presented by Grood & Suntay [62] is a widely used approach to assess knee rotations. Based on a medio-lateral axis of the femur, the longitudinal axis of the tibia and a floating axis, flexion/extension, tibial internal/external rotation and abduction/adduction are reported. To calculate clinically meaningful rotations, the rotational axis of the femur and tibia have to closely approximate the instantaneous axes of rotation. Rotations calculated around any other segment fixed axis are, to a certain amount, affected by kinematic cross-talk.

Within the present thesis, definition of the anatomical coordinate system for the femur and tibia was challenging. Despite a variety of definitions presented in the literature, replication of a previously used coordinate system was difficult, mostly due to the lack of clear descriptions. In addition, the chosen coordinate systems should have been least affected by subjective selections of the examiner. As a result, a femoral functional flexion axis (FFA) based on the fluoroscopic data of a deep knee bending trial and defined according to the symmetrical axis of rotation approach (SARA) [67], was used as the medio-lateral axis of the femoral anatomical coordinate system. The antero-posterior axis was then defined orthogonal to the FFA and a temporary shaft axis while the longitudinal axis completed the right-handed, orthogonal coordinate system (Figure 4.2 A). For the tibial anatomical coordinate system, a plane parallel to the tibial articular surface and two circles intersecting the outer surface, were manually defined. The longitudinal axis was defined parallel to the shaft axis while the antero-posterior axis was defined orthogonal to the longitudinal axis and the line connecting the circle centres. The tibial medio-lateral axis completed the right-handed, orthogonal coordinate system (Figure 4.2 B).

While the femoral anatomical coordinate system was completely independent of the examiner,

the definition of the initial tibial plane and the point selection for the circle fitted to the tibial cortex were performed manually. To increase independence of the examiner, the tibial plane was defined based on the most prominent points of the tibia along the medio-lateral and antero-posterior direction. As all anatomical coordinate systems were initialised by the same examiner, no inter-examiner variability was assessed.
For both coordinate systems, the definition of the axes were comparable to Gray et al. [74] to facilitate comparison between the studies. In addition, the presented coordinate systems are in line with the recently published recommendations by Hull [207]. We used a functional axis for the femur but a geometrical for the tibia fixed axis. While the determination of the functional flexion axis works well using isolated flexion activities such as deep knee bending, squats or lunges, extraction of the longitudinal axis of rotation is more challenging due to the reduced range of motion along this axis. As a result, no ideal movement has yet been presented in the literature.

Condylar translation has also been assessed using a variety of analysis approaches. To better understand differences presented in the literature, identical fluoroscopic data during deep knee bending as well as level walking were used to assess antero-posterior (A-P) translations of a medial and lateral condyle point using six different kinematic analysis approaches (Chapter 5). For both tasks, significant differences were observed between the approaches (Figure 5.2 & 5.3). Both contact point measures (nearest point (NP) and tibio-femoral separation (SEP)) showed significant differences to the FFA, transepicondylar axis (TEA), and cylinder axis (CA) but also the FFA and TEA were significantly different for certain flexion angles or periods of the gait cycle.
In general, the ranges of A-P translation of the medial condyle showed lower SD than for the lateral condyle, indicating comparable translational patterns between the subjects. Especially, for the NP and SEP approach, the lateral condyle showed higher inter-subject variability, especially at lower flexion angles during level walking. While the NP and SEP are influenced by the subjective definition of the tibial plane, a relative flat region on the later condyle for certain subjects, can also result in "jumps" of the contact measures during phases of knee extension.
Although any femur fixed axis (FFA, TEA, CA) is able to replicate the instantaneous axis of rotation for certain instances, deviations of this axis at other time points will result in translational movements caused by kinematic cross-talk. Within the present study, the FFA is assumed to best approximate this instantaneous axis, and therefore be least affected by kinematic cross-talk. However, it is entirely clear, that femur fixed axes and contact point measures report different aspects of the kinematic behaviour. While a femur fixed axis is able to report the position of

the femur relative to the tibia and therefore allow assessment of the 3D movement of the joint, contact point approaches seem to provide information about the regions of tibio-femoral contact on the condylar surfaces.
As a result, the kinematic analysis approach should be chosen based on the research problem to best address the question raised. For the kinematic analysis of the neutral, varus, and valgus subjects presented in this thesis, the FFA was used to limit kinematic cross-talk. In addition, the NP approach was also presented for each subject to enable comparison with previously published studies as well as to enhance an in-depth understanding of the underlying mechanisms.

7.2 Role of limb alignment and activity on knee joint motion

In the currently available literature, tibio-femoral kinematics are controversially discussed, especially during functional activities such as walking. Beside the aforementioned differences in the analysis method and presentation of the results, differences in the performance of the investigated activity are inherently plausible and can alter the reported tibio-femoral kinematics. In addition, only limited studies have analysed different activities within the same subject cohort and using identical analysis approaches [24, 51].

To understand the influence of the performed walking task on tibio-femoral kinematics, ten healthy subjects were analysed throughout multiple complete gait cycles of level walking, downhill walking and stair descent (Chapter 4). To successfully perform the activities, all subjects showed an increased range of flexion/extension from level walking to downhill walking and stair descent in both, the loaded stance and the unloaded swing phase (Table 4.1). Tibial internal/external rotation and abduction/adduction were less dependent on the performed task (Table 4.1) and only a minimal effect was found for the A-P translation of the medial and lateral condyle (Table 4.2). Although larger A-P forces have been reported for downhill walking [91], this did not seem to critically influence A-P translation of the condyles in the healthy knee. However, differences were found between the loaded stance and unloaded swing phases, critically emphasising the need to analyse complete gait cycles and not only portions of a gait cycle.

While the influence of subject-specific musculoskeletal and anatomical variations has not yet been studied in detail, varus or valgus limb alignment poses considerable challenges for surgical interventions. With the recent tendency towards kinematic alignment in total knee arthroplasty

(TKA) surgery, detailed knowledge of the role of limb alignment on tibio-femoral kinematics is needed. Kinematic differences were assessed in twelve subjects with neutral limb alignment, ten subjects with varus limb alignment, and five subjects with valgus limb alignment (Chapter 6). Surprisingly, limb alignment played only a minor role in governing tibio-femoral rotations and condylar translations (Figure 6.3, 6.4 & 6.5). The only differences were found for the translational patterns of the lateral condyle point during stair descent between the varus and valgus subjects (Figure 6.4). However, inter-subject variability was high, suggesting that other factors such as soft tissue structures are responsible for the individual differences and critically affect tibio-femoral kinematics.

All subjects were grouped according to their hip-knee-ankle (HKA) angle assessed in a standing, weight-bearing position using the EOS system. The measured HKA showed good correlation with the abduction/adduction angle during standing for most subjects and differences in abduction/adduction were visible between the groups (Figure 6.2). However, no significant differences in abduction/adduction were found between the groups for the dynamic gait activities. While the relationship between static and dynamic HKA is not yet fully understood, this data clearly emphasises the need to assess complete cycles of different functional activities, in weight-bearing and non-weight-bearing situations to gain improved understanding of the influence of individual anatomical variations on tibio-femoral kinematics.

7.3 Tibio-femoral kinematics in the healthy knee vs. in total knee arthroplasties

TKA has become a standard surgical procedure in patients suffering from late stage osteoarthritis. By substituting the joint surfaces using a femoral and tibial implant component, TKA surgeries aim to relieve pain and restore physiological knee function. Despite the overall high success rate, 16 - 30% of all patients undergoing TKA surgery remain uncertain or unsatisfied with resultant outcome, especially during functional activities [3, 4]. To better understand individual requirements and mechanisms leading to unsatisfactory results and thus support implant selection and implantation in subjects with different limb alignments, comparison of healthy tibio-femoral and TKA kinematics is crucial. However, only limited studies have directly compared healthy knees with TKAs using the same set-up [24, 210].

In a recent study, a patient cohort with three different implants was measured during complete gait cycles of level walking, downhill walking and stair descent using the Institute for Biomechanics' moving fluoroscope [194]. The study consisted of three groups of each ten subjects with either a conventional posterior-stabilised, fixed-bearing implant (GMK Primary PS), a conventional ultra-congruent, mobile-bearing implant (GMK Primary UC) or a novel implant with geometrical conformity providing a constrain to the medial condyle together with a flat, unconstrained lateral tibial surface allowing rotational freedom (GMK Sphere). All subjects were good outcome and analysed at least one year post-operative. In a first preliminary analysis, implant kinematics throughout level walking of these 30 subjects were compared with the before presented tibio-femoral kinematics of 27 healthy subjects with a neutral, varus or valgus alignment (Chapter 6).

For both studies, tibio-femoral rotations were analysed based on two segment coordinate system (femur and tibia) and according to Grood & Suntay [62]. While the GMK Sphere and GMK PS exhibited comparable ranges of flexion/extension to the healthy subject groups, the GMK UC subjects showed a reduced RoM (Table 7.1). All three implant groups showed slightly smaller RoM for both, tibial internal/external rotation and abduction/adduction (Table 7.1). The additional constrains of the implant geometry, especially for the GMK Sphere and the GMK UC, can therefore be assumed to restrict axial rotation resulting in lower ranges of rotation.
Condylar A-P translations were compared using two femur fixed axis. As previously presented, a medial and lateral point on the FFA was used for the healthy subjects. For the implant subjects, a medial and lateral point on the geometric centre axis (GCA), defined based on the implant geometry, was used. To compare A-P translations despite different condylar sizes, all translations were normalised to the mean femoral width of the neutral subjects and their respective mid-sagittal plane. Over the complete gait cycle, the GMK PS and GMK UC showed comparable ranges of translation for both condyles, with the GMK PS exhibiting slightly larger ranges of motion than the GMK UC (Table 7.1). As intended by the implant geometry, the GMK Sphere showed minimal A-P translation of the medial condyle point but allowed more translations on the lateral side (Table 7.1).
In addition, the position of the medial and lateral GCA and FFA points were used to calculate an overall centre of rotation (CoR) across all subjects of each group [67]. While the neutral, varus and GMK Sphere subjects exhibited a mean medial CoR, the valgus, GMK PS and GMK UC subjects demonstrated a more central CoR (Table 7.1 & Figure 7.1).

Table 7.1: Range of motion for all three tibio-femoral rotations, range of A-P translation of the medial and lateral condylar points as well as location of the centre of rotation in all three healthy subject groups and three TKA groups. Mean and standard deviations across all subjects of each group are presented for the complete gait cycle of level walking.
Flex/ex: flexion/extension, int/ext: tibial internal/external rotation, ab/add: abduction/adduction

		neutral	**varus**	**valgus**	**GMK Sphere**	**GMK PS**	**GMK UC**
range of tibio-femoral rotations [°]	flex/ex	66.1 ± 3.9	63.3 ± 4.0	63.5 ± 6.4	62.7 ± 4.9	63.5 ± 4.7	57.2 ± 4.8
	int/ext	15.5 ± 2.6	13.8 ± 1.6	13.3 ± 0.8	11.9 ± 4.2	10.5 ± 1.9	8.1 ± 2.5
	abd/add	7.0 ± 1.9	5.7 ± 1.6	7.6 ± 2.3	2.8 ± 0.8	2.9 ± 0.8	2.3 ± 0.6
range of A-P translation [mm]	medial condyle	8.8 ± 1.8	8.6 ± 1.0	9.8 ± 0.8	4.1 ± 1.2	12.9 ± 2.8	8.9 ± 1.6
	lateral condyle	10.9 ± 2.2	9.9 ± 2.1	10.3 ± 3.0	11.4 ± 4.7	12.4 ± 2.2	9.1 ± 2.0
location of CoR [mm]	A-P location	-8.7 ± 2.7	-8.6 ± 2.4	-8.7 ± 2.2	-4.9 ± 0.8	-5.2 ± 1.5	-3.9 ± 1.6
	M-L location	13.5 ± 10.4	17.4 ± 11.4	10.9 ± 13.5	20.3 ± 5.7	-0.5 ± 15.7	4.6 ± 16.9

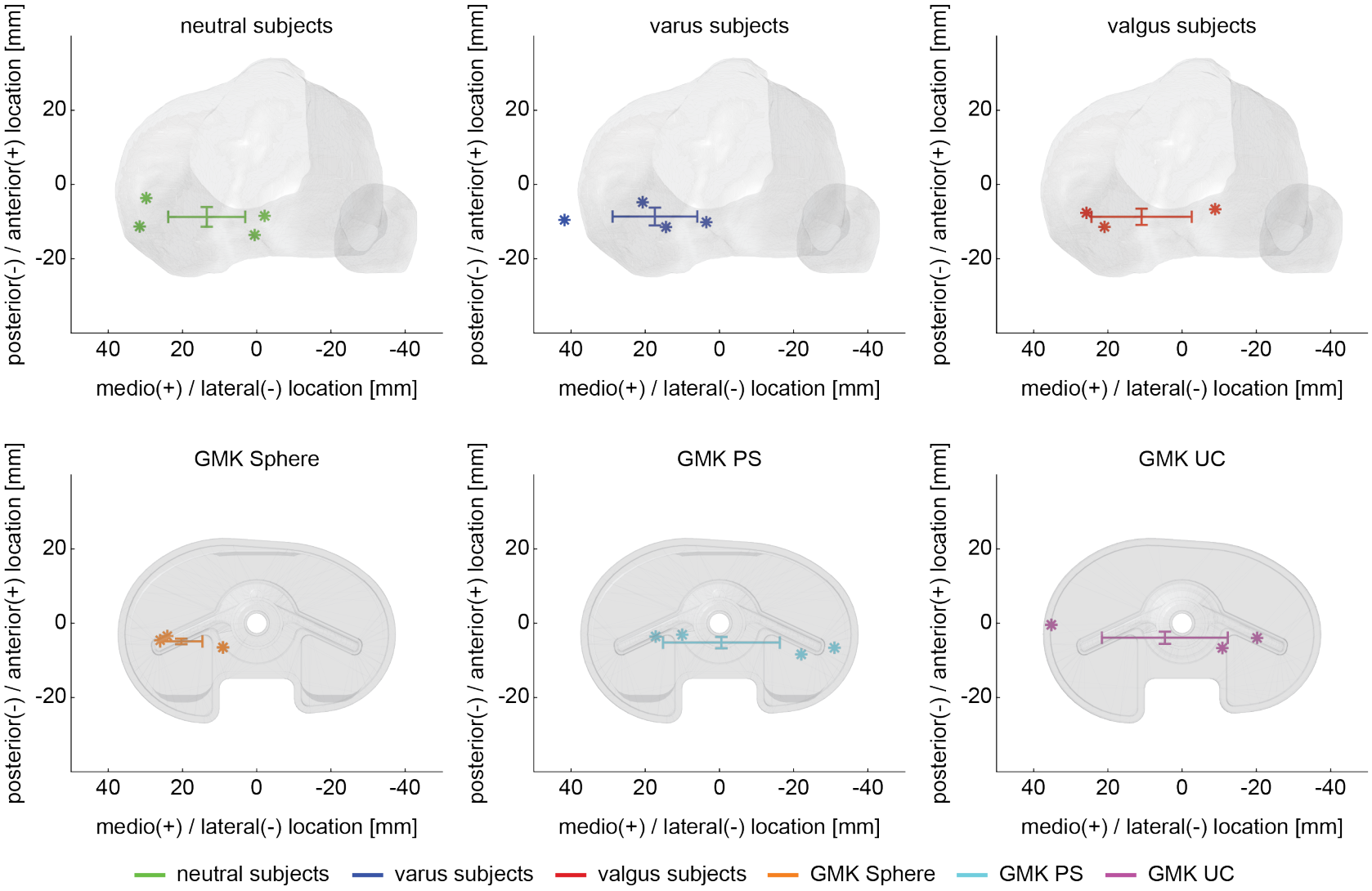

Figure 7.1: Location of the centre of rotation (CoR) over the complete gait cycle of level walking, shown on the tibial plateau for the neutral, varus and valgus subjects and on the tibial tray for the GMK Sphere, GMK PS and GMK UC subjects. The mean and standard deviations across all subjects of each group in the antero-posterior and medio-lateral direction are indicated. The most extreme points in each direction across all subjects of each group are presented as *

It is important to notice, that for all three alignment groups as well as in the GMK PS and GMK UC group, inter-subject variability was high and clear subject-specific differences were evident resulting in contrary translational behaviour for certain subjects.

After this first comparison, it seems, that individual tibio-femoral rotations and condylar translations can be guided by a specific implant geometry, but the necessity for different implant geometries to address individual functional needs is also evident. This data can provide a first basis to support clinical decision-making and help to further improve orthopaedic interventions aiming to restore physiological knee joint function but no clear conclusions on the resulting kinematic behaviour can be drawn based on subject specific limb alignment. As a result, intra-operative component alignment remains controversially discussed and further evidence especially on the desirable level of limb alignment correction is needed.

7.4 Limitations

Within this thesis, using the Institute for Biomechanics' moving fluoroscope has provided an unique measurement technology, enabling to not only measure *in vivo* tibio-femoral kinematics during isolated flexion activities but also throughout complete cycles of level walking, downhill walking and stair descent. However, the presented studies are subject to certain limitations.

For all three walking tasks, the subjects showed a reduced overall walking speed compared to free level walking or stair descent [143], which potentially influences the observed gait patterns of the individual subjects. In a control study, walking with the moving fluoroscope decreased the walking speed and small alterations to the kinematic gait parameters were observed. Despite this impact, the observed gait patterns were comparable to slow natural walking [203]. As the maximal walking speed is limited by the tracking capability of the moving fluoroscope, faster tracking and a better grip, using e.g. a rail system, would be needed to measure activities such as fast walking or running.

The greatest source of error is likely to arise from the single-plane set-up used. Caused by the imaging set-up, out-of-plane accuracy is limited, resulting in mean absolute out-of-plane registration errors of < 7.1 mm compared to much lower errors for in-plane translations (< 0.6 mm) and all three rotations ($< 1°$). With the imaging plane parallel to the main movement direc-

tion (sagittal plane), the main conclusions for A-P translation drawn within this thesis are least affected. However, the registration errors could affect the determination of the CoR in the transverse plane, whereas rotations and in-plane translations are less affected.
The performed validation study was based on radiopaque femur and tibia bone models, each analysed independently. As a result, relative translational and rotational errors between the femur and tibia are unknown. Registration errors for the individual bones could plausibly lead to larger total relative errors between the bones. However, to ensure relative medio-lateral alignment of the femur and tibia, each frame was manually checked. If needed, the out-of-plane registration was corrected and the bones were manually aligned.
Although x-ray images of the natural knee provide visible internal details, based on the internal structure of the bone rather than just a black silhouette, as for metal objects like TKA, they are subject to limited image contrast, further complicating the 2D/3D registration. In the current set-up, the contralateral knee is within the field of view and potentially overlapping the analysed knee twice per gait cycle, hence further challenging the 2D/3D registration at these instances.
The predominant drawback of using videofluoroscopy to study tibio-femoral kinematics, however is the subject's exposure to radiation. Within the study performed for this thesis, each subject was exposed to an average total effective dose for all fluoroscopic measurements of 0.17 ± 0.05 mSv, approximately equal to a chest x-ray or one and a half round trips New York – London [211]. To minimise radiation, especially in healthy young subjects, data collection using videofluoroscopy should be kept to a minimum.
To overcome the limitations with regard to the single-plane set-up, a dual-plane fluoroscope could provide considerable advantages to the currently used set-up, but would increase the overall radiation dose applied to each subject.

For the studies included in this thesis, only a limited number of subjects was analysed. The number of analysed subjects is comparable to other videofluoroscopic studies, which have rarely measured more than ten subjects. Nevertheless, a larger subject cohort would give a better representation of the tibio-femoral kinematics within the healthy population and the effect of individual outliers would be limited.
While the number of subjects within the groups with neutral (twelve subjects) and varus (ten subjects) limb alignment was comparable, only five subjects were included in the valgus group. With the limited number of valgus subjects among the healthy population [122], recruitment of subjects was challenging and resulted in the low number of subjects.
All subjects included, were healthy and generally young subjects with no history of knee injury

and no signs of knee disorders. Whereas this subject group provides unique knowledge of the healthy tibio-femoral kinematics, they are not directly comparable to subjects affected by osteoarthritis or undergoing TKA surgery. Subjects with extreme limb alignment (more than 10° of varus or valgus) and even pathological knees would increase our knowledge of the underlying injury mechanisms and enhance our understanding of factors leading to a successful or unsuccessful surgery. Therefore, further analysis of extreme and pathological cases is clearly needed. To recruit enough subjects, the subjects were not controlled for sex or the body side analysed. The overall distribution of subjects was by chance relatively balanced with fourteen female and thirteen male subjects allocated to twelve left and fifteen right knees. However, distribution within the different groups, especially for the varus and valgus subjects was more variable. In the literature, significant differences between women and men as well as between the dominant and non-dominant leg have been previously presented [53, 87]. However, these differences are in the range of the presented standard deviations for the individual groups and therefore the subject's gender and the analysed knee are assumed to only have a minimal impact on the presented results.

7.5 Outlook

This thesis has revealed large inter-subject variability for tibio-femoral rotations and especially condylar translations throughout complete cycles of different dynamic gait activities. The underlying data was the first to assess multiple complete gait cycles in a unique subject cohort with neutral, varus and valgus limb alignment. To further understand factors leading to subject-specific kinematics, additional analysis of the data set is needed. The following section contains ideas for future projects:

Each subject was not only analysed during dynamic gait activities but also while performing a squat, a deep knee bending activity and a passive flexion movement. This data can serve as a comparison to the previously published literature and can help to understand the differences between isolated flexion tasks and dynamic walking activities.

Furthermore, synchronised ground reaction forces and skin marker data was acquired for all trials. Analysis of the forces and moments acting on the knee joint can help to further examine the underlying mechanisms driving tibio-femoral kinematics.

Individual limb alignment has been shown to only play a minor role in governing tibio-femoral kinematics. Nevertheless, the impact of other anatomical parameters remains unknown. Femoral and tibial torsion are known to alter the relative position of the femur and tibia with respect to the hip and ankle joint and therefore influences on tibio-femoral kinematics are inherently conceivable. Based on the EOS assessment and CT scan of each subjects, additional anatomical factors, such as the femoral and tibial torsion or the joint line, can be defined and correlations with the already analysed tibio-femoral kinematics can be help to further understand the influence of anatomical variations on tibio-femoral kinematics.

Musculoskeletal modelling provides a great additional opportunity to better understand differences between the subjects by comparing the effect of the kinematic pattern on loading of the surrounding soft tissue structures. While regional dependency of the loading of the medial collateral ligament was found for the neutral subject, further analysis of the varus and valgus subject can help to better understand intra-operative soft tissue balancing during TKA surgery in cases with severe varus or valgus limb alignment.

Detailed comparison to the previously and currently measured subjects with a TKA can help to further understand potential factors leading to unsatisfied patients or unstable implants.

With the new mobile dual-plane fluoroscope, currently being built at the Institute of Biomechanics, measuring more challenging tasks will be possible and help to better understand the influence of demanding activities on individual tibio-femoral kinematics. In combination with further analysis of subjects with knee pathologies such as anterior cruciate ligament ruptures or severe osteoarthritis, a further understanding of the underlying injury can be achieved.

7.6 Conclusion

This doctoral thesis has investigated the role of limb alignment and activity in governing tibio-femoral kinematics of the natural knee. For the first time, tibio-femoral kinematics in subjects with neutral, varus and valgus limb alignment have been analysed throughout multiple, complete gait cycles of level walking, downhill walking as well as stair descent.

Limb alignment was found to only play a minor role in governing condylar translation and not influence tibio-femoral rotations. Despite significant differences in the range of flexion/extension, limited differences between the activities occurred for the ranges of tibial internal/external rotation, abduction/adduction as well as medial and lateral condylar translation. In addition, differences between the loaded stance and unloaded swing phase emphasise the need to assess complete gait cycles. Significant differences between kinematic analysis approaches also indicate the importance of reporting tibio-femoral kinematics, especially condylar translations, based on multiple analysis approaches.

Inter-subject variability in the resultant tibio-femoral kinematics can not only be explained by the individual limb alignment or the performed activity. It is entirely plausible, that other factors, such as soft tissue sufficiency, critically influence natural motion of the healthy knee. A comparison with previously measured kinematics in TKA patients, indicate, that identical implants can serve as an optimal solution for subjects with neutral, varus or valgus limb alignment. Overall, this data can provide a basis for clinical decision-making and can therefore help to further improve surgical procedures aiming to restore natural knee joint motion.

References

[1] T. P. Andriacchi, E. J. Alexander, M. K. Toney, C. Dyrby, and J. Sum. A point cluster method for in vivo motion analysis: applied to a study of knee kinematics. *J Biomech Eng*, 120(6):743–749, 1998.

[2] S. Kurtz, K. Ong, E. Lau, F. Mowat, and M. Halpern. Projections of primary and revision hip and knee arthroplasty in the united states from 2005 to 2030. *J Bone Joint Surg Am*, 89A(4):780–785, 2007.

[3] O. Robertsson, M. Dunbar, T. Pehrsson, K. Knutson, and L. Lidgren. Patient satisfaction after knee arthroplasty: a report on 27,372 knees operated on between 1981 and 1995 in sweden. *Acta Orthop Scand*, 71(3):262–267, 2000.

[4] R. B. Bourne, B. M. Chesworth, A. M. Davis, N. N. Mahomed, and K. D. Charron. Patient satisfaction after total knee arthroplasty: who is satisfied and who is not? *Clin Orthop Relat Res*, 468(1):57–63, 2010.

[5] M. A. R. Freeman and V. Pinskerova. The movement of the normal tibio-femoral joint. *J Biomech*, 38(2):197–208, 2005.

[6] M. Akbarshahi, A. G. Schache, J. W. Fernandez, R. Baker, S. Banks, and M. G. Pandy. Non-invasive assessment of soft-tissue artifact and its effect on knee joint kinematics during functional activity. *J Biomech*, 43(7):1292–1301, 2010.

[7] A. Cappozzo, U. D. Croce, A. Leardini, and L. Chiari. Human movement analysis using stereophotogrammetry. part 1: theoretical background. *Gait Posture*, 21(2):186–196, 2005.

[8] W. R. Taylor, R. M. Ehrig, G. N. Duda, H. Schell, P. Seebeck, and M. O. Heller. On the influence of soft tissue coverage in the determination of bone kinematics using skin markers. *J Orthop Res*, 23(4):726–734, 2005.

[9] A. Barré, R. Aissaoui, K. Aminian, and R. Dumas. Assessment of the lower limb soft tissue artefact at marker-cluster level with a high-density marker set during walking. *J Biomech*, 62:21–26, 2017.

[10] A. Cereatti, T. Bonci, M. Akbarshahi, K. Aminian, A. Barre, M. Begon, D. L. Benoit, C. Charbonnier, F. Dal Maso, S. Fantozzi, C. C. Lin, T. W. Lu, M. G. Pandy, R. Stagni, A. J. van den Bogert, and V. Camomilla. Standardization proposal of soft tissue artefact description for data sharing in human motion measurements. *J Biomech*, 62:5–13, 2017.

[11] A. Leardini, L. Chiari, U. Della Croce, and A. Cappozzo. Human movement analysis using stereophotogrammetry. part 3. soft tissue artifact assessment and compensation. *Gait Posture*, 21(2):212–225, 2005.

[12] B. M. Potvin, M. S. Shourijeh, K. B. Smale, and D. L. Benoit. A practical solution to reduce soft tissue artifact error at the knee using adaptive kinematic constraints. *J Biomech*, 62:124–131, 2017.

[13] D. L. Benoit, D. K. Ramsey, M. Lamontagne, L. Xu, P. Wretenberg, and P. Renstrom. In vivo knee kinematics during gait reveals new rotation profiles and smaller translations. *Clin Orthop Relat Res*, 454:81–88, 2007.

[14] Y. Ishii, K. Terajima, S. Terashima, and Y. Koga. Three-dimensional kinematics of the human knee with intracortical pin fixation. *Clin Orthop Relat Res*, 343:144–150, 1997.

[15] M. A. Lafortune, P. R. Cavanagh, H. J. Sommer, and A. Kalenak. Three-dimensional kinematics of the human knee during walking. *J Biomech*, 25(4):347–357, 1992.

[16] C. Reinschmidt, A. J. vandenBogert, A. Lundberg, B. M. Nigg, N. Murphy, A. Stacoff, and A. Stano. Tibiofemoral and tibiocalcaneal motion during walking: external vs. skeletal markers. *Gait Posture*, 6(2):98–109, 1997.

[17] P. Picerno. 25 years of lower limb joint kinematics by using inertial and magnetic sensors: A review of methodological approaches. *Gait Posture*, 51:239–246, 2017.

[18] J. Karrholm, S. Brandsson, and M. A. R. Freeman. Tibiofemoral movement 4: Changes of axial tibial rotation caused by forced rotation at the weight-bearing knee studied by rsa. *J Bone Joint Surg Br*, 82B(8):1201–1203, 2000.

[19] P. F. Hill, V. Vedi, A. Williams, H. Iwaki, V. Pinskerova, and M. A. Freeman. Tibiofemoral movement 2: The loaded and unloaded living knee studied by mri. *J Bone Joint Surg Br*, 82(8):1196–1198, 2000.

[20] H. Iwaki, V. Pinskerova, and M. A. R. Freeman. Tibiofemoral movement 1: The shapes and relative movements of the femur and tibia in the unloaded cadaver knee. *J Bone Joint Surg Br*, 82B(8):1189–1195, 2000.

[21] P. Johal, A. Williams, P. Wragg, D. Hunt, and W. Gedroyc. Tibio-femoral movement in the living knee. a study of weight bearing and non-weight bearing knee kinematics using 'interventional' mri. *J Biomech*, 38(2):269–276, 2005.

[22] A. McPherson, J. Karrholm, V. Pinskerova, A. Sosna, and S. Martelli. Imaging knee position using mri, rsa/ct and 3d digitisation. *J Biomech*, 38(2):263–268, 2005.

[23] J. M. Scarvell, P. N. Smith, K. M. Refshauge, H. R. Galloway, and K. R. Woods. Evaluation of a method to map tibiofemoral contact points in the normal knee using mri. *J Orthop Res*, 22(4):788–793, 2004.

[24] D. Dennis, R. Komistek, G. Scuderi, J. N. Argenson, J. Insall, M. Mahfouz, J. M. Aubaniac, and B. Haas. In vivo three-dimensional determination of kinematics for subjects with a normal knee or a unicompartmental or total knee replacement. *J Bone Joint Surg Am*, 83(2):104–115, 2001.

[25] C. R. Galvin, D. M. Perriman, P. M. Newman, J. T. Lynch, P. N. Smith, and J. M. Scarvell. Squatting, lunging and kneeling provided similar kinematic profiles in healthy knees-a systematic review and meta-analysis of the literature on deep knee flexion kinematics. *Knee*, 25(4):514–530, 2018.

[26] T. F. Grieco, A. Sharma, R. D. Komistek, and H. E. Cates. Single versus multiple-radii cruciate-retaining total knee arthroplasty: An in vivo mobile fluoroscopy study. *J Arthroplasty*, 31(3):694–701, 2016.

[27] P. Moewis, G. N. Duda, T. Jung, M. O. Heller, H. Boeth, B. Kaptein, and W. R. Taylor. The restoration of passive rotational tibio-femoral laxity after anterior cruciate ligament reconstruction. *PLoS One*, 11(7):e0159600, 2016.

[28] T. A. Moro-oka, S. Hamai, H. Miura, T. Shimoto, H. Higaki, B. J. Fregly, Y. Iwamoto, and S. A. Banks. Dynamic activity dependence of in vivo normal knee kinematics. *J Orthop Res*, 26(4):428–434, 2008.

[29] W. Anderst, R. Zauel, J. Bishop, E. Demps, and S. Tashman. Validation of three-dimensional model-based tibio-femoral tracking during running. *Med Eng Phys*, 31(1):10–16, 2009.

[30] S. Guan, H. A. Gray, F. Keynejad, and M. G. Pandy. Mobile biplane x-ray imaging system for measuring 3d dynamic joint motion during overground gait. *IEEE Trans Med Imaging*, 35(1):326–336, 2016.

[31] M. Kozanek, A. Hosseini, F. Liu, S. K. Van de Velde, T. J. Gill, H. E. Rubash, and G. Li. Tibiofemoral kinematics and condylar motion during the stance phase of gait. *J Biomech*, 42(12):1877–1884, 2009.

[32] G. Li, S. K. Van de Velde, and J. T. Bingham. Validation of a non-invasive fluoroscopic imaging technique for the measurement of dynamic knee joint motion. *J Biomech*, 41(7):1616–1622, 2008.

[33] L. E. DeFrate, H. Sun, T. J. Gill, H. E. Rubash, and G. Li. In vivo tibiofemoral contact analysis using 3d mri-based knee models. *J Biomech*, 37(10):1499–1504, 2004.

[34] S. Hamai, T. A. Moro-oka, N. J. Dunbar, H. Miura, Y. Iwamoto, and S. A. Banks. In vivo healthy knee kinematics during dynamic full flexion. *Biomed Res Int*, 2013:717546, 2013.

[35] F. Leszko, K. R. Hovinga, A. L. Lerner, R. D. Komistek, and M. R. Mahfouz. In vivo normal knee kinematics is ethnicity or gender an influencing factor? *Clin Orthop Relat Res*, 469(1):95–106, 2011.

[36] G. Li, L. E. DeFrate, S. E. Park, T. J. Gill, and H. E. Rubash. In vivo articular cartilage contact kinematics of the knee: an investigation using dual-orthogonal fluoroscopy and magnetic resonance image-based computer models. *Am J Sports Med*, 33(1):102–107, 2005.

[37] G. A. Li, J. M. Moses, R. Papannagari, N. P. Pathare, L. E. DeFrate, and T. J. Gill. Anterior cruciate ligament deficiency alters the in vivo motion of the tibiofemoral cartilage contact points in both the anteroposterior and mediolateral directions. *J Bone Joint Surg Am*, 88a(8):1826–1834, 2006.

[38] W. Qi, A. Hosseini, T. Y. Tsai, J. S. Li, H. E. Rubash, and G. A. Li. In vivo kinematics of the knee during weight bearing high flexion. *J Biomech*, 46(9):1576–1582, 2013.

[39] K. Kono, T. Tomita, K. Futai, T. Yamazaki, S. Tanaka, H. Yoshikawa, and K. Sugamoto. In vivo three-dimensional kinematics of normal knees during different high-flexion activities. *Bone Joint J*, 100b(1):50–55, 2018.

[40] O. Tanifuji, T. Sato, K. Kobayashi, T. Mochizuki, Y. Koga, H. Yamagiwa, G. Omori, and N. Endo. Three-dimensional in vivo motion analysis of normal knees using single-plane fluoroscopy. *J Orthop Sci*, 16(6):710–718, 2011.

[41] O. Tanifuji, T. Sato, K. Kobayashi, T. Mochizuki, Y. Koga, H. Yamagiwa, G. Omori, and N. Endo. Three-dimensional in vivo motion analysis of normal knees employing transepicondylar axis as an evaluation parameter. *Knee Surg Sports Traumatol Arthrosc*, 21(10):2301–2308, 2013.

[42] S. Yamaguchi, K. Gamada, T. Sasho, H. Kato, M. Sonoda, and S. A. Banks. In vivo kinematics of anterior cruciate ligament deficient knees during pivot and squat activities. *Clin Biomech*, 24(1):71–76, 2009.

[43] V. Pinskerova, P. Johal, S. Nakagawa, A. Sosna, A. Williams, W. Gedroyc, and M. A. Freeman. Does the femur roll-back with flexion? *J Bone Joint Surg Br*, 86(6):925–931, 2004.

[44] C. R. Galvin, D. M. Perriman, J. T. Lynch, M. R. Pickering, P. Newman, P. N. Smith, and J. M. Scarvell. Age has a minimal effect on knee kinematics: A cross-sectional 3d/2d image-registration study of kneeling. *Knee*, 26(5):988–1002, 2019.

[45] J. M. Scarvell, N. Hribar, C. R. Galvin, M. R. Pickering, D. M. Perriman, J. T. Lynch, and P. N. Smith. Analysis of kneeling by medical imaging shows the femur moves back to the posterior rim of the tibial plateau, prompting review of the concave-convex rule. *Phys Ther*, 99(3):311–318, 2019.

[46] D. A. Dennis, M. R. Mahfouz, R. D. Komistek, and W. Hoff. In vivo determination of normal and anterior cruciate ligament-deficient knee kinematics. *J Biomech*, 38(2):241–253, 2005.

[47] T. F. Grieco, A. Sharma, G. M. Dessinger, H. E. Cates, and R. D. Komistek. In vivo kinematic comparison of a bicruciate stabilized total knee arthroplasty and the normal knee using fluoroscopy. *J Arthroplasty*, 33(2):565–571, 2018.

[48] J. M. Scarvell, P. N. Smith, K. M. Refshauge, H. R. Galloway, and K. R. Woods. Comparison of kinematic analysis by mapping tibiofemoral contact with movement of the femoral condylar centres in healthy and anterior cruciate ligament injured knees. *J Orthop Res*, 22(5):955–962, 2004.

[49] T. Asano, M. Akagi, K. Tanaka, J. Tamura, and T. Nakamura. In vivo three-dimensional knee kinematics using a biplanar image-matching technique. *Clin Orthop Relat Res*, 388:157–166, 2001.

[50] T. Asano, M. Akagi, and T. Nakamura. The functional flexion-extension axis of the knee corresponds to the surgical epicondylar axis: in vivo analysis using a biplanar image-matching technique. *J Arthroplasty*, 20(8):1060–1067, 2005.

[51] R. D. Komistek, D. A. Dennis, and M. Mahfouz. In vivo fluoroscopic analysis of the normal human knee. *Clin Orthop Relat Res*, 410:69–81, 2003.

[52] Y. J. Koo and S. Koo. Three-dimensional kinematic coupling in the knee during normal walking. *J Biomech Eng*, 141(8):081012, 2019.

[53] T. Gale and W. Anderst. Asymmetry in healthy adult knee kinematics revealed through biplane radiography of the full gait cycle. *J Orthop Res*, 37(3):609–614, 2019.

[54] J. D. Yamokoski and S. A. Banks. Does close proximity robot motion tracking alter gait? *Gait Posture*, 34(4):508–513, 2011.

[55] S. A. Banks and W. A. Hodge. Accurate measurement of three-dimensional knee replacement kinematics using single-plane fluoroscopy. *IEEE Trans Biomed Eng*, 43(6):638–649, 1996.

[56] W. A. Hoff, R. D. Komistek, D. A. Dennis, S. M. Gabriel, and S. A. Walker. Three-dimensional determination of femoral-tibial contact positions under in vivo conditions using fluoroscopy. *Clin Biomech*, 13(7):455–472, 1998.

[57] M. R. Mahfouz, W. A. Hoff, R. D. Komistek, and D. A. Dennis. A robust method for registration of three-dimensional knee implant models to two-dimensional fluoroscopy images. *IEEE Trans Med Imaging*, 22(12):1561–1574, 2003.

[58] S. Zuffi, A. Leardini, F. Catani, S. Fantozzi, and A. Cappello. A model-based method for the reconstruction of total knee replacement kinematics. *IEEE Trans Med Imaging*, 18(10):981–991, 1999.

[59] B. J. Fregly, H. A. Rahman, and S. A. Banks. Theoretical accuracy of model-based shape matching for measuring natural knee kinematics with single-plane fluoroscopy. *J Biomech Eng*, 127(4):692–699, 2005.

[60] J. M. Scarvell, M. R. Pickering, and P. N. Smith. New registration algorithm for determining 3d knee kinematics using ct and single-plane fluoroscopy with improved out-of-plane translation accuracy. *J Orthop Res*, 28(3):334–340, 2010.

[61] T. Y. Tsai, T. W. Lu, C. M. Chen, M. Y. Kuo, and H. C. Hsu. A volumetric model-based 2d to 3d registration method for measuring kinematics of natural knees with single-plane fluoroscopy. *Med Phys*, 37(3):1273–1284, 2010.

[62] E. S. Grood and W. J. Suntay. A joint coordinate system for the clinical description of three-dimensional motions: application to the knee. *J Biomech Eng*, 105(2):136–144, 1983.

[63] M. H. Schwartz and A. Rozumalski. A new method for estimating joint parameters from motion data. *J Biomech*, 38(1):107–116, 2005.

[64] S. S. Gamage and J. Lasenby. New least squares solutions for estimating the average centre of rotation and the axis of rotation. *J Biomech*, 35(1):87–93, 2002.

[65] K. Halvorsen, M. Lesser, and A. Lundberg. A new method for estimating the axis of rotation and the center of rotation. *J Biomech*, 32(11):1221–1227, 1999.

[66] T. F. Besier, D. L. Sturnieks, J. A. Alderson, and D. G. Lloyd. Repeatability of gait data using a functional hip joint centre and a mean helical knee axis. *J Biomech*, 36(8):1159–1168, 2003.

[67] R. M. Ehrig, W. R. Taylor, G. N. Duda, and M. O. Heller. A survey of formal methods for determining functional joint axes. *J Biomech*, 40(10):2150–2157, 2007.

[68] R. A. Berger, H. E. Rubash, M. J. Seel, W. H. Thompson, and L. S. Crossett. Determining the rotational alignment of the femoral component in total knee arthroplasty using the epicondylar axis. *Clin Orthop Relat Res*, (286):40–47, 1993.

[69] R. A. Berger, L. S. Crossett, J. J. Jacobs, and H. E. Rubash. Malrotation causing patellofemoral complications after total knee arthroplasty. *Clin Orthop Relat Res*, (356):144–153, 1998.

[70] D. L. Churchill, S. J. Incavo, C. C. Johnson, and B. D. Beynnon. The transepicondylar axis approximates the optimal flexion axis of the knee. *Clin Orthop Relat Res*, (356):111–118, 1998.

[71] D. G. Eckhoff, T. F. Dwyer, J. M. Bach, V. M. Spitzer, and K. D. Reinig. Three-dimensional morphology of the distal part of the femur viewed in virtual reality. *J Bone Joint Surg Am*, 83-A Suppl 2(Pt 1):43–50, 2001.

[72] H. Kurosawa, P. S. Walker, S. Abe, A. Garg, and T. Hunter. Geometry and motion of the knee for implant and orthotic design. *J Biomech*, 18(7):487–499, 1985.

[73] T. J. Gill, S. K. Van de Velde, D. W. Wing, L. S. Oh, A. Hosseini, and G. Li. Tibiofemoral and patellofemoral kinematics after reconstruction of an isolated posterior cruciate ligament injury: in vivo analysis during lunge. *Am J Sports Med*, 37(12):2377–2385, 2009.

[74] H. A. Gray, S. Guan, L. T. Thomeer, A. G. Schache, R. de Steiger, and M. G. Pandy. Three-dimensional motion of the knee-joint complex during normal walking revealed by mobile biplane x-ray imaging. *J Orthop Res*, 37(3):615–630, 2019.

[75] J. S. Li, A. Hosseini, L. Cancre, N. Ryan, H. E. Rubash, and G. Li. Kinematic characteristics of the tibiofemoral joint during a step-up activity. *Gait Posture*, 38(4):712–716, 2013.

[76] G. Li, T. H. Wuerz, and L. E. DeFrate. Feasibility of using orthogonal fluoroscopic images to measure in vivo joint kinematics. *J Biomech Eng*, 126(2):314–318, 2004.

[77] S. Nakagawa, Y. Kadoya, S. Todo, A. Kobayashi, H. Sakamoto, M. A. Freeman, and Y. Yamano. Tibiofemoral movement 3: full flexion in the living knee studied by mri. *J Bone Joint Surg Br*, 82(8):1199–1200, 2000.

[78] E. Most, J. Axe, H. Rubash, and G. Li. Sensitivity of the knee joint kinematics calculation to selection of flexion axes. *J Biomech*, 37(11):1743–1748, 2004.

[79] S. J. Shefelbine, C. B. Ma, K. Y. Lee, M. A. Schrumpf, P. Patel, M. R. Safran, J. P. Slavinsky, and S. Majumdar. Mri analysis of in vivo meniscal and tibiofemoral kinematics in acl-deficient and normal knees. *J Orthop Res*, 24(6):1208–1217, 2006.

[80] S. Todo, Y. Kadoya, T. Moilanen, A. Kobayashi, Y. Yamano, H. Iwaki, and M. A. Freeman. Anteroposterior and rotational movement of femur during knee flexion. *Clin Orthop Relat Res*, (362):162–170, 1999.

[81] B. Akpinar, E. Thorhauer, J. J. Irrgang, S. Tashman, F. H. Fu, and W. J. Anderst. Alteration of knee kinematics after anatomic anterior cruciate ligament reconstruction is dependent on associated meniscal injury. *Am J Sports Med*, 46(5):1158–1165, 2018.

[82] S. Farrokhi, S. Tashman, A. B. Gil, B. A. Klatt, and G. K. Fitzgerald. Are the kinematics of the knee joint altered during the loading response phase of gait in individuals with concurrent knee osteoarthritis and complaints of joint instability? a dynamic stereo x-ray study. *Clin Biomech*, 27(4):384–389, 2012.

[83] V. Kefala, A. J. Cyr, M. D. Harris, D. R. Hume, B. S. Davidson, R. H. Kim, and K. B. Shelburne. Assessment of knee kinematics in older adults using high-speed stereo radiography. *Med Sci Sports Exerc*, 49(11):2260–2267, 2017.

[84] S. Koo and T. P. Andriacchi. The knee joint center of rotation is predominantly on the lateral side during normal walking. *J Biomech*, 41(6):1269–1273, 2008.

[85] G. Li, M. Kozanek, A. Hosseini, F. Liu, S. K. Van de Velde, and H. E. Rubash. New fluoroscopic imaging technique for investigation of 6dof knee kinematics during treadmill gait. *J Orthop Surg Res*, 4, 2009.

[86] F. Liu, M. Kozanek, A. Hosseini, S. K. Van de Velde, T. J. Gill, H. E. Rubash, and G. Li. In vivo tibiofemoral cartilage deformation during the stance phase of gait. *J Biomech*, 43(4):658–665, 2010.

[87] J. Clément, P. Toliopoulos, N. Hagemeister, F. Desmeules, A. Fuentes, and P. A. Vendittoli. Healthy 3d knee kinematics during gait: Differences between women and men, and correlation with x-ray alignment. *Gait Posture*, 64:198–204, 2018.

[88] T. Gale and W. Anderst. Knee kinematics of healthy adults measured using biplane radiography. *J Biomech Eng*, 142(10), 2020.

[89] M. Kuster, S. Sakurai, and G. A. Wood. Kinematic and kinetic comparison of downhill and level walking. *Clin Biomech*, 10(2):79–84, 1995.

[90] A. S. McIntosh, K. T. Beatty, L. N. Dwan, and D. R. Vickers. Gait dynamics on an inclined walkway. *J Biomech*, 39(13):2491–2502, 2006.

[91] A. N. Lay, C. J. Hass, and R. J. Gregor. The effects of sloped surfaces on locomotion: a kinematic and kinetic analysis. *J Biomech*, 39(9):1621–1628, 2006.

[92] S. Farrokhi, C. A. Voycheck, B. A. Klatt, J. A. Gustafson, S. Tashman, and G. K. Fitzgerald. Altered tibiofemoral joint contact mechanics and kinematics in patients with knee osteoarthritis and episodic complaints of joint instability. *Clin Biomech*, 29(6):629–635, 2014.

[93] T. Saari, L. Carlsson, J. Karlsson, and J. Karrholm. Knee kinematics in medial arthrosis. dynamic radiostereometry during active extension and weight-bearing. *J Biomech*, 38(2):285–292, 2005.

[94] A. Bowman, M. Shunmugam, A. R. Watts, D. C. Bramwell, C. Wilson, and J. Krishnan. Inter-observer and intra-observer reliability of mechanical axis alignment before and after total knee arthroplasty using long leg radiographs. *Knee*, 23(2):203–208, 2016.

[95] A. N. Colebatch, D. J. Hart, G. J. Zhai, F. M. Williams, T. D. Spector, and N. K. Arden. Effective measurement of knee alignment using ap knee radiographs. *Knee*, 16(1):42–45, 2009.

[96] D. Cooke, A. Scudamore, J. Li, U. Wyss, T. Bryant, and P. Costigan. Axial lower-limb alignment: comparison of knee geometry in normal volunteers and osteoarthritis patients. *Osteoarthritis Cartilage*, 5(1):39–47, 1997.

[97] R. Guggenberger, C. W. Pfirrmann, P. P. Koch, and F. M. Buck. Assessment of lower limb length and alignment by biplanar linear radiography: comparison with supine ct and upright full-length radiography. *AJR Am J Roentgenol*, 202(2):W161–167, 2014.

[98] G. McDaniel, K. L. Mitchell, C. Charles, and V. B. Kraus. A comparison of five approaches to measurement of anatomic knee alignment from radiographs. *Osteoarthritis Cartilage*, 18(2):273–277, 2010.

[99] J. R. Moreland, L. W. Bassett, and G. J. Hanker. Radiographic analysis of the axial alignment of the lower extremity. *J Bone Joint Surg Am*, 69(5):745–749, 1987.

[100] M. A. Hunt, P. J. Fowler, T. B. Birmingham, T. R. Jenkyn, and J. R. Giffin. Foot rotational effects on radiographic measures of lower limb alignment. *Can J Surg*, 49(6):401–406, 2006.

[101] L. Jud, T. Trache, T. Tondelli, P. Fürnstahl, S. F. Fucentese, and L. Vlachopoulos. Rotation or flexion alters mechanical leg axis measurements comparably in patients with different coronal alignment. *Knee Surg Sports Traumatol Arthrosc*, 28(10):3128–3134, 2019.

[102] A. V. Specogna, T. B. Birmingham, M. A. Hunt, I. C. Jones, T. R. Jenkyn, P. J. Fowler, and J. R. Giffin. Radiographic measures of knee alignment in patients with varus gonarthrosis: effect of weightbearing status and associations with dynamic joint load. *Am J Sports Med*, 35(1):65–70, 2007.

[103] D. Magee. *Orthopedic physical assessment*. Elsevier, 6th edition edition, 2014.

[104] J. Cibere, N. Bellamy, A. Thorne, J. M. Esdaile, K. J. McGorm, A. Chalmers, S. Huang, P. Peloso, K. Shojania, J. Singer, H. Wong, and J. Kopec. Reliability of the knee examination in osteoarthritis: effect of standardization. *Arthritis Rheum*, 50(2):458–468, 2004.

[105] S. R. Jonson and M. T. Gross. Intraexaminer reliability, interexaminer reliability, and mean values for nine lower extremity skeletal measures in healthy naval midshipmen. *J Orthop Sports Phys Ther*, 25(4):253–263, 1997.

[106] V. B. Kraus, T. P. Vail, T. Worrell, and G. McDaniel. A comparative assessment of alignment angle of the knee by radiographic and physical examination methods. *Arthritis Rheum*, 52(6):1730–1735, 2005.

[107] R. S. Hinman, R. L. May, and K. M. Crossley. Is there an alternative to the full-leg radiograph for determining knee joint alignment in osteoarthritis? *Arthritis Rheum*, 55(2):306–313, 2006.

[108] A. M. Navali, L. A. Bahari, and B. Nazari. A comparative assessment of alternatives to the full-leg radiograph for determining knee joint alignment. *Sports Med Arthrosc Rehabil Ther Technol*, 4(1):40, 2012.

[109] M. A. Hunt, T. B. Birmingham, T. R. Jenkyn, J. R. Giffin, and I. C. Jones. Measures of frontal plane lower limb alignment obtained from static radiographs and dynamic gait analysis. *Gait Posture*, 27(4):635–640, 2008.

[110] E. I. Kornaropoulos, W. R. Taylor, G. N. Duda, R. M. Ehrig, G. Matziolis, M. Müller, G. Wassilew, P. Asbach, C. Perka, and M. O. Heller. Frontal plane alignment: an imageless method to predict the mechanical femoral-tibial angle (mfta) based on functional determination of joint centres and axes. *Gait Posture*, 31(2):204–208, 2010.

[111] A. Mündermann, C. O. Dyrby, and T. P. Andriacchi. A comparison of measuring mechanical axis alignment using three-dimensional position capture with skin markers and radiographic measurements in patients with bilateral medial compartment knee osteoarthritis. *Knee*, 15(6):480–485, 2008.

[112] B. Vanwanseele, D. Parker, and M. Coolican. Frontal knee alignment: three-dimensional marker positions and clinical assessment. *Clin Orthop Relat Res*, 467(2):504–509, 2009.

[113] J. Clément, W. Blakeney, N. Hagemeister, F. Desmeules, N. Mezghani, V. Lowry, and P. A. Vendittoli. Hip-knee-ankle (hka) angle modification during gait in healthy subjects. *Gait Posture*, 72:62–68, 2019.

[114] L. D. Duffell, J. Mushtaq, M. Masjedi, and J. P. Cobb. The knee adduction angle of the osteo-arthritic knee: a comparison of 3d supine, static and dynamic alignment. *Knee*, 21(6):1096–1100, 2014.

[115] M. Wybier and P. Bossard. Musculoskeletal imaging in progress: the eos imaging system. *Joint Bone Spine*, 80(3):238–243, 2013.

[116] D. Folinais, P. Thelen, C. Delin, C. Radier, Y. Catonne, and J. Y. Lazennec. Measuring femoral and rotational alignment: Eos system versus computed tomography. *Orthop Traumatol Surg Res*, 99(5):509–516, 2013.

[117] B. Guenoun, F. Zadegan, F. Aim, D. Hannouche, and R. Nizard. Reliability of a new method for lower-extremity measurements based on stereoradiographic three-dimensional reconstruction. *Orthop Traumatol Surg Res*, 98(5):506–513, 2012.

[118] Y. Chaibi, T. Cresson, B. Aubert, J. Hausselle, P. Neyret, O. Hauger, J. A. de Guise, and W. Skalli. Fast 3d reconstruction of the lower limb using a parametric model and statistical inferences and clinical measurements calculation from biplanar x-rays. *Comput Methods Biomech Biomed Engin*, 15(5):457–466, 2012.

[119] R. Gheno, E. Nectoux, B. Herbaux, M. Baldisserotto, L. Glock, A. Cotten, and N. Boutry. Three-dimensional measurements of the lower extremity in children and adolescents using a low-dose biplanar x-ray device. *Eur Radiol*, 22(4):765–771, 2012.

[120] C. Delin, S. Silvera, C. Bassinet, P. Thelen, J. L. Rehel, P. Legmann, and D. Folinais. Ionizing radiation doses during lower limb torsion and anteversion measurements by eos stereoradiography and computed tomography. *Eur J Radiol*, 83(2):371–377, 2014.

[121] T. J. Dietrich, C. W. Pfirrmann, A. Schwab, K. Pankalla, and F. M. Buck. Comparison of radiation dose, workflow, patient comfort and financial break-even of standard digital radiography and a novel biplanar low-dose x-ray system for upright full-length lower limb and whole spine radiography. *Skeletal Radiol*, 42(7):959–967, 2013.

[122] J. Bellemans, W. Colyn, H. Vandenneucker, and J. Victor. The chitranjan ranawat award: is neutral mechanical alignment normal for all patients? the concept of constitutional varus. *Clin Orthop Relat Res*, 470(1):45–53, 2012.

[123] M. T. Hirschmann, S. Hess, H. Behrend, F. Amsler, V. Leclercq, and L. B. Moser. Phenotyping of hip-knee-ankle angle in young non-osteoarthritic knees provides better understanding of native alignment variability. *Knee Surg Sports Traumatol Arthrosc*, 27(5):1378–1384, 2019.

[124] M. O. Heller, W. R. Taylor, C. Perka, and G. N. Duda. The influence of alignment on the musculo-skeletal loading conditions at the knee. *Langenbecks Arch Surg*, 388(5):291–297, 2003.

[125] O. D. Schipplein and T. P. Andriacchi. Interaction between active and passive knee stabilizers during level walking. *J Orthop Res*, 9(1):113–119, 1991.

[126] S. Van Rossom, M. Wesseling, C. R. Smith, D. G. Thelen, B. Vanwanseele, V. A. Dieter, and I. Jonkers. The influence of knee joint geometry and alignment on the tibiofemoral load distribution: A computational study. *Knee*, 26(4):813–823, 2019.

[127] G. M. Brouwer, A. W. van Tol, A. P. Bergink, J. N. Belo, R. M. Bernsen, M. Reijman, H. A. Pols, and S. M. Bierma-Zeinstra. Association between valgus and varus alignment and the development and progression of radiographic osteoarthritis of the knee. *Arthritis Rheum*, 56(4):1204–1211, 2007.

[128] L. Sharma, J. Song, D. T. Felson, S. Cahue, E. Shamiyeh, and D. D. Dunlop. The role of knee alignment in disease progression and functional decline in knee osteoarthritis. *JAMA*, 286(2):188–195, 2001.

[129] L. Sharma, J. Song, D. Dunlop, D. Felson, C. E. Lewis, N. Segal, J. Torner, T. D. Cooke, J. Hietpas, J. Lynch, and M. Nevitt. Varus and valgus alignment and incident and progressive knee osteoarthritis. *Ann Rheum Dis*, 69(11):1940–1945, 2010.

[130] R. W. Hsu, S. Himeno, M. B. Coventry, and E. Y. Chao. Normal axial alignment of the lower extremity and load-bearing distribution at the knee. *Clin Orthop Relat Res*, 255:215–227, 1990.

[131] C. Baier, A. Benditz, F. Koeck, A. Keshmiri, J. Grifka, and G. Maderbacher. Different kinematics of knees with varus and valgus deformities. *J Knee Surg*, 31(3):264–269, 2018.

[132] G. Maderbacher, C. Baier, H. R. Springorum, F. Zeman, J. Grifka, and A. Keshmiri. Lower limb anatomy and alignment affect natural tibiofemoral knee kinematics: a cadaveric investigation. *J Arthroplasty*, 31(9):2038–2042, 2016.

[133] K. Turcot, S. Armand, A. Lübbeke, D. Fritschy, P. Hoffmeyer, and D. Suva. Does knee alignment influence gait in patients with severe knee osteoarthritis? *Clin Biomech*, 28(1):34–39, 2013.

[134] S. A. Banks, B. J. Fregly, F. Boniforti, C. Reinschmidt, and S. Romagnoli. Comparing in vivo kinematics of unicondylar and bi-unicondylar knee replacements. *Knee Surg Sports Traumatol Arthrosc*, 13(7):551–556, 2005.

[135] M. Foresti. *In vivo measurement of total knee joint replacement kinematics and kinetics during stair descent.* Phd thesis, 2009.

[136] M. Foresti, H. Gerber, and E. Stüssi. Biomechanics of the knee by means of a two degrees of freedom automated video fluoroscope and instrumented stairs. In *8th International Symposium on Computer Methods in Biomechanics and Biomedical Engineering*, 2008.

[137] M. S. Zihlmann, H. Gerber, A. Stacoff, K. Burckhardt, G. Szekely, and E. Stüssi. Three-dimensional kinematics and kinetics of total knee arthroplasty during level walking using single plane video-fluoroscopy and force plates: a pilot study. *Gait Posture*, 24(4):475–481, 2006.

[138] K. Burckhardt, G. Szekely, H. Notzli, J. Hodler, and C. Gerber. Submillimeter measurement of cup migration in clinical standard radiographs. *IEEE Trans Med Imaging*, 24(5):676–688, 2005.

[139] J. Weese, G. P. Penney, P. Desmedt, T. M. Buzug, D. L. Hill, and D. J. Hawkes. Voxel-based 2-d/3-d registration of fluoroscopy images and ct scans for image-guided surgery. *IEEE Trans Inf Technol Biomed*, 1(4):284–293, 1997.

[140] T. A. Moro-oka, M. Muenchinger, J. P. Canciani, and S. A. Banks. Comparing in vivo kinematics of anterior cruciate-retaining and posterior cruciate-retaining total knee arthroplasty. *Knee Surg Sports Traumatol Arthrosc*, 15(1):93–99, 2007.

[141] A. Sharma, F. Leszko, R. D. Komistek, G. R. Scuderi, Jr. Cates, H. E., and F. Liu. In vivo patellofemoral forces in high flexion total knee arthroplasty. *J Biomech*, 41(3):642–648, 2008.

[142] T. P. Andriacchi, J. O. Galante, and R. W. Fermier. The influence of total knee-replacement design on walking and stair-climbing. *J Bone Joint Surg Am*, 64(9):1328–1335, 1982.

[143] A. Stacoff, C. Diezi, G. Luder, E. Stüssi, and I. A. Kramers-de Quervain. Ground reaction forces on stairs: effects of stair inclination and age. *Gait Posture*, 21(1):24–38, 2005.

[144] F. Catani, A. Ensini, C. Belvedere, A. Feliciangeli, M. G. Benedetti, A. Leardini, and S. Giannini. In vivo kinematics and kinetics of a bi-cruciate substituting total knee arthroplasty: A combined fluoroscopic and gait analysis study. *J Orthop Res*, 27(12):1569–1575, 2009.

[145] S. Fantozzi, M. G. Benedetti, A. Leardini, S. A. Banks, A. Cappello, D. Assirelli, and F. Catani. Fluoroscopic and gait analysis of the functional performance in stair ascent of two total knee replacement designs. *Gait Posture*, 17(3):225–234, 2003.

[146] A. Leardini, C. Belvedere, L. Astolfi, S. Fantozzi, M. Viceconti, F. Taddei, A. Ensini, M. G. Benedetti, and F. Catani. A new software tool for 3d motion analyses of the musculo-skeletal system. *Clin Biomech*, 21(8):870–879, 2006.

[147] A. D. Dennis and R. D. Komistek. An in vivo analysis of the effectiveness of the osteoarthritic knee brace during heel strike and midstance of gait. *Acta Chir Orthop Traumatol Cech*, 66(6):323–327, 1999.

[148] S. K. Van de Velde, A. Hosseini, M. Kozanek, T. J. Gill, H. E. Rubash, and G. Li. Application guidelines for dynamic knee joint analysis with a dual fluoroscopic imaging system. *Acta Orthop Belg*, 76(1):107–113, 2010.

[149] D. Zhao, S. A. Banks, K. H. Mitchell, D. D. D'Lima, Jr. Colwell, C. W., and B. J. Fregly. Correlation between the knee adduction torque and medial contact force for a variety of gait patterns. *J Orthop Res*, 25(6):789–797, 2007.

[150] F. Alton, L. Baldey, S. Caplan, and M. C. Morrissey. A kinematic comparison of overground and treadmill walking. *Clin Biomech*, 13(6):434–440, 1998.

[151] S. J. Lee and J. Hidler. Biomechanics of overground vs. treadmill walking in healthy individuals. *J Appl Physiol*, 104(3):747–755, 2008.

[152] H. Stolze, J. P. Kuhtz-Buschbeck, C. Mondwurf, A. Boczek-Funcke, K. Johnk, G. Deuschl, and M. Illert. Gait analysis during treadmill and overground locomotion in children and adults. *Electroencephalogr Clin Neurophysiol*, 105(6):490–497, 1997.

[153] G. M. Strathy, E. Y. Chao, and R. K. Laughman. Changes in knee function associated with treadmill ambulation. *J Biomech*, 16(7):517–522, 1983.

[154] T. Warabi, M. Kato, K. Kiriyama, T. Yoshida, and N. Kobayashi. Treadmill walking and overground walking of human subjects compared by recording sole-floor reaction force. *Neurosci Res*, 53(3):343–348, 2005.

[155] J. R. Watt, J. R. Franz, K. Jackson, J. Dicharry, P. O. Riley, and D. C. Kerrigan. A three-dimensional kinematic and kinetic comparison of overground and treadmill walking in healthy elderly subjects. *Clin Biomech*, 25(5):444–449, 2010.

[156] E. Wass, N. F. Taylor, and A. Matsas. Familiarisation to treadmill walking in unimpaired older people. *Gait Posture*, 21(1):72–79, 2005.

[157] G. Stoquart, C. Detrembleur, and T. Lejeune. Effect of speed on kinematic, kinetic, electromyographic and energetic reference values during treadmill walking. *Neurophysiol Clin*, 38(2):105–116, 2008.

[158] S. A. Banks, C. Lightcap, and J. D. Yamokoski. A robotic radiographic imaging platform for observation of dynamic skeletal motion and tomography. *J Biomech*, 39(Supplement 1):S446, 2006.

[159] M. Foresti, H. Gerber, and E. Stüssi. Automated moving fluoroscope: a novel method to acquire video fluoroscopic data during level walking. *J Biomech*, 39(Supplement 1):S109, 2006.

[160] F. Liu, R. Komistek, W. Hamel, M. Mahfouz, and P. Gabriel. Automatically image controlled mobile fluoroscope system. *J Biomech*, 39(Supplement 1):S213, 2006.

[161] W. Gander and J. Hrebicek. *Least squares fit of point clouds*, book section 23, pages 339–349. Springer, 1997.

[162] P. Schütz, M. Angst, B. Postolka, M. Hitz, P. Schwilch, H. Gerber, WR. Taylor, and R. List. Knee implant kinematics of downhill walking by means of videofluoroscopy. In *14th Symposium on the 3-D Analysis of Human Movement*, 2016.

[163] R. List, M. Foresti, H. Gerber, J. Goldhahn, P. Rippstein, and E. Stüssi. Three-dimensional kinematics of an unconstrained ankle arthroplasty: a preliminary in vivo videofluoroscopic feasibility study. *Foot Ankle Int*, 33(10):883–892, 2012.

[164] M. P. Kadaba, H. K. Ramakrishnan, M. E. Wootten, J. Gainey, G. Gorton, and G. V. Cochran. Repeatability of kinematic, kinetic, and electromyographic data in normal adult gait. *J Orthop Res*, 7(6):849–860, 1989.

[165] I.A. Kramers de Quervain, E. Stüssi, and A. Stacoff. Ganganalyse beim gehen und laufen. *Sportmedizin und Sporttraumatologie*, 56(2):35–42, 2008.

[166] I.A. Kramers-de Quervain, E. Stüssi, R. Müller, T. Drobny, U. Munzinger, and N. Gschwend. Quantitative gait analysis after bilateral total knee arthroplasty with two different systems within each subject. *J Arthroplasty*, 12(2):168–179, 1997.

[167] Z. Zhu and G. Li. An automatic 2d–3d image matching method for reproducing spatial knee joint positions using single or dual fluoroscopic images. *Comput Methods Biomech Biomed Engin*, 15(11):1245–1256, 2012.

[168] K. De and V. Masilamani. Image sharpness measure for blurred images in frequency domain. *Procedia Eng*, 64:149–158, 2013.

[169] S. A. Banks, A. Z. Banks, F.F. Cook, and W. A. Hodge. Markerless three dimensional measurement of knee kinematics using single-plane fluoroscopy. In *20th Annual Meeting, American Society of Biomechanics*, 1996.

[170] W. R. Taylor, P. Schütz, G. Bergmann, R. List, B. Postolka, M. Hitz, J. Dymke, P. Damm, G. Duda, H. Gerber, V. Schwachmeyer, S. H. Hosseini Nasab, A. Trepczynski, and I. Kutzner. A comprehensive assessment of the musculoskeletal system: The cams-knee data set. *J Biomech*, 65:32–39, 2017.

[171] T. Yamazaki, T. Watanabe, Y. Nakajima, K. Sugamoto, T. Tomita, H. Yoshikawa, and S. Tamura. Improvement of depth position in 2-d/3-d registration of knee implants using single-plane fluoroscopy. *IEEE Trans Med Imaging*, 23(5):602–612, 2004.

[172] T. A. Moro-oka, S. Hamai, H. Miura, T. Shimoto, H. Higaki, B. J. Fregly, Y. Iwamoto, and S. A. Banks. Can magnetic resonance imaging-derived bone models be used for accurate motion measurement with single-plane three-dimensional shape registration? *J Orthop Res*, 25(7):867–872, 2007.

[173] A. Gueziec, P. Kazanzides, B. Williamson, and R. H. Taylor. Anatomy-based registration of ct-scan and intraoperative x-ray images for guiding a surgical robot. *IEEE Trans Med Imaging*, 17(5):715–728, 1998.

[174] A. Hamadeh, S. Lavallee, and P. Cinquin. Automated 3-dimensional computed tomographic and fluoroscopic image registration. *Comput Aided Surg*, 3(1):11–19, 1998.

[175] D. Tomazevic, B. Likar, T. Slivnik, and F. Pernus. 3-d/2-d registration of ct and mr to x-ray images. *IEEE Trans Med Imaging*, 22(11):1407–1416, 2003.

[176] W. Birkfellner, J. Wirth, W. Burgstaller, B. Baumann, H. Staedele, B. Hammer, N. C. Gellrich, A. L. Jacob, P. Regazzoni, and P. Messmer. A faster method for 3d/2d medical image registration–a simulation study. *Phys Med Biol*, 48(16):2665–2679, 2003.

[177] S. Jonic, P. Thevenaz, G. Zheng, L. P. Nolte, and M. Unser. An optimized spline-based registration of a 3d ct to a set of c-arm images. *Int J Biomed Imaging*, 2006, 2006.

[178] H. Livyatan, Z. Yaniv, and L. Joskowicz. Gradient-based 2-d/3-d rigid registration of fluoroscopic x-ray to ct. *IEEE Trans Med Imaging*, 22(11):1395–1406, 2003.

[179] G. P. Penney, J. Weese, J. A. Little, P. Desmedt, D. L. Hill, and D. J. Hawkes. A comparison of similarity measures for use in 2-d-3-d medical image registration. *IEEE Trans Med Imaging*, 17(4):586–595, 1998.

[180] D.B. Russakoff, T. Rohlfing, and C. R. Maurer. Fast intensity-based 2d-3d image registration of clinical data using light fields. In *9th IEEE International Conference on Computer Vision*, pages 416–422, 2003.

[181] D. B. Russakoff, T. Rohlfing, Jr. Adler, J. R., and Jr. Maurer, C. R. Intensity-based 2d-3d spine image registration incorporating a single fiducial marker. *Acad Radiol*, 12(1):37–50, 2005.

[182] D. B. Russakoff, T. Rohlfing, K. Mori, D. Rueckert, A. Ho, Jr. Adler, J. R., and Jr. Maurer, C. R. Fast generation of digitally reconstructed radiographs using attenuation fields with application to 2d-3d image registration. *IEEE Trans Med Imaging*, 24(11):1441–1454, 2005.

[183] S. D. Steppacher, M. Tannast, G. Zheng, X. Zhang, J. Kowal, S. E. Anderson, K. A. Siebenrock, and S. B. Murphy. Validation of a new method for determination of cup orientation in tha. *J Orthop Res*, 27(12):1583–1588, 2009.

[184] X. Zhang, G. Zheng, F. Langlotz, and L. P. Nolte. Assessment of spline-based 2d-3d registration for image-guided spine surgery. *Minim Invasive Ther Allied Technol*, 15(3):193–199, 2006.

[185] G. Zheng. Effective incorporating spatial information in a mutual information based 3d-2d registration of a ct volume to x-ray images. *Comput Med Imaging Graph*, 34(7):553–562, 2010.

[186] S. Schumann, B. Thelen, S. Ballestra, L. P. Nolte, P. Buchler, and G. Zheng. X-ray image calibration and its application to clinical orthopedics. *Med Eng Phys*, 36(7):968–974, 2014.

[187] Y. Pauchard, T. Fitze, D. Browarnik, A. Eskandari, I. Pauchard, W. Enns-Bray, H. Palsson, S. Sigurdsson, S. J. Ferguson, T. B. Harris, V. Gudnason, and B. Helgason. Interactive graph-cut segmentation for fast creation of finite element models from clinical ct data for hip fracture prediction. *Comput Methods Biomech Biomed Engin*, 19(16):1693–1703, 2016.

[188] R. List, B. Postolka, P. Schütz, M. Hitz, P. Schwilch, H. Gerber, S. J. Ferguson, and W. R. Taylor. A moving fluoroscope to capture tibiofemoral kinematics during complete cycles of free level and downhill walking as well as stair descent. *PLoS One*, 12(10):e0185952, 2017.

[189] G. Zheng, N. Gerber, D. Widmer, C. Stieger, M. Caversaccio, LP. Nolte, and S. Weber. Automated detection of fiducial screws from ct/dvt volume data for image-guided ent surgery. In *32nd Annual International Conference of the IEEE Engineering in Medicine and Biology*, 2010.

[190] R. O. Duda and P. E. Hart. Use of hough transformation to detect lines and curves in pictures. *Commun ACM*, 15(1):11–15, 1972.

[191] V. Lepetit, F. Moreno-Noguer, and P. Fua. Epnp: An accurate o(n) solution to the pnp problem. *Int J Comput Vis*, 81(2):155–166, 2009.

[192] J. M. Bland and D. G. Altman. Statistical methods for assessing agreement between two methods of clinical measurement. *Lancet*, 327(8476):307–310, 1986.

[193] P. Schütz, B. Postolka, H. Gerber, S. Ferguson, W. R. Taylor, and R. List. Knee implant kinematics are task-dependent. *J R Soc Interface*, 16(151), 2019.

[194] P. Schütz, W. R. Taylor, B. Postolka, S. F. Fucentese, P. P. Koch, M. A. R. Freeman, V. Pinskerova, and R. List. Kinematic evaluation of the gmk sphere implant during gait activities: A dynamic videofluoroscopy study. *J Orthop Res*, 37(11):2337–2347, 2019.

[195] M. Akter, A. J. Lambert, M. R. Pickering, J. M. Scarvell, and P. N. Smith. 3d ct to 2d low dose single-plane fluoroscopy registration algorithm for in-vivo knee motion analysis. In *36th Annual International Conference of the IEEE Engineering in Medicine and Biology Society*, 2014.

[196] A. A. Muhit, M. R. Pickering, J. M. Scarvell, T. Ward, and P. N. Smith. Image-assisted non-invasive and dynamic biomechanical analysis of human joints. *Phys Med Biol*, 58(13):4679–4702, 2013.

[197] S. Guan, H. A. Gray, A. G. Schache, J. Feller, R. de Steiger, and M. G. Pandy. In vivo six-degree-of-freedom knee-joint kinematics in overground and treadmill walking following total knee arthroplasty. *J Orthop Res*, 35(8):1634–1643, 2017.

[198] R. List, T. Gulay, M. Stoop, and S. Lorenzetti. Kinematics of the trunk and the lower extremities during restricted and unrestricted squats. *J Strength Cond Res*, 27(6):1529–1538, 2013.

[199] B. Postolka, R. List, B. Thelen, P. Schütz, W. R. Taylor, and G. Zheng. Evaluation of an intensity-based algorithm for 2d/3d registration of natural knee videofluoroscopy data. *Med Eng Phys*, 77:107–113, 2020.

[200] R. M. Ehrig, W. R. Taylor, G. N. Duda, and M. O. Heller. A survey of formal methods for determining the centre of rotation of ball joints. *J Biomech*, 39(15):2798–2809, 2006.

[201] S. H. Hosseini Nasab, C. R. Smith, P. Schütz, B. Postolka, R. List, and W. R. Taylor. Elongation patterns of the collateral ligaments after total knee arthroplasty are dominated by the knee flexion angle. *Front Bioeng Biotechnol*, 7, 2019.

[202] S. H. Hosseini Nasab, C. R. Smith, P. Schütz, P. Damm, A. Trepczynski, R. List, and W. R. Taylor. Length-change patterns of the collateral ligaments during functional activities after total knee arthroplasty. *Ann Biomed Eng*, 48(4):1396–1406, 2020.

[203] M. Hitz, P. Schütz, M. Angst, W. R. Taylor, and R. List. Influence of the moving fluoroscope on gait patterns. *PLoS One*, 13(7):e0200608, 2018.

[204] B. Postolka, P. Schütz, S. F. Fucentese, M.A.R. Freeman, V. Pinskerova, R. List, and W. R. Taylor. Tibiofemoral kinematics of the healthy knee joint throughout complete cycles of gait activities. *J Biomech*, 110, 2020.

[205] G. Taubin. Estimation of planar curves, surfaces, and nonplanar space-curves defined by implicit equations with applications to edge and range image segmentation. *IEEE Trans Pattern Anal Mach Intell*, 13(11):1115–1138, 1991.

[206] T. C. Pataky, M. A. Robinson, and J. Vanrenterghem. Region-of-interest analyses of one-dimensional biomechanical trajectories: bridging 0d and 1d theory, augmenting statistical power. *PeerJ*, 4:e2652, 2016.

[207] M. L. Hull. Coordinate system requirements to determine motions of the tibiofemoral joint free from kinematic crosstalk errors. *J Biomech*, 109:109928, 2020.

[208] M. T. Hirschmann, L. B. Moser, F. Amsler, H. Behrend, V. Leclercq, and S. Hess. Phenotyping the knee in young non-osteoarthritic knees shows a wide distribution of femoral and tibial coronal alignment. *Knee Surg Sports Traumatol Arthrosc*, 27(5):1385–1393, 2019.

[209] A. Trepczynski, I. Kutzner, P. Schütz, J. Dymke, R. List, P. von Roth, P. Moewis, G. Bergmann, W. R. Taylor, and G. N. Duda. Tibio-femoral contact force distribution is not the only factor governing pivot location after total knee arthroplasty. *Sci Rep*, 9(1):182, 2019.

[210] H. A. Gray, S. Guan, T. J. Young, M. M. Dowsey, P. F. Choong, and M. G. Pandy. Comparison of posterior-stabilized, cruciate-retaining, and medial-stabilized knee implant motion during gait. *J Orthop Res*, 38(8):1753, 2020.

[211] D. Biswas, J. E. Bible, M. Bohan, A. K. Simpson, P. G. Whang, and J. N. Grauer. Radiation exposure from musculoskeletal computerized tomographic scans. *J Bone Joint Surg Am*, 91(8):1882–1889, 2009.

Appendix A

Supplementary material Chapter 3

Supplementary material associated with Chapter 3:
Evaluation of an intensity-based algorithm for 2D/3D registration of natural knee videofluoroscopy data

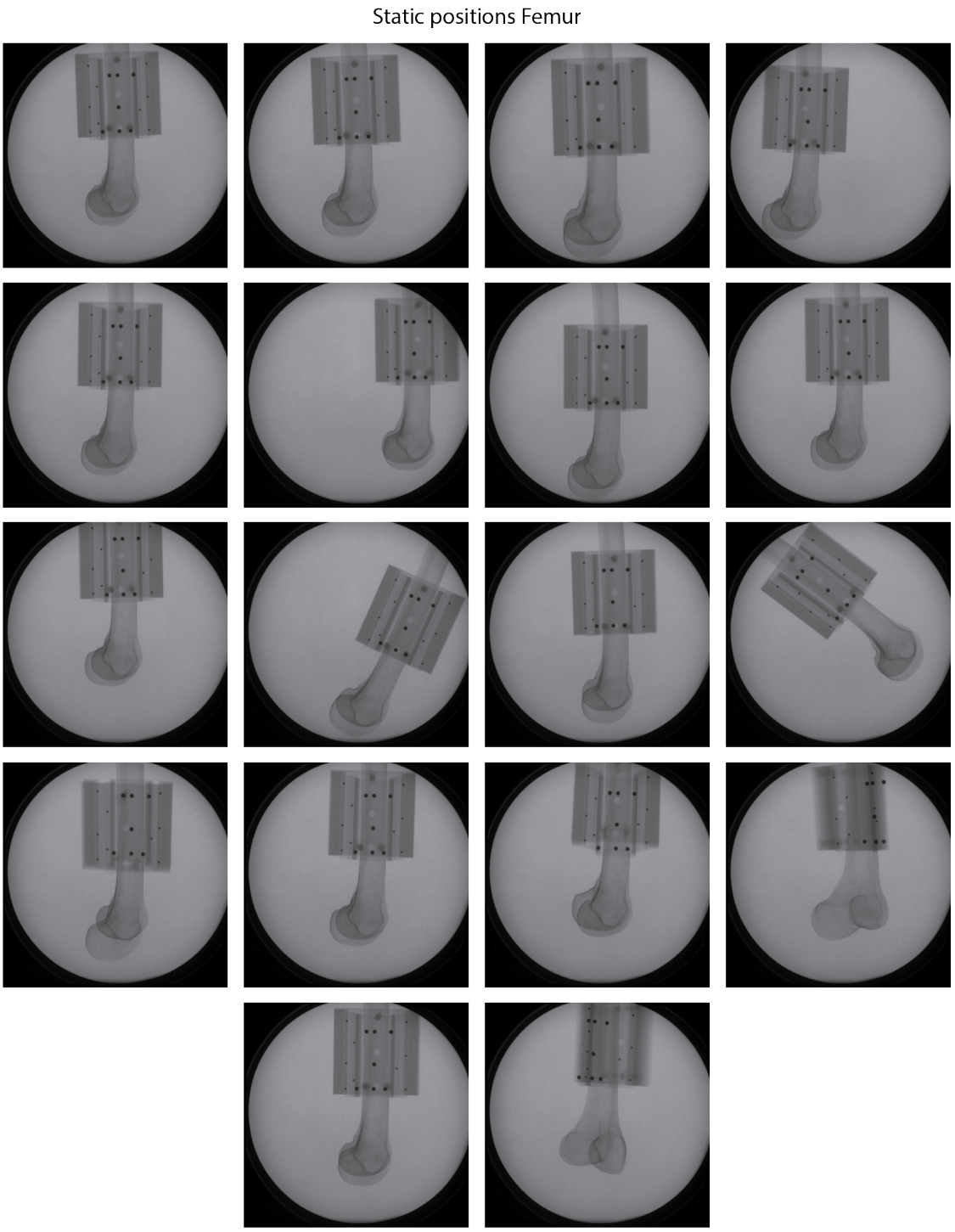

Figure A.1: 18 static positions of the radiopaque femur

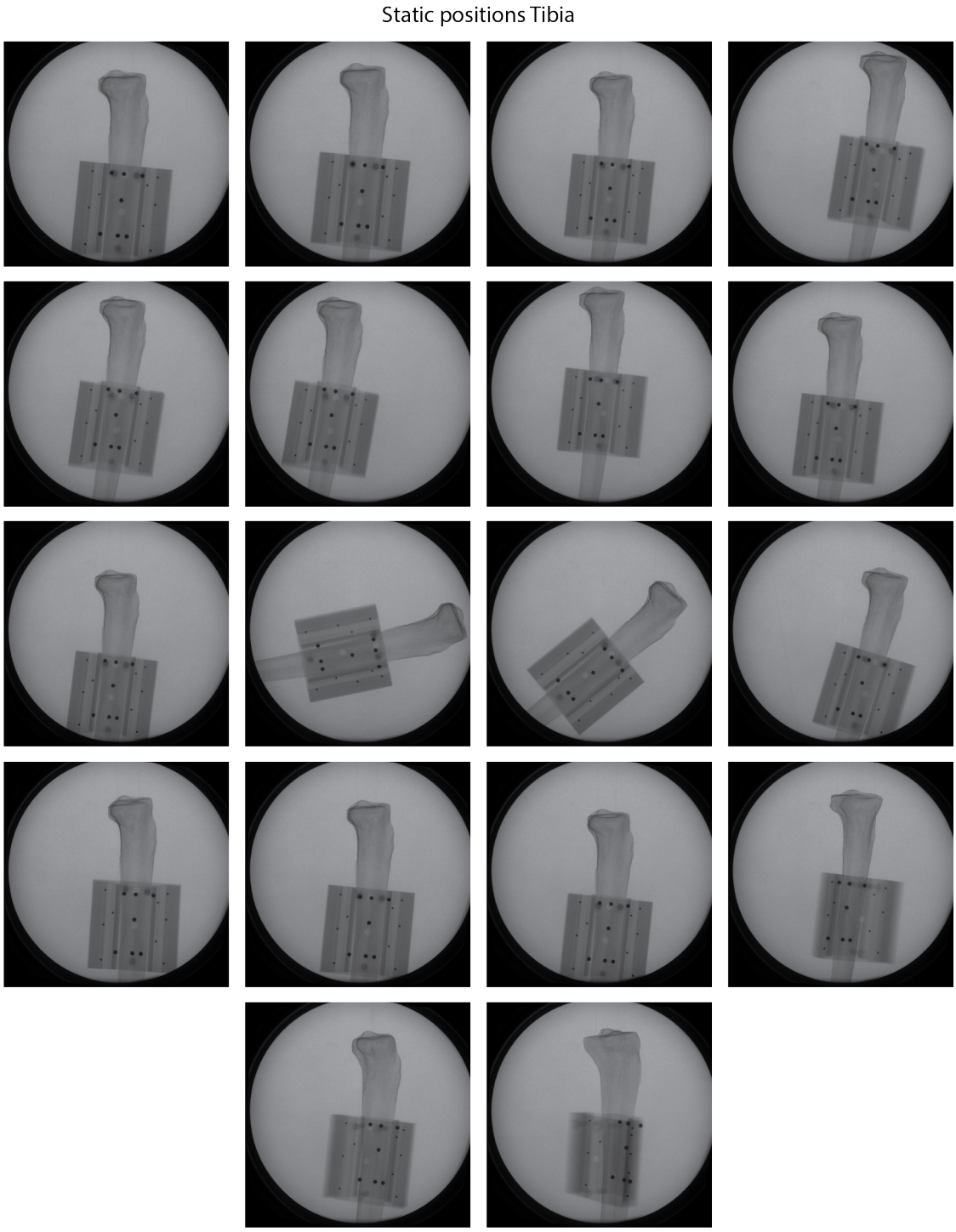

Figure A.2: 18 static positions of the radiopaque tibia

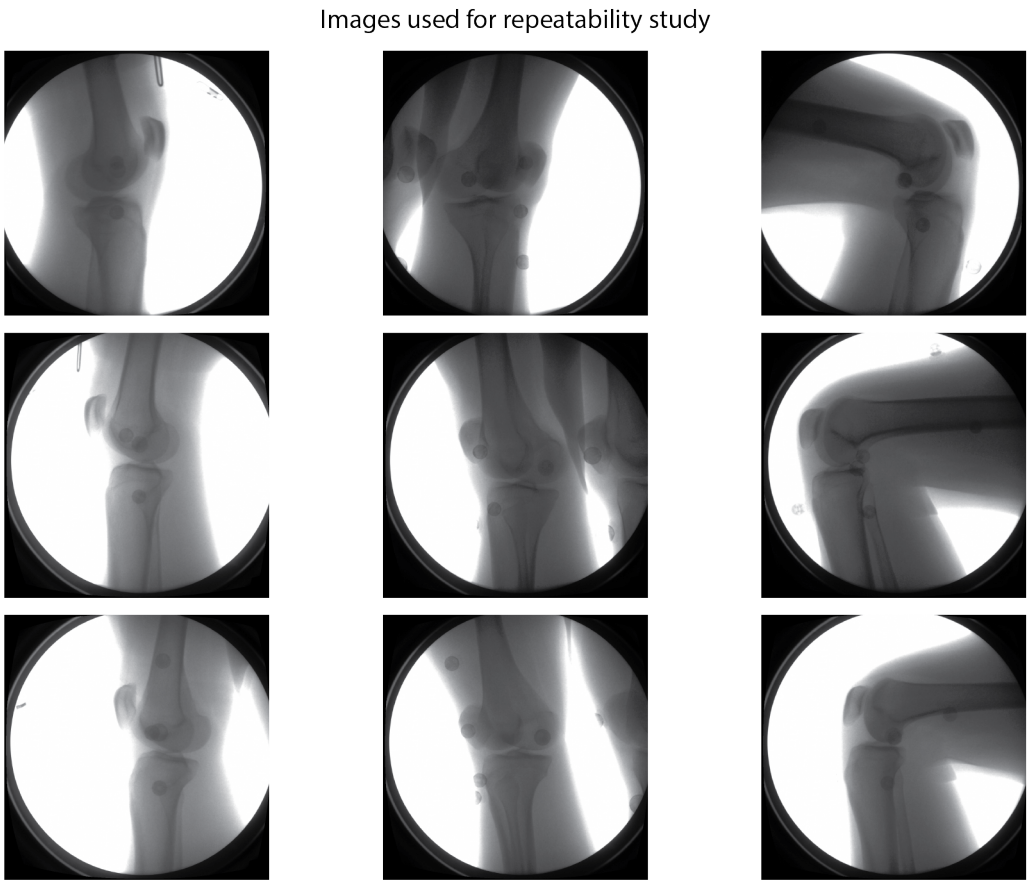

Figure A.3: Images used for the *in vivo* repeatability test

Appendix B

Supplementary material Chapter 4

Supplementary material associated with Chapter 4:

Tibio-femoral kinematics of the healthy knee joint throughout complete cycles of gait activities

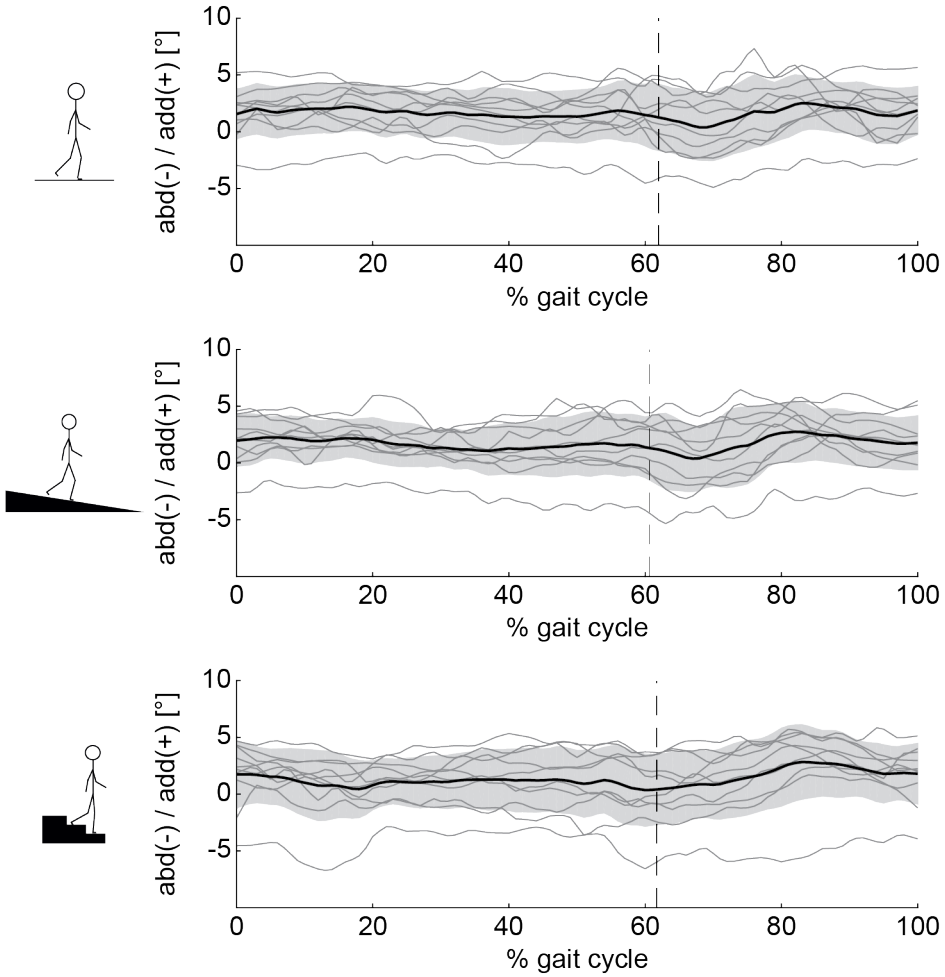

Figure B.1: Tibio-femoral abduction/adduction (abd/add) throughout complete cycles of level walking (top), downhill walking (middle) and stair descent (bottom). The mean across all subjects (black line), standard deviations across all subjects (grey shading), as well as means for every subject (dark grey lines) are presented. The average instance of toe-off across all subjects is indicated as a vertical dashed line.

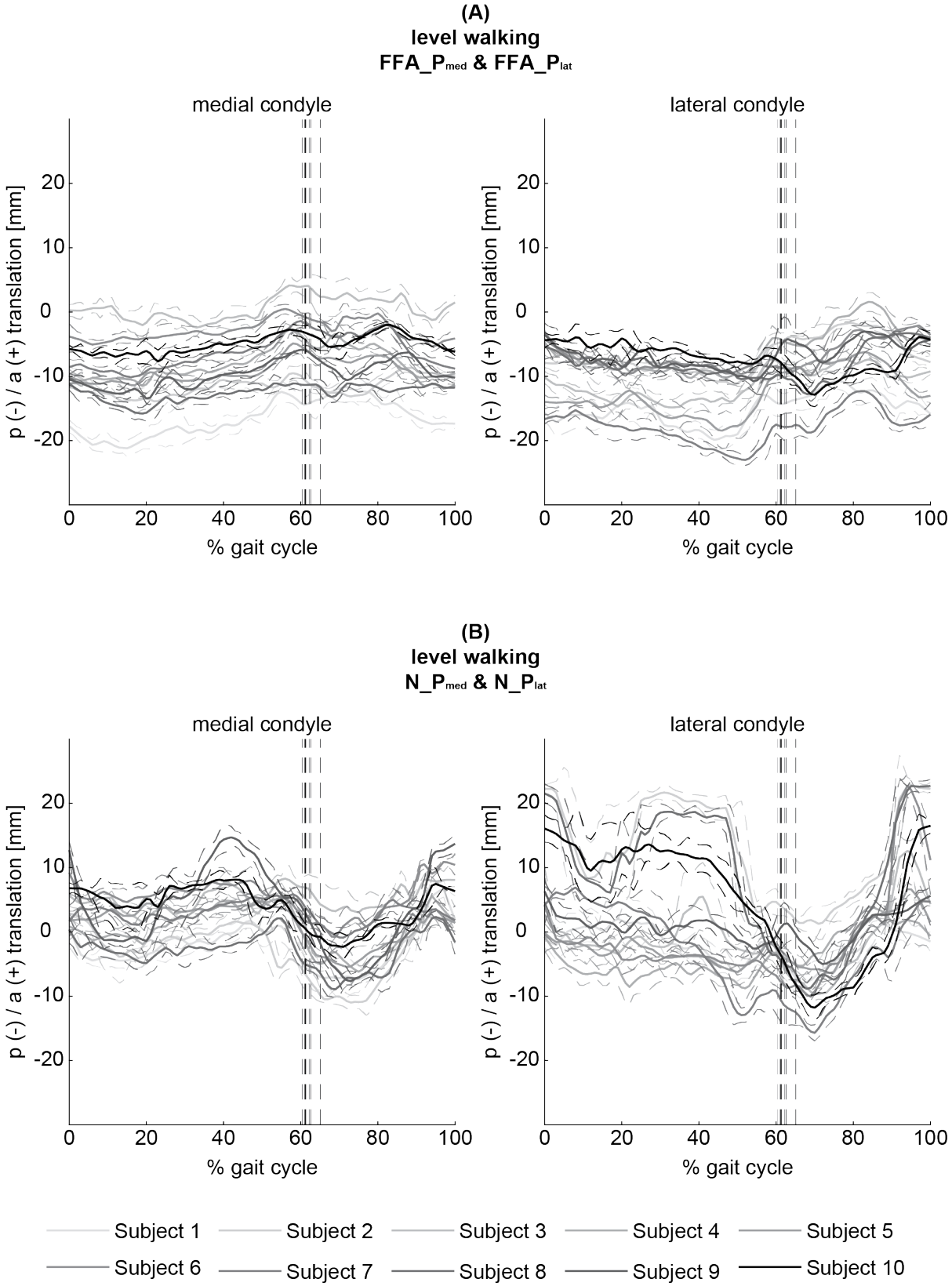

Figure B.2: Antero (a) – posterior (p) translation of the medial and lateral functional flexion axis points (A) as well as the nearest points (B) throughout complete cycles of level walking. The mean and standard deviation across all repetitions of each single subject are presented using different grey intensities. The average instance of toe-off for each subject is indicated as a vertical dashed line.

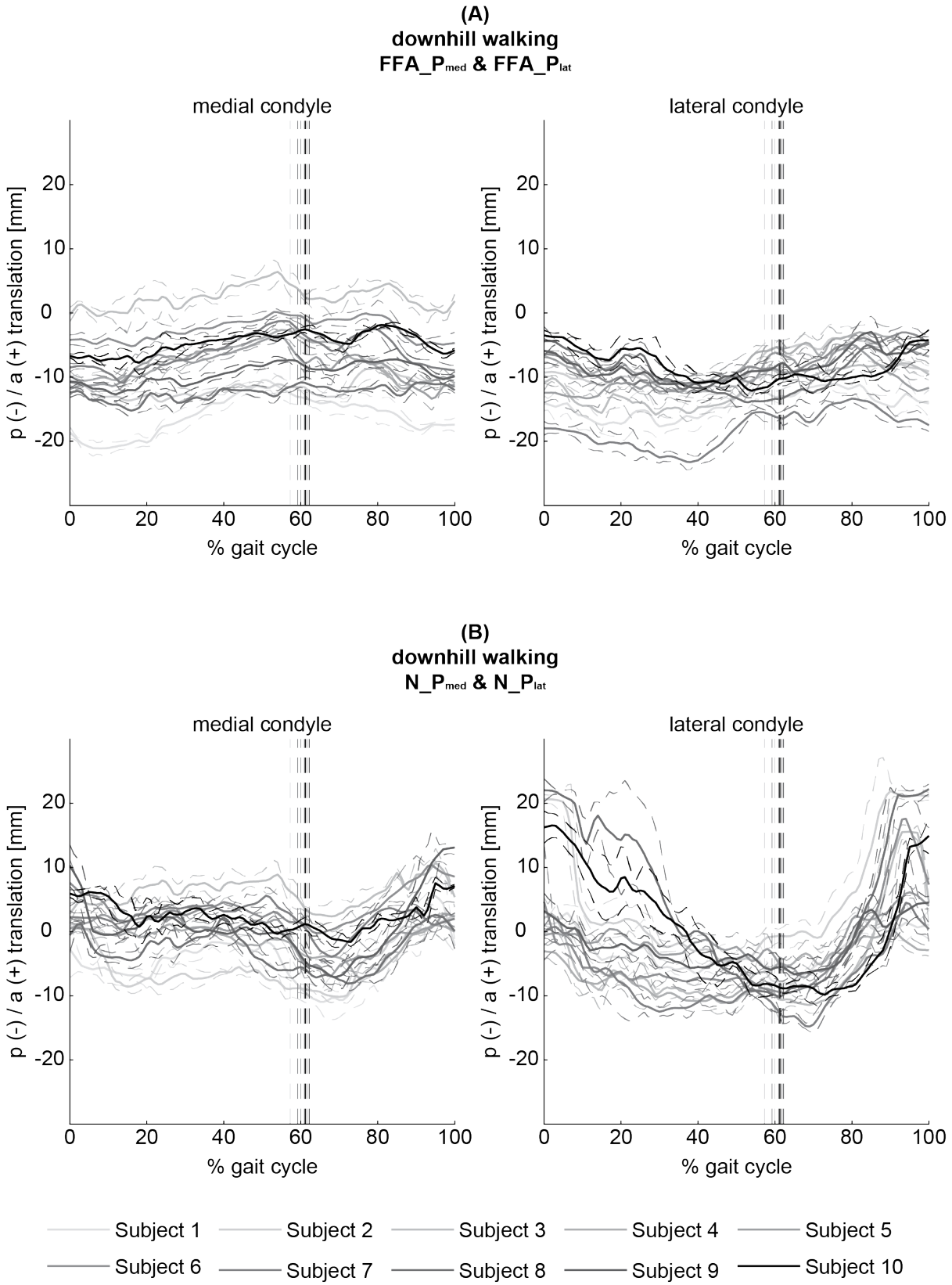

Figure B.3: Antero (a) – posterior (p) translation of the medial and lateral functional flexion axis points (A) as well as the nearest points (B) throughout complete cycles of downhill walking. The mean and standard deviation across all repetitions of each single subject are presented using different grey intensities. The average instance of toe-off for each subject is indicated as a vertical dashed line.

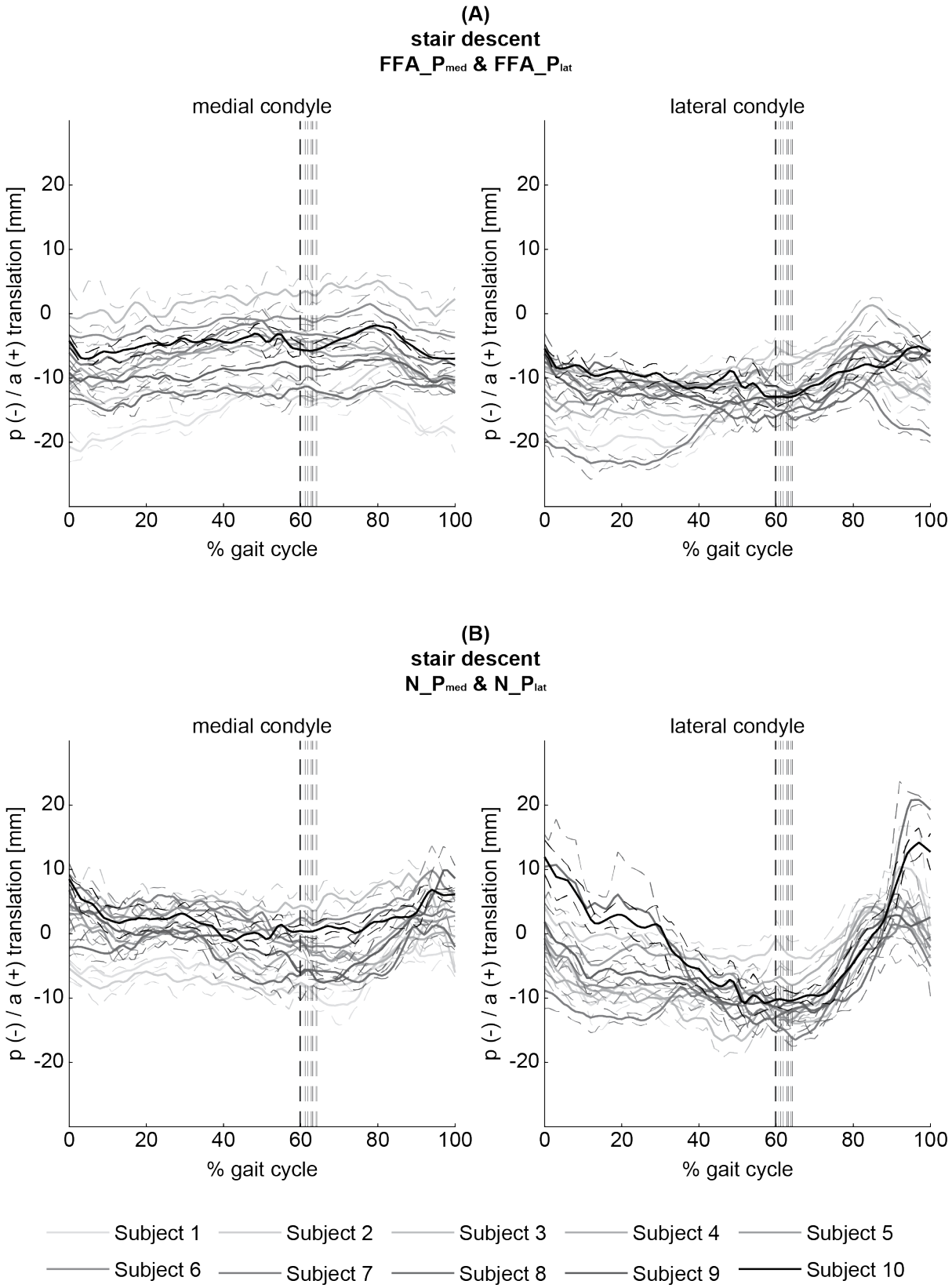

Figure B.4: Antero (a) – posterior (p) translation of the medial and lateral functional flexion axis points (A) as well as the nearest points (B) throughout complete cycles of stair descent. The mean and standard deviation across all repetitions of each single subject are presented using different grey intensities. The average instance of toe-off for each subject is indicated as a vertical dashed line.

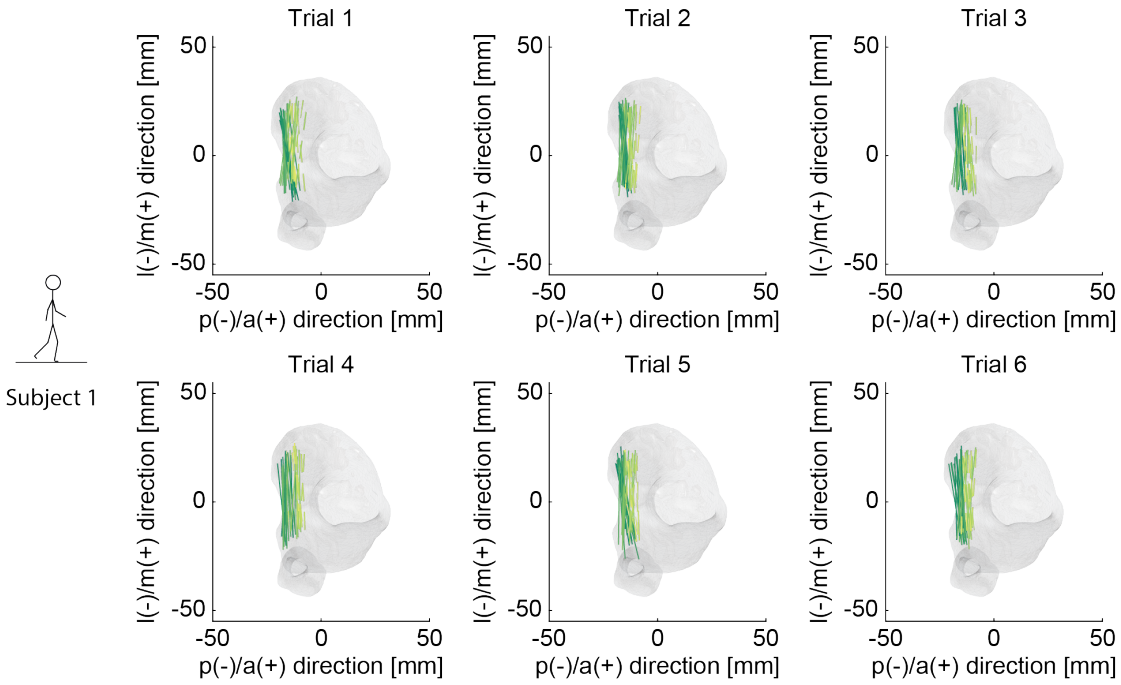

Figure B.5: Location and orientation of the femur relative to the tibia in medio (m)/lateral (l) and antero (a)/posterior (p) direction for all captured time frames during level walking is presented for Subject 1. Lines connect the FFA_P$_{med}$ and FFA_P$_{lat}$. Solid lines represent the loaded stance and dashed lines the unloaded swing phase. A continuous colour map is used from dark green (at heel strike) to yellow (end of swing phase)

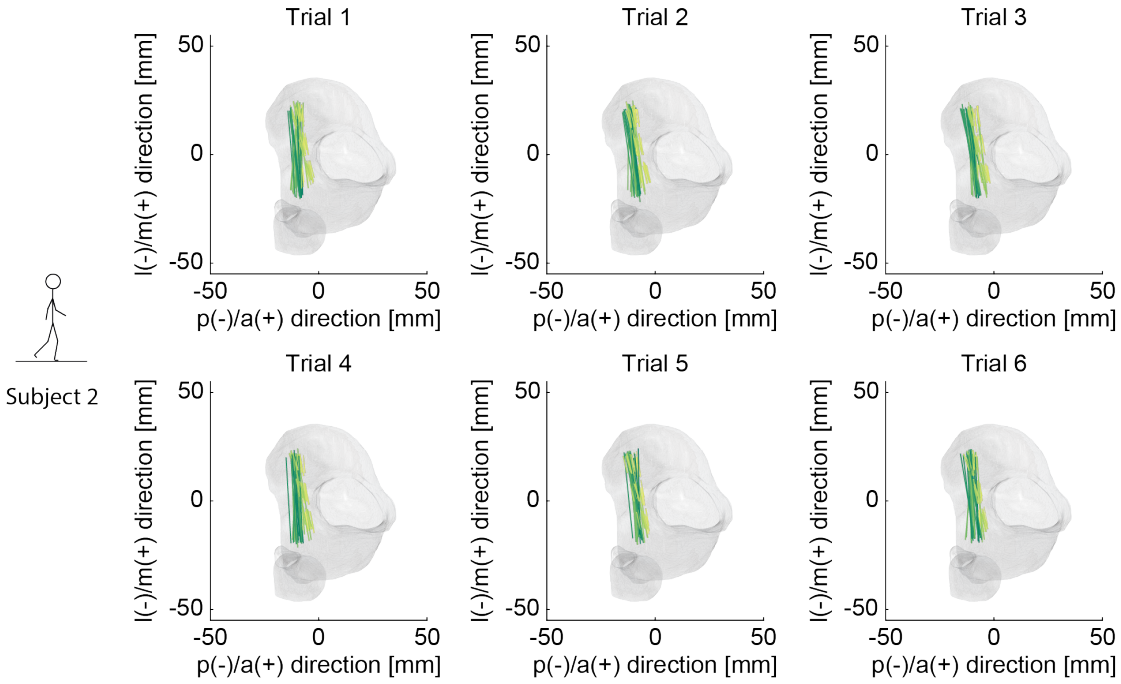

Figure B.6: Location and orientation of the femur relative to the tibia in medio (m)/lateral (l) and antero (a)/posterior (p) direction for all captured time frames during level walking is presented for Subject 2. Lines connect the FFA_P$_{med}$ and FFA_P$_{lat}$. Solid lines represent the loaded stance and dashed lines the unloaded swing phase. A continuous colour map is used from dark green (at heel strike) to yellow (end of swing phase)

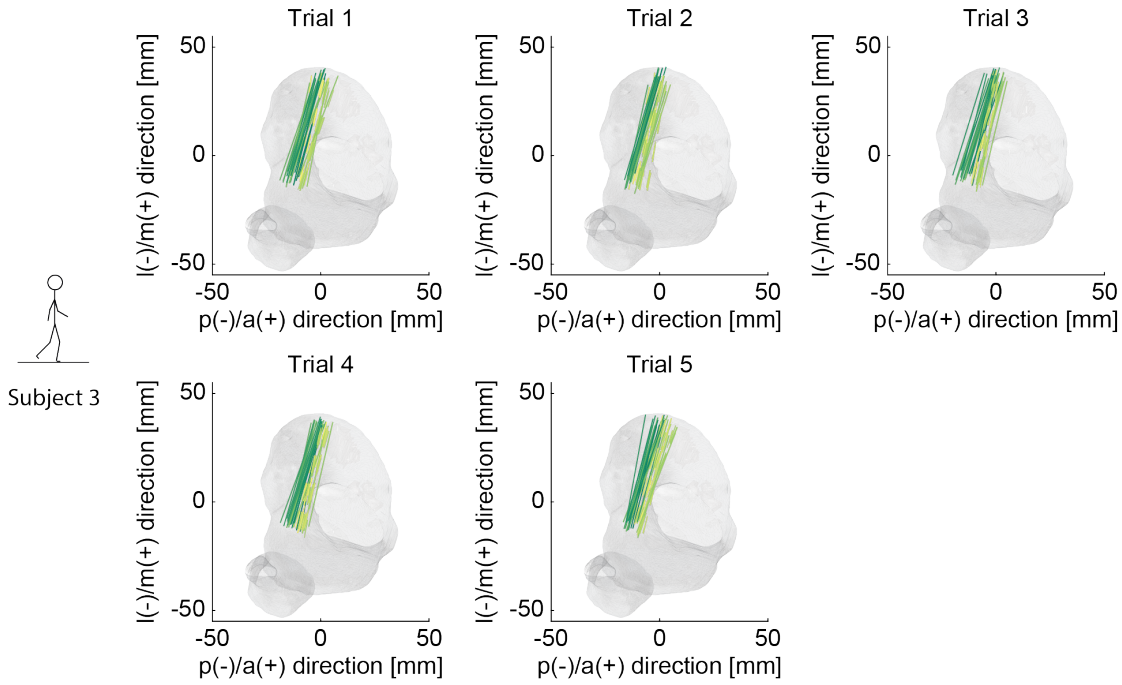

Figure B.7: Location and orientation of the femur relative to the tibia in medio (m)/lateral (l) and antero (a)/posterior (p) direction for all captured time frames during level walking is presented for Subject 3. Lines connect the FFA_P$_{med}$ and FFA_P$_{lat}$. Solid lines represent the loaded stance and dashed lines the unloaded swing phase. A continuous colour map is used from dark green (at heel strike) to yellow (end of swing phase)

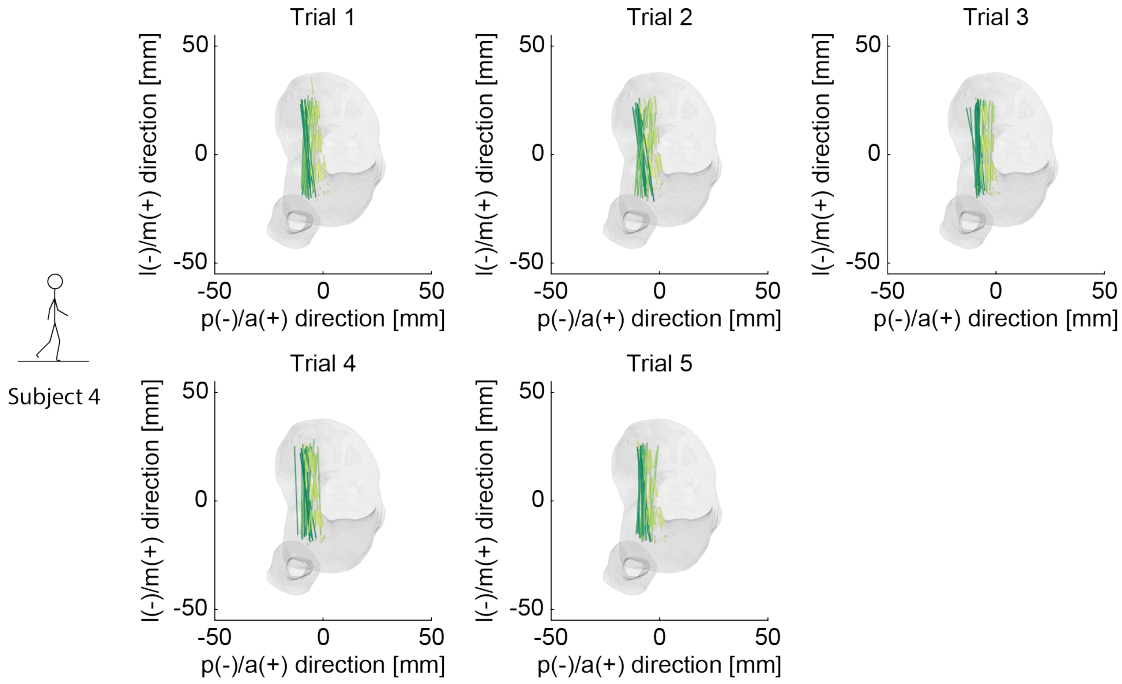

Figure B.8: Location and orientation of the femur relative to the tibia in medio (m)/lateral (l) and antero (a)/posterior (p) direction for all captured time frames during level walking is presented for Subject 4. Lines connect the FFA_P$_{med}$ and FFA_P$_{lat}$. Solid lines represent the loaded stance and dashed lines the unloaded swing phase. A continuous colour map is used from dark green (at heel strike) to yellow (end of swing phase)

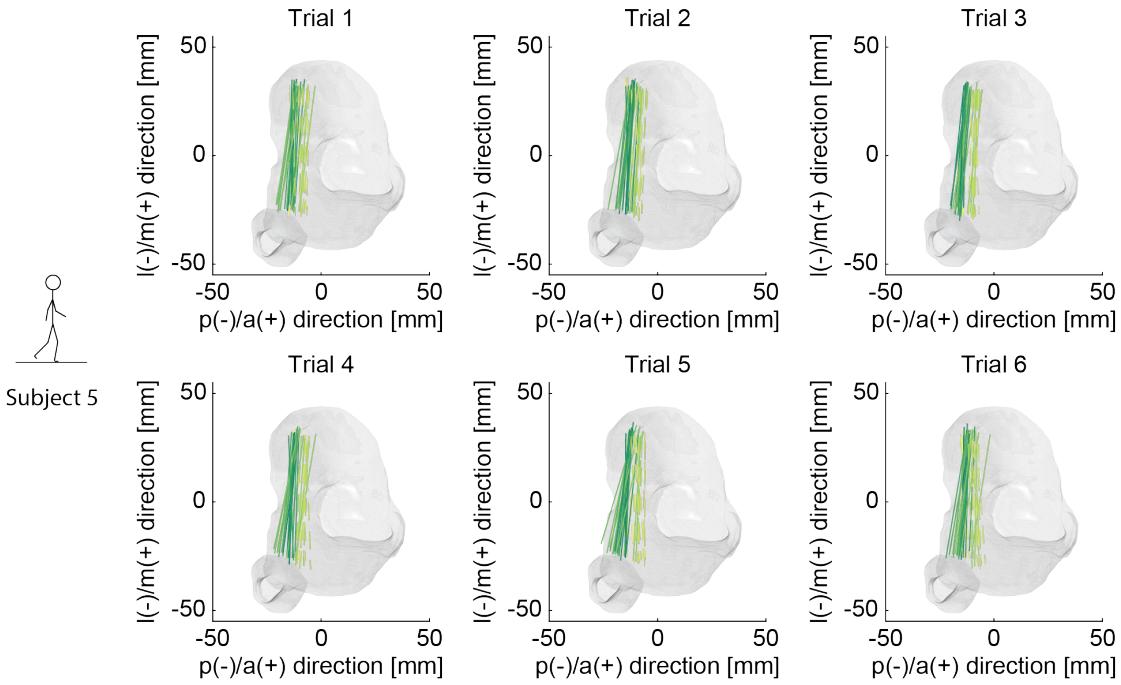

Figure B.9: Location and orientation of the femur relative to the tibia in medio (m)/lateral (l) and antero (a)/posterior (p) direction for all captured time frames during level walking is presented for Subject 5. Lines connect the FFA_P$_{med}$ and FFA_P$_{lat}$. Solid lines represent the loaded stance and dashed lines the unloaded swing phase. A continuous colour map is used from dark green (at heel strike) to yellow (end of swing phase)

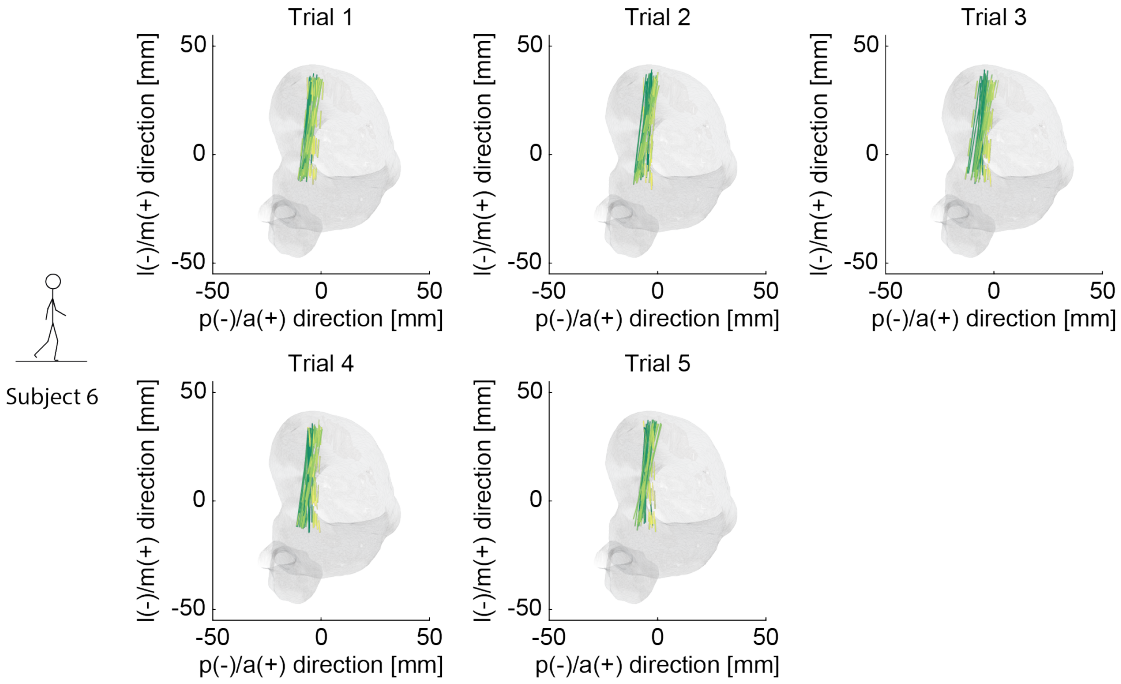

Figure B.10: Location and orientation of the femur relative to the tibia in medio (m)/lateral (l) and antero (a)/posterior (p) direction for all captured time frames during level walking is presented for Subject 6. Lines connect the FFA_P$_{med}$ and FFA_P$_{lat}$. Solid lines represent the loaded stance and dashed lines the unloaded swing phase. A continuous colour map is used from dark green (at heel strike) to yellow (end of swing phase)

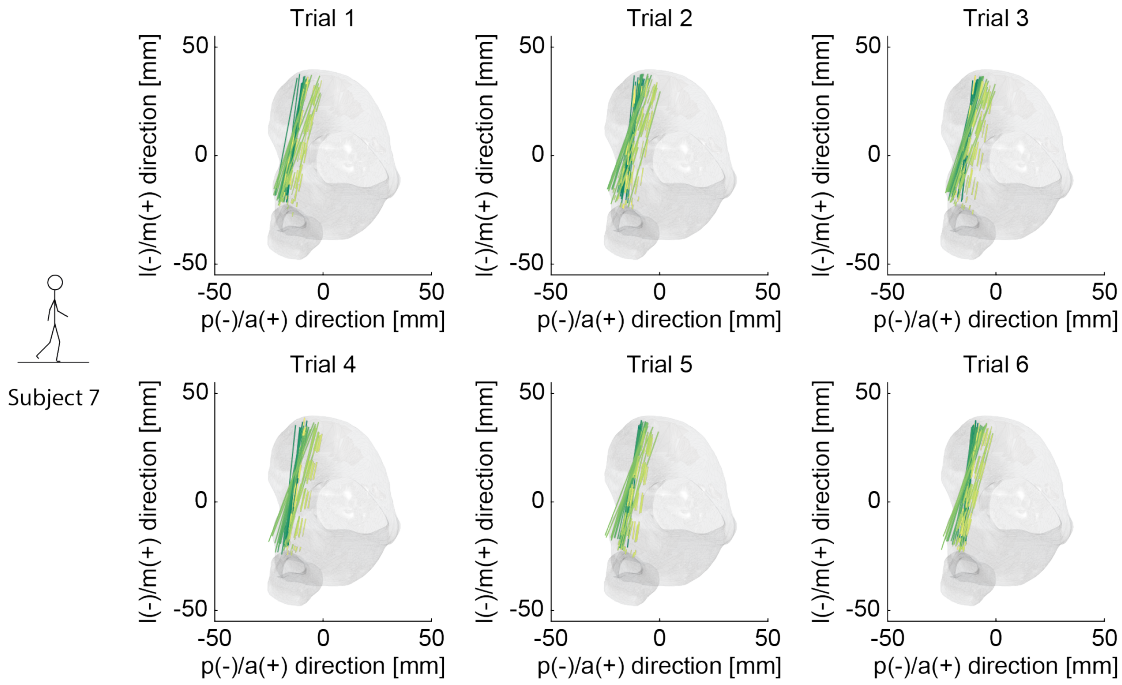

Figure B.11: Location and orientation of the femur relative to the tibia in medio (m)/lateral (l) and antero (a)/posterior (p) direction for all captured time frames during level walking is presented for Subject 7. Lines connect the FFA_P$_{med}$ and FFA_P$_{lat}$. Solid lines represent the loaded stance and dashed lines the unloaded swing phase. A continuous colour map is used from dark green (at heel strike) to yellow (end of swing phase)

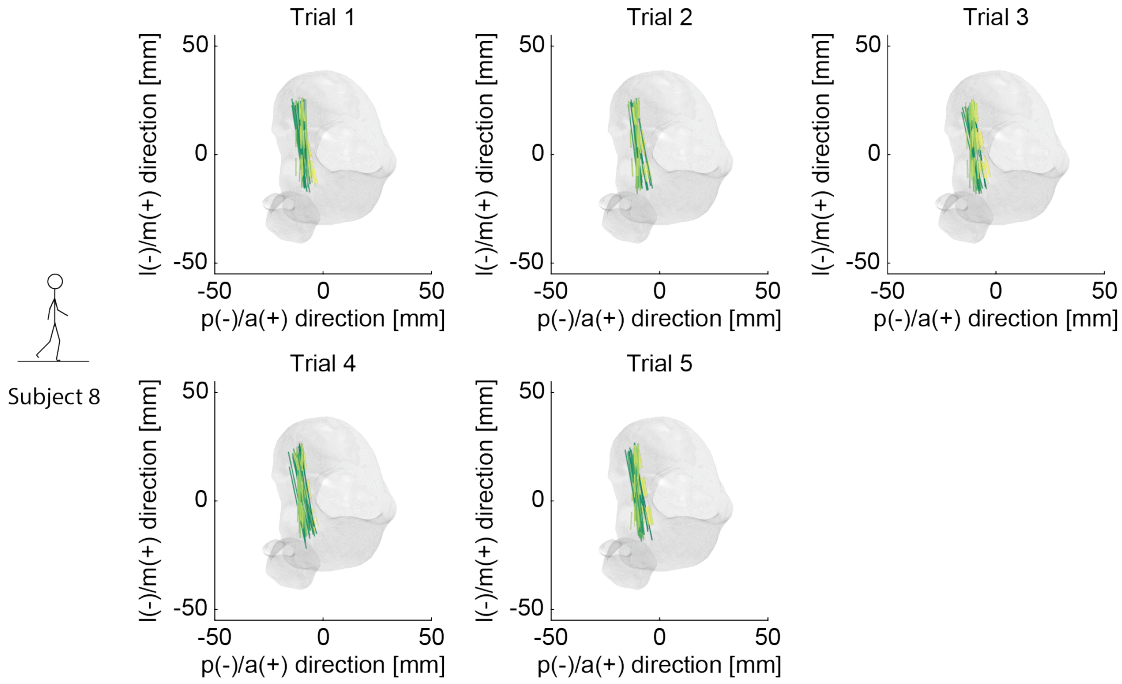

Figure B.12: Location and orientation of the femur relative to the tibia in medio (m)/lateral (l) and antero (a)/posterior (p) direction for all captured time frames during level walking is presented for Subject 8. Lines connect the FFA_P$_{med}$ and FFA_P$_{lat}$. Solid lines represent the loaded stance and dashed lines the unloaded swing phase. A continuous colour map is used from dark green (at heel strike) to yellow (end of swing phase)

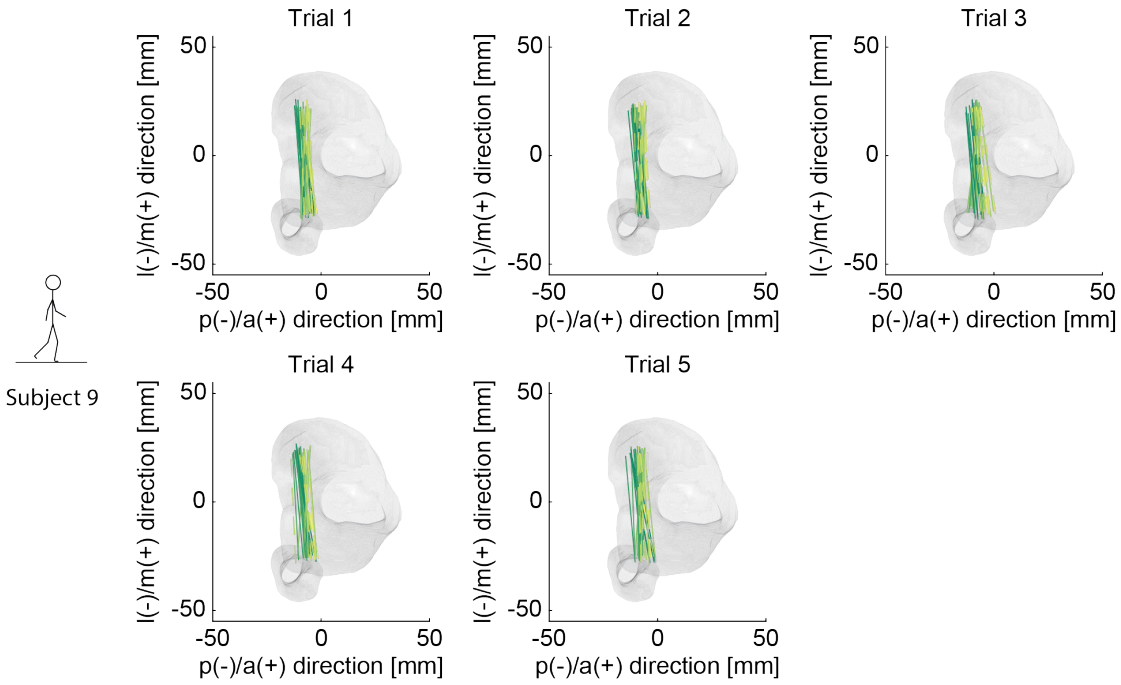

Figure B.13: Location and orientation of the femur relative to the tibia in medio (m)/lateral (l) and antero (a)/posterior (p) direction for all captured time frames during level walking is presented for Subject 9. Lines connect the FFA_P$_{med}$ and FFA_P$_{lat}$. Solid lines represent the loaded stance and dashed lines the unloaded swing phase. A continuous colour map is used from dark green (at heel strike) to yellow (end of swing phase)

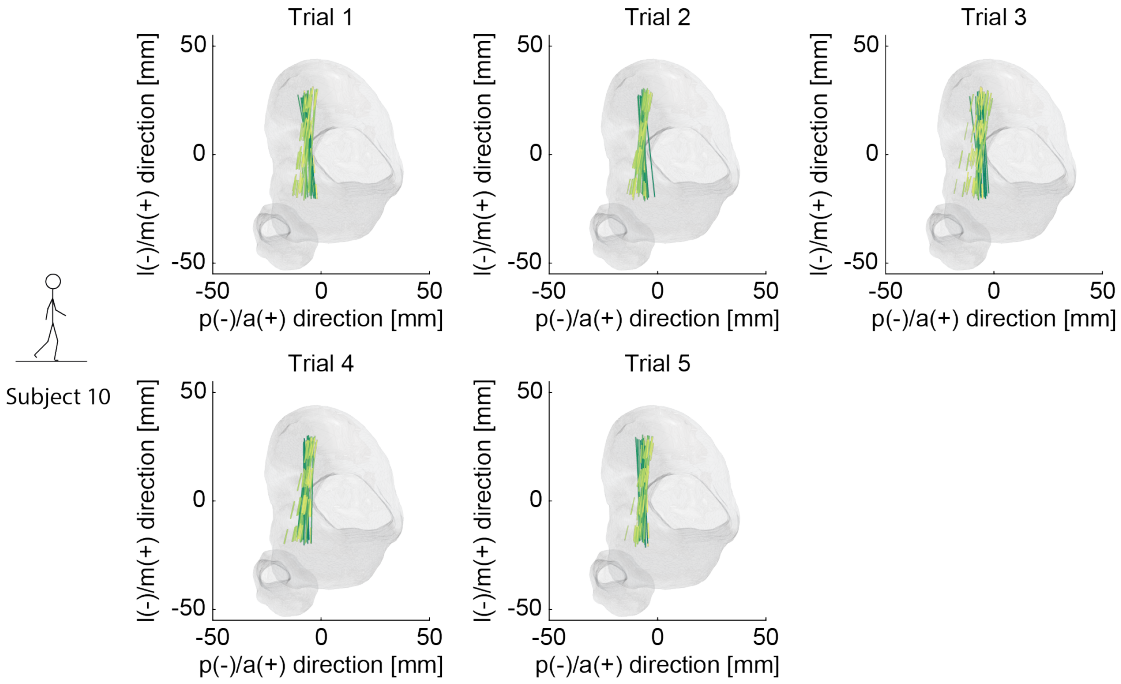

Figure B.14: Location and orientation of the femur relative to the tibia in medio (m)/lateral (l) and antero (a)/posterior (p) direction for all captured time frames during level walking is presented for Subject 10. Lines connect the FFA_P$_{med}$ and FFA_P$_{lat}$. Solid lines represent the loaded stance and dashed lines the unloaded swing phase. A continuous colour map is used from dark green (at heel strike) to yellow (end of swing phase)

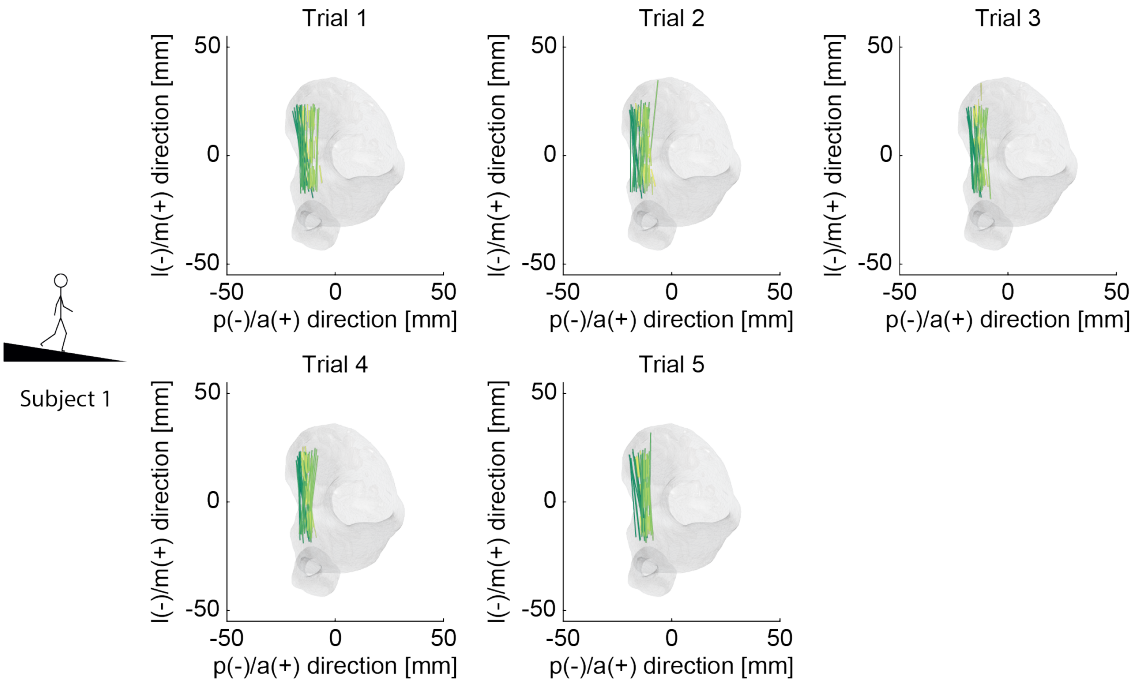

Figure B.15: Location and orientation of the femur relative to the tibia in medio (m)/lateral (l) and antero (a)/posterior (p) direction for all captured time frames during downhill walking is presented for Subject 1. Lines connect the FFA_P$_{med}$ and FFA_P$_{lat}$. Solid lines represent the loaded stance and dashed lines the unloaded swing phase. A continuous colour map is used from dark green (at heel strike) to yellow (end of swing phase)

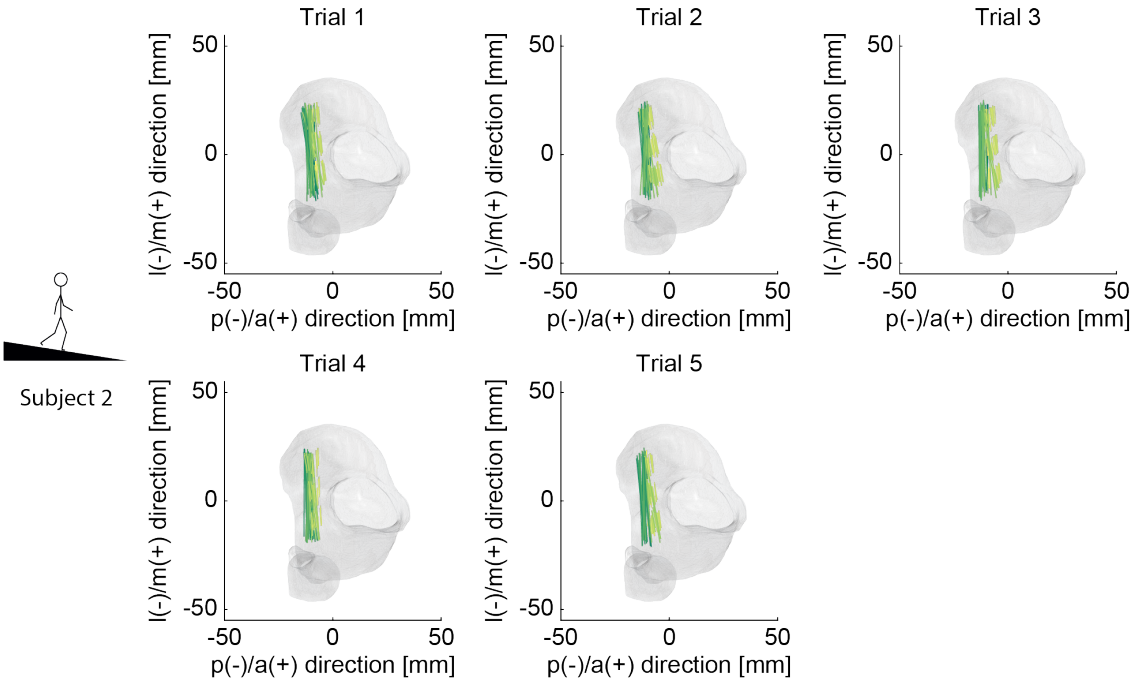

Figure B.16: Location and orientation of the femur relative to the tibia in medio (m)/lateral (l) and antero (a)/posterior (p) direction for all captured time frames during downhill walking is presented for Subject 2. Lines connect the FFA_P$_{med}$ and FFA_P$_{lat}$. Solid lines represent the loaded stance and dashed lines the unloaded swing phase. A continuous colour map is used from dark green (at heel strike) to yellow (end of swing phase)

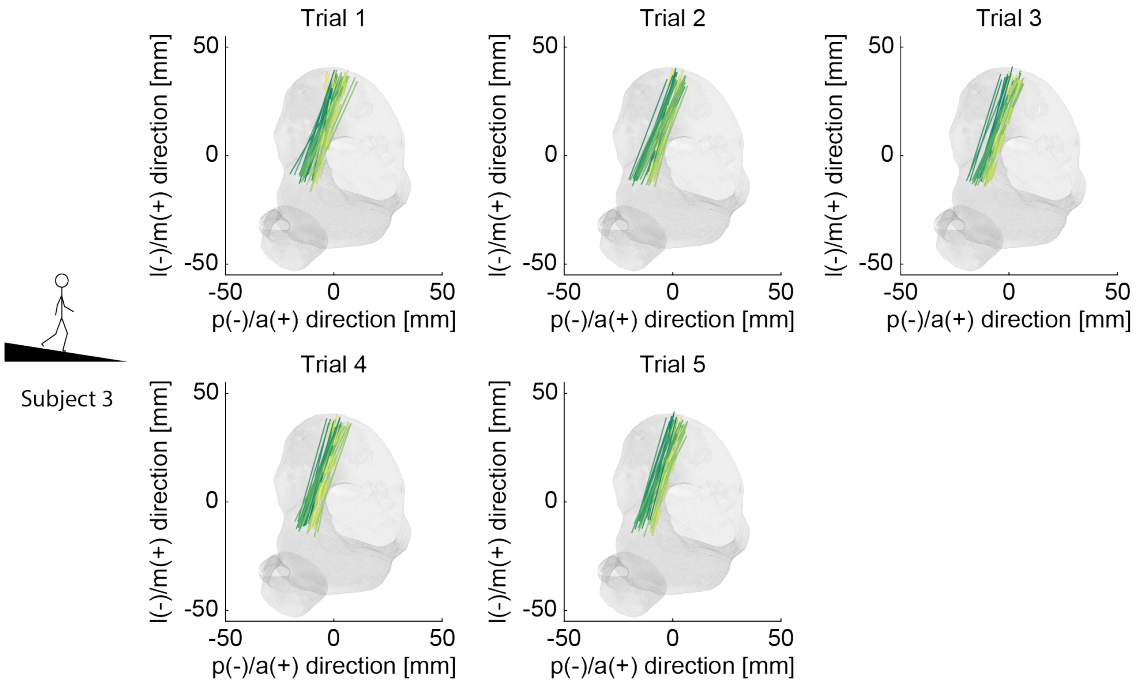

Figure B.17: Location and orientation of the femur relative to the tibia in medio (m)/lateral (l) and antero (a)/posterior (p) direction for all captured time frames during downhill walking is presented for Subject 3. Lines connect the FFA_P$_{med}$ and FFA_P$_{lat}$. Solid lines represent the loaded stance and dashed lines the unloaded swing phase. A continuous colour map is used from dark green (at heel strike) to yellow (end of swing phase)

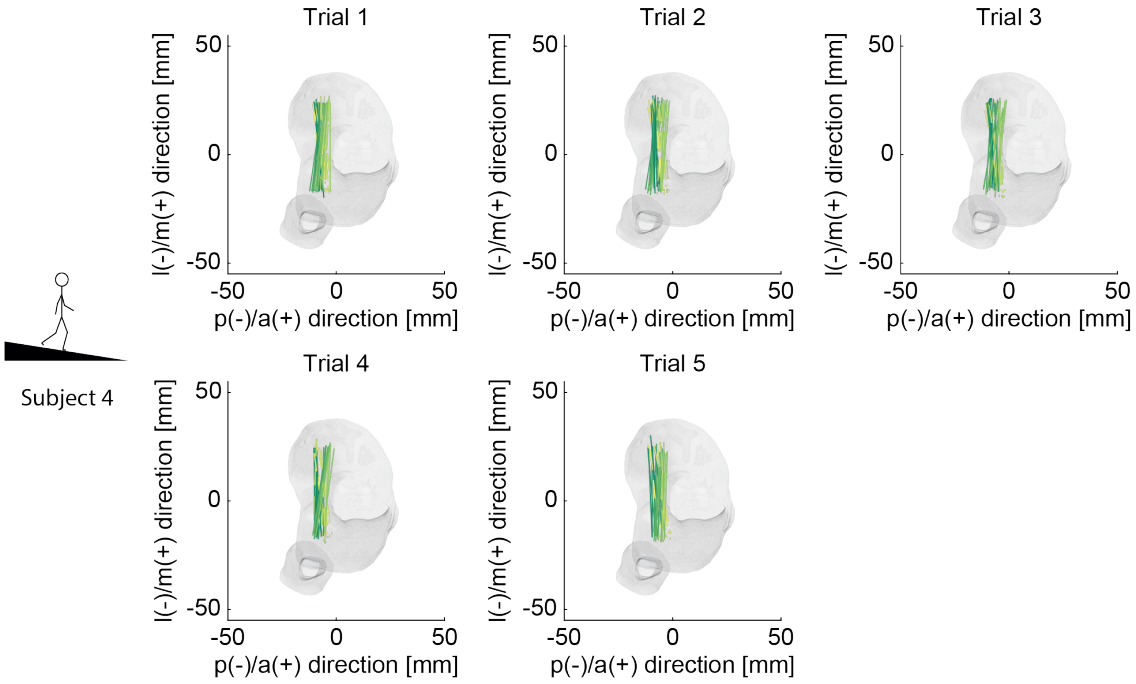

Figure B.18: Location and orientation of the femur relative to the tibia in medio (m)/lateral (l) and antero (a)/posterior (p) direction for all captured time frames during downhill walking is presented for Subject 4. Lines connect the FFA_P$_{med}$ and FFA_P$_{lat}$. Solid lines represent the loaded stance and dashed lines the unloaded swing phase. A continuous colour map is used from dark green (at heel strike) to yellow (end of swing phase)

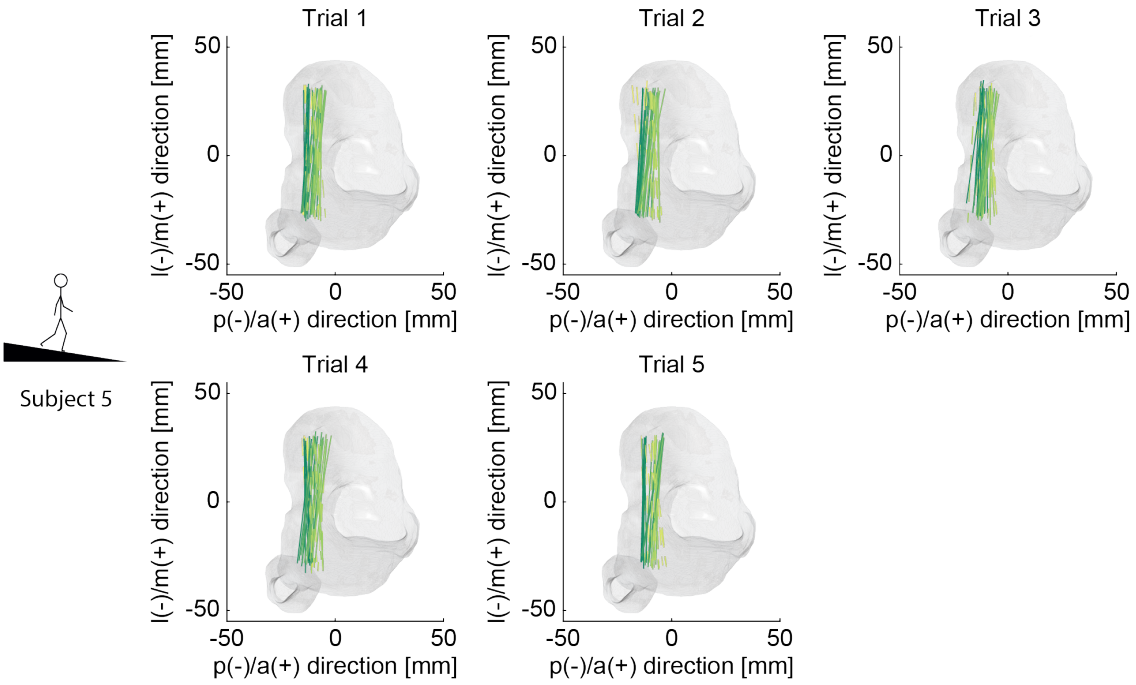

Figure B.19: Location and orientation of the femur relative to the tibia in medio (m)/lateral (l) and antero (a)/posterior (p) direction for all captured time frames during downhill walking is presented for Subject 5. Lines connect the FFA_P$_{med}$ and FFA_P$_{lat}$. Solid lines represent the loaded stance and dashed lines the unloaded swing phase. A continuous colour map is used from dark green (at heel strike) to yellow (end of swing phase)

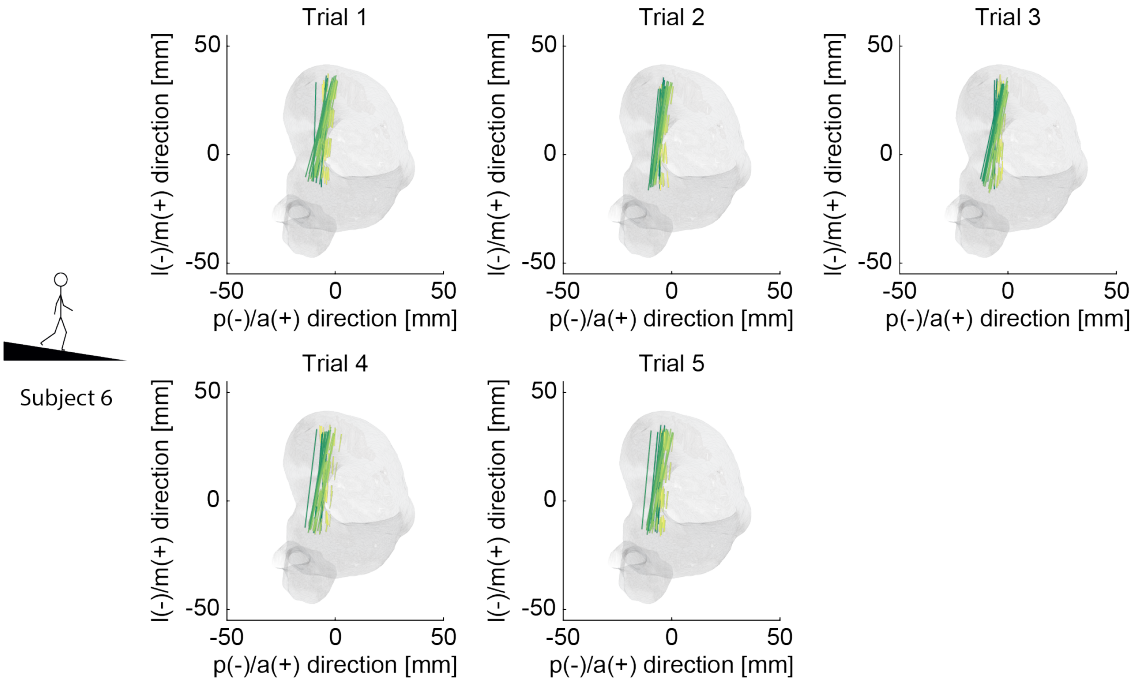

Figure B.20: Location and orientation of the femur relative to the tibia in medio (m)/lateral (l) and antero (a)/posterior (p) direction for all captured time frames during downhill walking is presented for Subject 6. Lines connect the FFA_P$_{med}$ and FFA_P$_{lat}$. Solid lines represent the loaded stance and dashed lines the unloaded swing phase. A continuous colour map is used from dark green (at heel strike) to yellow (end of swing phase)

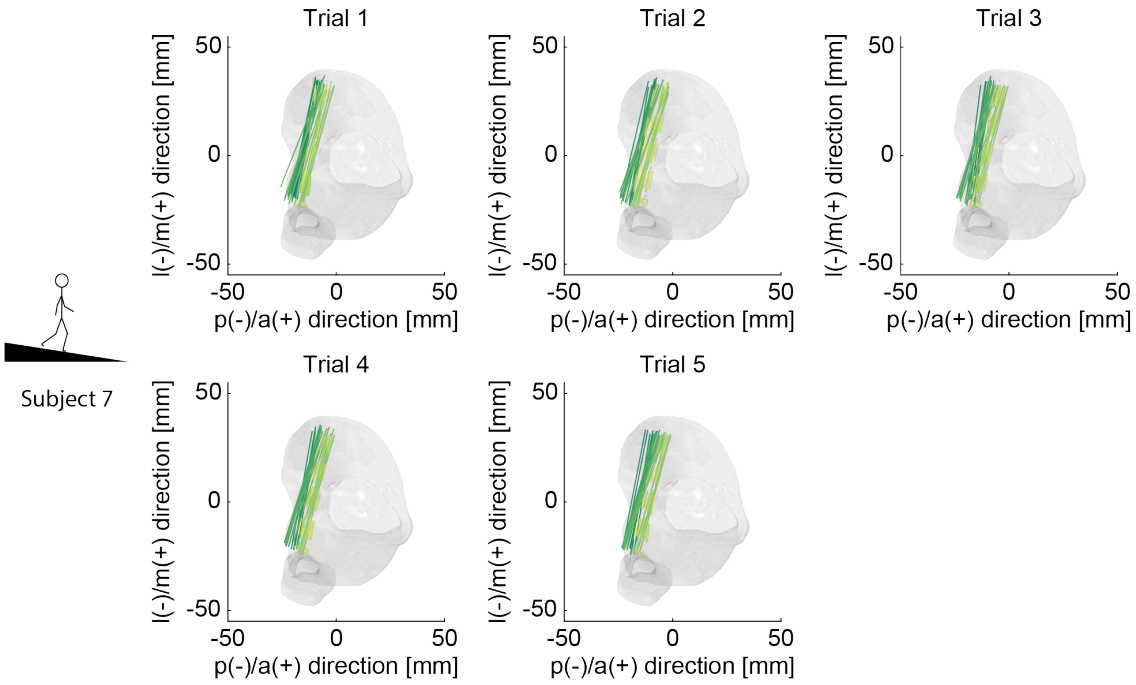

Figure B.21: Location and orientation of the femur relative to the tibia in medio (m)/lateral (l) and antero (a)/posterior (p) direction for all captured time frames during downhill walking is presented for Subject 7. Lines connect the FFA_P$_{med}$ and FFA_P$_{lat}$. Solid lines represent the loaded stance and dashed lines the unloaded swing phase. A continuous colour map is used from dark green (at heel strike) to yellow (end of swing phase)

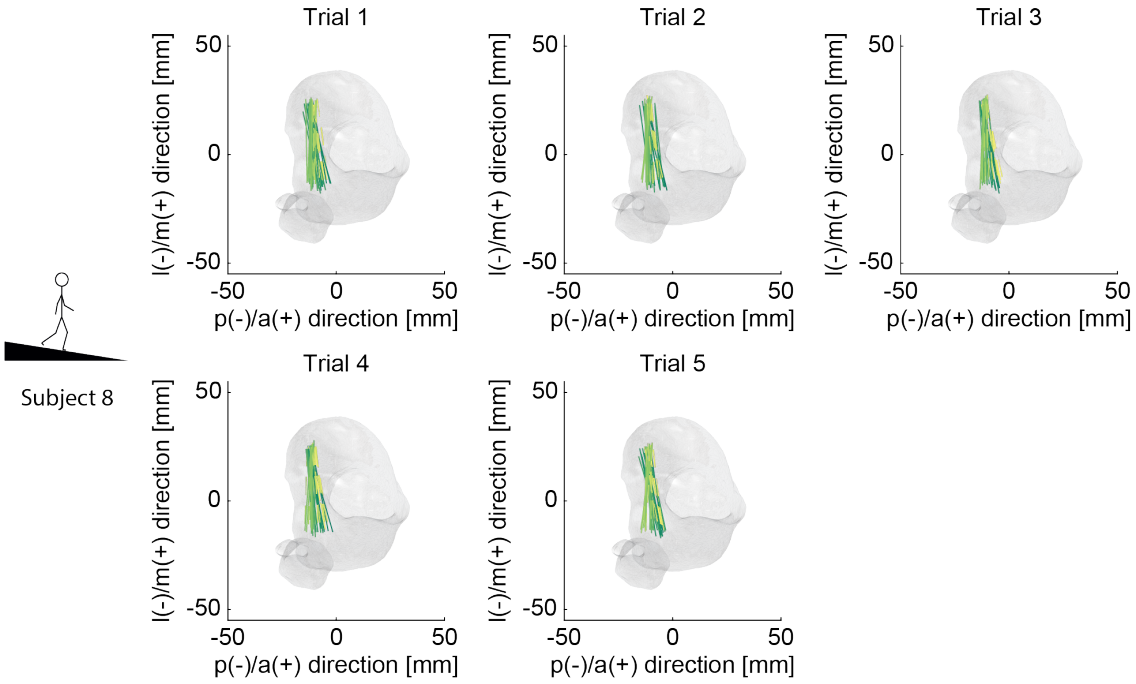

Figure B.22: Location and orientation of the femur relative to the tibia in medio (m)/lateral (l) and antero (a)/posterior (p) direction for all captured time frames during downhill walking is presented for Subject 8. Lines connect the FFA_P$_{med}$ and FFA_P$_{lat}$. Solid lines represent the loaded stance and dashed lines the unloaded swing phase. A continuous colour map is used from dark green (at heel strike) to yellow (end of swing phase)

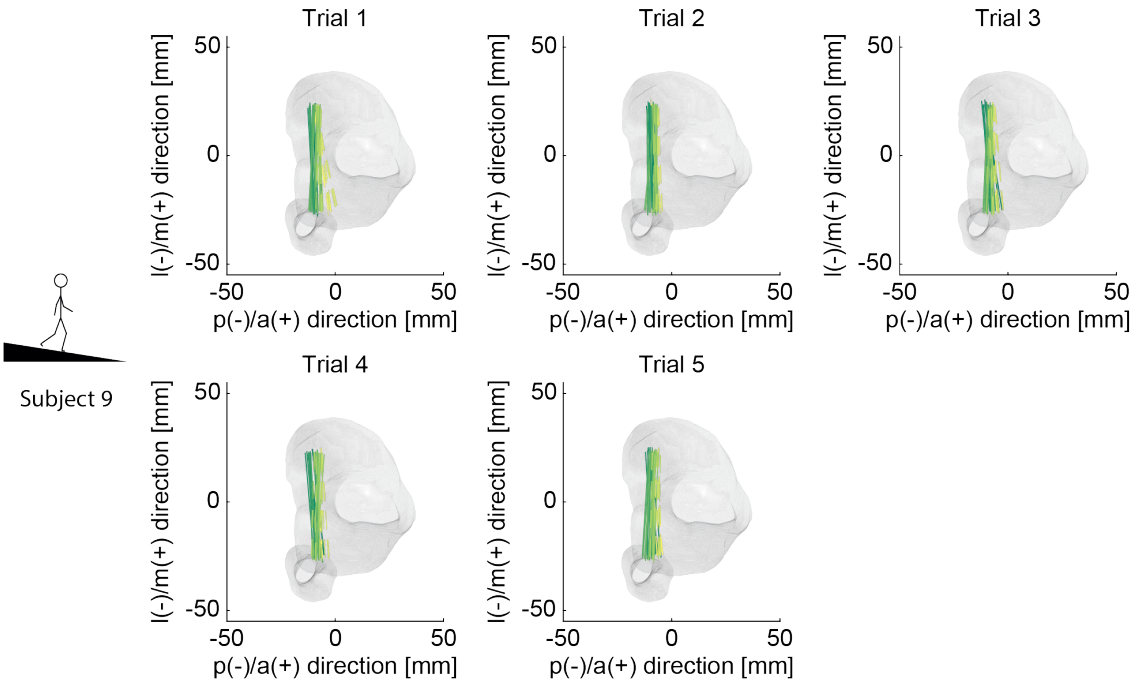

Figure B.23: Location and orientation of the femur relative to the tibia in medio (m)/lateral (l) and antero (a)/posterior (p) direction for all captured time frames during downhill walking is presented for Subject 9. Lines connect the FFA_P$_{med}$ and FFA_P$_{lat}$. Solid lines represent the loaded stance and dashed lines the unloaded swing phase. A continuous colour map is used from dark green (at heel strike) to yellow (end of swing phase)

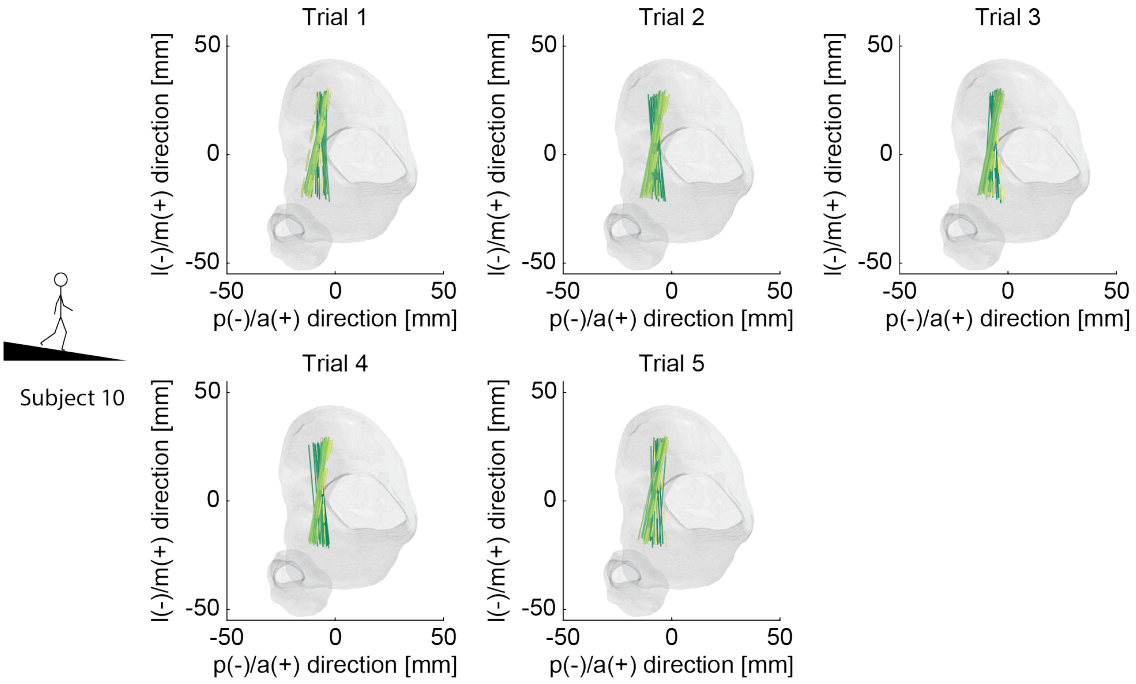

Figure B.24: Location and orientation of the femur relative to the tibia in medio (m)/lateral (l) and antero (a)/posterior (p) direction for all captured time frames during downhill walking is presented for Subject 10. Lines connect the FFA_P$_{med}$ and FFA_P$_{lat}$. Solid lines represent the loaded stance and dashed lines the unloaded swing phase. A continuous colour map is used from dark green (at heel strike) to yellow (end of swing phase)

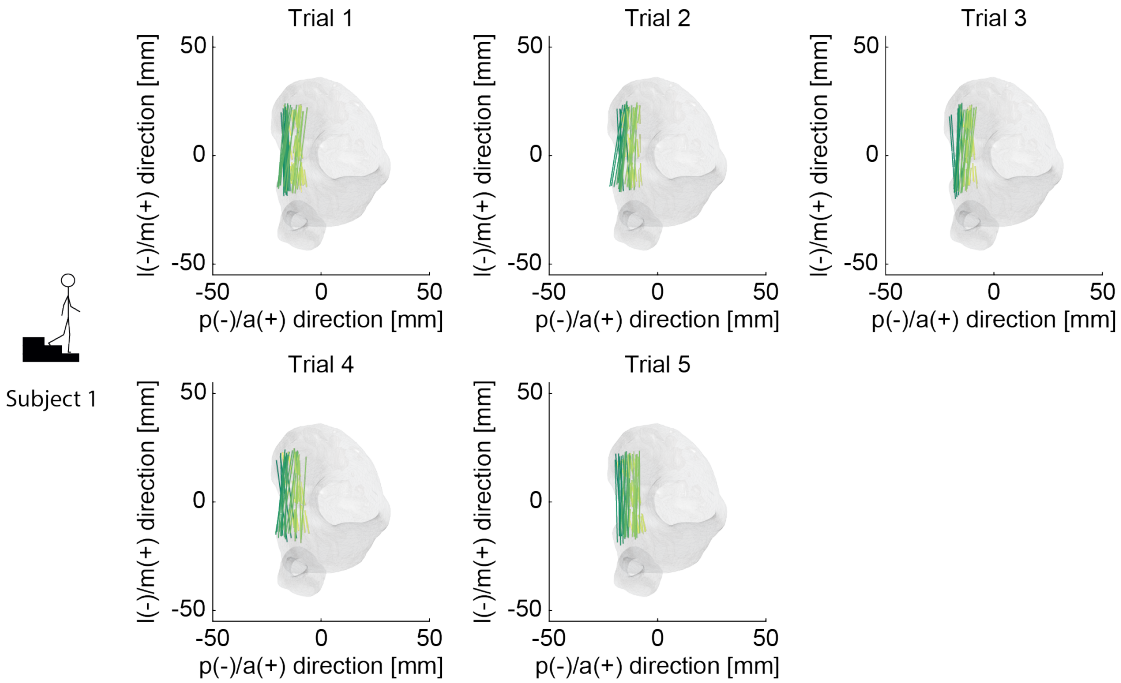

Figure B.25: Location and orientation of the femur relative to the tibia in medio (m)/lateral (l) and antero (a)/posterior (p) direction for all captured time frames during stair descent is presented for Subject 1. Lines connect the FFA_P$_{med}$ and FFA_P$_{lat}$. Solid lines represent the loaded stance and dashed lines the unloaded swing phase. A continuous colour map is used from dark green (at heel strike) to yellow (end of swing phase)

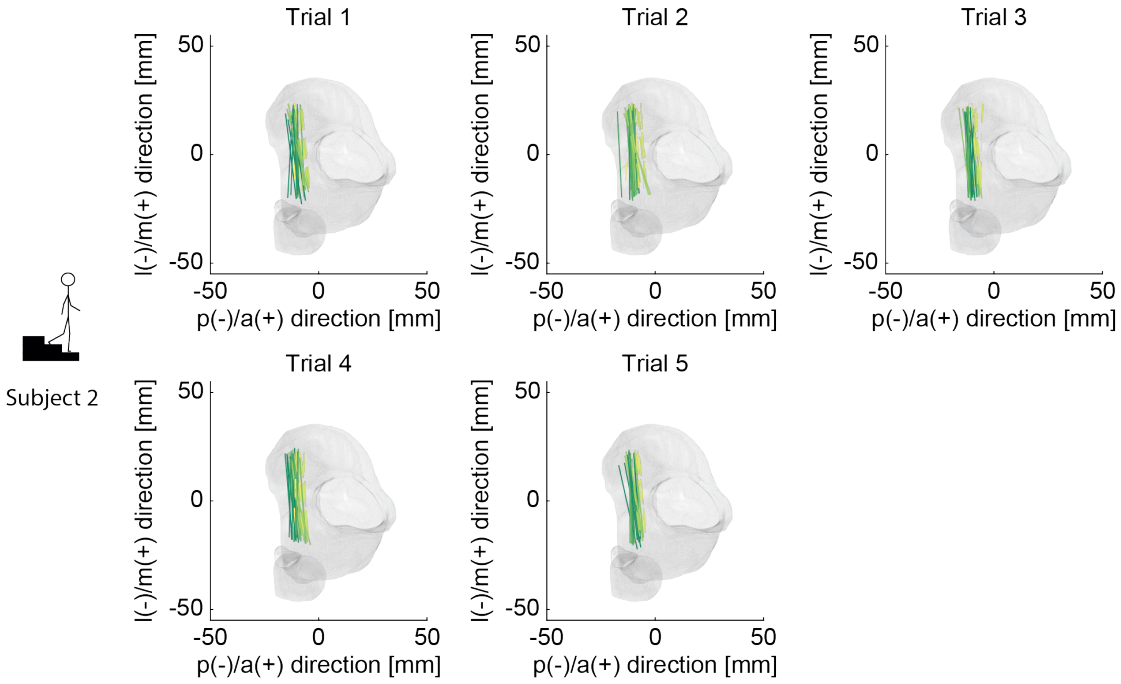

Figure B.26: Location and orientation of the femur relative to the tibia in medio (m)/lateral (l) and antero (a)/posterior (p) direction for all captured time frames during stair descent is presented for Subject 2. Lines connect the FFA_P$_{med}$ and FFA_P$_{lat}$. Solid lines represent the loaded stance and dashed lines the unloaded swing phase. A continuous colour map is used from dark green (at heel strike) to yellow (end of swing phase)

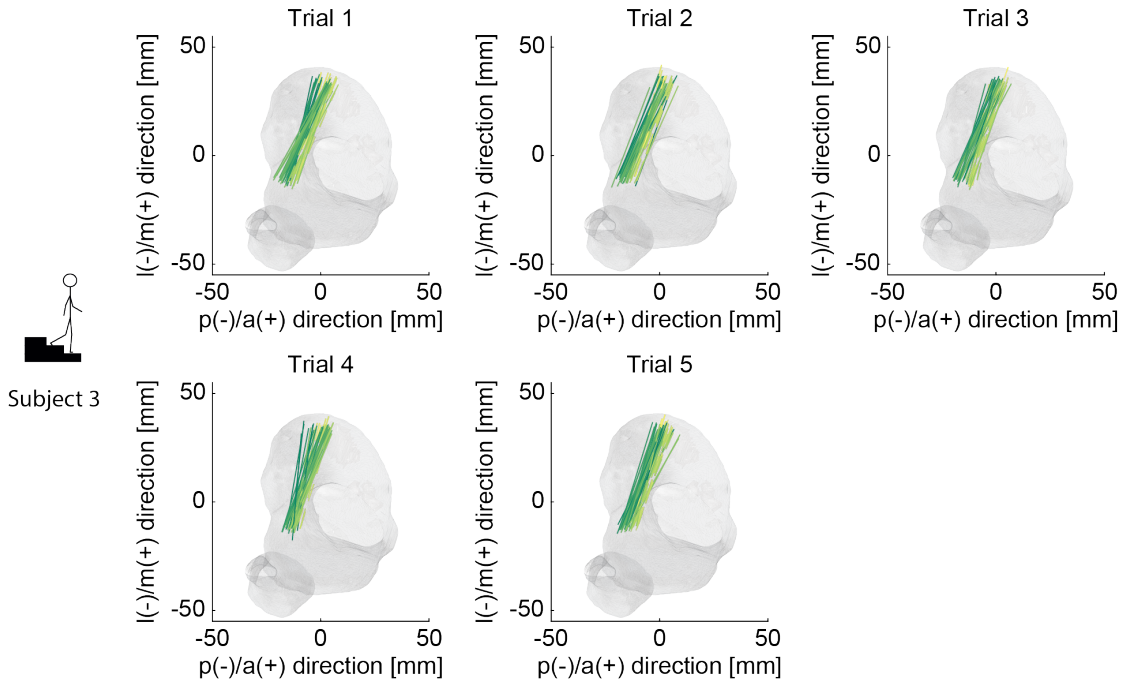

Figure B.27: Location and orientation of the femur relative to the tibia in medio (m)/lateral (l) and antero (a)/posterior (p) direction for all captured time frames during stair descent is presented for Subject 3. Lines connect the FFA_P$_{med}$ and FFA_P$_{lat}$. Solid lines represent the loaded stance and dashed lines the unloaded swing phase. A continuous colour map is used from dark green (at heel strike) to yellow (end of swing phase)

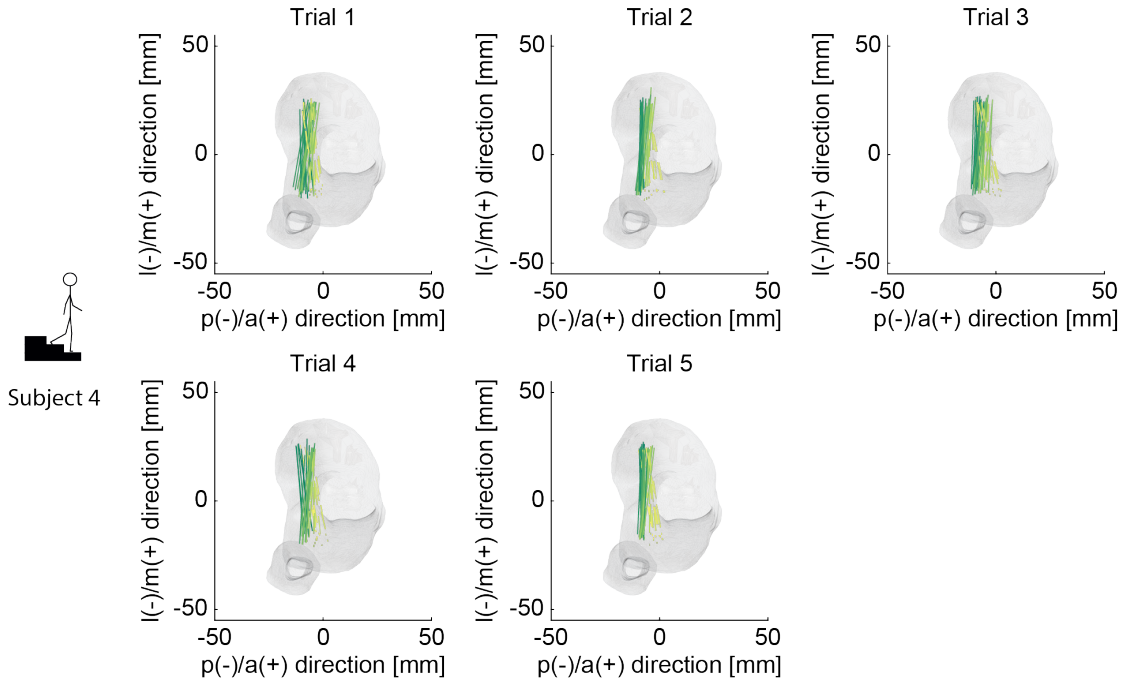

Figure B.28: Location and orientation of the femur relative to the tibia in medio (m)/lateral (l) and antero (a)/posterior (p) direction for all captured time frames during stair descent is presented for Subject 4. Lines connect the FFA_P$_{med}$ and FFA_P$_{lat}$. Solid lines represent the loaded stance and dashed lines the unloaded swing phase. A continuous colour map is used from dark green (at heel strike) to yellow (end of swing phase)

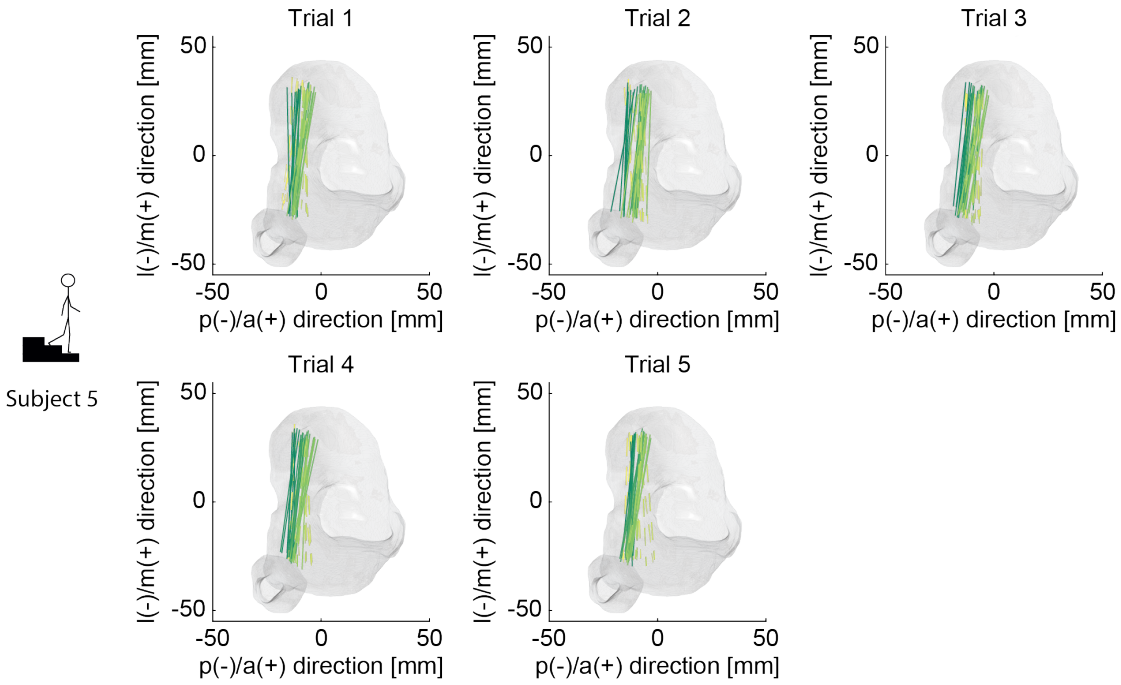

Figure B.29: Location and orientation of the femur relative to the tibia in medio (m)/lateral (l) and antero (a)/posterior (p) direction for all captured time frames during stair descent is presented for Subject 5. Lines connect the FFA_P$_{med}$ and FFA_P$_{lat}$. Solid lines represent the loaded stance and dashed lines the unloaded swing phase. A continuous colour map is used from dark green (at heel strike) to yellow (end of swing phase)

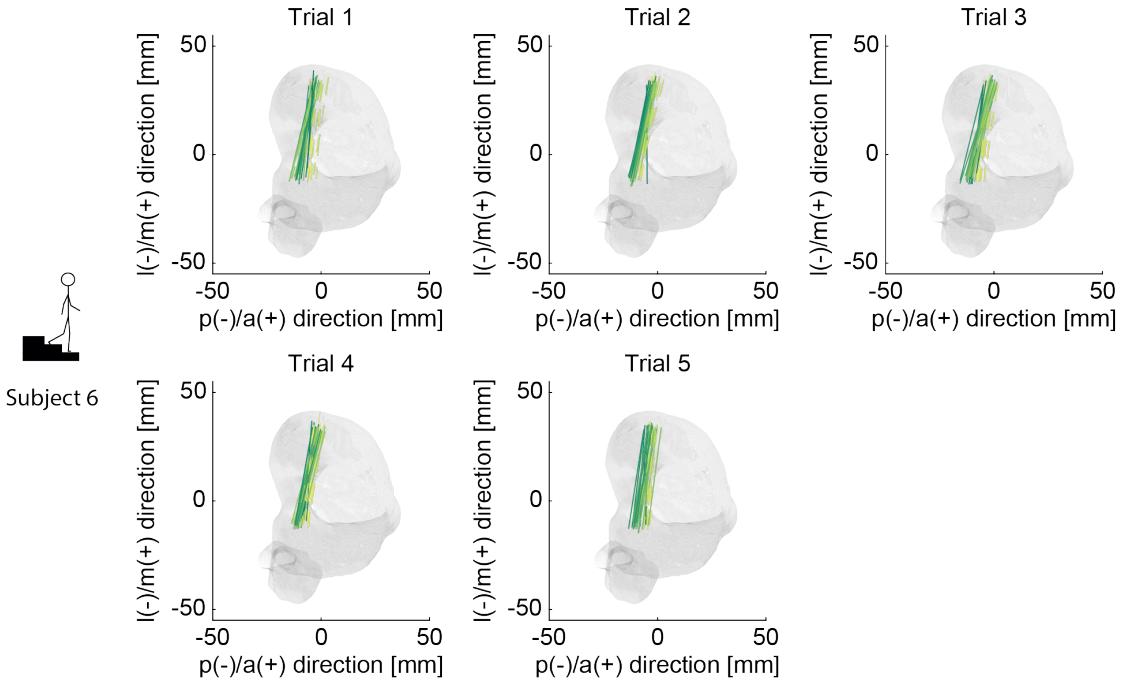

Figure B.30: Location and orientation of the femur relative to the tibia in medio (m)/lateral (l) and antero (a)/posterior (p) direction for all captured time frames during stair descent is presented for Subject 6. Lines connect the FFA_P$_{med}$ and FFA_P$_{lat}$. Solid lines represent the loaded stance and dashed lines the unloaded swing phase. A continuous colour map is used from dark green (at heel strike) to yellow (end of swing phase)

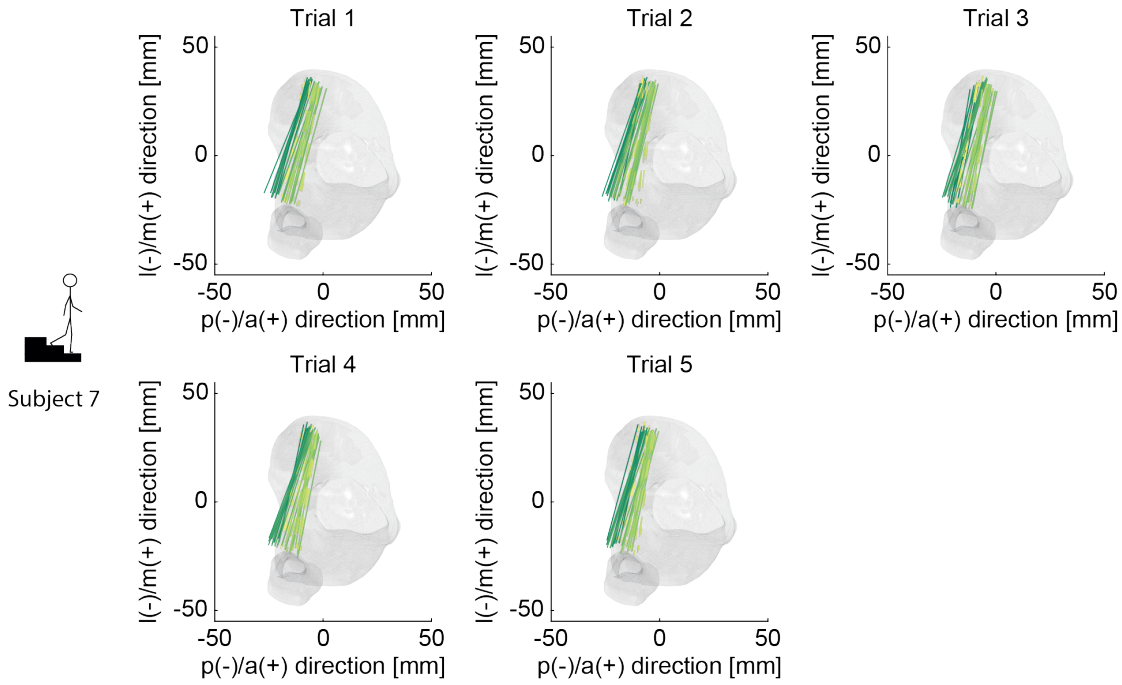

Figure B.31: Location and orientation of the femur relative to the tibia in medio (m)/lateral (l) and antero (a)/posterior (p) direction for all captured time frames during stair descent is presented for Subject 7. Lines connect the FFA_P$_{med}$ and FFA_P$_{lat}$. Solid lines represent the loaded stance and dashed lines the unloaded swing phase. A continuous colour map is used from dark green (at heel strike) to yellow (end of swing phase)

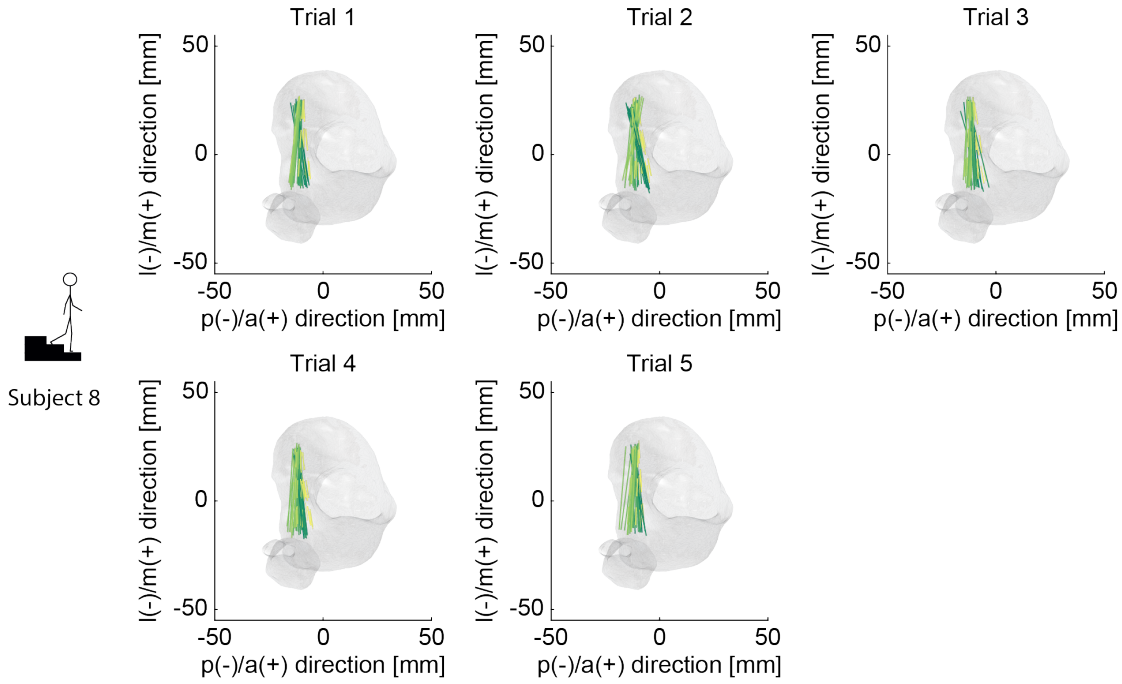

Figure B.32: Location and orientation of the femur relative to the tibia in medio (m)/lateral (l) and antero (a)/posterior (p) direction for all captured time frames during stair descent is presented for Subject 8. Lines connect the FFA_P$_{med}$ and FFA_P$_{lat}$. Solid lines represent the loaded stance and dashed lines the unloaded swing phase. A continuous colour map is used from dark green (at heel strike) to yellow (end of swing phase)

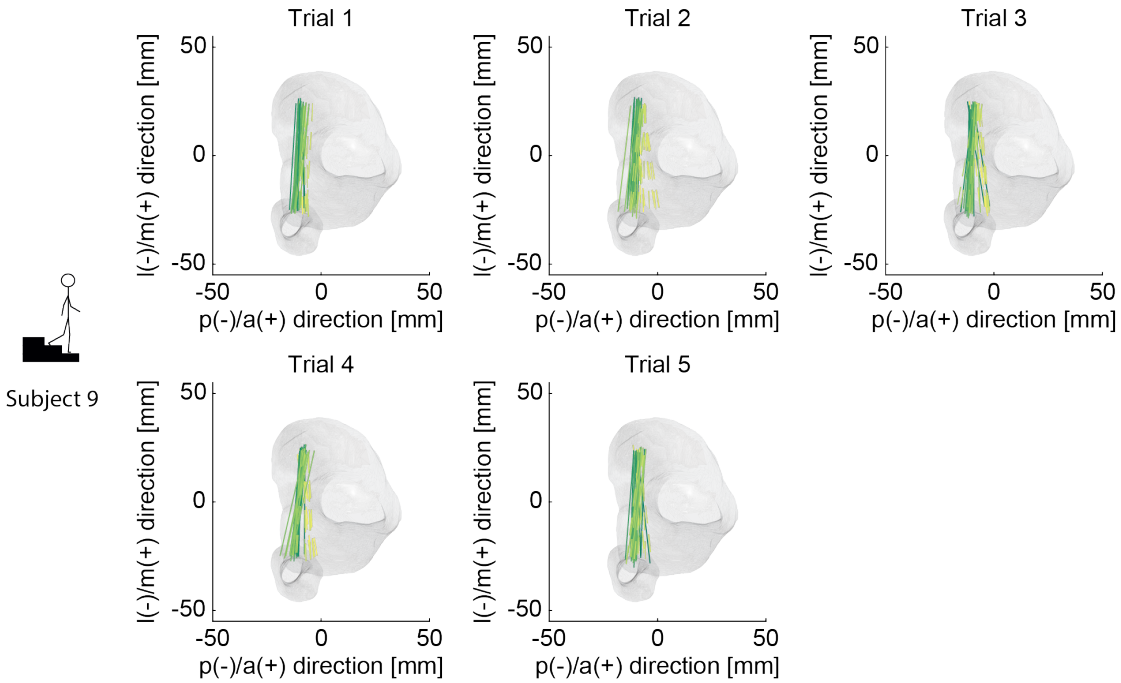

Figure B.33: Location and orientation of the femur relative to the tibia in medio (m)/lateral (l) and antero (a)/posterior (p) direction for all captured time frames during stair descent is presented for Subject 9. Lines connect the FFA_P$_{med}$ and FFA_P$_{lat}$. Solid lines represent the loaded stance and dashed lines the unloaded swing phase. A continuous colour map is used from dark green (at heel strike) to yellow (end of swing phase)

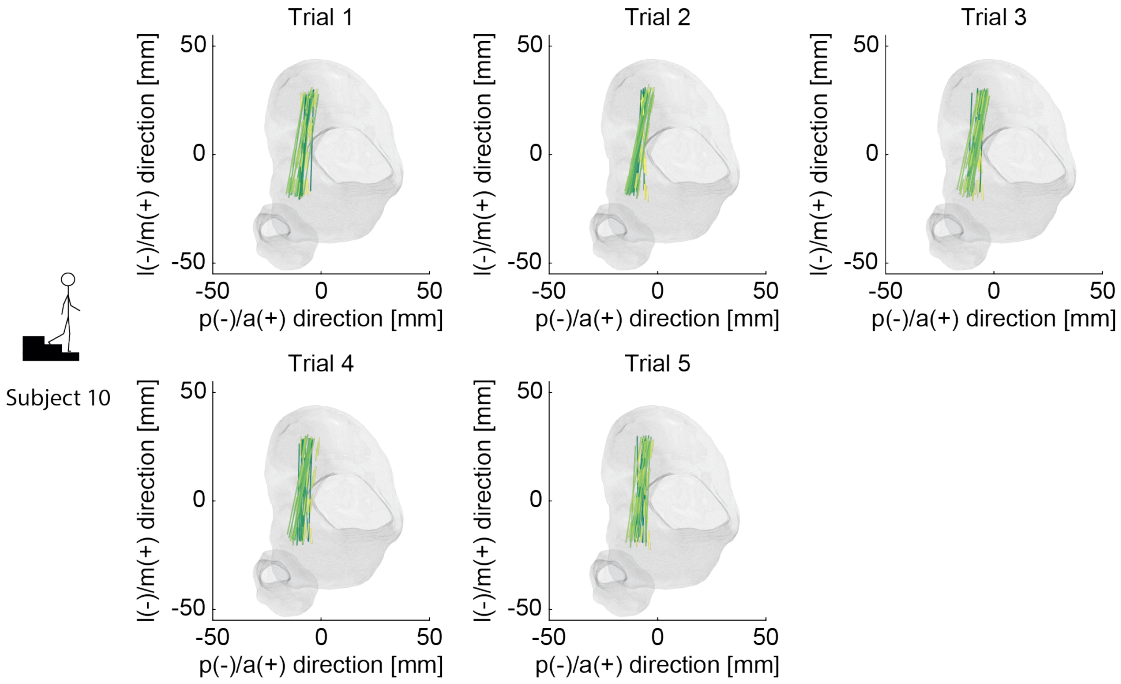

Figure B.34: Location and orientation of the femur relative to the tibia in medio (m)/lateral (l) and antero (a)/posterior (p) direction for all captured time frames during stair descent is presented for Subject 10. Lines connect the FFA_P$_{med}$ and FFA_P$_{lat}$. Solid lines represent the loaded stance and dashed lines the unloaded swing phase. A continuous colour map is used from dark green (at heel strike) to yellow (end of swing phase)

Table B.1: Location of the centre of rotation (CoR) during level walking in the antero-posterior (A-P), proximal-distal (P-D) and medio-lateral (M-L) direction. CoR for all trials of each individual subject, subject means and standard deviations (STD) as well as means and STDs across all subjects are presented for the loaded stance phase.

level walking		**loaded stance phase**						
		trial 1	trial 2	trial 3	trial 4	trial 5	trial 6	*mean ± STD*
Subject 1	A-P	-15.5	-15.1	-15.3	-14.7	-15.0	-14.5	*-15.0 ± 0.4*
	P-D	27.2	26.5	26.8	27.6	27.6	28.1	*27.3 ± 0.6*
	M-L	2.8	2.9	14.2	-6.8	-0.9	-7.7	*0.8 ± 8.0*
Subject 2	A-P	-10.2	-10.2	-9.8	-11.0	-10.0	-10.1	*-10.2 ± 0.4*
	P-D	28.6	28.5	28.3	29.1	28.6	28.9	*28.7 ± 0.3*
	M-L	2.8	3.5	2.9	16.3	8.4	5.9	*6.6 ± 5.2*
Subject 3	A-P	-6.2	-9.4	2.6	-2.1	-11.9		*-5.4 ± 5.8*
	P-D	31.0	31.2	29.5	30.4	32.2		*30.9 ± 1.0*
	M-L	14.5	2.3	45.6	29.8	-4.4		*17.6 ± 20.4*
Subject 4	A-P	-7.4	-7.6	-7.3	-7.7	-7.4		*-7.5 ± 0.2*
	P-D	24.7	24.9	25.6	25.5	25.4		*25.2 ± 0.4*
	M-L	1.0	-2.9	-13.3	1.9	0.4		*-2.6 ± 6.3*
Subject 5	A-P	-11.7	-11.2	-12.9	-12.4	-12.1	-12.5	*-12.1 ± 0.6*
	P-D	28.6	28.1	29.1	29.0	28.2	29.1	*28.7 ± 0.5*
	M-L	18.4	25.5	14.6	13.4	24.2	12.9	*18.2 ± 5.5*
Subject 6	A-P	-6.8	-5.8	-6.7	-6.3	-5.8		*-6.3 ± 0.5*
	P-D	31.0	30.3	30.8	30.6	30.1		*30.6 ± 0.3*
	M-L	1.6	10.4	7.0	7.2	8.9		*7.0 ± 3.3*
Subject 7	A-P	-13.0	-12.1	-13.7	-12.7	-11.2	-11.9	*-12.5 ± 0.9*
	P-D	32.5	31.8	31.7	32.0	31.7	32.1	*32.0 ± 0.3*
	M-L	9.8	12.0	7.0	10.7	16.6	13.1	*11.5 ± 3.2*
Subject 8	A-P	-9.4	-10.8	-10.8	-10.9	-10.3		*-10.4 ± 0.6*
	P-D	28.2	28.1	28.4	28.2	27.9		*28.2 ± 0.2*
	M-L	1.3	11.2	7.2	10.4	4.2		*6.9 ± 4.2*
Subject 9	A-P	-7.9	-8.3	-8.7	-7.9	-8.3		*-8.2 ± 0.3*
	P-D	26.9	26.8	26.7	26.7	26.3		*26.7 ± 0.2*
	M-L	-7.8	-8.9	5.0	-4.0	1.1		*-2.9 ± 5.9*
Subject 10	A-P	-6.1	-6.6	-6.1	-6.4	-6.6		*-6.4 ± 0.3*
	P-D	31.7	31.0	31.2	30.9	30.9		*31.2 ± 0.3*
	M-L	9.1	13.9	7.4	12.1	6.0		*9.7 ± 3.3*
mean ± STD	A-P	-9.4 ± 3.2						
	P-D	28.9 ± 2.2						
	M-L	7.2 ± 7.4						

Table B.2: Location of the centre of rotation (CoR) during level walking in the antero-posterior (A-P), proximal-distal (P-D) and medio-lateral (M-L) direction. CoR for all trials of each individual subject , subject means and standard deviations (STD) as well as means and STDs across all subjects are presented for the unloaded swing phase.

level walking		**unloaded swing phase**						
		trial 1	trial 2	trial 3	trial 4	trial 5	trial 6	*mean ± STD*
Subject 1	A-P	-12.7	-12.0	-10.7	-11.0	-12.8	-11.8	*-11.8 ± 0.8*
	P-D	25.4	26.4	26.7	25.5	25.2	25.8	*25.8 ± 0.6*
	M-L	5.0	-19.4	-27.2	-7.1	16.5	-7.5	*-6.6 ± 15.8*
Subject 2	A-P	-7.7	-8.5	-8.2	-7.4	-7.6	-8.0	*-7.9 ± 0.4*
	P-D	28.7	28.1	28.2	28.2	28.1	28.7	*28.3 ± 0.3*
	M-L	6.8	8.4	9.4	4.7	2.7	6.2	*6.4 ± 2.4*
Subject 3	A-P	-2.9	-0.7	0.1	-0.3	-2.6		*-1.3 ± 1.4*
	P-D	30.4	30.8	30.0	29.8	30.5		*30.3 ± 0.4*
	M-L	12.1	29.4	36.1	27.4	13.7		*23.7 ± 10.4*
Subject 4	A-P	-3.7	-3.7	-4.2	-5.0	-4.5		*-4.2 ± 0.6*
	P-D	24.7	24.9	24.4	24.5	24.7		*24.6 ± 0.2*
	M-L	2.1	1.5	0.1	4.9	4.8		*2.7 ± 2.1*
Subject 5	A-P	-9.8	-9.7	-9.8	-7.6	-10.0	-12.8	*-10.0 ± 1.7*
	P-D	25.7	26.4	27.3	24.0	26.0	22.5	*25.3 ± 1.8*
	M-L	45.4	21.5	11.3	61.1	28.0	70.5	*39.6 ± 23.3*
Subject 6	A-P	-3.8	-3.7	-3.7	-3.8	3.8		*-3.8 ± 0.1*
	P-D	29.5	29.9	30.0	29.9	29.7		*29.8 ± 0.2*
	M-L	15.6	14.1	14.1	14.5	15.9		*14.9 ± 0.9*
Subject 7	A-P	-6.4	-9.6	-6.5	-9.0	-2.2	-9.3	*-7.2 ± 2.8*
	P-D	29.3	29.5	29.1	29.7	28.6	28.9	*29.2 ± 0.4*
	M-L	24.3	11.1	25.2	8.8	50.7	14.3	*22.4 ± 15.5*
Subject 8	A-P	-10.4	-10.2	-11.0	-10.0	-10.8		*-10.5 ± 0.4*
	P-D	27.6	27.5	27.1	27.3	27.5		*27.4 ± 0.2*
	M-L	21.3	14.5	23.8	14.1	22.7		*19.3 ± 4.6*
Subject 9	A-P	-5.1	-7.2	-5.2	-7.3	-6.2		*-6.2 ± 1.0*
	P-D	26.4	25.2	25.4	25.1	25.6		*25.5 ± 0.5*
	M-L	-17.1	6.5	-11.6	4.3	-9.7		*-5.5 ± 10.3*
Subject 10	A-P	-5.9	-6.0	-5.4	-5.4	-5.6		*-5.7 ± 0.3*
	P-D	29.8	29.7	29.0	29.1	29.7		*29.5 ± 0.4*
	M-L	18.7	18.2	23.7	20.9	18.5		20.0 ± 2.3
mean ± STD	A-P	-6.8 ± 3.3						
	P-D	27.6 ± 2.1						
	M-L	13.7 ± 14.4						

Table B.3: Location of the centre of rotation (CoR) during level walking in the antero-posterior (A-P), proximal-distal (P-D) and medio-lateral (M-L) direction. CoR for all trials of each individual subject, subject means and standard deviations (STD) as well as means and STDs across all subjects are presented for the complete gait cycle.

level walking		**complete gait cycle**						
		trial 1	trial 2	trial 3	trial 4	trial 5	trial 6	*mean ± STD*
Subject 1	A-P	-14.3	-14.1	-14.3	-13.5	-13.9	-13.6	*-14.0 ± 0.3*
	P-D	26.5	26.3	26.0	26.6	26.9	27.3	*26.6 ± 0.5*
	M-L	2.1	-0.8	14.0	-2.5	0.1	-7.3	*0.9 ± 7.2*
Subject 2	A-P	-9.9	-10.3	-9.9	-10.7	-9.7	-10.0	*-10.1 ± 0.3*
	P-D	29.1	28.7	28.5	29.2	28.6	29.1	*28.9 ± 0.3*
	M-L	13.0	11.4	10.3	18.8	9.6	12.8	*12.6 ± 3.3*
Subject 3	A-P	-2.5	-1.6	0.9	0.9	-6.2		*-1.7 ± 2.9*
	P-D	30.5	30.6	29.8	30.0	31.1		*30.4 ± 0.5*
	M-L	22.7	28.6	39.8	37.6	9.9		*27.7 ± 12.1*
Subject 4	A-P	-6.3	-6.5	-6.4	-6.8	-6.4		*-6.5 ± 0.2*
	P-D	24.6	24.8	25.0	25.0	25.0		*24.9 ± 0.2*
	M-L	8.9	5.4	1.5	8.5	9.2		*6.7 ± 3.3*
Subject 5	A-P	-10.3	-10.1	-10.4	-9.7	-10.7	-11.1	*-10.4 ± 0.5*
	P-D	27.3	26.7	26.6	27.0	26.7	27.2	*26.9 ± 0.3*
	M-L	31.1	32.9	35.6	32.7	32.2	27.6	*32.0 ± 2.6*
Subject 6	A-P	-4.9	-4.5	-4.8	-4.8	-4.7		*-4.7 ± 0.2*
	P-D	30.1	29.9	29.9	30.1	29.7		*30.0 ± 0.2*
	M-L	13.4	15.4	16.6	15.3	15.3		*15.2 ± 1.2*
Subject 7	A-P	-9.8	-10.6	-9.9	10.3	-8.3	-11.1	*-10.0 ± 1.0*
	P-D	31.1	30.9	30.6	31.0	30.5	31.0	*30.9 ± 0.2*
	M-L	18.6	14.2	17.6	15.0	26.3	13.0	*17.5 ± 4.8*
Subject 8	A-P	-10.1	-10.7	-10.9	-10.7	-11.0		*-10.7 ± 0.3*
	P-D	27.9	27.9	27.9	27.9	27.7		*27.9 ± 0.1*
	M-L	13.8	14.0	13.4	12.2	14.9		*13.7 ± 1.0*
Subject 9	A-P	-7.3	-7.7	-8.2	-7.8	-7.7		*-7.8 ± 0.3*
	P-D	26.6	26.4	26.1	26.1	26.0		*26.2 ± 0.3*
	M-L	-6.4	-10.2	8.2	1.0	-0.6		*-1.6 ± 7.1*
Subject 10	A-P	-6.3	-6.5	-6.0	-5.8	-6.3		*-6.2 ± 0.3*
	P-D	30.8	30.5	30.1	30.0	30.3		*30.3 ± 0.3*
	M-L	14.8	16.0	18.2	19.5	13.2		*16.4 ± 2.5*
mean ± STD	A-P	-8.2 ± 3.5						
	P-D	28.3 ± 2.1						
	M-L	14.1 ± 10.5						

Table B.4: Location of the centre of rotation (CoR) during downhill walking in the antero-posterior (A-P), proximal-distal (P-D) and medio-lateral (M-L) direction. CoR for all trials of each individual subject , subject means and standard deviations (STD) as well as means and STDs across all subjects are presented for the loaded stance phase.

downhill walking		**loaded stance phase**					
		trial 1	trial 2	trial 3	trial 4	trial 5	*mean ± STD*
Subject 1	A-P	-13.0	-15.1	-14.0	-13.7	-12.6	*-13.7 ± 1.0*
	P-D	26.8	26.6	25.7	26.0	26.7	*26.4 ± 0.5*
	M-L	-10.6	-11.2	-3.9	-6.2	-13.7	*-9.1 ± 4.0*
Subject 2	A-P	-10.6	-11.4	-11.8	-11.5	-11.9	*-11.5 ± 0.5*
	P-D	27.5	27.5	28.1	27.7	27.2	*27.6 ± 0.3*
	M-L	4.8	12.5	23.9	18.1	16.9	*15.2 ±7.1*
Subject 3	A-P	-4.4	-1.4	-6.6	-4.6	-6.5	*-4.7 ± 2.1*
	P-D	30.1	29.5	29.9	29.4	29.2	*29.6 ± 0.3*
	M-L	14.7	23.7	10.1	16.8	11.3	*15.3 ± 5.4*
Subject 4	A-P	-7.7	-7.7	-7.1	-8.0	-6.8	*-7.5 ± 0.5*
	P-D	24.0	24.4	24.6	24.9	25.0	*24.6 ± 0.4*
	M-L	-0.6	2.9	-0.1	-7.2	-7.0	*-2.4 ± 4.5*
Subject 5	A-P	-10.2	-10.1	-10.1	-11.4	-10.4	*-10.5 ± 0.6*
	P-D	27.9	27.4	27.4	29.0	29.1	*28.2 ± 0.8*
	M-L	3.2	12.4	11.5	-9.0	-15.5	*0.5 ± 12.4*
Subject 6	A-P	-6.8	-5.8	-5.9	-7.2	-7.2	*-6.6 ± 0.7*
	P-D	29.6	29.1	29.5	29.5	29.5	*29.4 ± 0.2*
	M-L	8.2	8.1	11.0	8.7	5.6	*8.3 ± 1.9*
Subject 7	A-P	-10.2	-12.8	-13.5	-10.6	-14.1	*-12.3 ± 1.8*
	P-D	29.7	29.5	30.4	29.7	30.1	*29.9 ± 0.3*
	M-L	18.6	8.1	4.6	14.6	2.2	*9.6 ± 6.9*
Subject 8	A-P	-11.7	-11.3	-11.3	-11.7	-11.2	*-11.4 ± 0.3*
	P-D	27.5	27.6	27.2	27.2	27.5	*27.4 ± 0.2*
	M-L	16.1	15.4	15.5	18.3	13.6	*15.8 ± 1.7*
Subject 9	A-P	-9.6	-8.9	-8.9	-8.8	-9.4	*-9.1 ± 0.4*
	P-D	24.7	25.1	24.9	25.4	24.9	*25.0 ± 0.3*
	M-L	-2.0	-2.0	8.7	-7.2	4.1	*0.3 ± 6.2*
Subject 10	A-P	-6.5	-7.2	-6.8	-7.1	-6.6	*-6.9 ± 0.3*
	P-D	30.0	30.2	29.8	30.2	29.5	*29.9 ± 0.3*
	M-L	15.7	11.8	13.0	9.6	15.3	*13.1 ± 2.5*
mean ± STD	A-P	-9.4 ± 2.9					
	P-D	27.8 ± 2.0					
	M-L	6.7 ± 8.8					

Table B.5: Location of the centre of rotation (CoR) during downhill walking in the antero-posterior (A-P), proximal-distal (P-D) and medio-lateral (M-L) direction. CoR for all trials of each individual subject, subject means and standard deviations (STD) as well as means and STDs across all subjects are presented for the unloaded swing phase.

downhill walking		**unloaded swing phase**					
		trial 1	trial 2	trial 3	trial 4	trial 5	*mean ± STD*
Subject 1	A-P	-12.5	-11.9	-12.9	-12.9	-11.3	*-12.3 ± 0.7*
	P-D	24.3	25.8	25.5	25.4	27.4	*25.7 ± 1.1*
	M-L	17.3	-0.2	6.5	4.5	-13.5	*2.9 ± 11.2*
Subject 2	A-P	-7.4	-10.1	-7.8	-9.0	-9.8	*-8.8 ± 1.2*
	P-D	28.2	28.8	28.2	27.5	28.6	*28.3 ± 0.5*
	M-L	-0.9	16.9	3.0	5.4	14.3	*7.7 ± 7.6*
Subject 3	A-P	-3.1	-3.4	-0.1	-1.5	-0.7	*-1.8 ± 1.4*
	P-D	30.6	31.1	30.1	29.4	30.1	*30.3 ± 0.6*
	M-L	11.8	13.3	25.4	21.5	23.7	*19.1 ± 6.2*
Subject 4	A-P	-5.5	-4.9	-5.2	-5.9	-5.5	*-5.4 ± 0.4*
	P-D	25.5	25.5	25.3	25.2	25.7	*25.4 ± 0.2*
	M-L	-4.7	-7.5	-5.0	-7.9	2.6	*-4.5 ± 4.2*
Subject 5	A-P	-10.2	-11	-10.3	-10.2	-10.0	*-10.3 ± 0.4*
	P-D	26.7	26.6	28.6	27.5	25.5	*27.0 ± 1.1*
	M-L	24.2	23.7	11.3	13.5	25.7	*19.7 ± 6.7*
Subject 6	A-P	-4.3	-4.1	-3.5	-4.3	-4.2	*-4.1 ± 0.3*
	P-D	30.5	30.1	30.0	30.4	30.0	*30.2 ± 0.2*
	M-L	8.3	6.9	16.5	6.4	7.8	*9.2 ± 4.2*
Subject 7	A-P	-9.0	-6.2	-6.3	-9.4	-6.0	*-7.4 ± 1.7*
	P-D	29.3	29.4	29.7	29.6	29.3	*29.4 ± 0.2*
	M-L	18.4	28.6	29.8	11.7	29.4	*23.6 ± 8.2*
Subject 8	A-P	-10.1	-10.5	-10.8	-10.8	-10.4	*-10.5 ± 0.3*
	P-D	27.7	27.6	27.2	27.4	27.4	*27.5 ± 0.2*
	M-L	20.7	19.2	20.1	22.3	17.9	*20.0 ± 1.6*
Subject 9	A-P	-7.6	-7.1	-8.8	-7.2	-6.9	*-7.5 ± 0.8*
	P-D	25.6	26.8	23.8	25.5	25.7	*25.5 ± 1.1*
	M-L	9.9	-11.2	33.8	-0.1	-1.8	*6.1 ± 17.2*
Subject 10	A-P	-6.4	-6.0	-5.6	-5.9	-5.9	*-5.9 ± 0.3*
	P-D	29.5	29.6	30.0	29.9	29.3	*29.6 ± 0.3*
	M-L	17.0	13.5	12.6	11.6	13.5	*13.6 ± 2.1*
mean ± STD	A-P	-7.4 ± 3.2					
	P-D	27.9 ± 1.9					
	M-L	11.7 ± 9.0					

Table B.6: Location of the centre of rotation (CoR) during downhill walking in the antero-posterior (A-P), proximal-distal (P-D) and medio-lateral (M-L) direction. CoR for all trials of each individual subject, subject means and standard deviations (STD) as well as means and STDs across all subjects are presented for the complete gait cycle.

downhill walking		**complete gait cycle** trial 1	trial 2	trial 3	trial 4	trial 5	*mean ± STD*
	A-P	-12.6	-13.8	-13.5	-13.2	-12.1	*-13.0 ± 0.7*
Subject 1	P-D	26.1	25.6	25.6	25.7	27.0	*26.0 ± 0.6*
	M-L	-6.4	2.9	0.8	-0.1	-13.0	*-3.2 ± 6.5*
	A-P	-10.0	-11.4	-11.2	-10.9	-11.6	*-11.0 ± 0.6*
Subject 2	P-D	28.1	28.3	28.5	27.8	28.1	*28.2 ± 0.2*
	M-L	8.5	20.5	21.5	16.0	22.0	*17.7 ± 5.7*
	A-P	-2.2	-0.9	-2.0	-2.2	-2.2	*-1.9 ± 0.6*
Subject 3	P-D	30.0	30.1	29.9	29.3	29.4	*29.7 ± 0.4*
	M-L	19.3	24.4	21.4	22.4	21.4	*21.8 ± 1.9*
	A-P	-7.0	-7.0	-6.6	-7.1	-6.4	*-6.8 ± 0.3*
Subject 4	P-D	24.3	24.5	24.7	24.7	24.9	*24.6 ± 0.2*
	M-L	3.1	5.4	2.6	-2.2	3.8	*2.5 ± 2.9*
	A-P	-10.0	-10.3	-10.2	-10.4	-9.1	*-10.0 ± 0.5*
Subject 5	P-D	27.7	27.4	27.9	28.4	27.6	*27.8 ± 0.3*
	M-L	9.0	12.5	11.3	1.4	3.4	*7.5 ± 4.9*
	A-P	-5.0	-4.7	-4.1	-5.2	-4.8	*-4.8 ± 0.4*
Subject 6	P-D	29.6	29.3	29.4	29.5	29.2	*29.4 ± 0.2*
	M-L	13.8	12.1	18.6	15.3	16.8	*15.3 ± 2.5*
	A-P	-8.8	-8.8	-9.9	-8.6	-9.8	*-9.2 ± 0.6*
Subject 7	P-D	29.4	29.5	30.0	29.5	29.7	*29.6 ± 0.2*
	M-L	22.8	20.7	16.5	20.5	16.0	*19.3 ± 2.9*
	A-P	-11.0	-11.0	-11.1	-11.4	-10.9	*-11.1 ± 0.2*
Subject 8	P-D	27.6	27.6	27.2	27.3	27.5	*27.4 ± 0.2*
	M-L	16.2	17.6	18.4	19.9	14.4	*17.3 ± 2.1*
	A-P	-9.1	-8.3	-8.6	-8.2	-8.6	*-8.5 ± 0.3*
Subject 9	P-D	24.7	25.5	24.6	25.5	25.0	*25.1 ± 0.4*
	M-L	13.0	0.8	16.9	-6.7	9.1	*6.6 ± 9.6*
	A-P	-6.5	-6.9	-6.3	-6.8	-6.4	*-6.6 ± 0.3*
Subject 10	P-D	29.8	30.0	29.9	30.1	29.4	*29.8 ± 0.3*
	M-L	16.2	11.3	13.0	8.2	14.1	*12.6 ± 3.0*
	A-P			-8.3 ± 3.3			
mean ± STD	P-D			27.8 ± 2.0			
	M-L			11.7 ± 8.1			

Table B.7: Location of the centre of rotation (CoR) during stair descent in the antero-posterior (A-P), proximal-distal (P-D) and medio-lateral (M-L) direction. CoR for all trials of each individual subject, subject means and standard deviations (STD) as well as means and STDs across all subjects are presented for the loaded stance phase.

stair descent		**loaded stance phase** trial 1	trial 2	trial 3	trial 4	trial 5	*mean ± STD*
Subject 1	A-P	-15.7	-14.9	-16.7	-15.2	-14.3	*-15.3 ± 0.9*
	P-D	25.2	23.4	24.1	23.5	25.3	*24.3 ± 0.9*
	M-L	-9.1	5.8	-23.5	4.5	-22.1	*-8.9 ± 14.0*
Subject 2	A-P	-10.7	-11.2	-11.5	-11.2	-10.5	*-11.0 ± 0.4*
	P-D	27.1	27.6	27.1	27.0	26.8	*27.1 ± 0.3*
	M-L	5.2	8.6	7.8	6.8	5.2	*6.7 ± 1.5*
Subject 3	A-P	-7.3	-4.6	-8.1	-10.9	-13.6	*-8.9 ± 3.5*
	P-D	29.3	29.5	28.7	28.8	28.7	*29.0 ± 0.4*
	M-L	11.0	17.1	10.0	-0.7	-5.4	*6.4 ± 9.2*
Subject 4	A-P	-7.7	-7.9	-7.7	-7.9	-7.4	*-7.7 ± 0.2*
	P-D	23.9	23.9	25.1	24.5	24.5	*24.4 ± 0.5*
	M-L	3.7	-0.7	-0.3	-3.4	1.1	*0.1 ± 2.6*
Subject 5	A-P	-12.2	-9.4	-13.1	-13.0	-11.9	*-11.9 ± 1.5*
	P-D	28.6	26.0	27.5	27.5	27.6	*27.4 ± 0.9*
	M-L	-16.5	11.6	-14.0	-16.4	-8.1	*-8.7 ± 11.8*
Subject 6	A-P	-4.6	-5.7	-7.4	-6.2	-6.3	*-6.1 ± 1.0*
	P-D	28.4	29.3	29.4	28.9	29.1	*29.0 ± 0.4*
	M-L	23.7	15.8	7.8	11.2	10.2	*13.7 ± 6.3*
Subject 7	A-P	1.2	-4.0	-5.2	-2.6	-4.5	*-3.0 ± 2.5*
	P-D	29.6	29.5	29.8	28.8	29.4	*29.4 ± 0.4*
	M-L	51.3	37.8	31.5	41.2	35.5	*39.5 ± 7.5*
Subject 8	A-P	-11.6	-11.5	-11.8	-12.1	-11.8	*-11.8 ± 0.2*
	P-D	27.2	27.0	27.0	27.1	27.1	*27.1 ± 0.1*
	M-L	14.6	11.3	13.1	17.9	21.2	*15.6 ± 3.9*
Subject	A-P	-10.1	-9.2	-9.7	-10.1	-9.4	*-9.7 ± 0.4*
	P-D	24.2	24.4	24.6	24.9	24.4	*24.5 ± 0.3*
	M-L	3.8	20.9	19.5	2.3	3.9	*10.1 ± 9.3*
Subject 10	A-P	-5.7	-6.2	-6.7	-7.0	-6.6	*-6.4 ± 0.5*
	P-D	29.6	29.2	29.6	29.7	29.8	*29.6 ± 0.2*
	M-L	23.5	19.7	18.4	19.7	18.0	*19.9 ± 2.2*
mean ± STD	A-P	-9.2 ± 3.5					
	P-D	27.2 ± 2.1					
	M-L	9.4 ± 14.3					

Table B.8: Location of the centre of rotation (CoR) during stair descent in the antero-posterior (A-P), proximal-distal (P-D) and medio-lateral (M-L) direction. CoR for all trials of each individual subject, subject means and standard deviations (STD) as well as means and STDs across all subjects are presented for the unloaded swing phase.

stair descent		**unloaded swing phase** trial 1	trial 2	trial 3	trial 4	trial 5	*mean ± STD*
Subject 1	A-P	-11.6	-11.3	-12.5	-11.9	-11.4	*-11.7 ± 0.5*
	P-D	25.1	25.1	24.1	23.8	25.0	*24.6± 0.6*
	M-L	3.0	-4.8	21.8	10.7	2.9	*6.7 ± 10.0*
Subject 2	A-P	-8.8	-8.9	-8.6	-8.1	-8.2	*-8.5 ± 0.3*
	P-D	27.7	27.5	26.9	27.1	27.1	*27.3 ± 0.4*
	M-L	8.1	8.6	-1.1	-0.3	-0.9	*2.9 ± 5.0*
Subject 3	A-P	-4.1	-3.5	-6.7	-3.6	-2.5	*-4.1 ± 1.6*
	P-D	29.9	30.1	30.4	30.5	30.1	*30.2 ± 0.2*
	M-L	11.0	15.9	5.4	16.3	16.8	*13.1 ± 4.9*
Subject 4	A-P	-4.8	-4.7	-4.9	-4.5	-4.7	*-4.7 ± 0.2*
	P-D	24.5	24.0	24.4	24.8	23.8	*24.3 ± 0.4*
	M-L	0.5	6.8	5.4	3.8	7.1	*4.7 ± 2.7*
Subject 5	A-P	-8.1	-9.6	-9.2	-9.4	-9.7	*-9.2 ± 0.6*
	P-D	25.5	27.0	26.0	26.8	26.8	*26.4 ± 0.6*
	M-L	32.8	14	21.2	17.7	21.6	*21.5 ± 7.1*
Subject 6	A-P	-3.3	-5.9	-4.0	-3.9	-3.6	*-4.1 ± 1.0*
	P-D	29.6	30.2	29.4	29.4	29.1	*29.5 ± 0.4*
	M-L	18.0	5.9	14.5	15.4	18.9	*14.5 ± 5.2*
Subject 7	A-P	-6.2	-4.8	-5.4	-4.9	-5.0	*-5.3 ± 0.6*
	P-D	29.1	28.5	28.7	28.6	28.5	*28.7 ± 0.3*
	M-L	26.9	38.2	34.8	31.5	30.8	*32.5 ± 4.3*
Subject 8	A-P	-10.3	-11.2	-11.2	-11.8	-11.1	*-11.1 ± 0.5*
	P-D	26.6	27.5	27.0	27.4	27.0	*27.1 ± 0.4*
	M-L	27.6	29.6	26.0	27.9	28.2	*27.9 ± 1.3*
Subject 9	A-P	-8.2	-7.2	-8.0	-7.9	-8.6	*-8.0 ± 0.5*
	P-D	24.9	24.9	24.6	25.3	24.6	*24.9 ± 0.3*
	M-L	-3.9	18.4	14.6	11.4	9.5	*10.0 ± 8.5*
Subject 10	A-P	-7.2	-6.1	-6.7	-7.2	-6.7	*-6.8 ± 0.5*
	P-D	29.9	29.7	29.8	31.2	29.8	*30.1 ± 0.6*
	M-L	10.9	15.7	16.3	3.5	15.6	*12.4 ± 5.4*
mean ± STD	A-P	-7.3 ± 2.8					
	P-D	27.3 ± 2.3					
	M-L	14.6 ± 9.8					

Table B.9: Location of the centre of rotation (CoR) during stair descent in the antero-posterior (A-P), proximal-distal (P-D) and medio-lateral (M-L) direction. CoR for all trials of each individual subject, subject means and standard deviations (STD) as well as means and STDs across all subjects are presented for the complete gait cycle.

stair descent		**complete gait cycle** trial 1	trial 2	trial 3	trial 4	trial 5	*mean ± STD*
Subject 1	A-P	-13.6	-13.6	-13.8	-13.7	-13.3	*-13.6 ± 0.2*
	P-D	24.5	23.3	23.4	23.2	24.2	*23.7 ± 0.6*
	M-L	7.3	12.4	9.0	15.3	6.9	*10.2 ± 3.6*
Subject 2	A-P	-10.1	-10.5	-10.4	-10.2	-9.7	*-10.2 ± 0.3*
	P-D	27.7	27.7	27.1	27.2	26.9	*27.3 ± 0.4*
	M-L	10	10.4	4.0	6.4	3.2	*6.8 ± 3.3*
Subject 3	A-P	-5.0	-2.0	-4.7	-8.7	-7.2	*-5.5 ± 2.6*
	P-D	29.5	29.7	29.4	29.5	29.6	*29.5 ± 0.1*
	M-L	13.7	22.4	16.3	3.9	7.8	*12.8 ± 7.2*
Subject 4	A-P	-6.5	-6.3	-6.4	-6.6	-6.3	*-6.4 ± 0.1*
	P-D	23.8	23.4	24.0	24.1	23.8	*23.8 ± 0.3*
	M-L	10.0	13.3	12.0	8.4	13.3	*11.4 ± 2.2*
Subject 5	A-P	-10.2	-9.4	-9.7	-10.0	-9.8	*-9.8 ± 0.3*
	P-D	27.4	26.4	26.3	26.7	26.8	*26.7 ± 0.4*
	M-L	4.9	11.4	10.1	5.9	9.1	*8.3 ± 2.8*
Subject 6	A-P	-3.5	-5.3	-4.6	-4.7	-4.4	*-4.5 ± 0.7*
	P-D	28.5	29.4	29.1	28.9	28.9	*29.0 ± 0.3*
	M-L	26.0	14.7	17.4	16.2	19.1	*18.7 ± 4.4*
Subject 7	A-P	-4.4	-5.4	-6.4	-3.5	-4.8	*-4.9 ± 1.1*
	P-D	29.2	29.1	29.4	28.7	29.0	*29.1 ± 0.3*
	M-L	33.8	33.2	27.3	38.3	33.6	*33.2 ± 3.9*
Subject 8	A-P	-11.2	-11.1	-11.6	-11.9	-11.6	*-11.5 ± 0.3*
	P-D	27.1	27.1	27.0	27.2	27.1	*27.1 ± 0.1*
	M-L	17.4	14.3	16.2	21.7	22.7	*18.5 ± 3.6*
Subject 9	A-P	-9.1	-8.4	-9.1	-8.6	-9.0	*-8.8 ± 0.3*
	P-D	24.3	24.3	24.6	24.9	24.4	*24.5 ± 0.3*
	M-L	9.9	24.8	18.1	12.5	8.8	*14.8 ± 6.7*
Subject 10	A-P	-6.7	-6.1	-6.7	-7.0	-6.6	*-6.6 ± 0.3*
	P-D	29.7	29.3	29.7	30.2	29.8	*29.7 ± 0.3*
	M-L	15.2	18.4	17.4	15.4	16.8	*16.6 ± 1.3*
mean ± STD	A-P	-8.2 ± 3.1					
	P-D	27.1 ± 2.3					
	M-L	15.1 ± 7.6					

Appendix C

Supplementary material Chapter 5

Supplementary material associated with Chapter 5:
Interpretation of tibio-femoral kinematics critically depends upon the kinematic analysis approach: A survey and comparison of methodologies

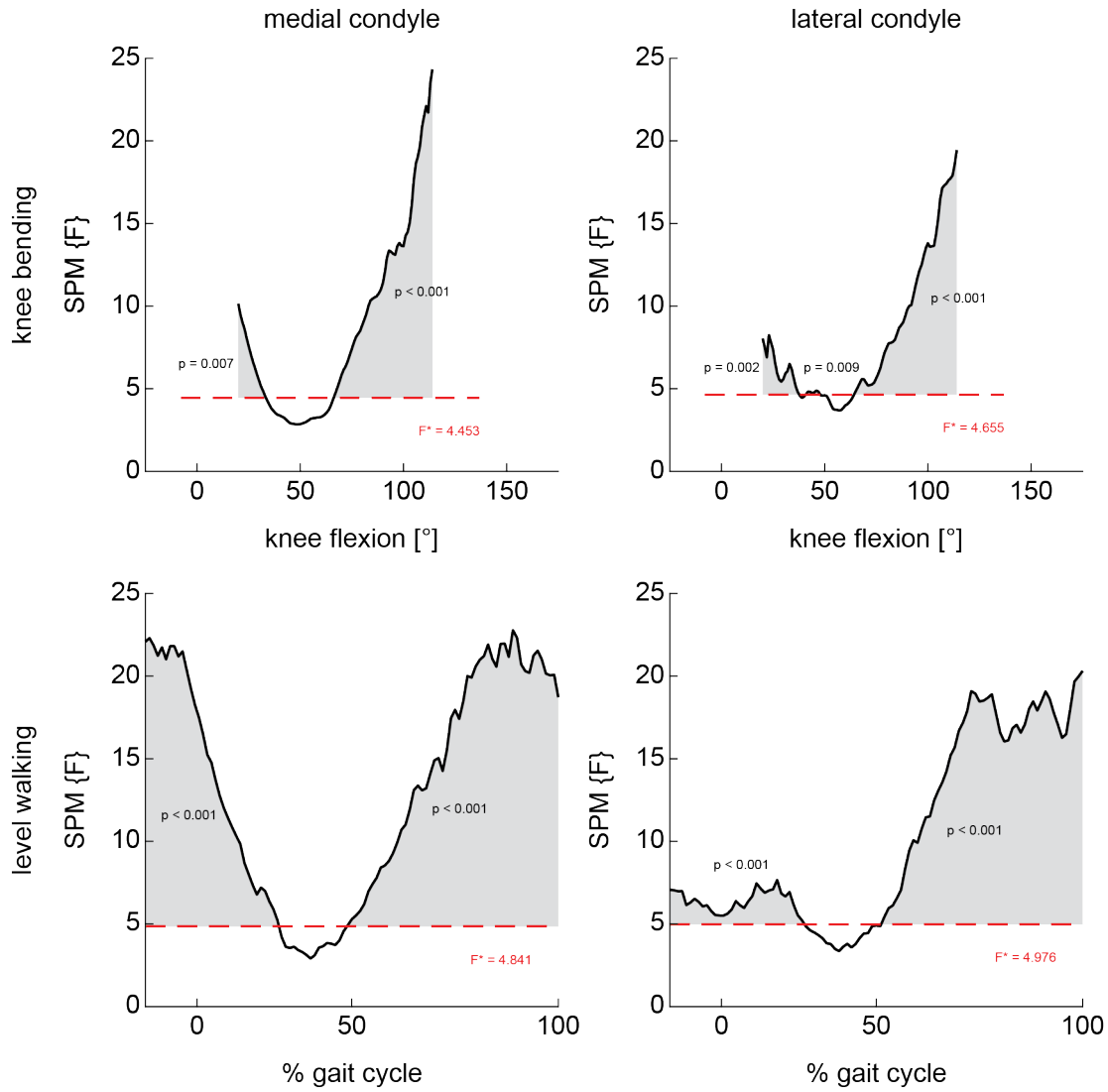

Figure C.1: F-value for the SPM ANOVA1d analysis to test for differences between the kinematic analysis approaches during continuous knee bending (top) and throughout the complete gait cycle of level walking (bottom) each for the medial (left) and lateral (right) femoral condyle. Significance was set to $\alpha = 0.0125$.

Table C.1: Location of the centre of rotation (CoR) in the transverse plane of the tibial anatomical coordinate system. Mean locations and standard deviations in the antero-posterior (A-P) and medio-lateral (M-L) direction are presented across all subjects as well as for each individual subject (Subject 1 – Subject 10) during continuous knee bending using the functional flexion axis (FFA), transepicondylar axis (TEA), cylinder axis (CA), extension facet centres and flexion facet centres (EFC/FFC), nearest point (NP) and tibio-femoral separation (SEP).

CoR location [mm]		**FFA**	**TEA**	**CA**	**EFC/FFC**	**NP**	**SEP**
continuous knee bending							
mean ± STD	**A-P location**	**-9.8 ± 2.6**	**-9.2 ± 6.3**	**3.75 ± 7.8**	**-1.4 ± 9.8**	**0.2 ± 2.9**	**0.2 ± 1.7**
	M-L location	**6.6 ± 10.5**	**31.8 ± 37.3**	**39.4 ± 25.6**	**40.1 ± 40.3**	**34.1 ± 17.2**	**27.2 ± 13.6**
Subject 1	A-P location	-10.3 ± 0.4	-24.6 ± 3.2	-13.9 ± 5.5	-16.6 ± 2.9	-4.6 ± 2.8	-2.4 ± 1.7
	M-L location	7.5 ± 5.9	-43.4 ±9.3	5.3 ± 39.2	-19.4 ± 19.6	-24.4 ± 20.4	24.4 ± 12.5
Subject 2	A-P location	-10.3 ± 0.3	-7.5 ± 1.7	-9.5 ± 0.7	-5.5 ± 1.6	-1.4 ± 0.9	-0.9 ± 0.8
	M-L location	21.7 ± 7.4	95.0 ± 14.5	42.7 ± 11.7	52.2 ± 1.6	34.6 ± 8.8	31.9 ± 9.7
Subject 3	A-P location	-8.6 ± 1.6	-5.0 ± 1.8	10.4 ± 5.9	6.7 ± 0.8	3.9 ± 2.5	1.9 ± 2.9
	M-L location	10.3 ± 4.8	32.3 ± 3.9	61.4 ± 13.8	46.3 ± 0.1	26.1 ± 3.0	16.1 ± 4.1
Subject 4	A-P location	-7.1 ± 1.0	-7.0 ± 3.4	-6.2 ± 0.3	-1.4 ± 1.3	-1.6 ± 2.4	-0.2 ± 0.6
	M-L location	-5.7 ± 3.9	6.5 ± 22.7	5.1 ± 4.5	43.4 ± 0.3	16.6 ± 10.0	16.3 ± 2.1
Subject 5	A-P location	-15.1 ± 9.1	-10.4 ± 1.6	3.1 ± 5.1	2.3 ± 1.0	1.7 ± 0.8	-0.4 ± 0.2
	M-L location	-9.0 ± 41.5	41.9 ± 12.0	81.8 ± 24.9	64.9 ± 1.7	37.7 ± 1.2	25.1 ± 2.3
Subject 6	A-P location	-7.8 ± 2.0	-1.4 ± 5.9	-4.9 ± 1.3	15.5 ± 2.9	-0.8 ± 1.1	0.1 ± 1.2
	M-L location	7.2 ± 11.8	41.4 ± 24.3	21.5 ± 8.5	102.4 ± 3.1	21.5 ± 3.8	17.0 ± 5.8
Subject 7	A-P location	-12.7 ± 6.0	-13.9 ± 0.4	5.0 ±1.3	1.1 ± 4.4	3.6 ± 1.3	-0.2 ± 0.6
	M-L location	1.0 ± 18.7	17.9 ± 1.6	61.2 ± 6.7	46.2 ± 1.1	31.4 ± 2.8	15.3 ± 2.8
Subject 8	A-P location	-10.7 ± 0.2	-7.3 ± 2.6	10.2 ± 1.0	-	-2.1 ± 0.4	-0.8 ± 0.8
	M-L location	13.2 ± 1.8	44.3 ± 11.4	44.9 ± 5.9	-	31.4 ± 0.9	35.8 ± 2.5
Subject 9	A-P location	-9.3 ± 0.8	-7.4 ± 2.7	-9.5 ± 0.6	-7.9 ± 1.6	0.1 ± 3.2	0.9 ± 2.6
	M-L location	-1.1 ± 8.1	68.9 ± 12.3	21.2 ± 13.6	51.1 ± 0.8	78.6 ± 12.3	59.7 ± 12.0
Subject 10	A-P location	-6.3 ± 0.3	-7.0 ± 5.7	-2.0 ± 1.1	-10.2 ± 1.1	4.1 ± 0.4	4.0 ± 0.3
	M-L location	21.4 ± 4.1	13.5 ± 39.0	48.5 ± 8.5	-26.4 ± 1.5	38.5 ± 1.5	30.1 ± 0.9

Table C.2: Location of the centre of rotation (CoR) in the transverse plane of the tibial anatomical coordinate system. Mean locations and standard deviations in the antero-posterior (A-P) and medio-lateral (M-L) direction are presented across all subjects as well as for each individual subject (Subject 1 – Subject 10) during level walking using the functional flexion axis (FFA), transepicondylar axis (TEA), cylinder axis (CA), extension facet centres and flexion facet centres (EFC/FFC), nearest point (NP) and tibio-femoral separation (SEP).

CoR location [mm]		**FFA**	**TEA**	**CA**	**EFC/FFC**	**NP**	**SEP**
level walking (complete cycle)							
mean ± STD	**A-P location**	**-8.7 ± 2.9**	**-1.7 ± 3.8**	**-4.5 ± 2.0**	**0.1 ± 6.2**	**0.5 ± 3.2**	**1.6 ± 2.3**
	M-L location	**14.3 ± 10.9**	**14.1 ± 12.4**	**14.2 ± 8.4**	**44.7 ± 33.5**	**24.8 ± 13.2**	**27.5 ± 11.7**
Subject 1	A-P location	-13.6 ± 0.3	-2.6 ± 0.6	-5.9 ± 0.2	-3.1 ± 0.5	-1.0 ± 0.4	-0.1 ± 0.2
	M-L location	0.6 ± 7.1	6.1 ± 6.1	4.5 ± 6.5	33.7 ± 0.8	9.9 ± 11.2	15.3 ± 7.1
Subject 2	A-P location	-10.5 ± 0.2	0.4 ± 1.1	-6.5 ± 0.4	-12.6 ± 1.1	-5.2 ± 1.1	0.3 ± 2.7
	M-L location	15.8 ± 3.3	-11.7 ± 7.1	5.3 ± 4.1	56.7 ± 0.5	36.2 ± 3.0	17.2 ± 11.5
Subject 3	A-P location	-3.6 ± 2.3	-3.3 ± 0.4	-1.0 ± 0.7	4.7 ± 0.7	3.5 ± 0.7	4.0 ± 0.3
	M-L location	29.8 ± 12.2	14.7 ± 3.6	12.8 ± 3.9	60.5 ± 4.4	27.4 ± 3.6	34.0 ± 7.2
Subject 4	A-P location	-6.9 ± 0.2	1.5 ± 0.3	-3.8 ± 0.3	0.5 ± 0.6	-1.4 ± 0.6	0.4 ± 0.2
	M-L location	6.7 ± 3.3	10.9 ± 2.1	12.1 ± 1.7	41.5 ± 0.6	6.4 ± 4.2	13.7 ± 1.2
Subject 5	A-P location	-11.3 ± 0.5	-6.3 ± 0.5	-4.6 ± 0.3	0.4 ± 0.6	-0.8 ± 0.5	0.1 ± 0.4
	M-L location	31.5 ± 2.6	8.9 ± 3.8	16.6 ± 3.2	51.2 ± 2.1	4.8 ± 3.2	21.3 ± 5.3
Subject 6	A-P location	-6.1 ± 0.1	3.4 ± 0.4	-3.4 ± 0.2	9.9 ± 1.4	2.7 ± 0.4	2.9 ± 0.4
	M-L location	14.5 ± 1.2	30.5 ± 1.8	18.9 ± 0.5	96.3 ± 3.1	31.5 ± 3.0	34.8 ± 2.3
Subject 7	A-P location	-10.1 ± 0.8	-8.7 ± 0.1	-4.4 ± 0.4	2.4 ± 0.5	3.6 ± 0.3	4.5 ±0.2
	M-L location	17.5 ± 4.9	17.7 ± 3.7	16.8 ± 2.4	43.6 ± 0.6	28.9 ± 2.1	32.7 ± 2.6
Subject 8	A-P location	-10.1 ± 0.3	-2.8 ± 0.5	-8.1 ± 0.7	-	-2.8 ± 0.3	-2.4 ± 0.6
	M-L location	12.8 ± 1.0	31.8 ± 4.3	28.4 ± 4.7	-	29.5 ± 1.8	41.9 ± 3.3
Subject 9	A-P location	-8.4 ± 0.4	-0.6 ± 0.3	-5.0 ± 0.2	-3.3 ± 0.7	1.9 ± 1.3	2.4 ± 0.8
	M-L location	-2.1 ± 7.1	13.1 ± 12.8	2.8 ± 2.4	49.6 ± 0.7	30.0 ± 15.7	18.0 ± 17.0
Subject 10	A-P location	-6.5 ± 0.2	2.2 ± 0.9	-2.8 ± 0.3	1.5 ± 1.3	4.2 ± 1.2	4.2 ± 0.5
	M-L location	16.1 ± 2.5	18.6 ± 7.2	23.4 ± 2.0	-30.9 ± 0.7	43.9 ± 3.2	45.7 ± 1.8

Table C.3: Resultant regions of significant differences between the kinematic analysis approaches based on statistical parameter mapping (SPM). Significant differences for continuous knee bending are indicated for specific flexion angles and significant differences for level walking are indicated for specific time points of the complete gait cycles (%). Significances are indicated based on an adjusted level of significance of $\alpha = 0.0033$.

	method (1)	**method (2)**	**medial condyle**	**lateral condyle**
continuous knee bending	FFA	TEA	97° – 119°	91° – 119°
	FFA	CA	–	–
	FFA	EFC/FFC	–	–
	FFA	NP	25° – 37°	25° / 26° / 28°
	FFA	SEP	25° – 41° / 118°/119°	25°– 52°
	TEA	CA	–	–
	TEA	EFC/FFC	111° – 119°	–
	TEA	NP	75° – 119°	82° – 119°
	TEA	SEP	71° – 119°	65° – 119°
	CA	EFC/FFC	–	–
	CA	NP	111° – 119°	–
	CA	SEP	102° – 119°	112° – 119°
	EFC/FFC	NP	–	–
	EFC/FFC	SEP	118°/119°	119°
	NP	SEP	–	–
level walking (complete cycle)	FFA	TEA	0 – 16% / 75% / 77 – 100%	58 – 100%
	FFA	CA	2 – 4% / 8 – 10%	–
	FFA	EFC/FFC	0 – 12%	–
	FFA	NP	0 – 32%	–
	FFA	SEP	0 – 37% / 74 – 100%	0 – 29%
	TEA	CA	–	–
	TEA	EFC/FFC	–	–
	TEA	NP	57 – 100%	58 – 100%
	TEA	SEP	53 – 100%	53 – 100%
	CA	EFC/FFC	–	–
	CA	NP	0 – 12% / 71 – 100%	–
	CA	SEP	0 – 18% / 62 – 100%	69 – 100%
	EFC/FFC	NP	–	–
	EFC/FFC	SEP	–	91% / 98 – 100%
	NP	SEP	–	–

Appendix D

Supplementary material Chapter 6

Supplementary material associated with Chapter 6:
Limb alignment plays only a minor role on tibio-femoral kinematics: A dynamic videofluoroscopy study

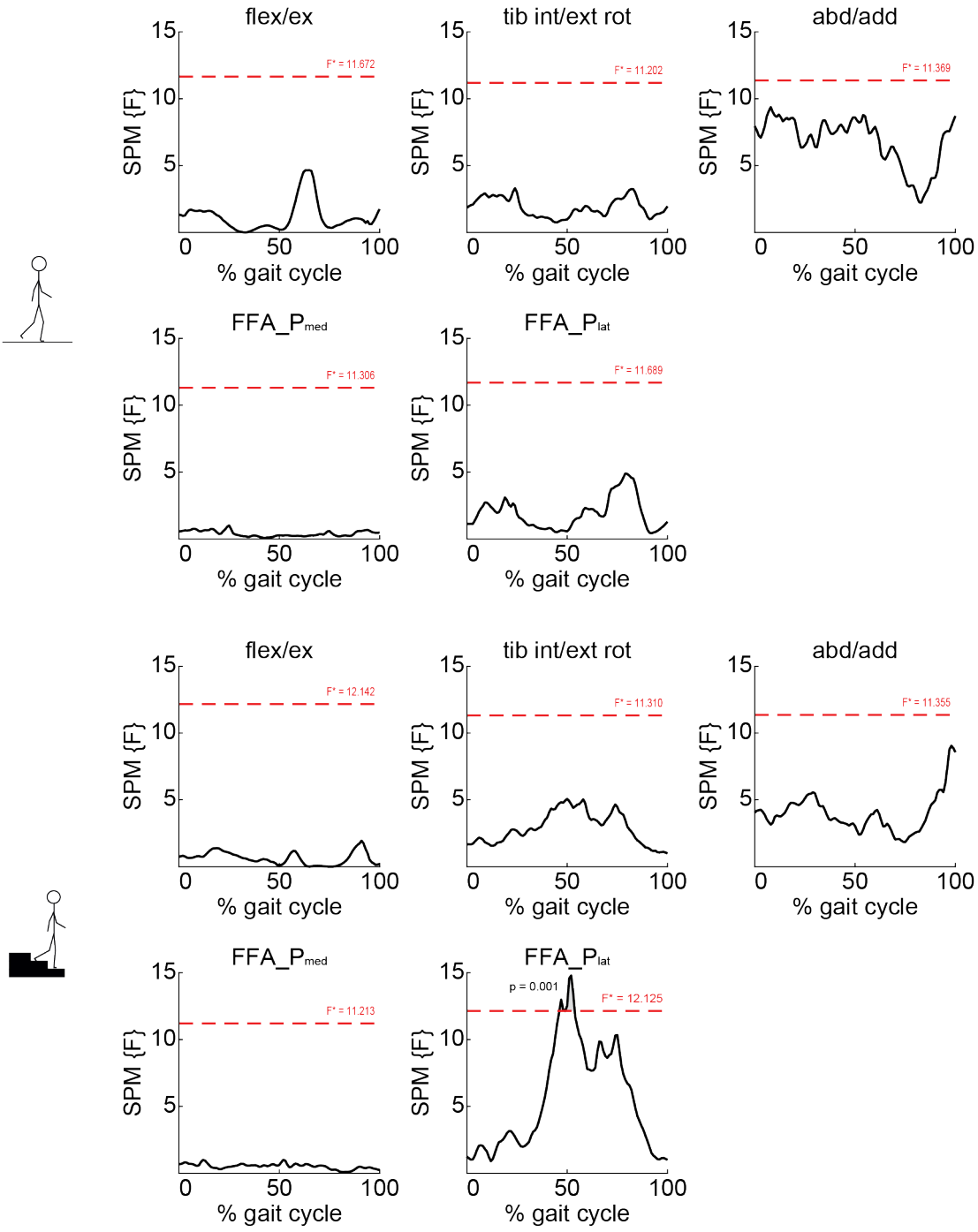

Figure D.1: F-value for the SPM ANOVA1d analysis for level walking (top) and stair descent (bottom), each rotation (flexion/extension (flex/ex), tibial internal/external rotation (tib int/ext rot), abduction/adduction (abd/add)) as well as A P translation of the medial and lateral point on the functional flexion axis (FFA_P$_{med}$ & FFA_P$_{lat}$). Significance was set to $\alpha = 0.005$.

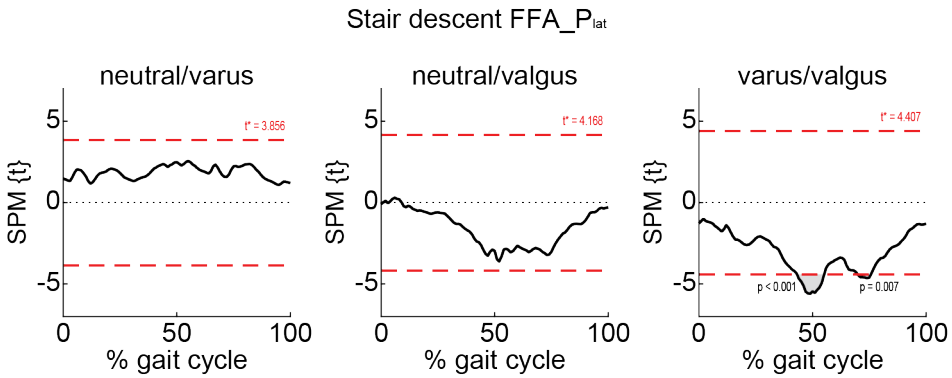

Figure D.2: T-value for the SPM t-test2 post-hoc analysis for the lateral functional flexion point (FFA_P$_{lat}$) during stair descent. Significance was set to $\alpha = 0.017$.

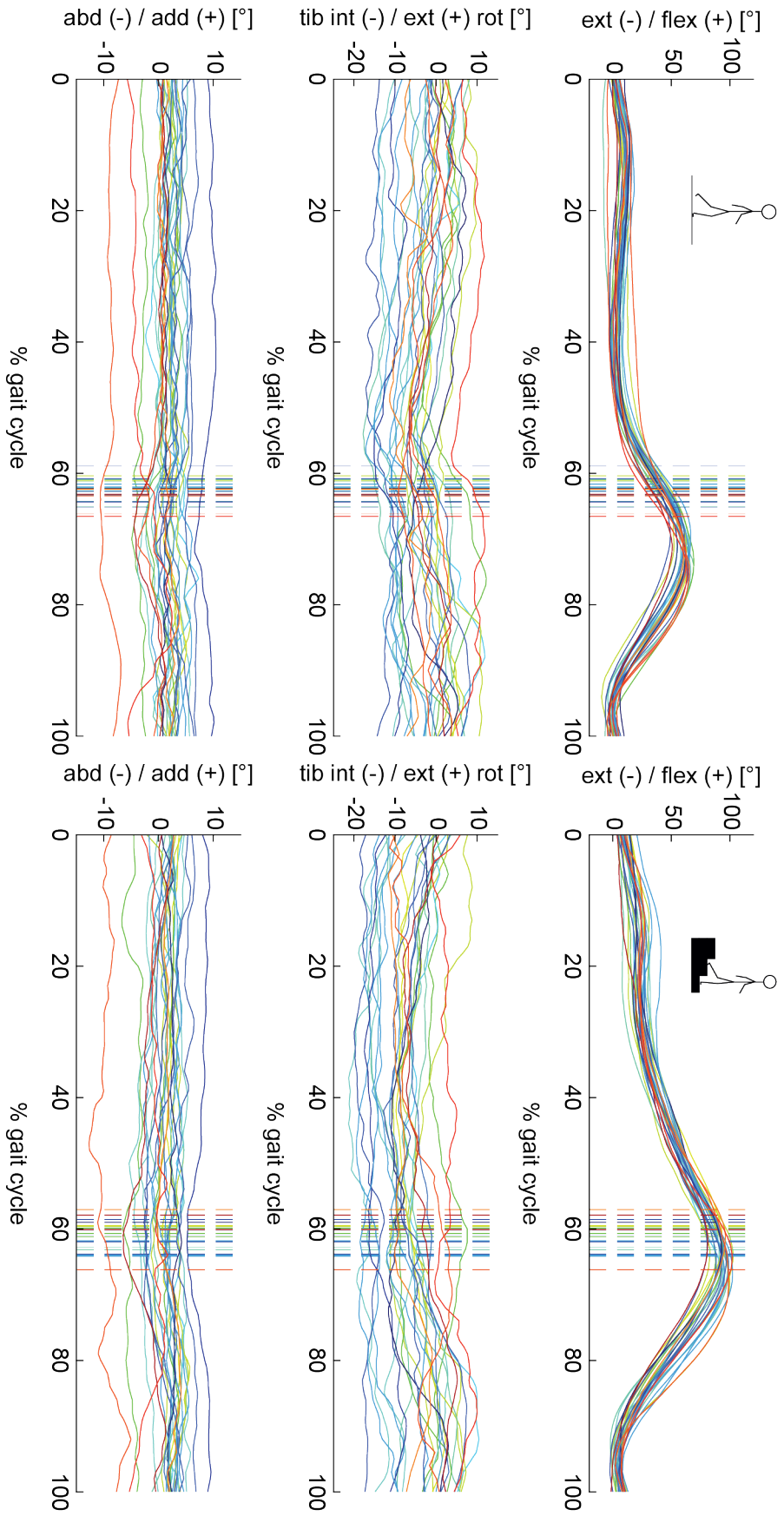

Figure D.3: Tibio-femoral flexion/extension (flex/ext), tibial internal/external rotation (tib int/ext rot) and abduction/adduction (abd/add) throughout complete cycles of level walking (left column) and stair descent (right column). The mean across all trials of each subject is presented. The average instance of toe-off for each subjects is indicated as a vertical dashed line

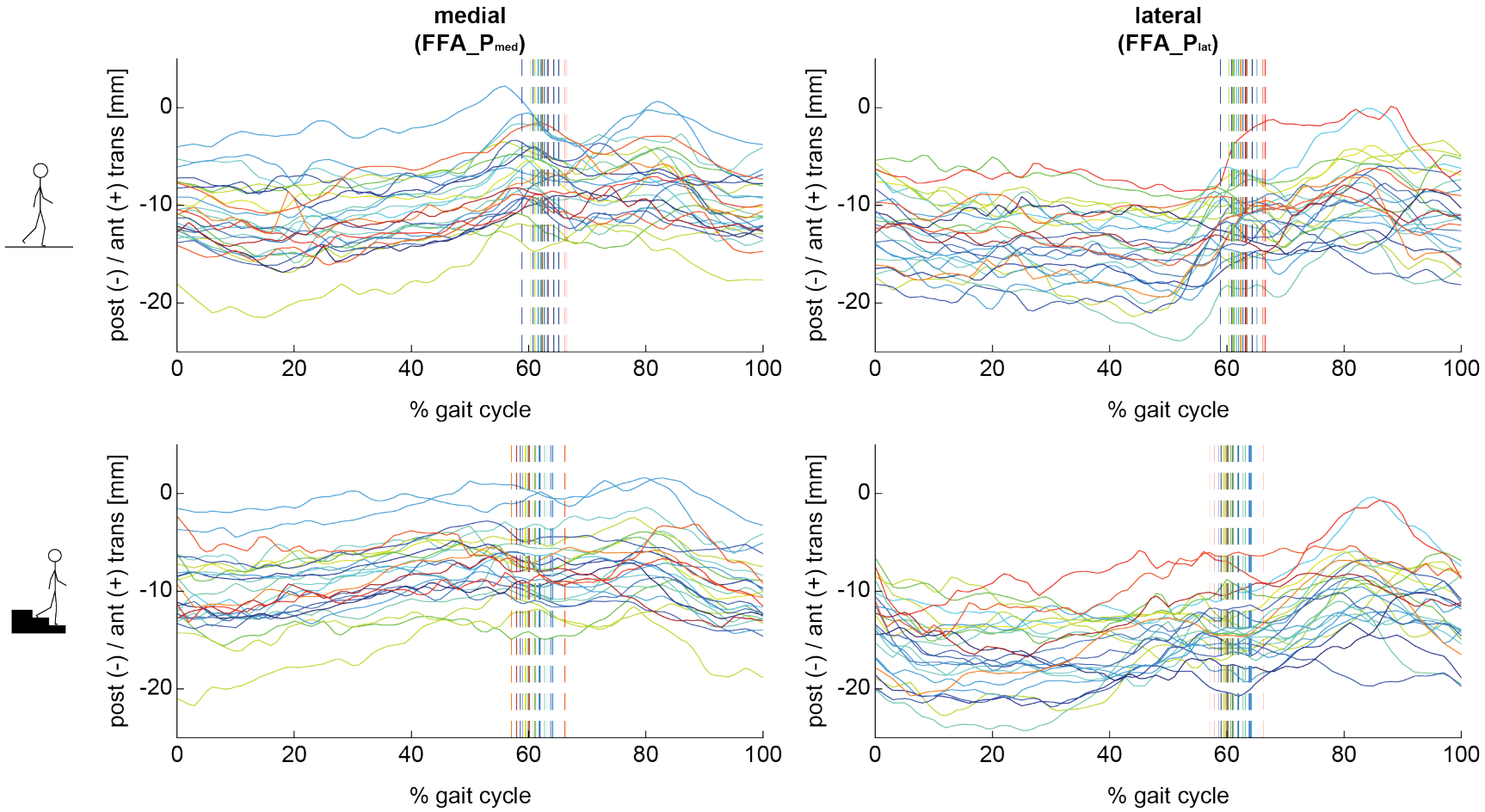

Figure D.4: Antero (ant) – posterior (post) translation of the medial and lateral functional flexion axis points throughout complete cycles of level walking (top) and stair decent (bottom). The mean across all trials of each subject is presented. The average instance of toe-off for each subject is indicated as a vertical dashed line.

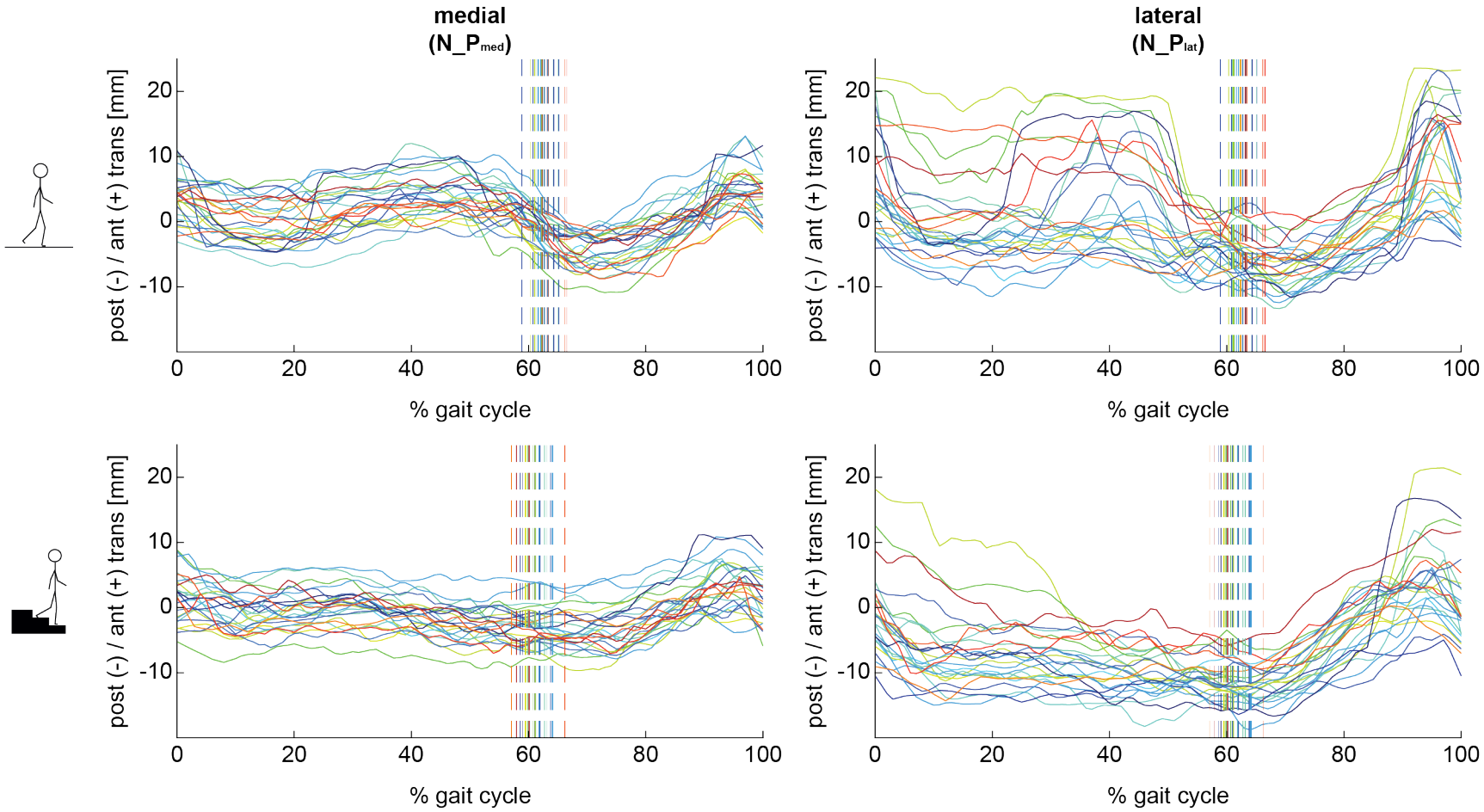

Figure D.5: Antero (ant) – posterior (post) translation of the medial and lateral nearest points throughout complete cycles of level walking (top) and stair decent (bottom). The mean across all trials of each subject is presented. The average instance of toe-off for each subject is indicated as a vertical dashed line.

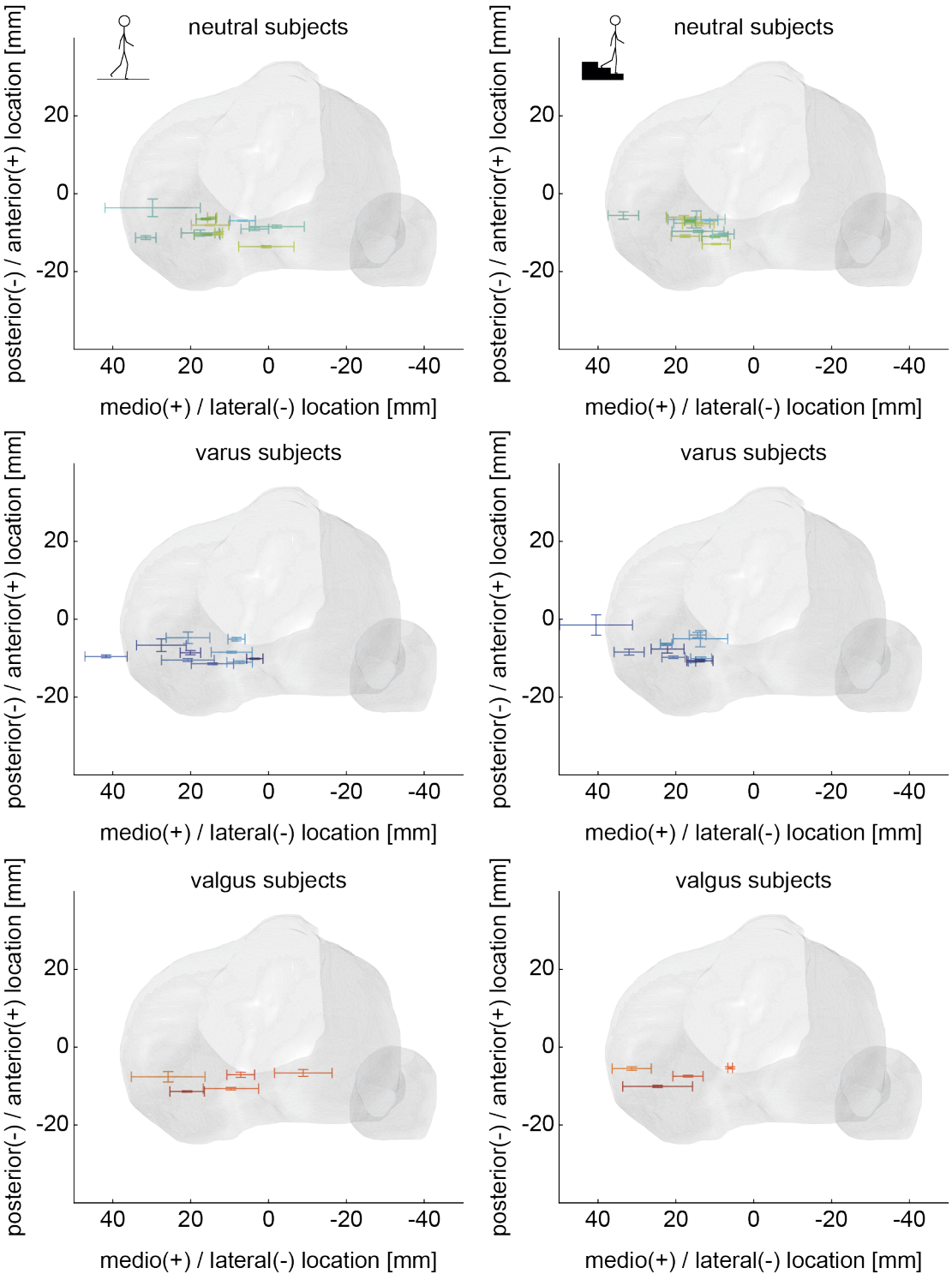

Figure D.6: Location of the centre of rotation (CoR) shown on the tibial plateau during complete cycles of level walking (left) and stair descent (right). The mean across all trials is presented for the neutral subjects (top), varus subjects (middle) and valgus subjects (bottom).